Natural Resources Canada | Ressources naturelles Canada

GEOLOGICAL SURVEY OF CANADA
OPEN FILE 8345

Application of indicator mineral methods to bedrock and sediments

M.B. McClenaghan and D. Layton-Matthews

2017

GEOLOGICAL SURVEY OF CANADA
OPEN FILE 8345

Application of indicator mineral methods to bedrock and sediments

M.B. McClenaghan[1] and D. Layton-Matthews[2]

[1]Geological Survey of Canada, 601 Booth Street, Ottawa, Ontario K1A 0E8
[2]Department of Geological Sciences, Queen's University, 30 Union Street, Kingston, Ontario K7L 3N6

2017

Permanent link: https://doi.org/10.4095/306305

This publication is available for free download through GEOSCAN (http://geoscan.nrcan.gc.ca/)

Recommended citation

McClenaghan, M.B. and Layton-Matthews, D., 2017. Application of indicator mineral methods to bedrock and sediments; Geological Survey of Canada, Open File 8345, 90 p. https://doi.org/10.4095/306305

Publications in this series have not been edited; they are released as submitted by the author.

Application of Indicator Mineral Methods to Bedrock Sediments

Convenors: M.B. McClenaghan and D. Layton-Matthews

October 22, 2017, Toronto, Ontario, Canada

INTRODUCTION

This report contains the workshop notes that were provided for a one-day short course during This open file report contains the workshop notes for “Workshop 5: Application of Indicator Mineral Methods to Bedrock and Sediments” that was convened on October 22, 2017 in Toronto, Canada, as part of Exploration ’17, the sixth decennial exploration and mining conference in a series that has been held in the seventh year of every decade since 1967 (http://www.exploration17.com/). The theme of the Exploration ’17 conference was “integrating the geosciences: the challenge of discovery”. Workshop 5 reviewed the principles, methods, and developments in the application of indicator mineral methods to mineral exploration around the world. The talks and workshop notes were presented by some of the most experienced practitioners in the field. Indicator mineral methods for the exploration for a broad range of deposit types were reviewed, including gold, diamonds, volcanogenic massive sulphide, porphyry copper, rare metals, and tungsten. Topics also included heavy mineral sample processing methods and microanalytical techniques. Support for convening the workshop and production of conference workshop notes and this report was generously provided by the Geological Survey of Canada through its Targeted Geoscience Initiative (TGI-5) and Geo-mapping for Energy and Minerals (GEM) programs.

Beth McClenaghan
Geological Survey of Canada
Natural Resources Canada

and

Dan Layton-Matthews
Department of Geological Sciences and Geological Engineering
Queen’s University

Overview of indicator mineral recovery methods for sediments and bedrock: 2017 update

M.B. McClenaghan

Geological Survey of Canada, 601 Booth Street, Ottawa, Ontario, Canada K1A 0E8
(e-mail: beth.mcclenaghan@canada.ca)

These workshop notes are a summary of a more detailed paper (McClenaghan, 2011) describing common sample processing methods used in mineral exploration programs to reduce sample volume, concentrate heavy minerals, and recover indicator minerals (Fig. 1). These notes are also an updated version of previously published workshop notes presented in 2009, 2011, and 2013 (McClenaghan, 2009, 2011, 2014). The application of indicator mineral methods to mineral exploration has expanded and developed significantly over the past three decades and these methods are now used around the world to explore for a broad spectrum of mineral deposit types. The recovery of indicator minerals from sediment samples has been reported for many deposit types including kimberlites (diamonds) (e.g. McClenaghan and Kjarsgaard, 2007), lode gold (e.g. McClenaghan and Cabri, 2011; Averill, 2017; Chapman et al., 2017), magmatic Ni-Cu-PGE (e.g. Averill, 2001, 2011; McClenaghan et al., 2011), metamorphosed VMS (e.g. McClenaghan et al., 2015), porphyry Cu (e.g. Kelley et al., 2011; Averill, 2011; Plouffe et al., 2016), Mississippi Valley-Type Pb-Zn (e.g. Paulen et al., 2011; McClenaghan et al. in press), intrusion-hosted Sn and W (McClenaghan et al., 2017a,b), and rare metals (e.g. Mackay et al., 2015; McClenaghan et al. this volume).

Indicator minerals, including ore, accessory, and alteration minerals, can be sparsely distributed or concentrated in zones in their host rocks. In sediments derived from these rocks, the indicator minerals may be even more sparsely distributed because of dilution from other rock debris; thus, sediment samples must be concentrated in order to recover and examine the indicator minerals. Most indicator minerals have a moderate to high specific gravity; therefore, most processing techniques use some type of density separation, often in combination with sizing and/or magnetic separation, to concentrate the minerals. The presence of specific indicator minerals in unconsolidated sediments provides evidence of a bedrock source and, in some cases, the chemical composition of the minerals may reflect the ore grade of the bedrock source. As little as one sand-sized grain of a specific indicator mineral in a 10 kg sediment sample may be significant. To recover such potentially small quantities (equivalent to ppb) of indicator minerals, samples are processed to reduce the volume of material that must be examined. The processing techniques employed must retain the indicator mineral(s) without contaminating the sample and must be reasonable in cost. Indicator minerals can be recovered from a variety of sample media, including stream, alluvial, glacial, beach, or eolian sediments, and residual soils. They can also be recovered from weathered and fresh bedrock, as well as mineralized float. The combinations of processing techniques used for recovering indicator minerals by exploration companies and government agencies are quite variable (e.g. Gregory and White, 1989; Peuraniemi, 1990; Davison, 1993; Towie and Seet, 1995; Chernet et al., 1999; McClenaghan et al., 1999; Gent et al., 2011; Plouffe et al., 2013). The processing methods used will depend on the commodities being sought as well as the cost per sample. Most oxide and silicate indicator minerals are easily recovered from the medium to coarse sand-sized (0.25–2.0 mm) fraction. Therefore, concentration tech-

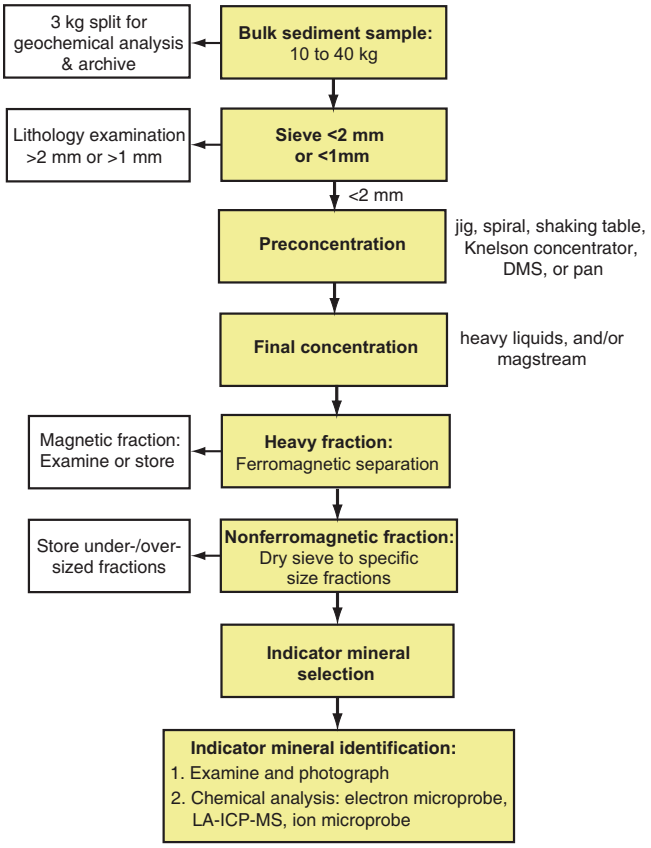

Figure 1. Generalized flow sheet showing steps in sample processing used to reduce sample weight, concentrate heavy minerals, and recover indicator minerals.

Table 1. Examples of variation in sample weight and processing procedures with sample and target type at Overburden Drilling Management Ltd.'s heavy mineral processing laboratory (Averill and Huneault, 2006).

Target	Typical Sample Weight (kg)	Required Separations				
		Table	Micropan	Heavy Liquid (specific gravity)	Ferro-magnetic separation?	Para-magnetic separation?
A. Sediment Samples						
Gold	10	Single	Yes	3.3	Yes	No
Kimberlite	10-30	Double	No	3.2	Yes	Yes
Massive sulphides (Ni-Cu-PGE, BHT, VMS, IOCG, MVT, skarn)	10	Single	Yes (PGM only)	3.2	Yes	Yes
Porphyry Cu	0.5	No	No	2.8, 3.2	Yes	Two
Uranium	10	Single	Yes	3.3	Yes	No
Heavy mineral sands (grade evaluation)	20	Triple	No	3.3	Yes	Optional
Tampering (investigation)	Variable	Optional	Yes	3.3	Yes	Optional
B. Rock Samples						
Gold, PGE, base metals	1	Optional	Yes	3.3	Yes	Optional
Kimberlite	1-10	Optional	No	3.2	Yes	Yes
Tampering (investigation)	1	No	Yes	3.3	Yes	Optional

niques that recover the sand-sized heavy minerals can be used. In contrast, a significant proportion of gold, platinum group minerals (PGM), sulphide minerals, and rare metal minerals (Laukkanen et al., 2011) are silt-sized (<0.063 mm), thus concentration of these indicator minerals requires a preconcentration technique that includes recovery of the silt- as well as the sand-sized fractions.

SAMPLE WEIGHT

The sample weight of material required for indicator mineral studies will vary depending on the type of surficial sediment collected, the grain size characteristics of the sample material, the commodity being sought, and shipping costs (Table 1). For example, in glaciated terrain clay-rich till samples may have to be 20 to 30 kg (or more) to recover a sufficient weight of sand-sized heavy minerals (Table 2, #5) (e.g. Spirito et al., 2011). In contrast, coarse-grained silty sand till typical of shield terrain requires smaller (10 to 15 kg) samples because it contains more sand-sized material in the matrix (Table 2, #1 to 4) (Spirito et al., 2011). Alluvial sand and gravel samples collected for recovery of porphyry Cu indicator minerals (PCIM) can be as small as ~0.5 kg because porphyry Cu alteration systems are large and rich in indicator minerals (Averill, 2007). Bedrock and float samples usually vary from 1 to 10 kg. The sample mass for indicator mineral studies will vary depending on the type of surficial sediment collected, the grain-size characteristics of the sample material, the commodity being sought, and shipping costs (Table 1). For example, in glaciated terrain, the mass of clay-rich till samples may have to be 20 to 30 kg (or more) to recover a sufficient quantity of sand-sized heavy minerals (Table 2, #5) (e.g. Spirito et al.,

Table 2. Weight of each fraction generated by a combination of tabling and heavy liquid separation to reduce till sample weight, concentrate heavy minerals, and recover indicator minerals: A) initial sample weight; B) sieving off <2 mm; C and D) tabling; E) heavy liquid separation; F) magnetic separation; G) final heavy mineral concentrate weight. Till samples are from (1) the South Pit of the Thompson Ni Mine, Thompson, Manitoba; (2) Broken Hammer Cu-PGE deposit, Sudbury, Ontario; (3) Pamour Mine, Timmins, Ontario; (4) Triple B kimberlite, Lake Timiskaming field, Ontario; and (5) Buffalo Head Hills, northern Alberta.

Location	Texture	A: total sample weight (kg)	B: weight >2 mm clasts (kg)	C: weight of sample put across shaking table (kg)	D: weight shaking table concentrate produced (g)	E: weight of heavy liquid light fraction (g)	F: weight magnetic fraction (g)	G: weight of non-magnetic heavy mineral concentrate (g) 0.25–2.0 mm
1. Thompson Ni Belt	silty sand till	15.0	3.0	12.0	1015.9	104.5	36.4	47.9
2. Sudbury	sandy till	15.0	5.6	9.4	1125.1	402.6	13.0	18.9
3. Timmins Gold camp	silty sand till	11.8	2.3	9.5	353.1	319.8	5.2	28.1
4. Triple B kimberlite	silty sand till	9.8	1.2	8.6	438.7	377.0	22.0	35.8
5. Northern Alberta	clayey till	67.4	2.4	65.0	1,307.0	1,235.2	5.6	11.5

2011; Plouffe et al., 2013). In contrast, coarse-grained silty sand till, which is typical of shield terrain, requires lighter (10 to 15 kg) samples because the sediment contains more sand-sized material in the matrix (Table 2, # 1 to 4) (Plouffe et al., 2013). Alluvial sand and gravel samples collected for recovery of porphyry Cu indicator minerals (PCIM) can be as small as ~0.5 kg because porphyry Cu alteration systems are large and rich in indicator minerals (Averill, 2007). Bedrock and float samples usually vary from 1 to 10 kg.

BEDROCK PREPARATION

Samples of bedrock or float (mineralized boulders) often need to be disaggregated or crushed prior to processing to reduce rock fragment/mineral grain size to <2 mm. Electric pulse disaggregation (EPD) using an electric current from a high-voltage power source in a water bath is an efficient means of liberating mineral grains from a rock (Cabri et al., 2008; Oberthür et al., 2010). The major advantage of this method compared to crushing is that individual mineral grains can be recovered in their original shape and form, regardless of grain size. Conventional rock crushers may also be used, however, they (1) are more difficult to clean between samples and thus pose a higher risk of cross contamination, (2) often cause rock fragments to break across grain boundaries, and (3) may mark/damage grains as they are liberated. Barren quartz can be disaggregated or crushed as a blank between routine rock samples to reduce and monitor contamination.

PRECONCENTRATION

If sample shipping costs are an issue, samples may be partly processed in the field to reduce the weight of the material needing to be shipped to a processing laboratory. Samples may be sieved to remove the coarse (>1 or >2 mm) fraction, which may reduce sample weights from a few % to 30% (e.g. Table 2, columns B-C). Preconcentrating samples using a pan, jig, sluice box, or centrifugal concentrator also may be carried out in the field to further reduce the weight of material to be shipped. These preconcentrates can be examined in the field, which significantly reduces the time waiting to obtain lab results in order to plan follow-up. However, preconcentrating in the field can itself be expensive and time consuming and the available methods may not provide optimal recovery of the indicator minerals of interest. Field setup of concentrating equipment may be more rudimentary than at the processing laboratory, thus extra care is required to avoid cross contamination or material loss during the preconcentration procedures.

Whether sieved off in the field or in the laboratory, the coarse >2 mm fraction may be examined to provide additional information about sample provenance and transport distance. The <2 mm (or <1 mm) fraction is most commonly preconcentrated using sieving and/or density methods (e.g. jig, shaking table, spiral concentrator, dense media separator, pan, centrifugal concentrator) to reduce the weight of material to be examined without losing indicator minerals. Some of the more common preconcentration equipment and techniques are described below.

Pans

Panning is the oldest method used to recover indicator minerals, primarily for gold and PGM (Theobald, 1957). Sediment is placed in a pan and shaken sideways in a circular motion while the pan is held just under the surface of the water. Heavy minerals sink to the bottom of the pan and light minerals rise and spill out over the top (Zeschke, 1961; Silva, 1986; English et al., 1987; Ballantyne and Harris, 1997). Pans have varying shapes (flat-bottomed or conical) and sizes, and can be made of plastic, metal, or wood. The advantages of this technique include that it can be done in the field- or in the laboratory, the equipment required is inexpensive, and if used in the field it reduces the weight of the sample to be shipped and thus shipping costs. If panning is undertaken in the field, indicator minerals can be examined immediately and results can be used to guide ongoing exploration while still in the field. Panning is often used in combination with other preconcentration and/or heavy liquid methods to recover silt-sized precious metal grains (e.g. Grant et al., 1991; Leake et al., 1991, 1998; Ballantyne and Harris, 1997; Wierchowiec, 2002). The disadvantages of this method are that it is slow and highly dependent on the experience and skill of the operator and therefore requires consistent personnel to perform the panning. It is considered to be a rough concentration method when used in the field and it should be followed up with further laboratory-based concentration techniques (e.g. Zantop and Nespereira, 1979; Stendal and Theobald, 1994).

Shaking tables

Preconcentration using a shaking (e.g. Wilfley) table is another one of the oldest methods for concentrating and separating heavy minerals based on density. It recovers silt- to coarse sand-sized heavy minerals for a broad spectrum of commodities, including diamonds, precious and base metals, and uranium (Averill and Huneault, 2006). A brief description of the method is summarized below from Sivamohan and Forssberg (1985), Silva (1986), and Stewart (1986). The shaking table consists of a deck with ≤1 cm-high riffles covering over half the surface. A motor mounted on one end drives a small arm that shakes the table along its length. A slurry of <2.0 mm sample material is put across the shaking table to prepare a preconcentrate. If kimberlite indicators are targeted, the sample is tabled twice to

ensure higher recovery of the key lower density minerals (Cr-diopside and forsteritic olivine) and the coarsest grains. The advantages of this method are the ability to recover both silt- and sand-sized indicator minerals for a broad spectrum of commodities at a moderate cost and that the operator is able observe the heavy minerals as the sample is being processed and can adjust the tabling efficiency during processing. It is a well established method for the recovery of precious metal mineral grains as well as kimberlite indicator minerals (e.g. English et al., 1987; McClenaghan et al., 1998, 2004). The disadvantages of this method include the loss of some coarse heavy minerals as well as the finer <0.10 mm grains (Gent et al., 2011), the lengthy time required to process each sample, and that its success is dependent on the skill of the operator.

Dense media separators

A micro-scale dense media separator (DMS) employs a gravity-based method to preconcentrate kimberlite indicator minerals. An overview of this method described below is outlined in Baumgartner (2006). Heavy mineral concentration is carried out using a gravity-fed high-pressure cyclone. The <1 mm fraction of a sample is mixed with fine-grained ferrosilicon (FeSi) to produce a slurry of a controlled density. The slurry is fed into the cyclone where the grains travel radially and helically, forcing the heavier particles toward the wall of the cyclone and the lighter particles toward the centre (Gent et al., 2011). The lighter and heavier particles exit the cyclone through different holes; the light fraction is discarded and the heavy fraction is collected on a 0.25 or 0.3 mm screen. The heavy mineral concentrate on the screen is then dried and cleaned to remove residual FeSi. A Tromp curve is used to define the efficiency and precision of the DMS separation. The DMS is calibrated to recover common kimberlite indicator minerals that have a specific gravity (SG) >3.1 — pyrope garnet, chrome-spinel, Mg-ilmenite, Cr-diopside, forsteritic olivine, and diamond — and it is tested using synthetic density tracers before processing samples. The density settings and cut points are checked once per day. The advantages of the micro DMS system are that it is fast, less susceptible to sample contamination than other heavy mineral concentrating techniques, and is not operator dependent. The method, however, is more expensive than the other methods described here and it does not recover the silt-sized precious and base metal indicator minerals.

Centrifugal concentrators

Centrifugal concentrators were originally designed for concentrating gold and platinum from placer and bedrock samples. However, in recent years they have also been used to recover kimberlite indicator minerals from sediment samples (e.g. Chernet et al., 1999; Lehtonen et al., 2005, 2015). Centrifugal concentrators can process particle sizes that range from >10 µm to a maximum of 6 mm. The general processing procedure for one type of centrifugal concentrator, the Knelson Concentrator, is summarized below from material provided on the manufacturer's website (http://www.knelsongravitysolutions.com). In summary, water is introduced into a concentrate cone through a series of holes in rings on the side of the cone. The sample slurry is then added into the concentrate cone from a tube at the top. When the slurry reaches the bottom of the cone, it is forced outward and up the cone wall by the centrifugal force generated by spinning the cone at high RPM. The slurry fills each ring on the inside wall of the cone to capacity, creating a concentrating bed. High specific gravity particles are captured in the rings and retained in the concentrating cone. At the end of the spin cycle, the concentrates are flushed from the cone into the sample collector.

The advantages of centrifugal concentrators are that they are fast, inexpensive, and when used in the field, they can reduce the volume of the material that must be shipped to the laboratory. However, problems that can occur include (1) poor recovery of indicator minerals from silt-poor sorted sediments (e.g. esker sand or stream sediments) due to the absence of fine-grained material to keep the slurry in suspension and (2) poor recovery of moderately heavy (~3.5–4.0 SG) grains that are <100 µm (Chernet et al., 1999; Lehtonen et al., 2015). Alternatively, too much fine-grained material can impede the settling of fine-grained heavy minerals.

Spiral concentrators

Heavy minerals can be recovered using a rotary spiral concentrator (Silva, 1986), which consists of a flat circular stainless-steel bowl with rubber ribs that spiral inward. The concentrator is mounted on a frame so it can be tilted and has a water wash bar extending laterally from one side of the bowl to the centre. As the bowl spins, water is sprayed from the bar and heavy mineral grains move up and inward along the spirals to the central opening where they are collected in a container behind the bowl. The water washes light minerals down to the bottom of the bowl. The heaviest minerals are recovered first. The advantages of the spiral concentrator are that it can be field-based and thus used to reduce sample weight to be shipped, it is inexpensive to acquire and operate, it requires little time if the material is sandy, and it recovers indicator minerals across a broad range of sizes, from silt- to sand-sized grains. The method, however, is dependent on the experience and skill of the operator, the lower density threshold is variable, there is some loss of heavy minerals, and the method is slow if the sample is clay-rich. It is used mainly for gold recovery (e.g. Maurice and Mercier

1986; Silva 1986; Maurice 1988; Sarala et al., 2009) but in recent years it also has been used for the recovery of kimberlite indicator minerals (e.g. Sarala and Peuraniemi, 2007).

Jigs

Jigging is one of the oldest gravity concentration methods; this method separates heavy minerals based on differential settling velocities of mineral grains in water (Stendal and Theobald 1994). Jigging is performed by hand or by mechanically jerking a partially filled screen of material up and down underwater for several minutes. While submersed in water, mineral grains separate through suspension and gravity effects into layers of varying specific gravity. Heavier grains concentrate on the surface of the screen, with the heaviest generally concentrating towards the centre of the screen forming an 'eye'. Very heavy minerals, such as ilmenite and magnetite, will be found at the very centre of the screen and lighter heavy mineral, such as garnet and pyroxene, will concentrate at the periphery of the eye. Diamonds tend to concentrate towards the centre, despite their moderate specific gravity (SG 3.51). A spoon is used to remove the heavy minerals in the eye for more detailed examination. For optimal recovery, the jig tailings should be re-jigged 2 to 3 times until no eye forms. This method is typically used for recovering gold (e.g. Silva 1986) and kimberlite indicator minerals (Muggeridge 1995). The advantages of using a jig are that it can be field-based, which reduces the volume of the samples to be shipped, is inexpensive to operate, is relatively fast, and works best for fine- to coarse-sand sized grains. However, it is best used in a fixed, laboratory-based setting by an experienced operator.

FINAL CONCENTRATION

Heavy liquid separation

A sample preconcentrate is usually further refined using heavy liquids of a precise density (Gent et al., 2011) to further reduce the volume of the sample prior to heavy mineral selection (Table 2, column E). Heavy liquid separation provides a sharp separation between heavy (sink) and light minerals (float) at an exact known density. This method is slow and expensive, and therefore is not economical for large volumes of sample material; hence, it is advantageous to use the preconcentration procedures described above to reduce the volume of the sample before this step (Stendal and Theobald 1994). It is common to remove the finer fraction (<0.063 mm) of a sample by sieving before using heavy liquid separation, as the small particle size of this material can make it difficult to separate (M. Lehtonen, pers. comm., 2013).

The heavy liquids most commonly used for heavy mineral separation include methylene iodide (MI) with a SG of 3.3 and tetrabromoethane (TBE) or low-toxicity heavy liquid lithium heteropolytungstates (LST), both of which have a SG of 2.9. The density of the heavy liquid to be used will depend on the target indicator minerals. Some laboratories use a combination of both heavy liquids for separation: using a lower density heavy liquid (SG ≈ 2.9) first to reduce the volume of material to be further separated using a higher density liquid (SG ≈ 3.2 or 3.3) (e.g. de Souza, 2006; Le Couteur and McLeod, 2006; Mircea, 2006). The recovery of lower density kimberlite and magmatic Ni-Cu-PGE indicator minerals (e.g. Cr-diopside and forsteritic olivine) requires separation using dilute methylene iodide with a SG of 3.2. Recovery of porphyry Cu indicator minerals requires separation using a liquid with a SG of 2.8 to 3.2 to recover the mid-density indicators such as tourmaline (dravite), alunite, jarosite, and turquoise (Averill, 2007; Plouffe et al., 2016). Some indicator minerals, such as apatite and fluorite, are of intermediate density but are recovered mainly from the mid-density rather than the heavy fraction.

Magnetic separation

Magnetic separation may be used to further refine heavy mineral concentrates and reduce concentrate volume before picking for mineral species with specific magnetic susceptibilities (Towie and Seet, 1995). The most common magnetic separation technique involves splitting the ferromagnetic from the non-ferromagnetic fraction. Ferromagnetic minerals can comprise a considerable proportion of the concentrate (e.g. Table 2, column F) and therefore removing the ferromagnetic minerals decreases the size of the concentrate prior to indicator mineral selection and removes any steel contaminants derived, in most instances, from sampling tools or drilling equipment. The ferromagnetic fraction may then be (1) set aside; (2) examined to determine the abundance and mineral chemistry of magnetite (e.g. Dare et al., 2014; Nadoll et al., 2015; Canil et al., 2016), pyrrhotite (McClenaghan et al., 2012), or magnetic Mg-ilmenite, as is the case for some kimberlites (e.g. McClenaghan et al., 1998); or (3) analyzed geochemically (e.g. Theobald et al., 1967). A hand magnet or plunger magnet is most commonly used to carry out this separation.

The non-ferromagnetic heavy mineral concentrate may be further separated electromagnetically into specific size fractions of different paramagnetic characteristics to reduce the volume of material to be examined for indicator minerals (Averill and Huneault, 2006). Minerals such as diamond are nonparamagnetic; pyrope garnet, eclogitic garnet, Cr-diopside and forsteritic olivine are nonparamagnetic to weakly paramagnetic; and Cr-spinel and Mg-ilmenite are moderately to strongly paramagnetic (see Table 1 in McClenaghan and Kjarsgaard, 2007). If the non- or

paramagnetic portion of the concentrate contains a significant amount of almandine garnet it may be processed through a magstream separator to separate the orange almandine from similar-looking eclogitic or pyrope garnet grains. In this case, magstream separation divides the concentrate into (1) a fraction containing most of the silicates (e.g. pyrope and eclogitic garnet) and no almandine, and (2) a fraction containing ilmenite, chromite, and other moderately magnetic minerals such as almandine (Baumgartner, 2006).

INDICATOR MINERAL SELECTION AND EXAMINATION

The non-ferromagnetic fraction is commonly sieved into two or three size fractions (e.g. 0.25–0.5 mm, 0.5–1.0 mm, 1.0–2.0 mm) for picking of indicator minerals; however, the final size range will depend on the commodity sought. For example, kimberlite indicator minerals are most abundant in the 0.25 to 0.5 mm fraction (McClenaghan and Kjarsgaard, 2007) and thus, to maximize recovery and minimize counting time and cost, the 0.25 to 0.5 mm fraction is most commonly picked.

Indicator minerals in the finer size (e.g. 0.25–0.5 mm, 0.3–0.5 mm, 0.25–0.86 mm) fractions are selected from the non-ferromagnetic heavy mineral concentrate during a visual scan, in most cases using a binocular microscope. The grains are counted and a number are removed from the sample for analysis by an electron microprobe (EMP) to confirm their identification. Methods for examining a sample for counting/picking vary from rolling conveyor belts to dishes/paper marked with lines or grids. If a concentrate is unusually large, then a split is examined and the indicator mineral counts are normalized to the total weight of the concentrate. If a split is picked, the weight of the split and the total weight should both be recorded. Not all grains counted in a sample will be removed for EMP analyses. If this is the case, both the total number of grains counted and the number of grains removed should be recorded.

Indicator minerals are visually identified in concentrates by their colour, crystal habit, and surface textures, which may include features such as kelyphite rims and orange-peel textures on kimberlitic garnet (e.g. Garvie, 2003; McClenaghan and Kjarsgaard, 2007). The morphology of gahnite (Zn spinel) may provide clues to the relative distance of glacial transport (McClenaghan et al., 2014). Minerals such as scheelite and zircon may be counted under shortwave ultraviolet light. Gold and PGM grains may be panned from the silt-sized fraction of concentrates (e.g. concentrates prepared by tabling). The grains may be counted and classified with the aid of optical or scanning electron microscopy. Commonly, gold grains are classified according to their shape and/or degree of wear (e.g. DiLabio, 1990; Averill, 2001), both of which are characteristics that can provide information about relative transport distances (McClenaghan and Cabri, 2011).

INDICATOR MINERAL CHEMISTRY

Mineral grains are characterized by measuring the abundances of major oxides, and minor and trace elements by scanning electron microscope -energy-dispersive X-ray spectroscopy (SEM-EDS), electron microprobe analysis (EMPA), laser ablation-inductively coupled plasma-mass spectrometry (LA ICP-MS), or secondary ion mass spectrometry (SIMS) (e.g. Ramsden et al., 1999; Belousova et al., 2002; Scott, 2003; Heimann et al., 2005; Layton-Matthews et al. this volume). For example, kimberlite indicator minerals are characterized by a specific range of compositions that reflect their mantle source and diamond grade (e.g. Fipke et al., 1995; Schulze, 1997; Grütter et al., 2004; Wyatt et al., 2004; Nowicki et al., 2007). Gold, PGM, and sulphide grains may be analyzed to determine their trace element chemistry or isotopic compositions (e.g. Grant et al., 1991; Leake et al., 1998; Chapman et al., 2009, 2017).

To provide quantitative mineralogical analysis and identification of indicator minerals in the 0.25 to 2.0 mm fraction or the rarely examined <0.25 mm fraction, polished epoxy grain mounts may be prepared for a portion of the heavy mineral concentrate. The grain mounts may then be examined using one the newer techniques, such as mineral liberation analysis (MLA) (e.g. Oberthür, et al., 2010; Wilton and Winter, 2012), computer-controlled scanning electron microscopy (CCSEM), or quantitative evaluation of materials by scanning electron microscopy (QEMSCAN). These methods can be used to identify indicator minerals of interest and prioritize grains for further detailed and more costly EMP analysis, thus reducing EMP analytical time and costs. The cost per sample for these new techniques is, in general, more expensive than conventional methods.

QUALITY CONTROL

To meet 43-101 reporting requirements, project geologists may use a combination of blank samples (which contain no indicator minerals), spiked samples (which contain a known quantity of introduced indicator mineral species or density blocks/beads (e.g. Gent et al., 2011; Plouffe et al., 2013)), and/or re-examination of ~10% of the heavy mineral concentrate samples to monitor a laboratory's potential sample contamination and the quality of their indicator mineral identification. In addition, heavy mineral processing and identification laboratories can be asked to report their own quality control monitoring procedures and test results.

Quality assurance and control measures implemented at the Geological Survey of Canada for indicator mineral surveys are described in Plouffe et al. (2013).

SUMMARY

These workshop notes describe some of the procedures available for processing surficial media and rocks to recover indicator minerals for mineral exploration. The processing method used will depend on the sample media, commodities being sought, budget, bedrock and surficial geology of the survey area, as well as the processing methods used for previous batches of samples. When reporting indicator mineral results in company assessment files, government reports, or scientific papers, it is helpful to report the laboratory name, processing methods used, and initial sample weights. A complete list of metadata that should be reported so that the indicator mineral data can be fully understood, interpreted, compared to other surveys, and archived is reported in Plouffe et al. (2013). Monitoring of quality control is essential at each stage in the processing, picking, and analytical procedures described here and should be monitored both by the processing laboratories and their clients. Geologists are encouraged to visit processing and picking laboratories so that they have a clear understanding of the procedures being used and can discuss customizations needed for specific sample batches.

REFERENCES

Averill, S.A., 2001. The application of heavy indicator minerals in mineral exploration with emphasis on base metal indicators in glaciated metamorphic and plutonic terrains, *In*: McClenaghan, M.B., Bobrowsky, P.T., Hall, G.E.M and Cook, S. (eds) *Drift Exploration in Glaciated Terrain*; Geological Society of London, Special Volume 1985, p. 69 82.

Averill, S.A., 2007. Recent advances in base metal indicator mineralogy: An update from Overburden Drilling Management Limited; *EXPLORE, Newsletter of the Association of Applied Geochemists*, v. 134, p. 2–6.

Averill, S.A., 2011. Viable indicator minerals in surficial sediments for two major base metal deposit types: Ni-Cu-PGE and porphyry Cu; *Geochemistry: Exploration, Environment, Analysis*, v. 11, p. 279–292.

Averill, S.A., 2017. The Blackwater gold-spessartine-pyrolusite glacial dispersal train, British Columbia, Canada; influence of sampling depth on indicator mineralogy and geochemistry; *Geochemistry: Exploration, Environment, Analysis*, v. 17, p. 43–60.

Averill, S.A. and Huneault. R., 2006. Overburden Drilling Management Ltd: Exploring heavy minerals; *EXPLORE, Newsletter of the Association of Applied Geochemists*, v. 133, p. 1–5.

Ballantyne, S.B and Harris, D.C., 1997. Alluvial platinum-group minerals and gold in Alberta: Results from the "Orientation Studies Project" and their significance to exploration, *In:* Macqueen, R.W. (ed), *Exploring for Minerals in Alberta*; Geological Survey of Canada Geoscience Contributions, Canada-Alberta Agreement on Mineral Development (1992–1995), Geological Survey of Canada, Bulletin 500, p. 279–329.

Baumgartner, M., 2006. Industry leading laboratory services for diamond explorers; *EXPLORE, Newsletter of the Association of Applied Geochemists*, v. 133, p. 5–10.

Belousova, E.A., Griffin, W.L., O'Reilly, S., and Fisher, N.I., 2002. Apatite as an indicator mineral for mineral exploration: Trace element compositions and their relationship to host rock type; *Journal of Geochemical Exploration*, v. 76, p. 45–69.

Cabri, L.J., Rudashevsky, N.S., Rudashevsky, V.N., and Oberthür, T., 2008. Electric-Pulse Disaggregation (EPD), Hydroseparation (HS) and their use in combination for mineral processing and advanced characterization of ores, *In: Proceedings*; Canadian Mineral Processors 40th Annual Meeting, Paper 14, p. 211–235.

Canil, D., Grondahl, C., Lacourse, T., and Pisiak, L.K., 2016. Trace elements in magnetite from porphyry Cu–Mo–Au deposits in British Columbia, Canada; *Ore Geology Reviews*, v. 72, p. 1116–1128.

Chapman, R.J., Leake, R.C., Bond, D.P.G., Stedra, V., and Fairgrieve, B., 2009. Chemical and mineralogical signatures of gold formed in oxidizing chloride hydrothermal systems and their significance within populations of placer gold grains collected during reconnaissance; *Economic Geology*, v. 104, p. 563–585.

Chapman, R.J., Mileham, T., Allan, M., and Mortensen, J., 2017. A distinctive Pd-Hg signature in detrital gold derived from alkali Cu-Au porphyry systems; *Ore Geology Reviews*, v. 83, p. 84–102.

Chernet, T. Marmo, J., and Nissinen, A., 1999. Technical note. Significantly improved recovery of slightly heavy minerals from Quaternary samples using GTK modified 3" Knelson preconcentrator; *Minerals Engineering,* v. 12, p. 1521–1526.

Dare, S.A.S., Barnes, S-J., Beaudoin, G., Méric, J., Boutroy, E., and Potvin-Doucet, C., 2014. Trace elements in magnetite as petrogenetic indicators; *Mineralium Deposita*, v. 49, p. 785–796.

Davison, J.G., 1993. Diamond exploration samples: laboratory processing, *In:* Sheahan P. and Chater, A. (Chairmen) *Diamond: Exploration, Sampling and Evaluation*; Prospectors and Developers Association of Canada, Short Course Proceedings, Toronto, March 27, 1993, p. 315–341.

de Souza, H., 2006. Indicator mineral processing at SGS Minerals Services; *EXPLORE, Newsletter of the Association of Applied Geochemists,* v. 133, p. 13–15.

DiLabio, R.N.W., 1990. Classification and interpretation of the shapes and surface textures of gold grains from till on the Canadian Shield, *In: Current Research, Part C*; Geological Survey of Canada, Paper 90-1C, p. 323–329.

English, B.L., Desborough, G.A., and Raymond, W.H., 1987. *A mechanical panning technique for separation of fine-grained gold and other heavy minerals*; United States Geological Survey, Open File Report 97-0364.

Fipke, C.E., Gurney, J.J., and Moore, R.O., 1995. *Diamond exploration techniques emphasizing indicator mineral geochemistry and Canadian examples;* Geological Survey of Canada, Bulletin 423.

Garvie, O.G., 2003. Surface textures found on kimberlite indicator minerals, *In: Indicator mineral methods in mineral exploration*; Prospectors and Developers Association of Canada, Short Course 2, March 8, p. 23.

Gent, M., Menendez, M., Toraño, J., and Torno, S., 2011. A review of indicator minerals and sample processing methods for geochemical exploration; Journal of Geochemical Exploration, v. 110, p. 47–60.

Grant, A.H., Lavin. O.P., and Nichol, I., 1991. The morphology and chemistry of transported gold grains as an exploration tool; *Journal of Geochemical Exploration*, v. 40, p. 73–94.

Gregory, G.P. and White, D.R., 1989. Collection and treatment of diamond exploration samples, *In:* Ross, J. (ed) *Kimberlites and Related Rocks Volume 2 Their Crust/Mantle Setting, Diamonds and Diamond Exploration*; Geological Society of Australia, Special Publication 14, Blackwell Scientific Publications, Oxford, p. 1123–1134.

Grütter, H.S., Gurney, J.J., Menzies, A.H., and Winter, F., 2004. An updated classification scheme for mantle-derived garnet, for use by diamond explorers; *Lithos*, v. 77, p. 841–857.

Heimann, A., Spry, P., and Teale, G.S., 2005. Zincian spinel associated with metamorphosed Proterozoic base-metal sulfide occurrences, Colorado: A re-evaluation of gahnite composition as a guide in exploration; *The Canadian Mineralogist*, v. 43, p. 601–622.

Kelley, K.D., Eppinger, R.G., Lang, J., Smith, S.M., and Fey, D.L., 2011. Porphyry copper indicator minerals (PCIMs) in glacial till samples as an exploration tool: example from the giant Pebble porphyry Cu-Au-Mo deposit; *Geochemistry: Exploration, Environment, Analysis*, v. 11, p. 321–334.

Laukkanen, J., Lehtonen, M., and Sarala, P., 2011. Exploring RE and REE mineralization using indicator minerals, *In*: *Workshop 3: Indicator Mineral Methods in Mineral Exploration*; 26th International Applied Geochemistry Symposium, Association of Applied Geochemists, p. 13–18.

Leake, R.C., Bland, D.J., Styles, M.T., and Cameron, D.G., 1991. Internal structure of Au-Pd-Pt grains from south Devon, England, in relation to low temperature transport and deposition; *Transactions of the Institute of Mining and Metallurgy*, Section B, Applied Earth Sciences, v. 100, p. B159–B178.

Leake, R.C., Chapman, R.J., Bland, D.J., Stone, P., Cameron, D.G., and Styles, M.T., 1998. The origin of alluvial gold in the Leadhills areas of Scotland: evidence from interpretation of internal characteristics; *Journal of Geochemical Exploration*, v. 63, p. 7–36.

Lehtonen, M.L., Marmo, J.S., Nissinen, A.J., Johanson, B.S., and Pakkanen, L.K., 2005. Glacial dispersal studies using indicator minerals and till geochemistry around two eastern Finland kimberlites; *Journal of Geochemical Exploration*, v. 87, p. 19–43.

Lehtonen, M.L., Lahaye, Y., O'Brien, H., Lukkari, S. Marmo, J.S., and Sarala, P., 2015. Novel technologies for indicator mineral-based exploration, *In:* Sarala, P. (ed.), *Novel Technology for Greenfield Exploration*; Geological Survey of Finland, Special Paper 57, p. 23–62.

Le Couteur, P.C. and McLeod, J.A., 2006. Heavy mineral processing at Vancouver Indicator Processors Inc./Teck Cominco Global Discovery Lab; *EXPLORE, Newsletter of the Association of Applied Geochemists*, v. 133, p. 5–18.

Mackay, D.A.R., Simandl, G.J., Ma, W., Redfearn, M., and Gravel, J., 2015. Indicator mineral-based exploration for carbonatites and related specialty metals deposits- a QEMSCAN® orientation survey, British Columbia, Canada. *Journal of Geochemical. Exploration*, v. 165, p. 159–173.

Maurice, Y.T., 1988. Regional alluvial heavy mineral geochemistry as a prospecting method in glaciated Appalachian Terrain: a case history from the southern Quebec placer-gold belt, *In:* MacDonald D.R. and K.A. Mills, K.A. (eds.), *Prospecting in Areas of Glaciated Terrain - 1988*; Canadian Institute of Mining and Metallurgy, p. 185–203.

McClenaghan, M.B., 2009. Processing methods for recovery of indicator minerals from sediment and bedrock, *In: Workshop B Indicator mineral methods in mineral exploration*; 26th International Applied Geochemistry Symposium, Association of Applied Geochemists, p. 13–20.

McClenaghan, M.B., 2011. Overview of common processing methods for recovery of indicator minerals from sediment and bedrock in mineral exploration; *Geochemistry: Exploration, Environment, Analysis*, v. 11, p. 265–278.

McClenaghan, M.B and Cabri, L.J., 2011. Review of gold and platinum group element indicator minerals methods for surficial sediment sampling; *Geochemistry: Exploration, Environment, Analysis*, v. 11, p. 251–263.

McClenaghan, M.B., 2014. Processing methods for recovery of indicator minerals from sediment and bedrock, *In:* McClenaghan, M.B., Plouffe, A., and Layton-Matthews, D. (eds), *Application of Indicator Mineral Methods to Mineral Exploration*; Geological Survey of Canada, Open File 7553, (also 26th International Applied Geochemistry Symposium Short Course SC07, November 17, 2103, Rotarua, New Zealand), p. 1–8.

McClenaghan, M.B. and Cabri, L.J., 2011. Review of gold and Platinum Group Element indicator minerals methods for surficial sediment sampling; *Geochemistry: Exploration, Environment, Analysis*, v. 11, p. 251–263.

McClenaghan, M.B. and Kjarsgaard, B.A., 2007. Indicator mineral and surficial geochemical exploration methods for kimberlite in glaciated terrain, examples from Canada, *In:* Goodfellow, W.D. (ed.) *Mineral Resources of Canada: A Synthesis of Major Deposit Types, District Metallogeny, the Evolution of Geological Provinces and Exploration Methods*; Geological Association of Canada, Special Publication No. 5, p. 983–1006.

McClenaghan, M.B. and Paulen, R.C., 2017. Mineral exploration in glaciated terrain, *In:* Menzies, J. and van der Meer, J. (eds) *Modern and Past Glacial Environments 2nd Edition*. Elsevier, in press.

McClenaghan, M.B., Paulen R.C., Ayer, J.A., Trowell, N.F., and Bauke, S., 1998. R*egional till and humus geochemistry of the Timmins-Kamiskotia (NTS 42A/11, 12, 13, 14) area, northeastern Ontario*. Geological Survey of Canada, Open File 3675.

McClenaghan, M.B., Kjarsgaard B.A., Kjarsgaard I.M., and Paulen, R.C., 1999. *Mineralogy and geochemistry of the Peddie kimberlite and associated glacial sediments, Lake Timiskaming, Ontario*. Geological Survey of Canada, Open File 3775.

McClenaghan, M.B., Kjarsgaard, I.M., and Kjarsgaard, B.A., 2004. *Kimberlite indicator mineral chemistry and till geochemistry around the Seed and Triple B kimberlites, Lake Timiskaming, Ontario*; Geological Survey of Canada, Open File 4822.

McClenaghan, M.B., Averill, S.A., Kjarsgaard, I.M., Layton-Matthews, D., and Matile, G., 2011. Indicator mineral signatures of magmatic Ni-Cu deposits, Thompson Nickel Belt, central Canada, *In:* McClenaghan, M.B. and Layton-Matthews, D. (conv.) *Workshop 3: Indicator mineral methods in mineral exploration*; 26th International Applied Geochemistry Symposium, Association of Applied Geochemists, p. 67–72.

McClenaghan, M.B., Budulan, G., Averill, S.A., Layton-Matthews, D., and Parkhill, M.A., 2012. *Indicator mineral abundance data for bedrock and till samples from the Halfmile Lake Zn-Pb-Cu volcanogenic massive sulphide deposit*, *Bathurst Mining Camp, New Brunswick*; Geological Survey of Canada, Open File 7076.

McClenaghan, M.B., Holmes, D.R.S., Averill, S.A., Paulen, R.C., and Layton-Matthews, D., 2014. P*hysical features indicating the glacial transport distance of gahnite from the Izok Lake Cu-Zn-Pb-Ag VMS deposit, Nunavut*. Geological Survey of Canada, Open File 7603.

McClenaghan, M.B., Paulen, R.C., Layton-Matthews, D., Hicken, A.K., and Averill, S.A., 2015. Glacial dispersal of gahnite from the Izok Lake Zn-Cu-Pb-Ag VMS deposit, northern Canada; *Geochemistry: Exploration, Environment, Analysis*, v. 15, p. 333–349.

McClenaghan, M.B., Parkhill, M.A., Pronk, A.G., Seaman, A.A., McCurdy, M., and Leybourne, M.I., 2017a. Indicator mineral and geochemical signatures associated with the Sisson W-Mo

deposit, New Brunswick, Canada. *Geochemistry: Exploration, Environment, Analysis*, online doi 10.1144/geochem2015-396.

McClenaghan, M.B., Parkhill, M.A., Pronk, A.G., and Sinclair, W.D., 2017b. Indicator mineral signatures of Sn-W deposits: examples from the Mount Pleasant Sn-W-Mo-Bi-In deposit, New Brunswick, Canada; *Journal of Geochemical Exploration*, v. 172, p. 151–166.

McClenaghan, M.B., Paulen, R.C., and Oviatt, N.M., in press. Geometry of indicator mineral and till geochemistry dispersal fans from the Pine Point Mississippi Valley-type Pb-Zn district, Northwest Territories, Canada; *Journal of Geochemical Exploration*.

McClenaghan, M.B., Paulen, R.C., Kjarsgaard, I.M., and Fortin, R., this volume. Indicator mineral signatures of the Strange Lake REE deposit, Quebec and Labrador, Canada, *In:* McClenaghan, M.B. and Layton-Matthews (conv.), *Workshop 5: Application of indicator mineral methods to bedrock sediments*. Exploration 2017.

Mircea, C., 2006. Kimberlite indicator mineral services offered by SRC Geoanalytical Laboratories; *EXPLORE, Newsletter of the Association of Applied Geochemists*, v. 133, p. 10–13.

Muggeridge, M.T., 1995. Pathfinder sampling techniques for locating primary source of diamond: recovery of indicator minerals, diamonds and geochemical signatures; *Journal Geochemical Exploration*, v. 53, p. 183–204.

Nadoll, P.N., Mauk, J.L., Leveille, R.A., and Koenig, A.E., 2015. Chemistry of magnetite from porphyry and skarn deposits in the southwestern United States; *Mineralium Deposita*, v. 50, p. 493–515.

Nowicki, T.E., Moore, R.O., Gurney, J.J., and Baumgartner, M.C., 2007. Diamonds and associated heavy minerals in kimberlite: a review of key concepts and applications; *Developments in Sedimentology*, v. 58, p. 1235–1267.

Oberthür, T., Melcher, F., and Sitnikova, M., 2010. Advances in the study of platinum mineralization by combining novel and classic mineralogical and geochemical methods, *In: 11th International Platinum Symposium*; Ontario Geological Survey, Miscellaneous Release –Data 269.

Paulen, R.C., Paradis, S., Plouffe, A., and Smith, I.R., 2011. Pb and S isotopic composition of indicator minerals in glacial sediments from northwest Alberta, Canada: implications for Zn-Pb base metal exploration; *Geochemistry: Exploration, Environment, Analysis*, v. 11, p. 309–320.

Peuraniemi, V., 1990. Chapter 10. Heavy minerals in glacial sediment, *In:* Kujansuu, R. and Saarnisto, M. (eds), *Glacial Indicator Tracing*; A.A. Balkema, Rotterdam, p. 165–185.

Plouffe, A., McClenaghan, M.B., Paulen, R.C., McMartin, I., Campbell, J.E., and Spirito, W.A., 2013. Processing of glacial sediments for the recovery of indicator minerals: protocols used at the Geological Survey of Canada; *Geochemistry: Exploration, Environment, Analysis*, v. 13, p. 303–316.

Plouffe, A., Ferbey, T., Hashmi. S., and Ward. B.C., 2016. Till geochemistry and mineralogy: vectoring towards Cu porphyry deposits in British Columbia, Canada; *Geochemistry: Exploration, Environment, Analysis*, 16, 213–232.

Ramsden, A.R., Griffin, W.L., and French, D.H., 1999. Application of resistate indicator mineralogy to metalliferous exploration: tourmaline, *In*: *Research Review*; CSIRO Exploration and Mining, p. 49–52.

Sarala, P. and Peuraniemi, V., 2007. Exploration using till geochemistry and heavy minerals in the ribbed moraine area of southern Finnish Lapland; *Geochemistry: Exploration, Environment, Analysis*, v. 7, p. 195–205.

Sarala, P., Pulkkinen, E., Juhani Ojala, V., and Peltoniemi-Taivalkoski, A., 2009. Gold exploration using till at Petäjälehto, northern Finland; *Geochemistry: Exploration, Environment, Analysis*, v. 9, p. 247–255.

Schulze, D.J., 1997. The significance of eclogite and Cr-poor megacryst garnets in diamond exploration; *Exploration and Mining Geology*, v. 6, p. 349–366.

Scott, K., 2003. Rutile geochemistry as a guide to mineralization at the Northparkes porphyry copper deposit, New South Wales, Australia, *In: Programme and Abstract*; International Geochemical Exploration Symposium, 2003 North Atlantic Minerals Symposium 2003, p. 44.

Silva, M., 1986. *Placer gold recovery methods*. California Department of Conservation, Division of Mines and Geology, Special Publication 87.

Sivamohan, R. and Forssberg, E., 1985. Principles of tabling. *International Journal of Mineral Processing*, v. 15, p. 281–295.

Spirito, W., McClenaghan, M.B., Plouffe, A., McMartin, I., Campbell, J.E., Paulen, R.C., Garrett, R.G., and Hall, G.E.M., 2011. *Till sampling and analytical protocols for GEM projects: from field to archive*; Geological Survey of Canada, Open File 6850.

Stendal, H. and Theobald, P.K., 1994. Heavy-mineral concentrates in geochemical exploration, *In:* Hale, M. and Plant, J.A. (eds), *Drainage Geochemistry*; Handbook of Exploration Geochemistry, v. 6, p. 185–225.

Stewart, R., 1986. Routine heavy mineral analysis using a concentrating table; *Journal of Sedimentary Research*, 56, 555–556.

Theobald, P.K., 1957. *The gold pan as a quantitative geologic tool*; United States Geological Survey, Bulletin 1071-A.

Theobald, P.K., Overstreet, W.C., and Thompson, C.E., 1967. *Minor elements in alluvial magnetite from the Inner Piedmont Belt, North and South Carolina;* United States Geological Survey, Professional Paper 554-A.

Towie, N.J. and Seet, L.H., 1995. Diamond laboratory techniques; *Journal of Geochemical Exploration*, v. 53, p. 205–212.

Wierchowiec, J., 2002. Morphology and chemistry of placer gold grains – indicators of the origin of the placers: an example from the East Sudetic Foreland, Poland; *Acta Geologica Polonica*, v. 52, p. 563–576.

Wilton, D.H.C. and Winter, L.S., 2012. *SEM-MLA (Scanning electron microscope- mineral liberation analyzer) research on indicator minerals in till and stream sediments - an example from the exploration for awaruite in Newfoundland and Labrador*; Mineralogical Association of Canada, Short Course 42, p. 265–284.

Wyatt, B.A., Baumgartner, M., Anckar, E., and Grütter, H., 2004. Compositional classification of kimberlitic and non-kimberlitic ilmenite; *Lithos*, v. 77, p. 819–840.

Zantop, H. and Nespereira, J., 1979. Heavy-mineral panning techniques in the exploration for tin and tungsten in NW Spain, *In:* Watterson, J.R. and Theobald, P.K. (eds), *Geochemical Exploration 1978*; Association of Exploration Geochemists, p. 329–336.

Zeschke, G., 1961. Prospecting for ore deposits by panning heavy minerals from river sands; *Economic Geology*, v. 56, p. 1250–1257.

Modern techniques and applications of mineral chemistry to exploration

D. Layton-Matthews[1*], C. Hamilton[2], and M.B. McClenaghan[3]

[1]Department of Geological Sciences, Queen's University, Kingston, Ontario, Canada K7L 3N6
[2]Systems for Research, #45, 155 Tycos Drive, Toronto, Ontario, Canada M6B 1W6
[3]Geological Survey of Canada, 601 Booth Street, Ottawa, Ontario, Canada K1A 0E8
*(*Corresponding author's e-mail: dlayton@queensu.ca)*

It is likely that undiscovered ore reserves are currently buried under recently deposited sedimentary cover. As such, our capacity to see through the complexities of this cover and to perceive the nature of the underlying bedrock ore environment has become a fundamental aspect of modern mineral exploration and ore deposit science. To date, the recognition of buried mineral deposits has been aided by our ability to (1) identify indicator minerals in bedrock sources, (2) identify and separate these same indicator minerals from sediment samples, and (3) measure the unique chemical and isotopic composition of these indicator minerals.

A substantial amount of research has been devoted to understanding the chemical and physical dispersal of minerals and elements at the Earth's surface and recognition of the dispersal patterns that are related to mineral deposits. The aerial and spatial extent of these footprint models has been partially limited by our incomplete understanding of the processes involved in physical and chemical dispersal, but moreover, by the technological challenges of detecting and measuring subtle mineral and chemical changes in these footprint sediments. Within mineral deposit footprints, the examination of the physical dispersal of relatively large (>63 μm) and heavy (>2.85 g/cm) minerals eroded from bedrock and transported during glaciation has met with great success. Many examples for different deposit types have now been published, including those for kimberlite (e.g. McClenaghan and Kjarsgaard, 2001, 2007; McClenaghan et al., 2002; Lehtonen et al., 2005;), porphyry Cu (e.g. Averill, 2011; Eppinger et al., 2011; Kelley et al., 2011; Plouffe et al., 2016), volcanogenic massive sulphide (VMS) (e.g. Averill, 2001; McClenaghan et al., 2012a,b, 2015a,b), granite-hosted Sn and W (McClenaghan et al., 2016, 2017a), Mississippi Valley-type Pb-Zn (Oviatt et al., 2015), magmatic Ni-Cu-PGE (Averill, 2011; McClenaghan et al., 2013), gold (e.g. Averill and Zimmerman, 1986; Sauerbrei et al., 1987; Averill, 2001, 2013, 2017; McClenaghan and Cabri, 2011), and more recently, rare earth elements (McClenaghan et al., this volume).

By using the abundance, size, shape, and chemistry of these indicator minerals, which have been separated from sediments using complex and expensive techniques (e.g. sieving, tabling, heavy liquids, magnetic separation, and hand-picking), the recognition of the spatial extent of the mineral deposit footprint has increased from 100s of metres to 1000s of metres. In this paper, we present an overview of the current methods and the applications of mineral chemistry using indicator minerals recovered from sediment cover. We also discuss new methods and instrumental developments, highlight current research on mineral chemistry, indicator minerals, and mineral exploration, and consider future research directions.

MINERAL IDENTIFICATION AND MINERAL CHEMISTRY

Indicator minerals, by definition, are minerals that have physical or chemical characteristics that allow them to be readily recovered from stream, alluvial, glacial, or aeolian sediments, or soils samples (Averill, 2001; McClenaghan, 2005, 2011; McClenaghan and Kjarsgaard, 2007). Traditionally, the identification and separation of indicator minerals relied on characteristics largely related to the minerals' chemistry, i.e., visual distinctiveness and moderate to high density.

Optical techniques

Indicator minerals are traditionally selected from heavy mineral concentrates (HMC) after the samples have undergone heavy mineral separation (see McClenaghan, 2011, this volume). Indicator minerals are "picked" from concentrates during an optical examination under a stereoscopic microscope, a process that may require up to 3 hours per sample. A few grains to several thousand grains may be separated into vials based on colour and mineral habit (Fig. 1). The production of high-quality HMCs, mineral identification, and mineral picking by experienced technicians are all vitally important in the first critical step of any indicator mineral chemical study.

Electron-based techniques

Once indicator minerals have been recovered, they are commonly epoxy-mounted, polished, and carbon-coated for examination using micro-analytical techniques (Fig. 2a,b). Most mineral chemical investigations examine these indicator mineral mounts using an

Figure 1. Examples of the colour and habit variations in kimberlite indicator minerals that can be observed using optical techniques (modified from McClenaghan and Paulen, in press): **a)** purple to pink Cr-pyrope; **b)** Cr-pyrope with dark green-grey kelyphite rims (k); **c)** Cr-diopside; **d)** eclogitic garnet; **e)** Mg-ilmenite; **f)** chromite showing resorbed crystal faces; **g)** forsteritic olivine; **h)** diamond. Mineral photography by Michael J. Bainbridge. Eclogitic garnet grains provided by Mineral Services; diamonds provided by Herb Helmstaedt, Queen's University. Figure from McClenaghan and Paulen (in press).

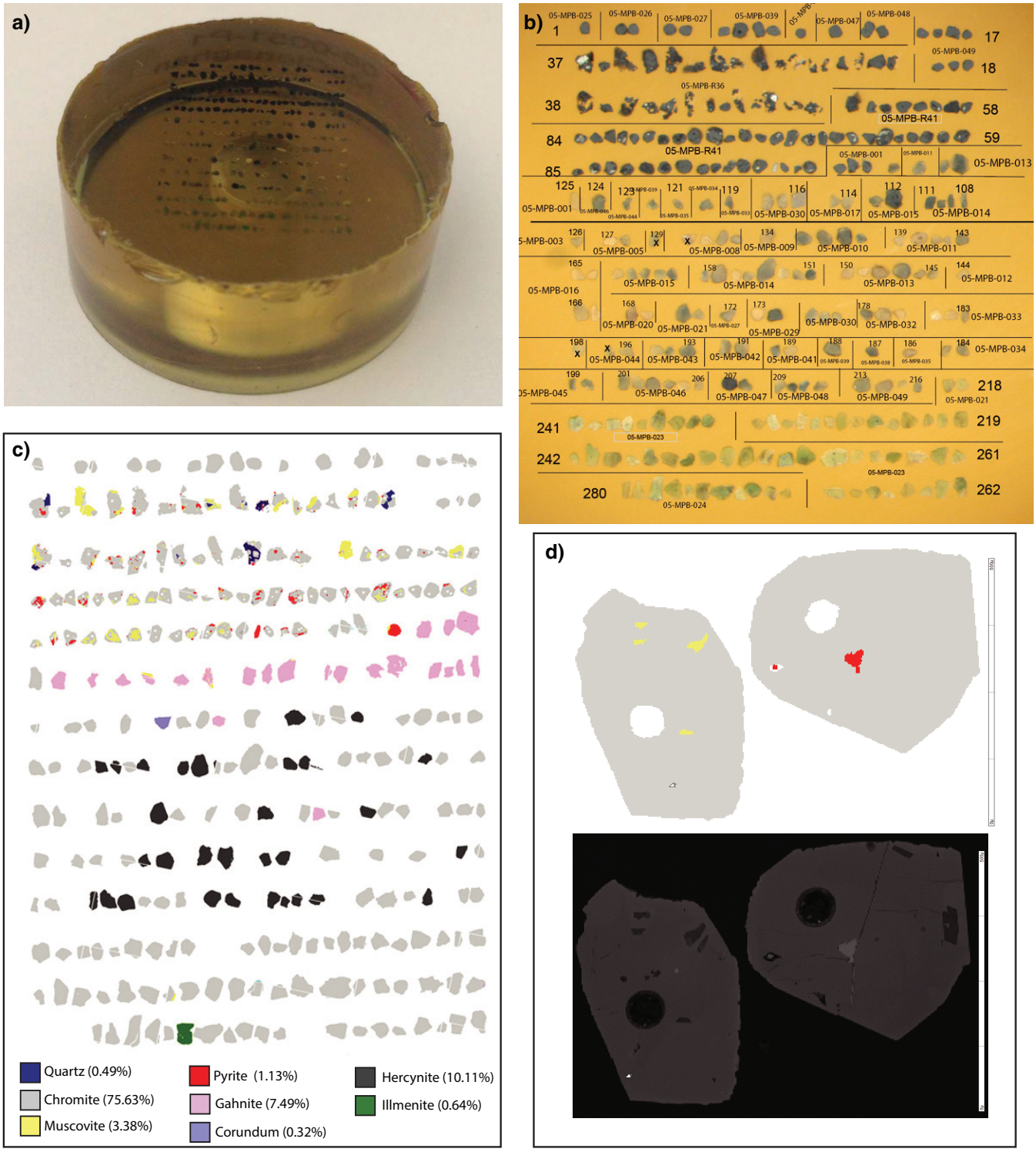

Figure 2. Example of the indicator mineral chemistry workflow from epoxy mount to laser ablation. **a)** Epoxy-mounted mineral grains after mineral separation. **b)** Optical stereo binocular photomicrograph. **c)** False-colour processed Mineral Liberation Analysis (MLA) image. **d)** MLA image of chromite (upper) and corresponding Backscatter secondary electron image (lower). Note the circular 50 micron laser ablations spots in each grain.

electron-based instrument. Traditionally, a scanning electron microscope (SEM) is used to examine the spatial distribution of backscatter secondary electrons (BSE), which is a reflection of differences in the average atomic number of an area of a grain. This scanning is done in combination with energy dispersive spectrometry (EDS) to identify relative element concentrations within mineral phases (Fig. 3) and mineralogy.

The goals of using an SEM are to (1) confirm of mineralogy that has been determined through visual

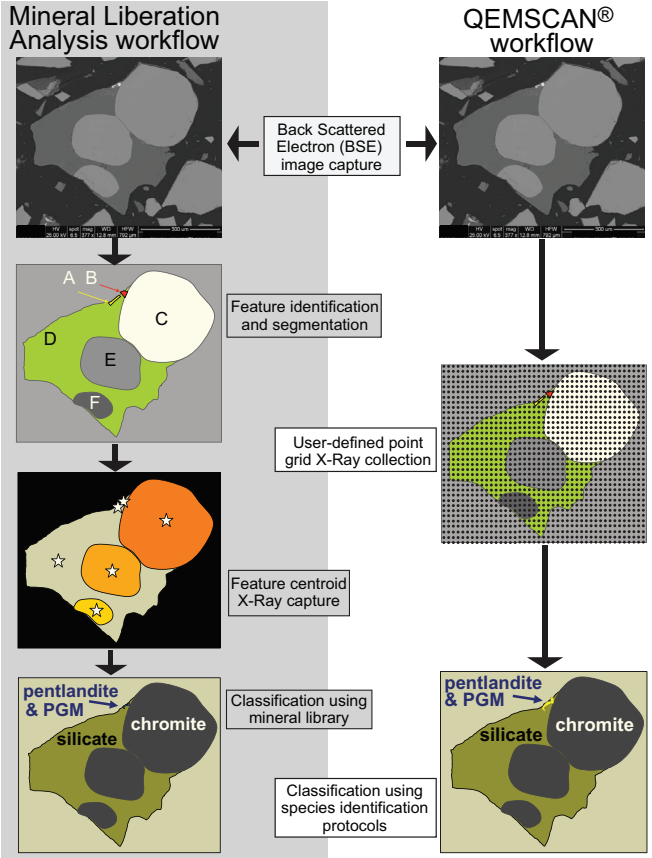

Figure 3. Comparison of the workflow of a sample when automated mineralogy using **(a)** Mineral Liberation Analysis (MLA) and **(b)** QEMSCAN® software.

mineral identification, (2) document mineral associations, (3) document mineral textures and morphology (shape, rounding, size, etc.), and (4) identify optimal mineral grains for further, more costly, mineral chemical characterization. The full characterization of a single epoxy mount with 200 to 500 grains can take 6 to 12 hours on a traditional SEM. Recent advances in automated scanning electron microscopy coupled with energy-dispersive X-Ray spectroscopy (EDS) are transforming the analysis of mineral grain mounts. Time-consuming and qualitative mineral descriptions are now been replaced with fast, quantitative, and repeatable SEM analyses. These automated SEM methods provide confirmation of mineralogy, quantification of mineral textures and morphology, and reduces grain mount analysis time to 1 to 2 hours.

The most popular automated SEM supplier is FEI; the company currently offers tungsten-based or field emission gun-based hardware that can be coupled with either QEMSCAN® or MLA software. Mineral Liberation Analysis (MLA) was initially developed for the mining industry by the University of Queensland, Australia (JKTech) (Burrows and Gu, 2006; Gu et al., 2012); QEMSCAN® was developed for the mining industry by CSIRO, Australia (Butcher et al., 2000; Gottlieb et al., 2000; Pirrie et al., 2004; Pirrie and Rollinson, 2009). However, both software packages are currently licensed and sold through FEI and their regional supply companies (e.g. Systems for Research, Canada).

MLA-automated mineralogy is based on high-resolution BSE images, image analyses, and elemental chemistry from EDS. Collections of BSE images are combined to create a mosaic image of an epoxy grain mount (Fig. 3). Each BSE image is used to remove epoxy from the image, and centroid image analysis segments grains and minerals into individual particles. The MLA software then collects a full X-ray spectrum (EDS) at the centre of each particle (Fig. 3). In post-collection processing, the full X-ray spectrum is compared with a user-defined mineral EDS library and the BSE image to create a coherent data set, which includes a false-colour mineral map (Fig. 2c), modal mineralogy, grain size, mineral associations (occurrence and interlocking), particle properties (roundness, area, shape), and mineral liberation.

QEMSCAN®-automated mineralogy is fundamentally different from MLA, in that is based on fast mineral identification using point analysis on a finely spaced grid. Like to MLA, QEMSCAN® collects BSE images to create a mosaic image of an epoxy grain mount; however, during automated measurement, the system collects EDS spectra along a pre-defined grid (similar to modal counting using a petrographic microscope). QEMSCAN® uses the EDS spectra in combination with the BSE image data to determine areas of epoxy and areas of mineral, minimizing the collection of background data. On scanning of mineral phases, a low-count EDS spectrum is collected that allows for ultra-fast discrimination of most minerals. QEMSCAN® also differs from MLA in the way that mineralogy is determined. In MLA, minerals are identified through comparison of unknown EDS with a user-defined EDS database of known minerals. In QEMSCAN®, a built-in library of 72 elemental reference spectra are used to build a composite elemental spectrum that is then used in conjunction with user-defined Species Identification Protocols (SIP) to identify discrete minerals. In addition to output data similar to MLA, QEMSCAN® produces elemental maps and mineral maps.

MLA- or QEMSCAN®-generated BSE and false-colour images of a mineral concentrate (Fig. 2c) have many advantages over traditional optical microscopy (Hartner et al., 2011; Gu et al., 2012; Sylvester, 2012; Mackay et al., 2016): 1) measurement of compositional data, 2) measurement of thousands of points per sample mount, 3) repeatable and quantitative measurements, 4) fully automated workflow, 5) faster processing time, 6) less training required, 7) modal mineralogy calculated assay data, 8) micron-scale resolution, 9) ability to measure and compare grain size, and 10) better determination of analysis points for texturally difficult

(i.e. polymineralic) grains and for choosing grains for *in situ* chemical or isotopic analyses.

The occurrence and modal quantification of distinct heavy minerals in till is of great importance in the definition of glacial dispersal trains in many ore exploration programs (i.e. gold); however, many HMC grain mounts are further characterized for individual mineral chemistry. Many indicator mineral studies (e.g. McClenaghan et al., 2002, 2013; Morris et al., 2002; Lehtonen et al., 2005, and references therein) have demonstrated the use of major and minor element mineral chemistry to identify the bedrock provenance and assess fertility.

The quantification of major elements can be obtained quickly for many elements from EDS software using a SEM with detection limits between 2000 and 10,000 ppm (Z>4). However, because EDS requires that individual X-Ray spectra be separated from other X-Ray spectra in a mineral analysis, some X-Ray energies cannot be separated from background radiation (high detection limit) or from X-Ray spectra of other elements (i.e. peak overlap). Most modern EDS detectors have an energy resolution of 130 to 160 eV (Full Width Half Max). For example, the quantitative analysis of molybdenite (MoS_2) by EDS is not possible because the Mo L alpha line is at 2.2930 keV and overlaps with the S K alpha line at 2.3070 keV.

More commonly, indicator minerals are analyzed for major and minor elements using electron probe microanalyzer (EPMA). In principle, an EPMA is very similar to a SEM, as the electron source and focusing column are nearly identical. However, an EPMA and a SEM collect X-Ray data differently. Both instruments collect chemical spectra using an EDS detector, but on an EPMA, spectra are also collected using wavelength dispersive spectroscopy (WDS). During the collection of WDS, spectra are separated by the mechanical diffraction of X-Rays into wavelengths that are individually measured by a detector. Most modern EPMA have up to 5 wavelength dispersive spectrometers that allow the simultaneous measurement of five elements. EDS and WDS each have advantages and disadvantages. EDS can quickly collect a full X-Ray spectrum in 10s of seconds; whereas WDS is time consuming, requiring the movement of a diffraction crystal to measure each individual element. Much of the spectral interference encountered during EDS can be eliminated by the high-energy resolution of WDS (~10 eV). The biggest disadvantage of both EDS and WDS systems are the detection limits (~0.1 and 0.01%, respectively) for most elements in the characterization of mineral chemistry.

Mass spectrometry-based techniques

The use of laser ablation inductively coupled plasma mass spectrometry (LA-ICP-MS) for characterization of mineral chemistry has grown since its first application to geological media (Hale et al., 1984; Jackson et al., 1992). Conceptually the application of laser ablation for mineral chemical and isotopic analyses is a straightforward, albeit destructive, technique. A short-pulsed (femto- to nanosecond) laser ablates a small volume (~8000 μm^3) of a mineral sample over a period of 10s of seconds. During ablation the mineral is converted into vapour and aerosol components. This material is then continually transferred in an Ar or He carrier gas to be ionized in an inductively coupled plasma and mass analyzed in either a quadrupole or magnetic-sector mass spectrometer.

There are several instrument parameters that must be optimized to measure element and isotopic compositions of a mineral by LA-ICP-MS (Arevalo et al., 2010; Rogers et al., 2010; Koch and Gunther, 2011); these include (1) laser pit-size, (2) laser wavelength, (3) laser pulse-rate, (4) mass spectrometer, (5) matrix-match standards, and (6) curve calibration. Most laser ablation instruments are capable of adjusting the laser beam size from 1–2 to 300 microns, however, most analyses are completed at ~30 microns (Fig. 2d). If a laser pit is too small, not enough material is ablated to create a suitable signal in the mass spectrometer. If a laser pit is too large, the mass spectrometer detector may become saturated or go beyond the element calibration curve.

Numerous studies have examined the analyses of geological media using variable laser wavelengths (Motelica-Hieno and Donard, 2001; Guillong et al., 2005; Jochum et al., 2007; Gaboardi and Humayun, 2009) and laser pulse-rates (Poitrasson et al., 2003; Gonzalez et al., 2007; Horn, 2008; Saetveit et al., 2008; Glaus et al., 2010), and collectively using similar laser energies. There is consensus that shorter wavelengths and higher laser pulse rates produce superior data that require fewer corrections for elemental and isotopic bias. In mineral analysis, a shorter wavelength laser (i.e. 193 nm vs 213 nm) produces a flat-bottomed and sharp-walled ablation pit. The higher pulse rate (i.e. femtosecond vs nanosecond) of the mineral, produces less thermal heating with a lower abundance of secondary condensates (Gunther and Heinrich, 1999; Gunther et al., 2000; Poitrasson et al., 2003; Hirata et al., 2004).

Ultimately, the ability of LA-ICP-MS to measure low-concentration elemental and isotopic data is a function of the mass spectrometer paired with the laser ablation system. There are three options for inductively coupled plasma mass spectrometers for use in laser ablation: 1) quadrupole, 2) high-resolution single collector, and 3) high-resolution multi-collector.

By far the most common mass spectrometer used in laser ablation studies of mineral chemistry is the quadrupole mass analyzer. These instruments filter

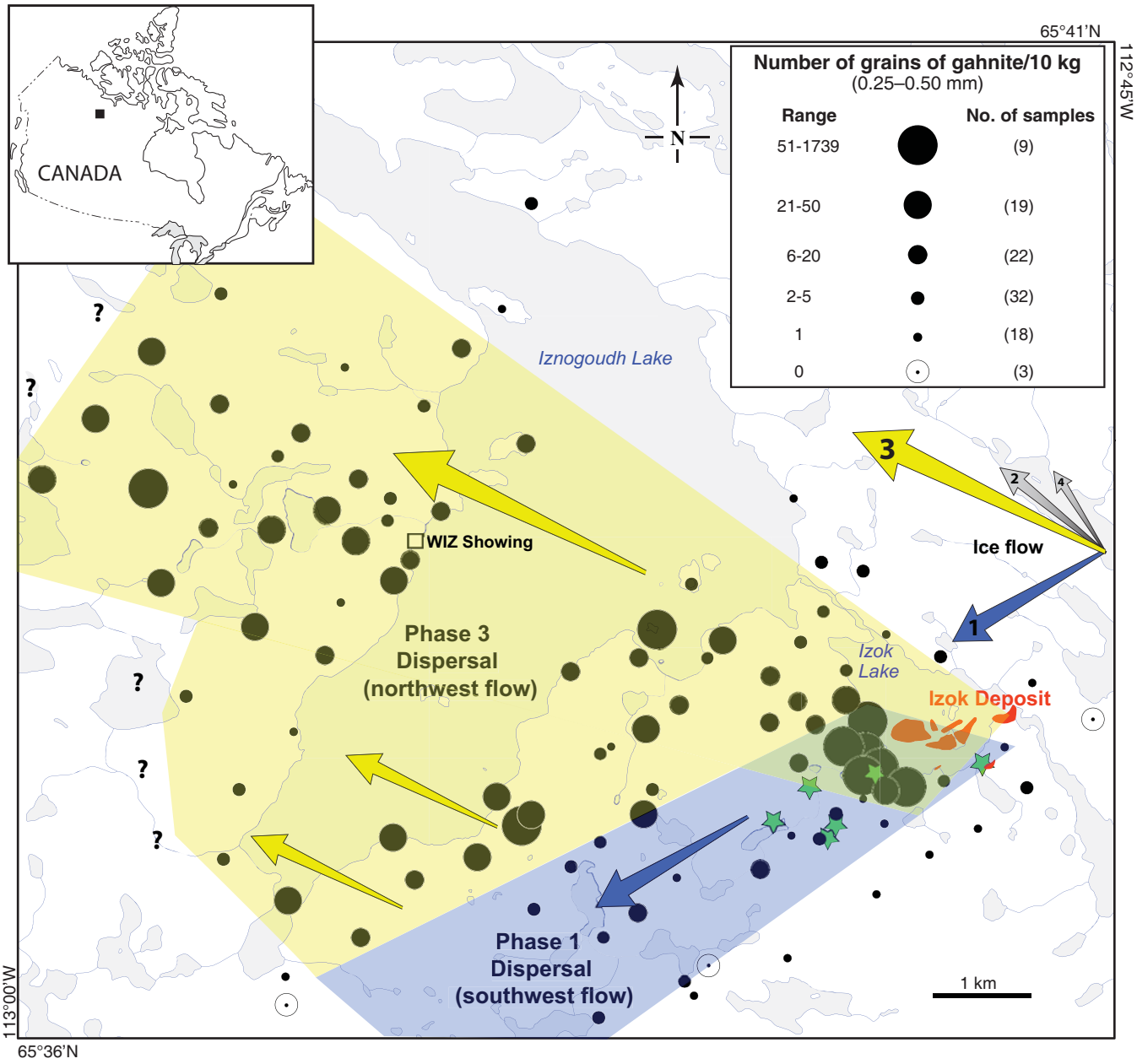

Figure 4. Fan-shaped glacial dispersal train of gahnite abundance in the 0.25–0.5 mm fraction of till (normalized to a 10 kg) down-ice of the Izok Lake volcanogenic massive sulphide deposit in northern Canada. The train fan formed by two phases of ice flow towards the southwest and northwest (modified from McClenaghan et al., 2015b). Arrows indicate relative ice-flow chronology (1 = oldest) and vigor (arrow size) of flow events. Blue-shaded polygon represents dispersal by the southwest (Phase 1) ice flow and yellow-shaded polygon represents dispersal by northwest (Phase 3) ice flows. Locations of gahnite-bearing rocks indicated by green stars and location of massive sulphide indicated by solid red polygons

ions created in the plasma by mass and charge (m/z) as they travel to the detector using variable DC voltages on four parallel stainless steel rods. By adjusting the DC voltage on the quadrupoles, the transient ions created in laser ablation can be filtered and analyzed for most elements on the periodic table in milliseconds (Hill, 2007).

In high-resolution mass spectrometers, ions created in laser ablation and in the inductively coupled plasma are passed along a curved flight path through magnetic and electrical fields to disperse ions according to their momentum and translational energy (Willard, 1988). By adjusting the magnetic and electrostatic fields, the transient ions arriving at the detector(s) can be varied on the basis of mass. Because of this geometry, the mass resolution of these instruments is superior to that of quadrupole instruments (e.g. ~10,000 versus ~600, respectively). As such, fractions of mass unit can be effectively separated during analysis, allowing for separation of polyatomic interferences (Hill, 2007).

For effective ion transmission through both the magnetic and electrical sectors, ions are accelerated at

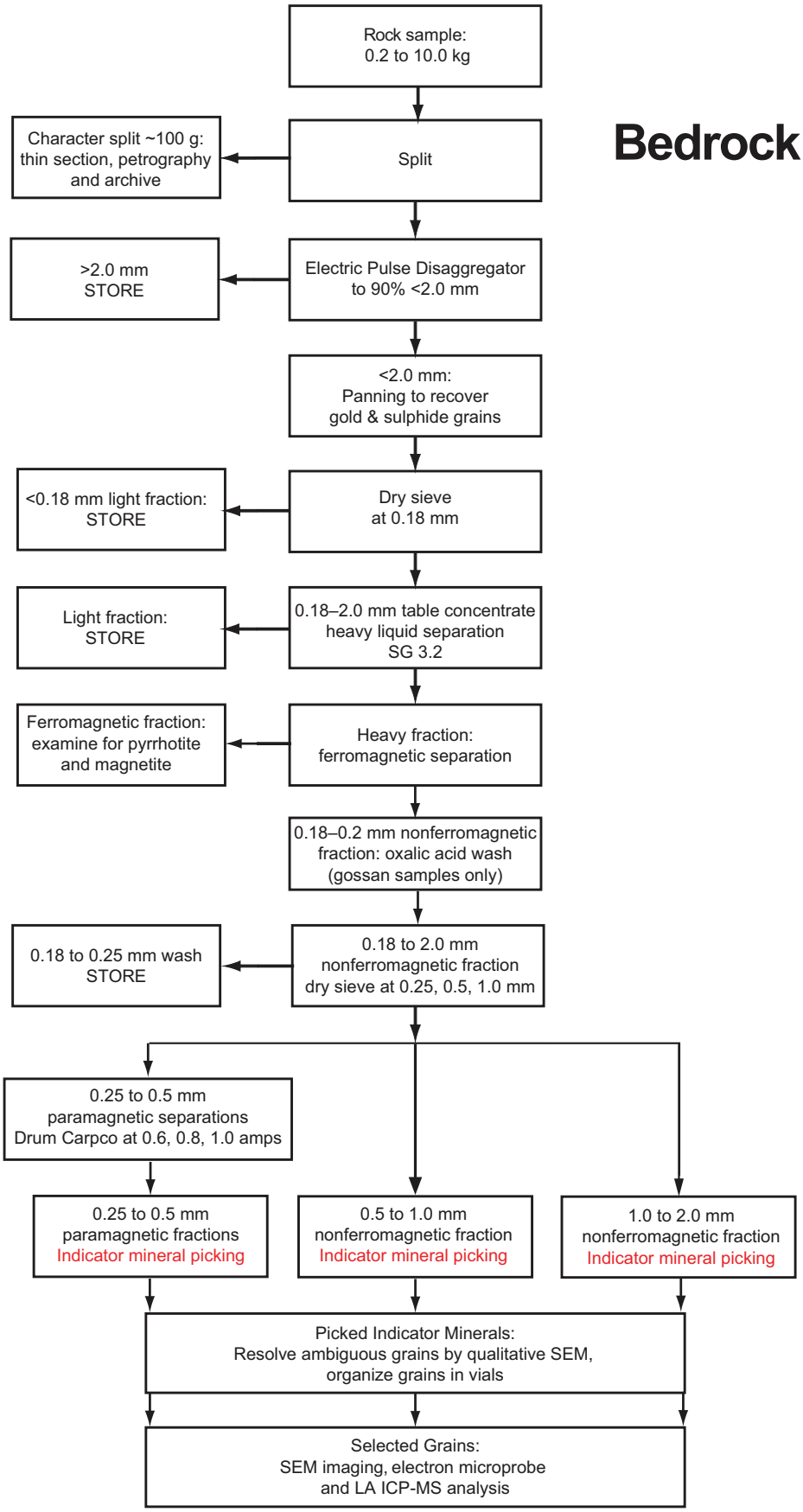

Figure 5. Flow sheet outlining the sample processing and picking procedure for bedrock samples processed from the Izok Lake deposit area (McClenaghan et al., 2012a).

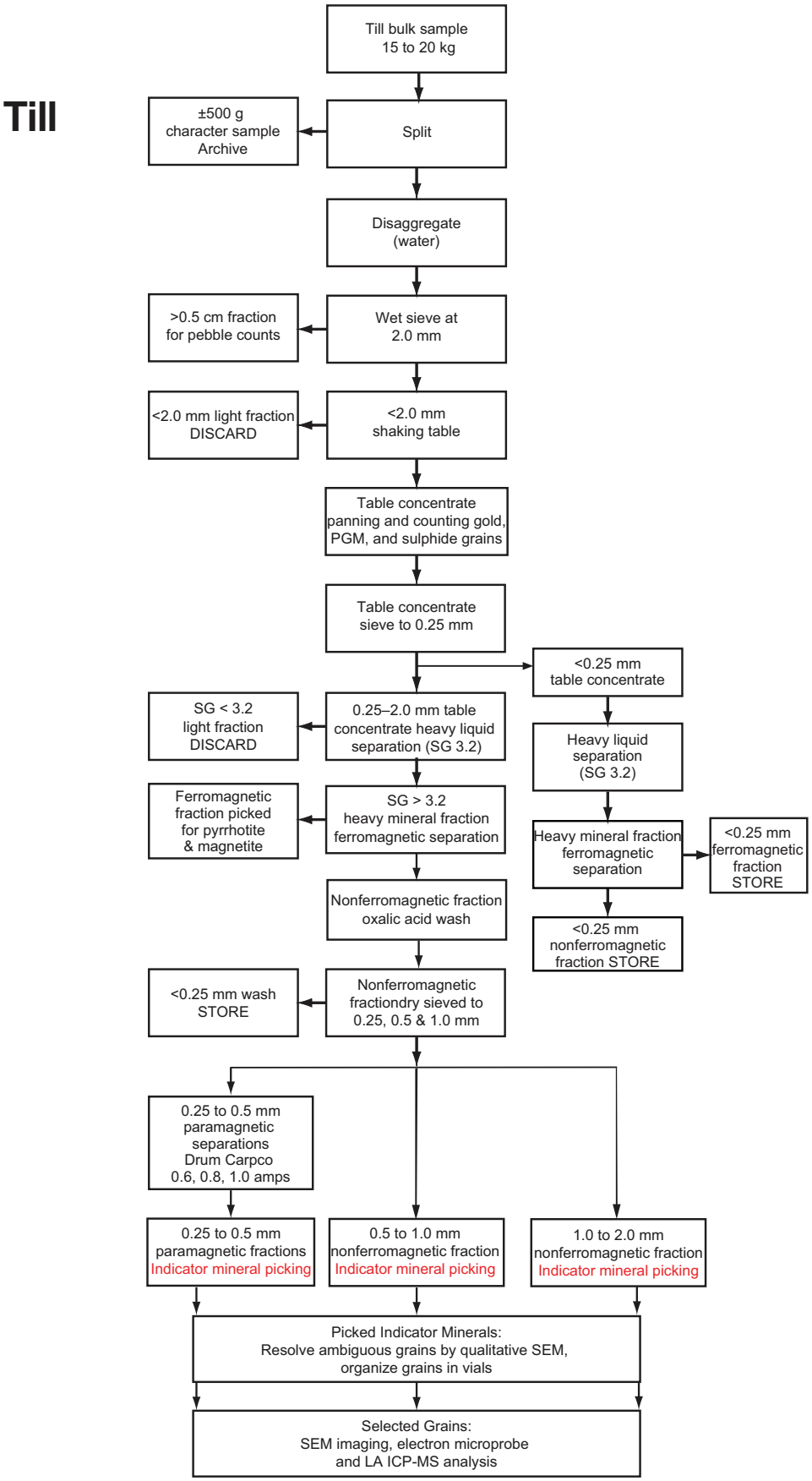

Figure 6. Flow sheet outlining the sample processing and picking procedure for till samples processed from the Izok Lake deposit area (McClenaghan et al., 2012a).

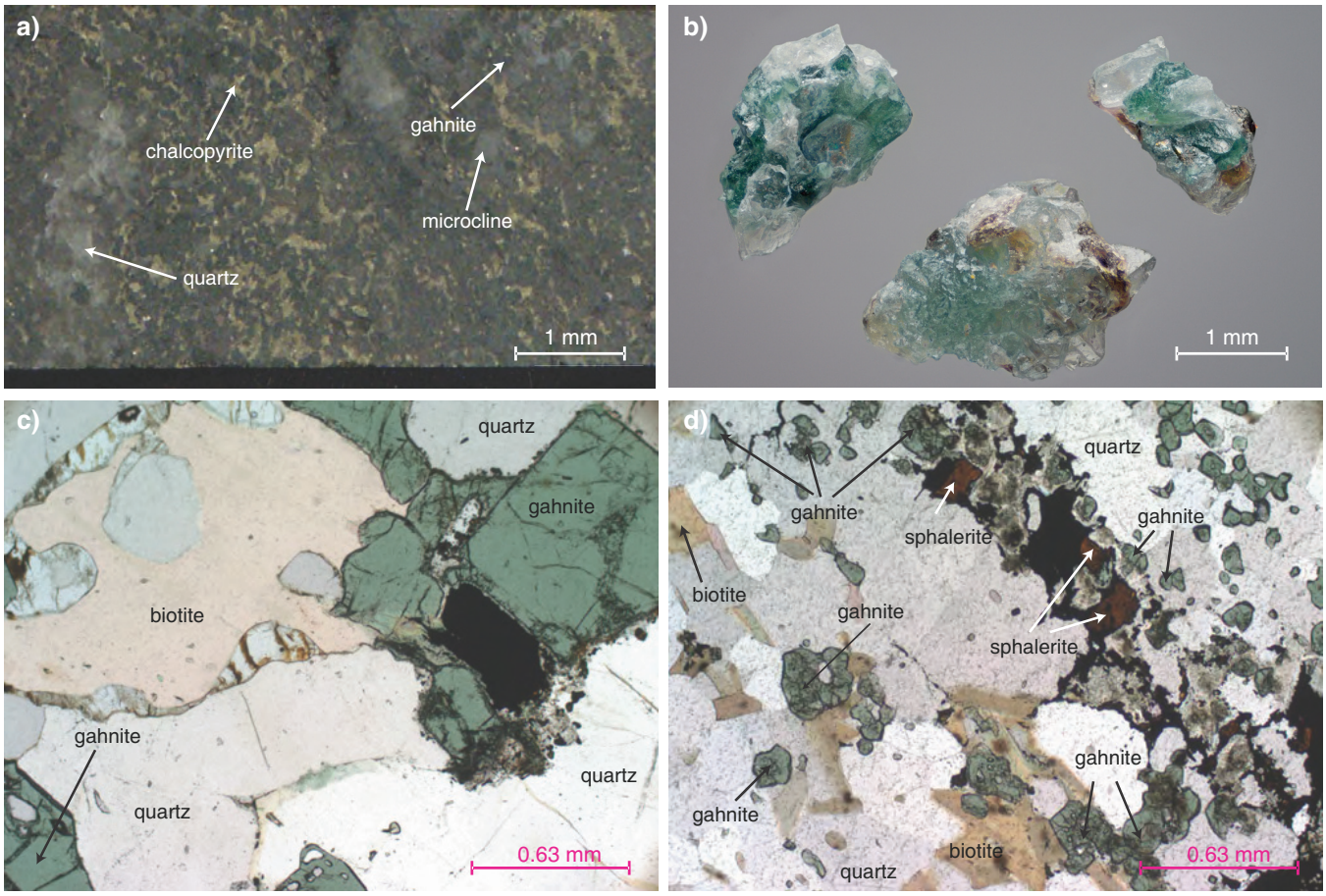

Figure 7. Gahnite **(a)** in a polished slab of drill core (sample 09-MPB-R69); **(b)** with adhering minerals in a till heavy mineral concentrate indicating proximity to the bedrock source (from McClenaghan and Paulen, in press); and **(c and d)** in polished thin sections (sample 09-MPB-R37 and 09-MPB-R41B, respectively).

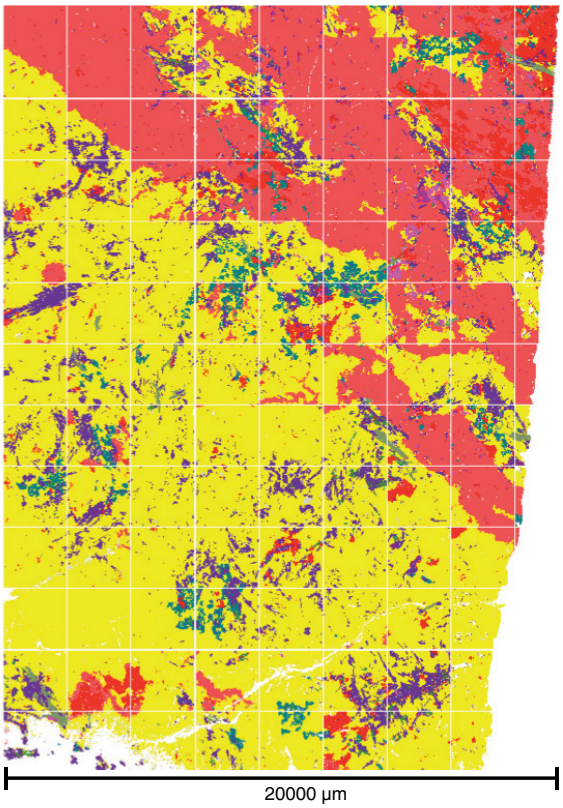

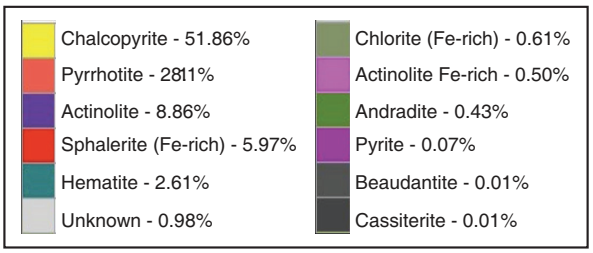

Figure 8. MLA image of 09-MPB-R60 (massive sulphide) from Izok Lake showing percentages of chalcopyrite, pyrrhotite, actinolite, sphalerite, hematite/magnetite, and trace minerals (Hicken, 2012).

Table 1. Comparison of sizes (mm) of key indicator minerals observed in polished thin sections, heavy mineral concentrates, and pan concentrates.

Mineral	Size Range in Polished Thin Section (mm)	Size Range in Heavy Mineral Concentrate (mm)	Size Range in Pan Concentrate (µm)
Pyrite	0.1–6	0.25–1.0	25–200
Chalcopyrite	0.1–5	0.25–1.0	15–200
Sphalerite	0.2–5	0.25–1.0	15–100
Galena	0.01–0.6	0.25–0.50	15–100
Gahnite	0.2–3.0	0.25–1.0	n/a
Staurolite	0.2–1.3	0.25–0.50	n/a
Axinite	0.4–2.0	0.25–0.50	n/a

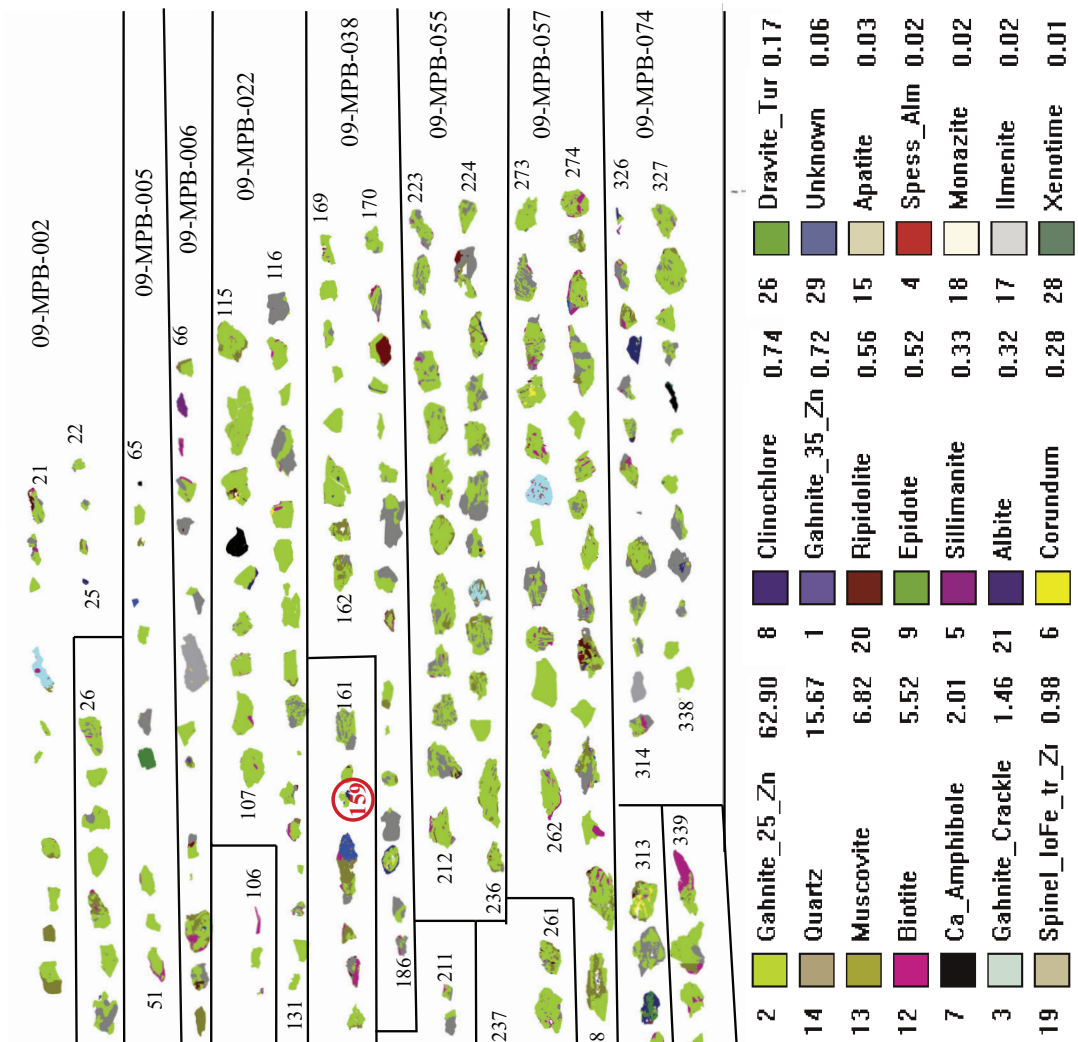

Figure 9. MLA image of 09-MPB-R60 (massive sulphide) from Izok Lake showing percentages of chalcopyrite, pyrrhotite, actinolite, sphalerite, hematite/magnetite, and trace minerals (Hicken, 2012).

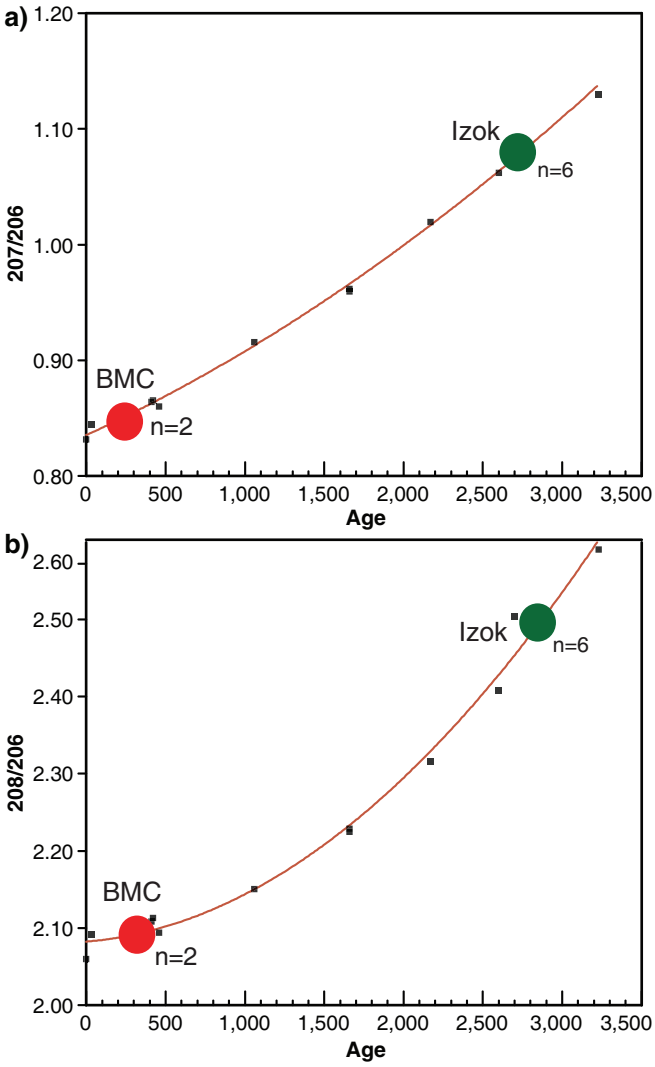

Figure 10. LA-ICP-MS quadrupole Pb isotopic ratios for gahnite. **a)** $^{207}Pb/^{206}Pb$ age relations for Izok Lake (green circles) and Halfmile Lake (Bathurst Mining Camp, New Brunswick: red circles); **b)** $^{208}Pb/^{206}Pb$ age relations for Izok Lake (green circles) and Halfmile Lake (Bathurst Mining Camp, New Brunswick: red circles). Red line is an approximation of terrestrial lead isotopic evolution (Stacey and Kramers, 1975). High-precision U/Pb ages for Halfmile Lake is 465 Ma (van Staal et al. 2003), for is Izok Lake is 2623 ± 20 Ma (Mortensen et al., 1988), and for Izok Lake is 2680.5 +7/-3 Ma (J. Gebert, unpub., 1995).

much higher energies than in quadrupole instruments (e.g. 10 kV versus 10 eV, respectively). As such, less ion scatter is created and lower detection limits are observed using high-resolution instruments. For many mineral chemical applications, a high-resolution mass spectrometer commonly has only one detector. However, in applications where isotopic ratios are measured, high-resolution instruments commonly have several detectors (known as multi-collector). These instruments can measure individual isotopes (i.e. ^{204}Pb, ^{206}Pb, ^{207}Pb, ^{208}Pb) simultaneously, without adjustment of the magnetic or electric sectors, which yields superior isotopic ratios.

Quadrupole and high-resolution mass spectrometers each have advantages and disadvantages in mineral chemical analyses using laser ablation. In quadrupole instruments, a wide range of elements (i.e. *m/z*) can be analyzed very quickly, compared to magnetic and electrical field sector instruments. In high-resolution instruments, the magnetic sector must be adjusted and allowed to stabilize before analyzing the next mass range (Giessmann and Greb, 1994; Jakubowski et al., 1998). Given the transient nature of laser ablation analysis, a quadrupole instrument is much better suited for mineral analyses of samples with varied element mass (i.e. rare earth elements, U, Pb). When there are narrow mass differences (<30%), very small laser ablation pits (<10 µm) or isotopic ratios are needed, for which high-resolution mass spectrometers offer vastly superior precision and detection limits.

Multi-element trace element analysis by LA-ICP-MS has not been universally adopted for mineral analysis because of the inadequate number of suitable reference materials with similar matrix compositions. Furthermore, there has been a limited effort to find or create matrix-matched standards with variable concentrations of trace elements (i.e. 10, 100, 500 ppm), which is necessary to create standard calibration curves and element quantification. Recently there have been several geological glasses that have been created from rock powder standards (Jochum et al., 2000, 2006, 2012; Jochum and Nohl, 2008) or by the doping of rock powder standards at variable concentrations (Guillong et al., 2005; Jochum et al., 2005; Kaiyun et al., 2013). The use of these standards in conjunction with EPMA data now allows the reliable quantification of many trace elements in minerals using LA-ICP-MS.

APPLICATIONS IN INDICATOR MINERAL STUDIES

During this workshop, several recent examples will outline the use of mineral chemistry in indicator mineral studies illustrating the methods described above. Due to brevity of an extended abstract, only one case study will be presented here.

In exploration for volcanogenic massive sulphide (VMS) deposits in northern Canada, an indicator mineral survey was completed around the Izok Lake Zn-Cu-Pb-Ag deposit (Fig. 4) in Nunavut, Canada (Hicken, 2012; Paulen et al., 2013; McClenaghan et al., 2015b). The direction of the ice flow rotated clockwise from southwest to northwest in a series of discrete ice-flow phases (Paulen et al., 2013). An early southwest ice flow was followed by strong west- to west-northwest-trending flow. Surface morphology and ice-flow indicators (e.g. striations) within the area reflect this dominant northwest phase (Paulen et al., 2013).

Field documentation of ice flow in the Izok Lake area was followed by till sampling up- and down-ice of the deposit (Fig. 4). Both bedrock and till samples were processed to recover HMCs (>3.2 g/cm^3 (Figs. 5, 6) from which the 0.25–0.5, 0.5–1.0, and 1.0–2.0 mm non-ferromagnetic heavy mineral fractions were examined using optical techniques (Fig. 7) and indicator minerals counted. Table 1 summarizes the size range of indicator minerals identified in bedrock and till. Thin sections and grain mounts were examined using MLA-ESEM (Figs. 8, 9) to quantify modal mineralogy, mineral associations, grain shape, and grain size. EPMA was completed on a selection of indicator minerals and LA-ICP-MS was conducted on gahnite (Zn-spinel) grains for trace elements and Pb/Pb dating (Fig. 10).

FUTURE DIRECTIONS IN MINERAL CHEMISTRY

Need for novel methods

The identification of discrete indicator minerals in till has greatly influenced mineral exploration. There are well established methods for separation and identification of minerals in HMC. Indicator mineral chemistry has been used to identify bedrock sources and assess their fertility. The question then becomes, "Why do we need new techniques in the application of mineral chemistry to indicator minerals?"

Successful mineral exploration using sediments and HMC requires a high degree of specialization. This type of work requires a person with not only a background in bedrock geology and ore deposits, but also a person with training in sample collection and preparation, mineralogy, analytical chemistry, and Quaternary geology. Current exploration models use a team approach, where each individual contributes their own area of expertise. At present, mineral separation methods have been well established for size-fractions larger than 0.063 mm, but these methods are slow, expensive, and require a highly qualified mineralogist.

New HMC and mineral chemical methods are currently being tested to utilize the smaller grain size (i.e. <0.25 mm) (e.g. Wilton and Winter, 2012; Lehtonen et al., 2015; Mackay et al., 2016) and less dense fractions (i.e. <2.85 g/cm^3) of sediments, and to incorporate new, faster, and more accessible analytical instruments (i.e. hyperspectral, MLA express). Development of these new methods will decrease the need for extensive specialized training, decrease the time and cost of HMC characterization, extend the spatial footprint of dispersal trains (i.e. smaller and farther), and ultimately lead to the identification of new indicator minerals in uncharacterized mineralized systems.

REFERENCES

Arevalo, R., Bellucci, J., and McDonough, W.F., 2010. GGR Biennial review: Advances in laser ablation and solution ICP-MS from 2008 to 2009 with particular emphasis on sensitivity enhancements, mitigation of fractionation effects and exploration of new applications; *Geostandards and Geoanalytical Research*, v. 34, p. 327–341.

Averill, S.A., 2001. The application of heavy indicator minerals in mineral exploration with emphasis on base metal indicators in glaciated metamorphic and plutonic terrain, *In:* McClenaghan, M.B., Bobrowsky, P.T., Hall, G.E.M., and Cook, S. (eds.) *Drift Exploration in Glaciated Terrain*; Geological Society of London, Special Volume 185, p. 69–82.

Averill, S.A., 2011. Viable indicator minerals in surficial sediments for two major base metal deposit types; Ni-Cu-PGE and porphyry Cu; *Geochemistry: Exploration, Environment, Analysis*, v. 11, p. 279–291.

Averill, S.A., 2013. Discovery and delineation of the Rainy River gold deposit using glacially dispersed gold grains sampled by deep overburden drilling; a 20 year odyssey, *In:* Paulen, R.C., and McClenaghan, M.B. (eds), *New Frontiers for Exploration in Glaciated Terrain*; Geological Survey of Canada, Open File 7374, p. 37–46.

Averill, S.A., 2017. The Blackwater gold-spessartine-pyrolusite dispersal train, British Columbia, Canada; Influence of sampling depth on indicator mineralogy and geochemistry; *Geochemistry: Exploration, Environment, Analysis*, v. 17, p. 43–60.

Averill, S.A., and Zimmerman, J.R., 1986. The riddle resolved: the discovery of the Partridge gold zone using sonic drilling in glacial overburden at Waddy Lake, Saskatchewan; *Canadian Geology Journal of the Canadian Institute of Mining and Metallurgy*, v. 1, p. 14–20.

Burrows, D., and Gu, Y., 2006. JKMRC mineral liberation analyser – a modern tool for ore characterisation and plant optimization, *In: Proceedings Metallurgical Plant Design and Operating Strategies 2006*. The Australasian Institute of Mining and Metallurgy: Melbourne, p. 125–139.

Butcher, A.R., Helms, T.A., Gottlieb, P., Bateman, R., Ellis, S., and Johnson, N.W., 2000. Advances in the quantification of gold deportment by QemSCAN, *In: Proceedings of 7th Mill Operators Conference, October 12–14, 2000, Kalgoorlie, Australia 2000*; Australasian Institute of Mining and Metallurgy, p. 267–271.

Eppinger, R.G., Kelley, K.D., Fey, D.L., Giles, S.A., and Smith, S.M., 2011. Exploration case study using indicator minerals in till at the giant Pebble porphyry Cu-Au-Mo deposit, southwest Alaska, USA; *Vuorimiesyhdistyksen Tutkimusseloste, Sarja B*, v. 92-4, p. 41–48.

Gaboardi, M., and Humayun, M., 2009. Elemental fractionation during LA-ICP-MS analysis of silicate glasses: implications for matrix-independent standardization; *Journal of Analytical Atomic Spectrometry*, v. 24, p. 1188–1197.

Giessmann, U., and Greb, U., 1994. High-resolution ICP-MS — a new concept for elemental mass-spectrometry; *Journal of Analytical Chemistry*, v. 350, p. 186–193.

Glaus, R., Kaegi, R., Krumeich, F., and Gunther, D., 2010. Phenomenological studies on structure and elemental composition of nanosecond and femtosecond laser-generated aerosols with implications on laser ablation inductively coupled plasma mass spectrometry; *Spectrochimica Acta Part B-Atomic Spectroscopy*, v. 65, p. 812–822.

Gonzalez, J.J., Liu, C.Y., Wen, S.B., Mao, X.L., and Russo, R.E., 2007. Metal particles produced by laser ablation for ICP-MS measurements; *Talanta*, v. 73, p. 567–576.

Gottlieb, P., Butcher, A.R., Tun, E.H., and Sutherland, D.N., 2000. Applications of automated process mineralogy, *In: Proceedings. International Congress on Applied Mineralogy*, v. 6, p. 321–323.

Gu, Y., Schouwstra, R., and Rule, C., 2012. The value of automated mineralogy, *In: Innovative Processing for Sustainable Growth.*

26th International Mineral Processing Congress, September 24–28 2012, New Delhi, India, p. 1726–1732.

Guillong, M., Hametner, K., Reusser, E., Wilson, S.A., and Guenther, D., 2005. Preliminary characterisation of new glass reference materials (GSA-1G, GSC-1G, GSD-1G and GSE-1G) by laser ablation-inductively coupled plasma-mass spectrometry using 193 nm, 213 nm and 266 nm wavelengths; *Geostandards and Geoanalytical Research*, v. 29, p. 315–331.

Gunther, D. and Heinrich, C.A., 1999. Comparison of the ablation behaviour of 266 nm Nd: YAG and 193 nm ArF excimer lasers for LA-ICP-MS analysis; *Journal of Analytical Atomic Spectrometry,* v. 14, p. 1369–1374.

Gunther, D., Horn, I., and Hattendorf, B., 2000. Recent trends and developments in laser ablation-ICP-mass spectrometry; *Fresenius Journal of Analytical Chemistry*, v. 368, p. 4–14.

Hale, M., Thompson, M., and Wheatley, M.R., 1984, Laser ablation of stream-sediment pebble coatings for simultaneous multi-element analysis in geochemical exploration; *Journal of Geochemical Exploration*, v. 21, p. 361–371.

Hartner, R., Walters, S.G., and Berry, R., 2011. Optical and SEM-based microscopy integration for optimisation of geometallurgical modelling and ore deposit characterisation. *In: Proceedings*; 1st AusIMM International Geometallurgy Conference 2011, GeoMet 2011, September 5–7 2011, Brisbane, p. 157–162.

Hicken, A., 2012, *Glacial Dispersal Of Indicator Minerals From The Izok Lake Zn-Cu-Pb-Ag Vms Deposit, Nunavut, Canada*; M.Sc. thesis, Queen's University, Kingston, Ontario.

Hill, S.J., 2007. *Inductively Coupled Plasma Spectrometry and its Applications*; Wiley-Blackwell.

Hirata, T., Asada, Y., Apinya, T., Ohno, T., Iizuka, T., Hayano, Y., Tanimizu, M., and Orihashi, Y., 2004. Improvements in the precision and accuracy of elemental and isotopic analyses of geochemical samples by a laser ablation-ICP-mass spectrometer; *Bunseki Kagaku*, v. 53, p. 491–501.

Horn, I., 2008. Comparison of femtosecond and nanosecond laser interactions with geologic matrices and their influence on accuracy and precision of LA-ICP-MS data; *Mineralogical Association of Canada*, Short Course 40, p. 53–65.

Jackson, S.E., Longerich, H.P., Dunning, G.R., and Fryer, B.J., 1992. The application of laser-ablation microprobe - inductively coupled plasma-mass spectrometry (LAM-ICP-MS) to in situ trace-element determinations in minerals; *The Canadian Mineralogist*, v. 30, p. 1049–1064.

Jakubowski, N., Moens, L., and Vanhaecke, F., 1998. Sector field mass spectrometers in ICP-MS; *Spectrochimica Acta Part B-Atomic Spectroscopy*, v. 53, p. 1739–1763.

Jochum, K.P., and Nohl, U., 2008, Reference materials in geochemistry and environmental research and the GeoReM database. *Chemical Geology*, v. 253, p. 50–53.

Jochum, K.P., Dingwell, D.B., Rocholl, A., Stoll, B., Hofmann, A.W., Becker, S., Besmehn, A., Bessette, D., Dietze, H. J., Dulski, P., Erzinger, J., Hellebrand, E., Hoppe, P., Horn, I., Janssens, K., Jenner, G. A., Klein, M., McDonough, W.F., Maetz, M., Mezger, K., Muenker, C., Nikogosian, I.K., Pickhardt, C., Raczek, I., Rhede, D., Seufert, H.M., Simakin, S.G., Sobolev, A.V., Spettel, B., Straub, S., Vincze, L., Wallianos, A., Weckwerth, G., Weyer, S., Wolf, D., and Zimmer, M., 2000. The preparation and preliminary characterisation of eight geological MPI-DING reference glasses for in-situ microanalysis; *Geostandards and Geoanalytical Research*, v. 24, p. 87–133.

Jochum, K.P., Willbold, M., Raczek, I., Stoll, B., and Herwig, K., 2005. Chemical characterisation of the USGS reference glasses GSA 1G, GSC-1G, GSD-1G, GSE-1G, BCR-2G, BHVO-2G and BIR-1G using EPMA, Id-Tims, ID-ICP-MS and LA-ICP-MS; *Geostandards and Geoanalytical Research*, v. 29, p. 285–302.

Jochum, K. P., Stoll, B., Herwig, K., Willbold, M., Hofmann, A. W., Amini, M., Aarburg, S., Abouchami, W., Hellebrand, E., Mocek, B., Raczek, I., Stracke, A., Alard, O., Bouman, C., Becker, S., Duecking, M., Braetz, H., Klemd, R., de Bruin, D., Canil, D., Cornell, D., de Hoog, C.-J., Dalpe, C., Danyushevsky, L., Eisenhauer, A., Gao, Y., Snow, J. E., Groschopf, N., Guenther, D., Latkoczy, C., Guillong, M., Hauri, E.H., Hoefer, H.E., Lahaye, Y., Horz, K., Jacob, D.E., Kasemann, S.A., Kent, A.J.R., Ludwig, T., Zack, T., Mason, P.R.D., Meixner, A., Rosner, M., Misawa, K., Nash, B.P., Pfaender, J., Premo, W.R., Sun, W.D., Tiepolo, M., Vannucci, R., Vennemann, T., Wayne, D., and Woodhead, J.D., 2006. MPI-DING reference glasses for in situ microanalysis; new reference values for element concentrations and isotope ratios; *Geochemistry: Geophysics, Geosystems*, v. 7, doi:10.1029/2005GC001060

Jochum, K.P., Stoll, B., Herwig, K., and Willbold, M., 2007. Validation of LA-ICP-MS trace element analysis of geological glasses using a new solid-state 193 nm Nd: YAG laser and matrix-matched calibration; *Journal of Analytical Atomic Spectrometry*, v. 22, p. 112–121.

Jochum, K.P., Nohl, U., Rothbarth, N., Schwager, B., Stoll, B., and Weis, U., 2012. Geostandards and geoanalytical research bibliographic review 2011; *Geostandards and Geoanalytical Research*, v. 36, p. 415–419.

Kaiyun, C., Honglin, Y., Zhian, B., Chunlei, Z., and Mengning, D., 2014. Precise and accurate in situ determination of lead isotope ratios in NIST, USGS, MPI-DING and CGSG glass reference materials using femtosecond laser ablation MC-ICP-MS; *Geostandards and Geoanalytical Research*, v. 38, p. 5–21.

Kelley, K.D., Eppinger, R.G., Lang, J., Smith, S.M., and Fey, D.L., 2011. Porphyry Cu indicator minerals in till as an exploration tool: example from the giant Pebble porphyry Cu-Au-Mo deposit, Alaska, USA; *Geochemistry: Exploration, Environment, Analysis*, v. 11, p. 321–334.

Koch, J., and Gunther, D., 2011. Review of the state-of-the-art of laser ablation inductively coupled plasma mass spectrometry; *Applied Spectroscopy*, v. 65, p. 155A–162A.

Lehtonen, M.L., Marmo, J.S., Nissinen, A.J., Johanson, B.S., and Pakkanen, L.K., 2005. Glacial dispersal studies using indicator minerals and till geochemistry around two eastern Finland kimberlites; *Journal of Geochemical Exploration*, v. 87, p. 19–43.

Lehtonen, M.L., Lahaye, Y., O'Brien, H., Lukkari, S. Marmo, J.S., and Sarala, P., 2015. Novel technologies for indicator mineral-based exploration; Geological Survey of Finland, Special Paper v. 57, p. 23–62.

Mackay, D.A.R., Simandl, G.J., Ma, W., Redfearn, J., and Gravel, J., 2016. Indicator mineral-based exploration for carbonatites and related specialty metal deposits – A QEMSCAN® orientation survey, British Columbia, Canada; *Journal of Geochemical Exploration*, v. 165, p. 159–173.

McClenaghan, M.B., 2005. Indicator mineral methods in mineral exploration; *Geochemistry: Exploration, Environment, Analysis*, v. 5, p. 233–245.

McClenaghan, M.B., 2011. Overview of common processing methods for recovery of indicator minerals from sediment and bedrock in mineral exploration; *Geochemistry: Exploration, Environment, Analysis*, v. 11, p. 265–278.

McClenaghan, M.B., 2017. Overview of indicator mineral recovery methods for sediments and bedrock: 2017 update, *In:* McClenaghan M.B., and Layton-Matthews, D. (conv.), *Application of Indicator Mineral Methods to Bedrock and Sediments*; Workshop 5, Exploration '17, Toronto, Ontario, October 22, 2017, p. 1–8.

McClenaghan, M.B., and Cabri, L.J., 2011. Gold and platinum group element indicator minerals in surficial sediments; *Geochemistry: Exploration, Environment, Analysis*, v. 11, p. 251–263.

McClenaghan, M.B. and Kjarsgaard, B.A., 2001. Indicator mineral and geochemical methods for diamond exploration in glaciated terrain in Canada, *In:* McClenaghan, M.B., Bobrowsky, P.T., Hall, G.E.M and Cook, S.J. (eds) *Drift Exploration in Glaciated Terrain*; Geological Society of London, Special Publication 185, p. 83–123.

McClenaghan, B. and Kjarsgaard, B.A., 2007. Indicator mineral and surficial geochemical exploration methods for kimberlite in glaciated terrain: examples from Canada, *In:* Goodfellow, W.D. (ed.) *Mineral Deposits of Canada: A Synthesis of Major Deposit Types, District Metallogeny, the Evolution of Geological Provinces, and Exploration Methods*; Geological Association of Canada, Mineral Deposits Division, Special Publication 5, p. 983–1006.

McClenaghan, M.B. and Paulen, R.C. in press. Mineral exploration in glaciated terrain, *In:* Menzies, J. and van der Meer, J.J-M. (eds) *Past Glacial Environments (Sediments, Forms and Techniques) A new and revised edition;* Elsevier.

McClenaghan, M.B., Ward, B.C., Kjarsgaard, I.M., Kjarsgaard, B.A., Kerr, D.E., and Dredge, L.A., 2002. Indicator mineral and till geochemical dispersal patterns associated with the Ranch Lake kimberlite, Lac de Gras region, NWT, Canada; *Geochemistry: Exploration, Environment, Analysis*, v. 2, p. 299–319.

McClenaghan, M.B., Hicken, A.K., Averill, S.A, Paulen, R.C., and Layton-Matthews, D., 2012a. *Indicator mineral abundance data for bedrock and till samples from the Izok Lake Zn-Cu-Pb-Ag volcanogenic massive sulphide deposit, Nunavut*; Geological Survey of Canada, Open File 7075.

McClenaghan, B., Budulan, G., Averill, S., Layton-Matthews, D., and Parkhill, M.A., 2012b. *Indicator mineral abundance data for bedrock and till samples from the Halfmile Lake Zn-Pb-Cu volcanogenic massive sulphide deposit, Bathurst Mining Camp, New Brunswick*; Geological Survey of Canada, Open File 7076.

McClenaghan, M.B., Kjarsgaard, I.M., Averill, S.A., Layton-Matthews, D., Crabtree, D., Matile, G., McMartin, I., and Pyne, M., 2013. *Indicator mineral signatures of magmatic Ni-Cu deposits, Thompson Nickel Belt, Manitoba part 2- till data*; Geological Survey of Canada, Open File 7200.

McClenaghan, M.B., Peter, J.M., and Layton-Matthews, D., 2015a. Overview of VMS exploration in glaciated terrain using indicator minerals, till geochemistry, and boulder tracing: A Canadian perspective, *In:* Peter, J.M. and Mercier-Langevin, P. (eds), *Targeted Geoscience Initiative 4 Contributions to the Understanding of Volcanogenic Massive Sulphide Genesis and Exploration Methods Development*; Geological Survey of Canada, Open File 7853, p. 81–100.

McClenaghan, M.B., Paulen, R.C., Layton-Matthews, D., Hicken, A.K., and Averill, S.A., 2015b. Glacial dispersal of gahnite from the Izok Lake Zn-Cu-Pb-Ag VMS deposit, northern Canada; *Geochemistry: Exploration, Environment, Analysis*, v. 15, p. 333–349.

McClenaghan, M.B., Parkhill, M.A., Pronk, A.G., and Sinclair, W.D., 2016. Indicator mineral and till geochemical signatures of the Mount Pleasant W-Mo-Bi and Sn-Zn-In deposits, New Brunswick, Canada; *Journal of Geochemical Exploration*, v. 172, p. 151–166.

McClenaghan, M.B., Parkhill, M.A., Pronk, A.G., Seaman, A.A., McCurdy, M., and Leybourne, M.I., 2017a. Indicator mineral and geochemical signatures associated with the Sisson W-Mo deposit, New Brunswick, Canada; *Geochemistry: Exploration, Environment, Analysis*. doi:10.1144/geochem2015-396

McClenaghan, M.B., Paulen, R.C., Kjarsgaard, I.M., and Fortin, R., 2017b. Rare earth element indicator minerals: an example from the Strange Lake deposit, Quebec and Labrador, eastern Canada, *In:* McClenaghan M.B., and Layton-Matthews, D. (conv.), *Application of Indicator Mineral Methods to Bedrock and Sediments*; Workshop 5, Exploration '17, Toronto, Ontario, October 22, 2017, p. 75–82.

Morris, T.F., Sage, R.P. Ayer, J.A., and Crabtree, D.C., 2002. A study in clinopyroxene composition: implications for kimberlite exploration; *Geochemistry: Exploration, Environment, Analysis*, v. 2, p. 321–331.

Mortensen, J.K., Thorpe, R.I., Padgham, W.A., King, J.E., and Davis, W.J., 1988. U-Pb zircon ages for felsic volcanism in Slave Province, N.W.T., *In: Radiogenic Age and Isotopic Studies: Report 2*; Geological Survey of Canada, Paper 88-2, p. 85–95.

Motelica-Hieno, M. and Donard, O.F.X., 2001. Comparison of UV and IR laser ablation ICP-MS on silicate reference materials and implementation of normalisation factors for quantitative measurements; *Geostandards Newsletter-the Journal of Geostandards and Geoanalysis*, v. 25, p. 345–359.

Oviatt, N.M., Gleeson, S.A., Paulen, R.C., McClenaghan, M.B., and Paradis, S., 2015. Characterization and dispersal of indicator minerals associated with the Pine Point Mississippi Valley-type (MVT) district, Northwest Territories, Canada; *Canadian Journal of Earth Sciences*, v. 52, p. 776–794.

Paulen, R.C., McClenaghan, B., and Hicken, A.K., 2013. Regional and local ice-flow history in the vicinity of the Izok Lake Zn-Cu-Pb-Ag deposit, Nunavut; *Canadian Journal of Earth Sciences*, v. 50, p. 1209–1222.

Pirrie, D. and Rollinson, G., 2009. Use of automated mineral analysis using QEMSCAN® in the characterisation of mine tailings; *Applied Earth Science*, v. 118, p. 32.

Pirrie, D., Butcher, A.R., Power, M.R., Gottlieb, P., and Miller, G.L., 2004. Rapid quantitative mineral and phase analysis using automated scanning electron microscopy (QEMSCAN®); potential applications in forensic geoscience, *In:* Pye, K., and Croft, D.J. (eds), *Forensic Geoscience, Principles, Techniques and Applications*; Geological Society, Special Publication 232, p. 123–136.

Plouffe, A., Ferbey, T., Hashmi. S., and Ward, B.C., 2016. Till geochemistry and mineralogy: vectoring towards Cu porphyry deposits in British Columbia, Canada; *Geochemistry: Exploration, Environment, Analysis*, v. 16, p. 213–232.

Poitrasson, F., Mao, X.L., Mao, S.S., Freydier, R., and Russo, R.E., 2003. Comparison of ultraviolet femtosecond and nanosecond laser ablation inductively coupled plasma mass spectrometry analysis in glass, monazite, and zircon; *Analytical Chemistry*, v. 75, p. 6184–6190.

Rogers, R.R., Fricke, H.C., Addona, V., Canavan, R.R., Dwyer, C.N., Harwood, C.L., Koenig, A.E., Murray, R., Thole, J.T., and Williams, J., 2010. Using laser ablation-inductively coupled plasma-mass spectrometry (LA-ICP-MS) to explore geochemical taphonomy of vertebrate fossils in the upper cretaceous two medicine and Judith River formations of Montana; *Palaios*, v. 25, p. 183–195.

Saetveit, N.J., Bajic, S.J., Baldwin, D.P., and Houk, R.S., 2008. Influence of particle size on fractionation with nanosecond and femtosecond laser ablation in brass by online differential mobility analysis and inductively coupled plasma mass spectrometry; *Journal of Analytical Atomic Spectrometry*, v. 23, p. 54–61.

Sauerbrei, J.A., Pattison, E.F., and Averill, S.A., 1987. Till sampling in the Casa-Berardi gold area, Quebec: a case history in orientation and discovery (Canada); *Journal of Geochemical Exploration*, v. 28, p. 297–314.

Stacey, J.S. and Kramers, J.D., 1975, Approximation of terrestrial lead isotope evolution by a two-stage model; *Earth Planet. Science Letters*, v. 26, p. 207–221.

Sylvester, P.J., 2012. Use of the mineral liberation analyzer (MLA) for mineralogical studies of sediments and sedimentary rocks, *In:* Sylvester, P.J. (ed.), *Quantitative Mineralogy and Microanalysis of Sediments and Sedimentary Rocks*; Mineralogical Association of Canada, Short Course 42, p. 1–16.

van Staal, C.R., Wilson, R.A., Rogers, N., Fyffe, L.R., Langton, J.P., McCutcheon, S.R., McNicoll, V., and Ravenhurst, C.E., 2003. Geology and tectonic history of the Bathurst Supergroup, Bathurst mining camp, and its relationships to coeval rocks in southwestern New Brunswick and adjacent mine; a synthesis. *In:* Goodfellow, W.D., McCutcheon, S.R., and Peter, J.M. (eds.) *Massive Sulfide Deposits of the Bathurst Mining Camp, New Brunswick, and Northern Maine*; Economic Geology, Monograph v. 11, p. 37–60.

Willard, H.H., 1988, *Instrumental Methods of Analysis*. Wadsworth Publishing Company, 895 p.

Wilton, D.H.C. and Winter, L.S., 2012. SEM-MLA (Scanning electron microscope- mineral liberation analyzer) research on indicator minerals in till and stream sediments - an example from the exploration for awaruite in Newfoundland and Labrador, Chapter 14 *In:* Sylvester, P. (ed.), *Quantitative Mineralogy and Microanalysis of Sediments and Sedimentary Rock;* Mineralogical Association of Canada, Short Course 42, p. 265–284.

Trace element chemistry of indicator silicates and oxides as vectors to metamorphosed sediment-hosted Pb-Zn-Ag and Cu-Au deposits in the Cambrian Kanmantoo Group, South Australia

P.G. Spry[1*], M.V. Pollock[1], K.A. Tott[1], A.E. Koenig[2], R.A. Both[3], and J.A. Ogierman[4]

[1]Department of Geological and Atmospheric Sciences, 253 Science I, 2237 Osborn Drive, Iowa State University, Ames, Iowa 50011-3212, U.S.A.

[2]U.S. Geological Survey, Denver Federal Center, Denver, Colorado 80225, U.S.A.

[3]23 Windsor Street, Fullarton, South Australia 5063, Australia

[4]Robust Resources, Level 2, 179 Grey Street, South Bank, Queensland 4101, Australia

*(*Corresponding author's e-mail: pgspry@iastate.edu)*

The presence of resistate indicator minerals (e.g. garnet, gahnite, magnetite, Cr diopside, ilmenite, olivine, and gold) in surficial sediments (e.g. glacial, eolian, stream, alluvial, beach, and residual soils) and bedrock have been used to explore for various types of mineral deposits, including porphyry Cu, lode gold, magmatic Ni-Cu-PGE, metamorphosed volcanogenic massive sulphide (VMS), rare metals, and iron oxide-copper-gold (IOCG) (Averill, 2001, 2007; McClenaghan, 2005, 2013). Optical- and electron- (e.g. scanning electron microscope coupled with QEMSCAN® or MLA™ software, electron microprobe analysis (EMPA), and mass spectrometry (e.g. laser ablation-inductively coupled plasma-mass spectrometry (LA-ICP-MS)) based techniques are used to identify indicator minerals, with EMPA and LA-ICP-MS techniques being able to determine their major and trace element compositions (e.g. Layton-Matthews et al., 2013). Laser ablation-inductively coupled plasma-mass spectrometry allows for the measurement of many elements at concentrations as low as parts per billion (e.g. Jackson et al., 1992).

In the past, individual studies using trace elements to vector to mineral deposits have generally only included one or two minerals (e.g. hematite and magnetite (Schmidt Mumm et al., 2012)); however, there are exceptions. Ismail et al. (2014) analyzed multiple minerals (feldspar, calcite, garnet, pyroxene, amphibole, allanite, epidote-group minerals, titanite, and apatite) in a study of the Hillside IOCG deposit, South Australia. In addition, Spry et al. (2015) analyzed garnet, biotite, and magnetite in the metamorphosed Stollberg Zn-Pb-Ag and magnetite field, Sweden. Trace element studies have been utilized to explore for metamorphosed massive sulphide deposits, including tourmaline (Griffin et al., 1996), sulphide minerals (George et al., 2016), garnet (Spry et al., 2007; Heimann et al., 2011), and gahnite (O'Brien et al., 2015a,b). However, these studies focused mostly on minerals spatially associated with Broken Hill-type Pb-Zn-Ag (BHT) deposits. By contrast, there are relatively few trace element studies of minerals associated with metamorphosed VMS and sedimentary-exhalative deposits, two of which were done by Makvandi et al. (2016a,b) for magnetite in various metamorphosed VMS deposits. Here, we have analyzed the trace and major element compositions of common rock-forming silicates (garnet, biotite, staurolite, chlorite, and muscovite) and oxides (gahnite, ilmenite, and magnetite) in sediment-hosted massive sulphide Cu-Au (Kanmantoo, South Australia) and Pb-Zn-Ag deposits (Wheal Ellen, Angas, Scotts Creek, Aclare, Strathalbyn, and St. Ives, South Australia), which were metamorphosed to amphibolite facies. Minerals were analyzed by EMP and LA-ICP-MS methods, the details of which are given in O'Brien et al. (2015a) and are not repeated here. The aim of study is to evaluate the use of trace elements of multiple minerals to guide exploration in the Kanmantoo area and metamorphosed sediment-hosted sulphide deposits, in general.

GEOLOGICAL SETTING

The Cu-Au and Pb-Zn-Ag deposits occur in a structurally thickened package (~7–8 km) of metamorphosed pelitic and psammitic (including metaturbidite) sediments of the Cambrian Kanmantoo Group, South Australia, within an extensional fault-controlled back-arc basin (Kanmantoo Trough). Up to five deformation events have affected the deposits, with peak metamorphic conditions (amphibolite facies) coinciding with the second deformation event (e.g. Spry et al., 1988). The Cu-Au and Pb-Zn-Ag deposits occur in the Tapanappa Formation, primarily in a stratigraphic interval, several hundred metres wide, in garnet-andalusite-biotite±staurolite schist that we consider to be a regional, stratabound, metamorphosed hydrothermal alteration zone. This zone extends intermittently for more than 30 km, from about 10 km north of Kanmantoo toward Strathalbyn, and has been, in the past, a major focus of exploration for base metal sulphides in the Kanmantoo Group (Fig. 1).

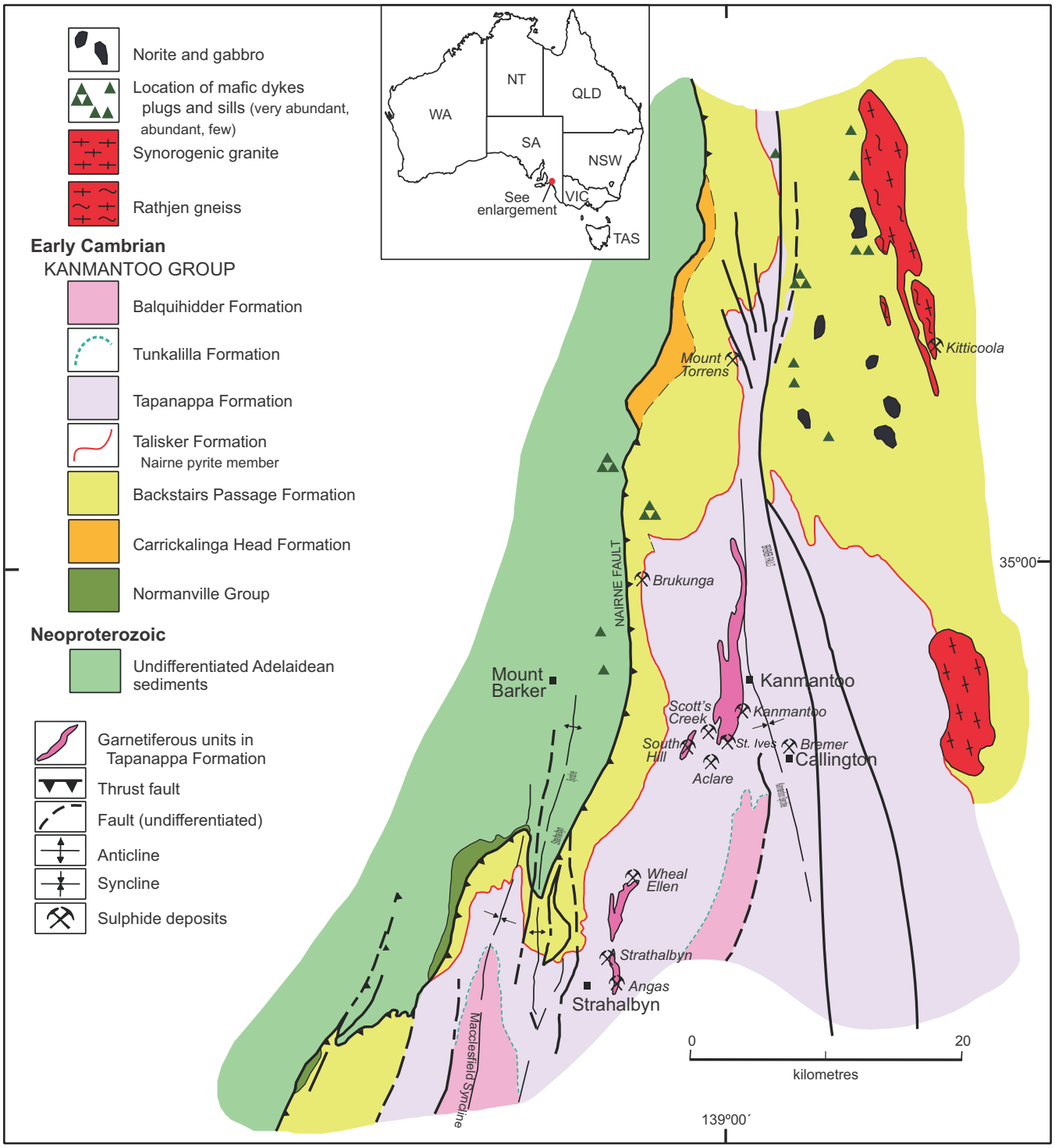

Figure 1. Geological map of the Kanmantoo region showing the location of Cu-Au and Pb-Zn-Ag deposits in the Kanmantoo Group, South Australia (modified after Toteff, 1999).

Rock types associated with sulphide mineralisation include quartz-mica schist, quartz-biotite-garnet-andalusite±chlorite± staurolite±magnetite rock, and biotite-garnet-chlorite rock, the last of which is the immediate host for much of the sulphides. Minor rock types include exhalite (e.g. quartz garnetite, garnet-quartz-cummingtonite schist, plagioclase rock, banded iron formation: Toteff, 1999), gahnite-bearing mica schist, pyritic schist, and calc-silicate rocks. The Kanmantoo Cu-Au deposit (34.5 Mt @ 0.6% Cu and 0.1 g/t Au; http://www.hillgroveresources.com.au/section/Projects/Kanmantoo), which is the largest Cu-Au deposit in the Kanmantoo Group, is characterized by discordant and pipe-like orebodies (e.g. Kavanagh, Spitfire, and Emily), and concordant mineralisation (Nugent). The Pb-Zn-Ag deposits are mostly concor-

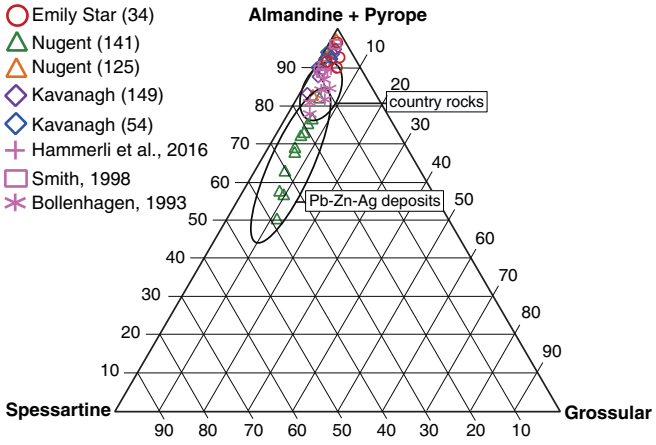

Figure 2. Ternary plot of garnet compositions from the Kanmantoo deposit (Emily Star, Kavanagh, and Nugent orebodies) and country rock schist (Bollenhagen, 1993; Smith, 1998; Hammerli et al., 2016) shown by an ellipse. The compositional field of garnet associated with Pb-Zn-Ag deposits is shown as a separate ellipse.

dant to bedding, with both Cu-Au and Pb-Zn-Ag types exhibiting local remobilization of sulphides. The discovery of gahnite- and spessartine garnet-bearing rocks were key to finding the Angas Pb-Zn-Ag deposit (3.04 Mt @ 8.0% Zn, 3.1% Pb, 0.3% Cu, 34 g/t Ag, and 0.5 g/t Au; http://www.portergeo.com.au/database/mineinfo.asp?mineid=mn1287), the largest known Pb-Zn-Ag occurrence in the Kanmantoo Group. The metallic minerals of the Cu-Au deposits consist mostly of chalcopyrite, pyrrhotite, magnetite, Bi minerals, and pyrite, whereas those associated with Pb-Zn-Ag deposits are primarily sphalerite, pyrite, galena, chalcopyrite, pyrrhotite, and cobaltian arsenopyrite. A zone of chalcopyrite-magnetite-rich rocks at the Wheal Ellen Pb-Zn-Ag deposit, which shows a metallic mineral assemblage almost identical to the most common assemblage at Kanmantoo, suggests a genetic link between the Pb-Zn-Ag deposits and Cu-Au mineralisation. The presence of both Cu and Pb-Zn-Ag zones at the Strathalbyn deposit also supports this concept.

MINERAL CHEMISTRY

Garnet

Although Fe-rich (Mn-poor) garnet is common in most orebodies at Kanmantoo (2–4 wt% MnO), country rock mica schists and unmineralized altered rocks in the Kanmantoo Group contain slightly higher concentrations of Mn (~3–7 wt% MnO) (Bollenhagen, 1993; Smith1998; Hammerli et al., 2016), whereas the composition of garnet is more Mn-rich in and proximal to Pb-Zn-Ag mineralisation (up to 30 wt% MnO), and the concordant Nugent orebody (up to 18 wt% MnO) at Kanmantoo (Fig. 2). Furthermore, the Zn concentration of garnet associated with Pb-Zn-Ag mineralisation is high (100–252 ppm Zn) relative to that spatially associated with the Kanmantoo Cu-Au deposit and the

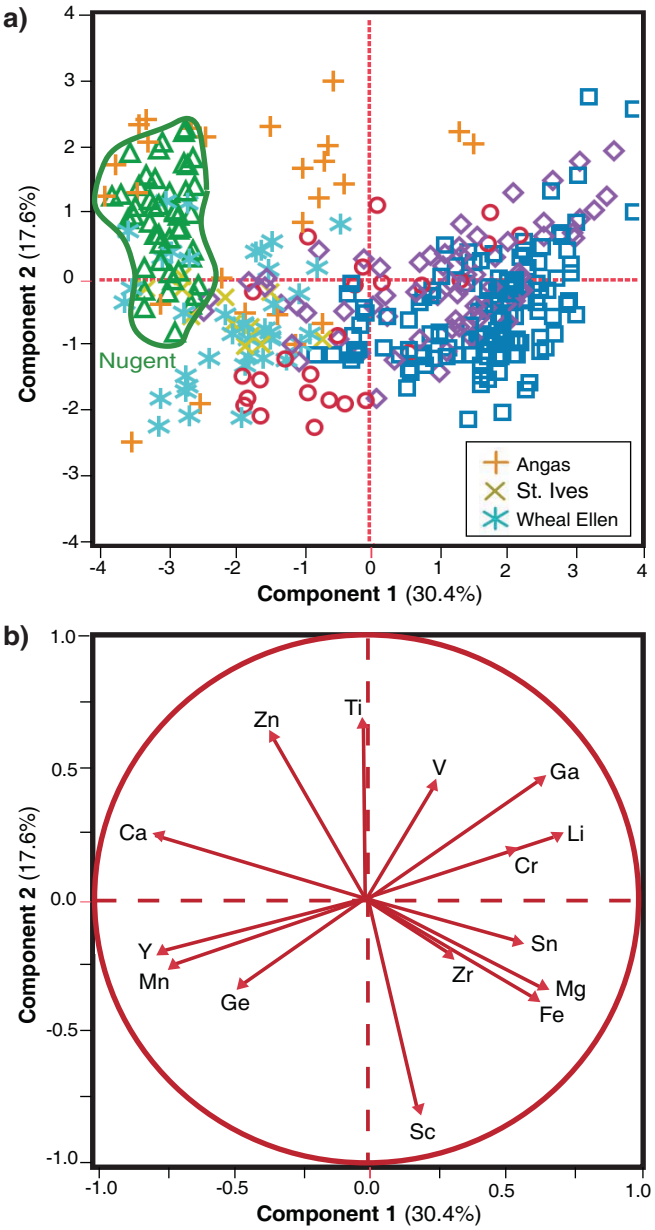

Figure 3. Principal component analysis of garnet using 15 elements, Ca, Cr, Fe, Ga, Ge, Li, Mg, Mn, Sc, Sn, Ti, V, Y, Zn, and Zr. **a)** Score plot of the first two principal components with percent variance for component 1 and 2 on the x and y axis, respectively. **b)** Loading plot showing the vector representation of data projected onto the score plot for each element. Symbols same as shown in Figure 2 for Kanmantoo orebodies.

country rocks (<26 ppm Zn). A principal component analysis of garnet from Pb-Zn-Ag deposits overlaps that of the Nugent orebody at Kanmantoo (Fig. 3), which is spatially associated with laminated quartz-garnet rocks.

Gahnite

Gahnite is spatially associated with the Pb-Zn-Ag deposits (e.g. Angas, Wheal Ellen, Strathalbyn, Aclare, and St. Ives) but it also locally occurs in schists imme-

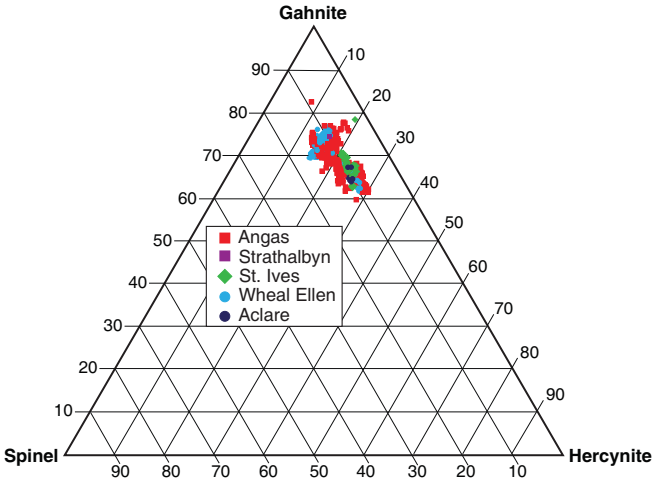

Figure 4. Ternary plot of gahnite compositions from the Aclare, Angas, St. Ives, Strathalbyn and Wheal Ellen Pb-Zn-Ag deposits, in terms of the gahnite-hercynite-spinel *sensu stricto* spinel endmembers.

diately north and south of the Kanmantoo deposit (Toteff, 1999). Gahnite in the Pb-Zn-Ag occurrences has major element compositions (Zn, Mg, and Fe) that overlap compositions of gahnite in metamorphosed massive sulphide deposits found elsewhere in the world (i.e. 28–34 wt% ZnO) (Fig. 4). Gahnite is enriched in Cu (up to 39 ppm), and the first series transition elements, which include up to 3,600 ppm Mn, up to 90 ppm Co, up to 320 ppm V, up to 1,000 ppm Cr, and up to 217 ppm Ga. The trace element compositions of gahnite from Pb-Zn-Ag deposits generally overlap with each other but those from St. Ives are more enriched in Co.

Staurolite

The Zn and Mn contents of staurolite are also high in the Pb-Zn-Ag deposits (up to 6.3 wt% ZnO and up to ~5,000 ppm Mn) relative to those associated with staurolite in the Kanmantoo deposit (up to 1.6 wt% ZnO (with one outlier of 3.2 wt% ZnO), 344 ppm Co, 285 ppm V, and 2070 ppm Mn) (Fig. 5).

Biotite

Biotite in the Cu-Au and Pb-Zn-Ag deposits has compositions generally close to the phlogopite-annite boundary. Biotite in the Pb-Zn-Ag deposits is unusually enriched in various trace elements, including up to 2,600 ppm Mn, 6,400 ppm Cu, and 1,200 ppm Zn in the St. Ives deposit, and up to 1,200 ppm Zn, 5,400 ppm Mn, and 5 wt% Tl in the Angas deposit. The Tl content of biotite is amongst the highest yet reported for biotite in nature. These elemental concentrations are in contrast to those associated with biotite in the Kanmantoo deposit, which are less enriched in metallic trace elements (e.g. <200 ppm MnO and ZnO, and <2 ppm Tl).

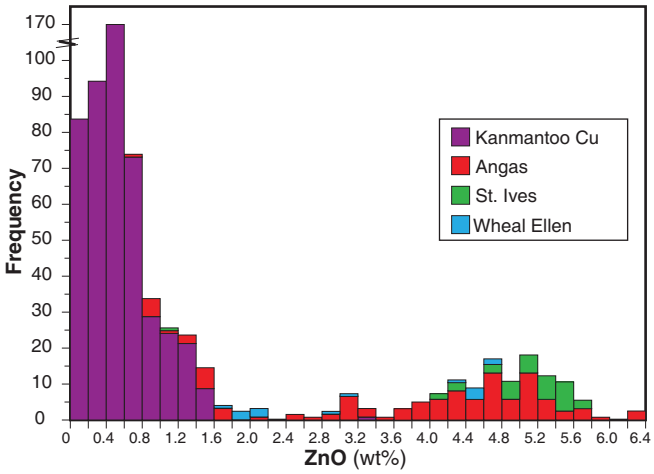

Figure 5. Histogram of Zn content of staurolite. Some data for Angas are from McElhinney (1994).

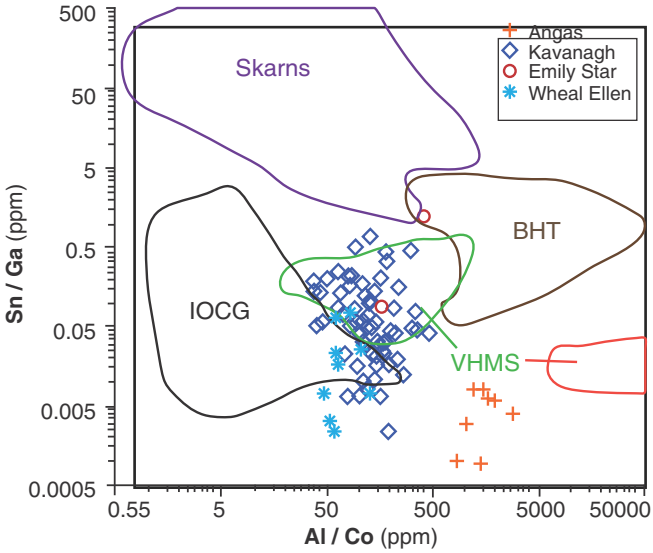

Figure 6. Plot of Sn/Ga (ppm) vs. Al/Co (ppm) used for provenance of hydrothermal ore deposits (after Singoyi et al., 2006). Please note that the symbols used in this figure are different than those used in the other figures.

Chlorite

Mg-rich chlorite in sulphide mineralization at Kanmantoo contains up to 2,300 ppm Mn and 1600 ppm Zn, whereas Fe-rich chlorite contains up to 628 ppm Mn and 202 ppm Zn. Chlorite in Emily Star is characterized by an enrichment in Cu (up to 593 ppm) relative to all other samples that typically contain <10 ppm Cu. The reason for this is unclear. Chlorite spatially associated with Pb-Zn-Ag sulphides contains up to 8922 ppm Mn, 6970 ppm Zn and 321 ppm Cu.

Muscovite

Trace element compositions of muscovite in unaltered country rocks and altered rocks spatially associated with the Kanmantoo deposit contain up to 724 ppm V, 973 ppm Sr, 482 ppm Pb, ppm Cu, 212 ppm Zn, and

31,023 ppm Ba, whereas those associated with the Pb-Zn-Ag deposits contain up to 324 ppm V, 204 ppm Sr, 721 ppm Pb, 101 ppm Cu, 661 ppm Zn, and 17,227 ppm Ba. Muscovite from country rocks elsewhere in the Kanmantoo Group contain lower amounts of these elements (up to 298 ppm V, 125 ppm Sr, 32 ppm Pb, 70 ppm Cu, 51 ppm Zn, and 3,072 ppm Ba: Hammerli et al., 2016).

Ilmenite

Ilmenite in the Kanmantoo deposit is essentially end-member $FeTiO_3$, with up to 0.5 wt% MnO and 0.1 wt% ZnO, differing greatly from that at St. Ives, which contains up to 22.9 wt% ZnO, close to ecandrewsite ($ZnTiO_3$). Ilmenite in the Angas deposit is enriched in Mn, with concentrations ranging from 1.7 to 8.4 wt% MnO, and up to 0.5 wt% ZnO.

Magnetite

Magnetite is intergrown with chlorite, chalcopyrite, and pyrrhotite in the Kanmantoo Cu-Au deposit. Concentrations of select elements in magnetite in the Kanmantoo Cu-Au and Pb-Zn-Ag deposits, respectively, contain up to 7070 and 5394 ppm Al, 4520 and 1195 ppm Ti, 5085 and 4506 ppm V, 1285 and 1775 ppm Cr, 23200 and 983 ppm Cu, 12715 and 509 ppm Zn, and 252 and 607 ppm Ga. A plot of Sn/Ga vs. Al/Co was developed by Singoyi et al. (2006) to assess the provenance of hydrothermal magnetite from skarn, IOCG, Broken Hill-type Pb-Zn-Ag, and VMS deposits. Although there is no designated field for sediment-hosted deposits, it should be noted that most magnetite from the Kanmantoo and Pb-Zn-Ag deposits generally overlap the compositions of magnetite associated with VMS deposits (Fig. 6).

DISCUSSION AND CONCLUSIONS

The enrichment of Zn, Mn, Co, V, Cr, and Cu in gahnite, Mn and Zn in garnet and ilmenite, and Zn, Mn, Cu, and Tl in biotite in Pb-Zn-Ag and Cu-Au deposits relative to those found in the same minerals in unmineralized rocks, constitutes a potential pathfinder to metamorphosed sediment-hosted massive sulphide deposits in the Kanmantoo Group. The enrichment of Co in gahnite at St. Ives may not be surprising since Co is enriched in sulphides in the Kanmantoo Group (e.g. pyrite in pyritic schists, and cobaltian arsenopyrite at Wheal Ellen). Like those obtained here, garnet, gahnite, and biotite in BHT deposits contain elevated concentrations of Mn and Zn. Common rock-forming minerals, such as biotite, muscovite, chlorite, ilmenite, garnet, magnetite, gahnite and staurolite, some of which are resistate minerals, serve as potential chemical vectors in the exploration for SEDEX deposits in the Kanmantoo Group and in other metamorphic terranes.

ACKNOWLEDGEMENTS

This project was financially supported by a grant from the Department for Manufacturing, Innovation, Trade, Resources, and Energy (DMITRE – Geological Survey of South Australia) to PGS, as well by Graduate Student Fellowships from the Society of Economic Geologists to MVP and KAT, and a grant to KAT from the Geological Society of America. Sincere thanks go to David Rawlins (Hillgrove Resources), and to Stephen Hill and John Keeling (DMITRE) for facilitating the project, and to Elizabeth Ambrose for assisting with editing the manuscript.

REFERENCES

Averill, S.A., 2001. The application of heavy indicator mineralogy in mineral exploration with emphasis on base metal indicators in glaciated metamorphic and plutonic terrains, *In:* McClenaghan, M.B., Bobrowsky, P.T., Hall, G.E.M., and Cook, S. (eds), *Drift Exploration in Glaciated Terrain*; Geological Society of London, Special Volume 1985, p. 69–82.

Averill, S.A., 2007. Viable indicators in surficial sediments for two major base metal deposit types: Ni-Cu-PGE and porphyry Cu, *In: Workshop 3: Indicator Mineral Methods in Mineral Exploration*; Exploration 07, International Conference on Mineral Exploration, Toronto, September 9, 2007, p. 33–42.

Bollenhagen, W.J., 1993. *The influence of bulk rock MnO on garnet development in metamorphic rocks of andalusite-staurolite grade; Kanmantoo, South Australia*; B.Sc. Honours thesis, University of Adelaide, Australia.

George, L.L., Cook, N.J., and Ciobanu, C.L., 2016. Partitioning of trace elements in co-crystallized sphalerite–galena–chalcopyrite hydrothermal ores; *Ore Geology Reviews*, v. 77, p. 97–116.

Griffin, W.L., Slack, J.F., Ramsden, A.R., Win, T.T., and Ryan, C.G., 1996. Trace elements in tourmalines from massive sulfides deposits and tourmalinites; geochemical controls and exploration applications; *Economic Geology*, v. 91, p. 657–675.

Hammerli, J., Spandler, C., and Oliver, N.H.S., 2016. Element redistribution and mobility during upper crustal metamorphism of metasedimentary rocks: an example from the eastern Mount Lofty Ranges, South Australia; *Contributions to Mineralogy and Petrology,* v. 36, p. 1–21.

Heimann, A., Spry, P.G., and Teale, G.S., 2011. Chemical and crystallographic constraints on the geochemistry of garnet in garnet-rich rocks, southern Proterozoic Curnamona Province, Australia; *Mineralogy and Petrology*, v. 101, p. 49–74.

Ismail, R., Ciobanu, C.L., Cook, N.J., Teale, G.S., Giles, D., Schmidt Mumm, A., and Wade, B., 2014. Rare earths and other trace elements in minerals from skarn assemblages, Hillside iron oxide-copper-gold deposit, Yorke Peninsula, South Australia; *Lithos*, v. 184-187, p. 456–477.

Jackson, S.E., Longerich, H.P., Dunning, G.R., and Freyer, B.J., 1992. The application of laser-ablation microprobe; inductively coupled plasma-mass spectrometry (LAM-ICP-MS) to in situ trace-element determinations in minerals; *Canadian Mineralogist*, v. 30, p. 1049–1064.

Layton-Matthews, D., Hamilton, D.C., and McClenaghan, M.B., 2013. Mineral chemistry: modern techniques and applications to exploration, *In: Application of Indicator Mineral Methods to Mineral Exploration*; 26th International Applied Geochemistry, Rotorua, New Zealand, Short Course Notes, p. 9–18.

Makvandi S., Ghasemzadeh-Barvarz, M., Beaudoin, G., Grunsky, E.C., McClenaghan, B.M., and Duchesne, C., 2016a. Principal component analysis of magnetite composition from volcanogenic massive sulfide deposits: case studies from the Izok

Lake (Nunavut, Canada) and Halfmile Lake (New Brunswick, Canada) deposits; *Ore Geology Reviews*, v. 72, p. 60–85.

Makvandi S., Ghasemzadeh-Barvarz, M., Beaudoin, G., Grunsky, E.C., McClenaghan, B.M. Duchesne, C., and Boutroy, E., 2016b. Partial least squares-discriminant analysis of trace element compositions of magnetite from various VMS deposit subtypes: Application to mineral exploration; *Ore Geology Reviews*, v. 78, p. 388–408.

McClenaghan, M.B., 2005. Indicator mineral methods in mineral exploration; *Geochemistry: Exploration, Environment, Analysis*, v. 5, p. 233–245.

McClenaghan, M.B., 2013. Overview of indicator mineral recovery methods for sediments and bedrock:, 2013 update, *In: Application of Indicator Mineral Methods to Mineral Exploration*; 26th International Applied Geochemistry, Rotorua, New Zealand, Short Course Notes, p. 1–7.

McElhinney, R., 1994. *Style and genesis of base metal sulphide mineralization of Angas Prospect, Strathalbyn area, South Australia*; B.Sc. Honours thesis, University of Adelaide, Australia.

O'Brien, J.J., Spry, P.G., Teale, G.S., Jackson, S.E., and Koenig, A.E., 2015a, Gahnite composition as a means to fingerprint metamorphosed base metal deposits; *Journal of Geochemical Exploration*, v. 159, p. 48–61.

O'Brien, J.J., Spry, P.G., Teale, G.S., Jackson, S.E., and Rogers, D., 2015b. Major and trace element chemistry of gahnite as an exploration guide to Broken Hill-type Pb-Zn-Ag mineralization in the Broken Hill domain, New South Wales, Australia; *Economic Geology*, v. 110, p. 1027–1057.

Schmidt Mumm, A., Dart, R.C., and Say, P., 2012. Hematite/maghemite trace element geochemistry in base metal exploration; *Journal of Geochemical Exploration*, v. 118, p. 1–13.

Singoyi, B., Danyushevsky, L., Davidson, G.J., Large, R. and Zaw, K., 2006. *Determination of trace elements in magnetites from hydrothermal deposits using the LA ICP-MS technique*; Society of Economic Geologists Conference, Keystone, Colorado, CD-ROM.

Smith, M.K., 1998. *A comparative petrological and geochemical study of garnetiferous rocks associated with base metal deposits in the Kanmantoo Trough: meta-exhalites or synmetamorphic alteration zones?* B.Sc. Honours thesis, University of Adelaide, Australia.

Spry, P.G., Heimann, A., Messerly, J.D., Houk, R.S., and Teale, G.S., 2007. Discrimination of metamorphic and metasomatic processes at the Broken Hill lead-zinc-silver deposit, Australia: Rare earth element signatures of garnet in garnet-rich rocks; *Economic Geology*, v. 102, p. 471–494.

Spry, P.G., O'Brien, J.J., Frank, K.S., Teale, G. S., Koenig, A., Jansson, N., Allen, R., and Raat, H., 2015. Trace element compositions of silicates and oxides as exploration guides to metamorphosed massive sulphide deposits: examples from Broken Hill, Australia, and Stollberg, Sweden, *In: Application of Indicator Mineral Methods to Mineral Exploration*; 27th International Applied Geochemistry, Tucson, Arizona, Short Course Notes, p. 23–29.

Spry, P.G., Schiller, J.C., and Both, R.A., 1988. Structure and metamorphic setting of base metal mineralisation in the Kanmantoo Group, South Australia; *Australasian Institute of Mining and Metallurgy Proceedings*, v. 293, p. 57–65.

Tedesco, A., 2009. *Late-stage orogenic model for Cu-Au mineralisation at Kanmantoo Mine: New insights from titanium in quartz geothermometry, fluid inclusions and geochemical modelling*; B.Sc. Honours thesis, Adelaide, University of Adelaide, Australia.

Toteff, S., 1999. *Cambrian sediment-hosted exhalative base metal mineralisation, Kanmantoo Trough, South Australia*; Geological Survey of South Australia, Report of Investigations 57.

Testing the applicability of tourmaline as a tool in the exploration for mineralized porphyry systems: insights and advances

A.M. McDonald* and C.E. Beckett-Brown

Harquail School of Earth Sciences, Laurentian University, 995 Ramsey Lake Road, Sudbury, Ontario, Canada P3E 2C6

*(*Corresponding author's e-mail: amcdonald@laurentian.ca)*

Tourmaline [general formula; $XY_3Z_6T_6O_{18}(BO_3)_3V_3W$] is represented by a large family of borosilicate minerals capable of incorporating a wide range of elements, from alkalis (Na,K,Rb), alkaline earths (Mg,Ca,Sr), high field-strength elements (Ti,Y,Nb) to metals (Fe,Mn,Ni,Cu) and halogens (F,Cl,Br). This, coupled with its resistivity to chemical and physical degradation in the natural environment, makes tourmaline ideal as an indicator mineral. Furthermore, the mineral is a relatively common constituent of mineralized porphyry systems, where it frequently develops in highly brecciated areas that can be host to significant mineralization (Cu-Au-Mo) as well as in veins or in disseminations (Fig. 1). On this basis, studies have been undertaken to examine the relationship between the crystal chemistry of tourmaline from mineralized porphyry systems in south-central British Columbia (Shaft Creek, Highland Valley) and southern Yukon (Casino), specifically focusing on the evaluation of (1) textural variations in tourmaline and their relationship to mineralization processes, (2) chemical changes (major, minor, trace) and insights into fluid chemistry, (3) chemical zonation patterns and linkages to crystallization processes, and (4) inclusions within tourmaline and how these vary inter- and intra-deposit. This presentation will highlight some (but not all) of the key findings of an on-going research program to creating a baseline database of tourmaline characteristics in mineralized porphyry systems.

The host lithologies for all samples examined are granodiorite to feldspar porphyries with variable degrees of potassic alteration. At Shaft Creek, tourmaline developed in veins, as disseminations, and in breccias. That found in veins occurs as densely packed aggregates composed of randomly arranged, prismatic crystals. The grains are relatively small (20–100 μm in length) and have, commonly developed at vein boundaries. Intergranular space is infilled with quartz and sulphide minerals and is frequently found with apatite and rutile. In disseminations, the tourmaline developed in radial aggregates of coarse grains (average 0.5 mm, but individual grains can be up to several millimetres in length) that are overgrown by sulphide minerals. In breccias, individual, euhedral grains of tourmaline, which range in size from <100 μm to several mm, have interesting zonation patterns that can be observed in

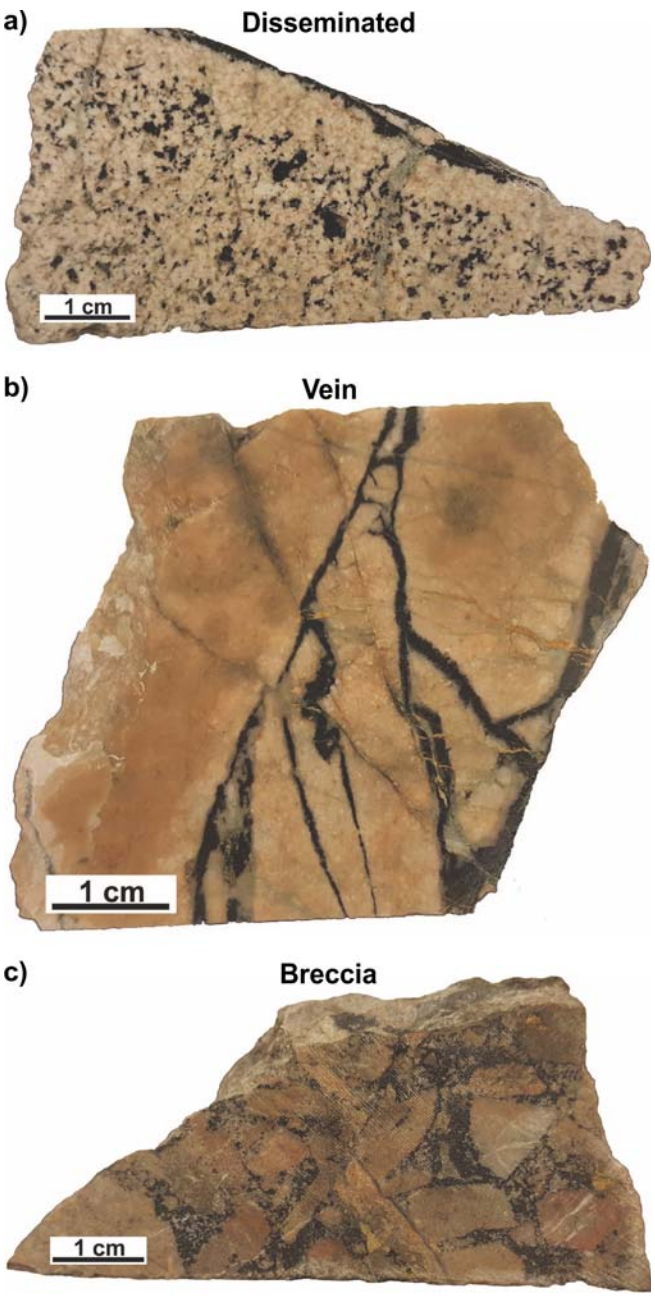

Figure 1. Examples from Schaft Creek of the depositional and textural variance of tourmaline observed in this study. **a)** Disseminated tourmaline (black mineral) showing its relationship to the host rock and the sulphide mineralization. **b)** Tourmaline (black mineral) occurring as veins. **c)** Tourmaline (black mineral) occurring in the breccia matrix together with quartz and sulphide minerals (chalcopyrite and pyrite).

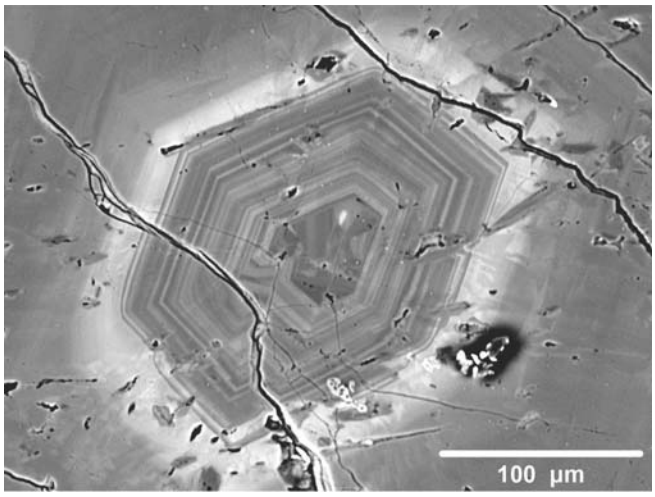

Figure 2. Oscillatory zonation characteristic of tourmaline examined in this study. Light zones correspond to Fe-enrichment, darker zones to Mg-enrichment. Schaft Creek, British Columbia.

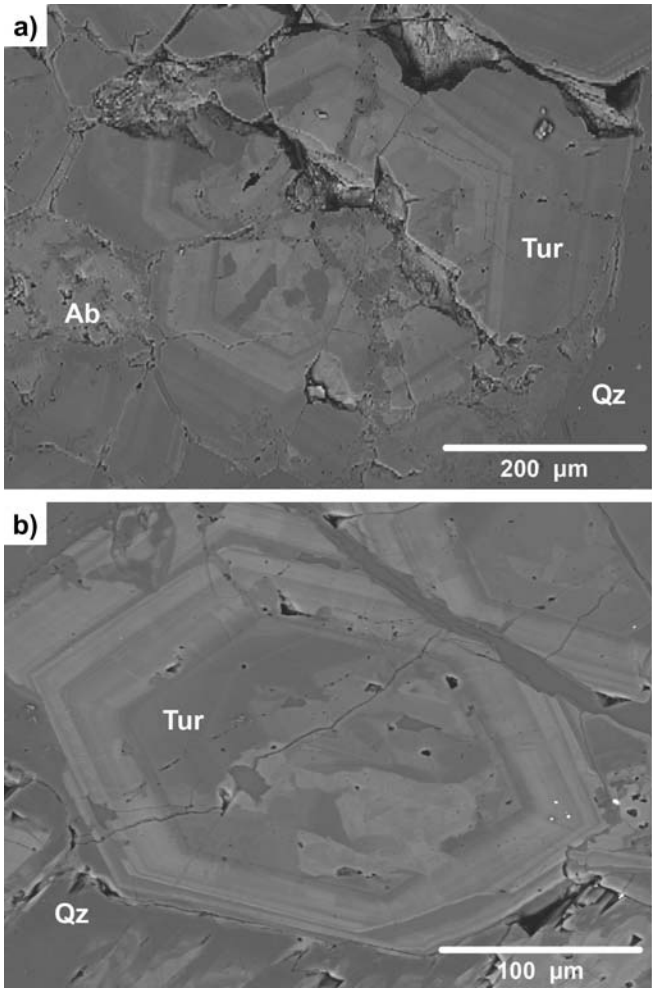

Figure 3. Backscattered-electron image showing the chaotic, dismembered tourmaline cores. Samples from the breccia zone at Schaft Creek, British Columbia. Abbreviations: Ab = albite; Tur = tourmaline, Qz = quartz.

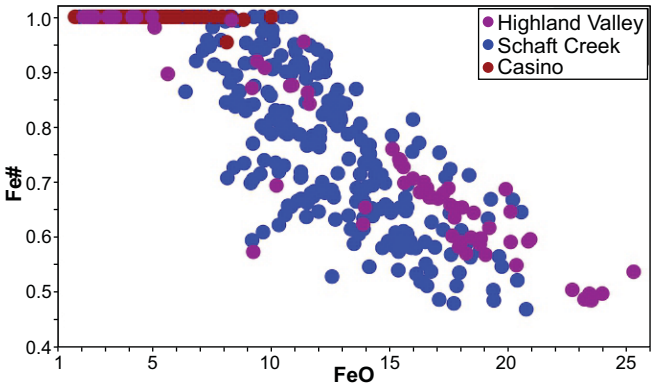

Figure 4. Plot of Fe# ($Fe^{2+}/Fe^{2+}+Fe^{3+}$) versus FeO showing a decrease in Fe^{2+} as FeO_{total} increases.

thin section: large, homogeneous cores, which are predominately red-brown in colour, are partially to wholly overgrown by fine-grained, grey-green rims. At least two generations have been observed: earlier formed, coarse grains that are 'cemented' by finer grained tourmaline along with quartz and sulphide (predominantly chalcopyrite). It is noteworthy that the tourmaline, regardless of its mode of occurrence, is typically pre- to syn-formational (paragenetically) to associated sulphide minerals. At Casino, tourmaline has to-date only been found in disseminations, where it occurs as acicular grains, typically <200 µm in length, that exhibit a wide range of colours in thin section (green, red, brown). The tourmaline is paragenetically early, with sulphide minerals (pyrite, chalcopyrite, tennantite) occurring as both overgrowths and fracture-fillings. At Highland Valley, the tourmaline developed as radiating clusters composed of blue-green to tan-brown crystals up to 4 mm in length, occasionally with fine-grained tourmaline overgrowths. The material analyzed was from sulphide-poor alteration zones and the paragenetic relationship between the two tourmaline types is still to be determined.

The tourmaline examined in this study frequently exhibits complex oscillatory zonation (most obvious under backscattered-electron imaging) that correlates with Mg-Fe variations (lighter areas being Fe-enriched; Fig. 2). The tourmaline typically possesses cores with irregular patchy zonation that have been subsequently overgrown by tourmaline exhibiting oscillatory zonation patterns (Fig. 3).

Results from the mineral-chemistry study show that tourmaline from all three occurrences (Shaft Creek, Highland Valley and Casino) is enriched in Mg and tends to be Fe^{2+}-dominant. Tourmaline from Shaft Creek has an average 2.12 *apfu* Mg (*apfu* = atom per formula unit) with 1.48 *apfu* Fe but it was observed that the tourmaline shows a wider range in Fe content than Mg content (0.26–3.14 *apfu* Fe vs. 1.35–2.89 *apfu* Mg). At Casino, the tourmaline has an average Mg content of 1.99 *apfu* and Fe content of 0.61 *apfu*. It is

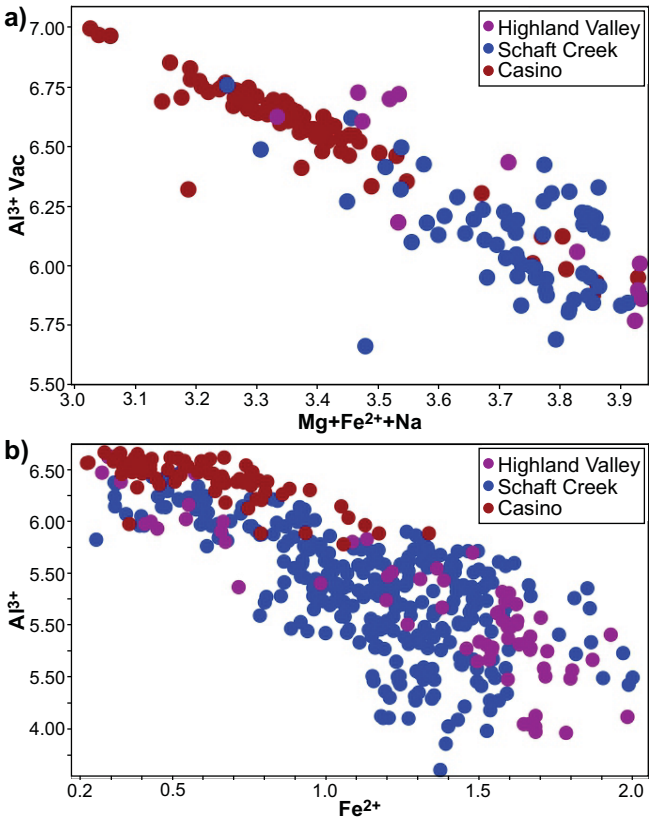

Figure 5. Plots of **(a)** R^{2+} versus Al^{3+} vacancy and **(b)** Al^{3+} versus Fe^{2+}, both of which show strong, negative correlations.

notably Fe-poor with a smaller range (0.23–1.33 *apfu* Fe). Neither F nor Cl were found to be present above detection limits (~0.1 and 0.15 wt%, respectively). Tourmaline from Highland Valley is, on average, the most Fe-rich (2.06 *apfu* vs. 1.86 *apfu* Mg) examined in this study and shows the widest range in chemical variation (0.28–3.81 *apfu* Fe vs. 1.12–2.70 *apfu* Mg). The calculated *Fe#* ($Fe^{2+}/Fe^{2+}+Fe^{3+}$) varies considerably amongst the three sites: for Shaft Creek, the tourmaline has an average *Fe#* of 0.81 (range 1–0.47), from Casino the *Fe#* is 1 (range 1–0.95), and for Highland Valley, the *Fe#* is 0.73 (range 1–0.49). A negative correlation between *Fe#* and FeO_{tot} (Fig. 4) has been observed at all three sites.

In general, deficiencies (vacancies) in the alkali site (X) of tourmaline are variable. Tourmaline from Casino shows the highest vacancy content (average: 0.17 *apfu*, range: 0.05–0.43 *apfu*), and tourmaline from Shaft Creek and Highland Valley are similar, both having relatively insignificant concentrations (average 0.01 and 0.02 *apfu*, respectively; ranges of 0–0.32 and 0–0.17 *apfu*, respectively). Results show that these vacancy abundances positively correlate with Al concentration and negatively with both (Mg+Fe) concentrations, which is consistent with the substitution of $R^{2+} + Na \leftrightarrow Al^{3+} + \square$ ($R^2 = 0.93$; Fig. 5a). A negative, but weaker ($R^2 = 0.77$) correlation between Fe^{2+} and

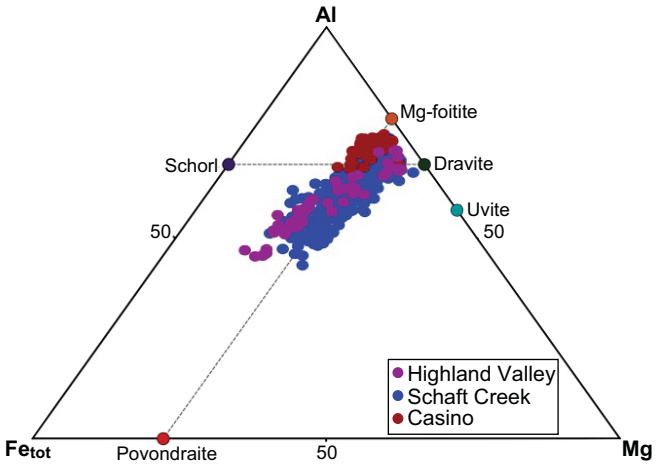

Figure 6. Ternary diagram of Fe_{tot}-Al-Mg plot of tourmaline examined in this study. Notice the data cluster along the dravite-schorl series, with pronounced extensions towards povondraite.

Al^{3+} is also noted, possibly reflecting the substitution $Fe^{2+} + (OH)^- \leftrightarrow Al^{3+} + O^{2-}$ (Fig. 5b).

Tourmaline analyzed in this study ranged in composition from dravite (Na-Mg tourmaline, $NaMg_3Al_6Si_6O_{18}(BO_3)_3(OH)_4$) to schorl (Na-$Fe^{2+}$ tourmaline, $NaFe^{2+}{}_3Al_6Si^6O_{18}(BO_3)_3(OH)_4$) and when plotted on a binary Mg-Fe plot, a general tendency could be observed for most tourmaline compositions to plot closer to that of dravite (i.e. Mg-dominant), regardless of whether the sample is from an earlier or later generation (Fig. 6). However, when tourmaline compositions are plotted on a Fe-Mg-Al ternary diagram, there is a noticeable tendency for a significant portion of the data to trend towards povondraite (Na-Fe^{3+} tourmaline, $NaFe^{3+}{}_3Fe^{3+}{}_4Mg_2Si_6O_{18}(BO_3)_3(OH)_4$), as is seen in samples from Schaft Creek and Highland Valley (Fig. 4). The exception is tourmaline from Casino, where the data tightly cluster along the dravite-schorl join, possibly with slightly elevated Al contents (Fig. 6).

Textural analyses of the tourmaline from this study show that the development of chaotic, dismembered cores followed by regular, oscillatory zoned rims is ubiquitous. This could reflect early formed tourmaline in the cores, likely with the commonly observed oscillatory zonation patterns, being shattered or dismembered and then reconsolidated and overgrown by tourmaline arising from a second period of growth (also exhibiting the typical oscillatory zonation patterns), probably during relatively quiescent periods of crystallization. Mineral-chemical data indicate that the tourmaline in the chaotic cores as well as in the oscillatory-zoned rims show the same chemical characteristics, including *Mg#* ($100Mg/(Mg+Fe_{tot})$ and *Fe#*, with the same magnitudes of variation, implying broad similarities in the composition of the fluids form which they were crystallized. The shattered cores could reflect

boiling and an increase in pressure, which would, in turn, lead to overpressure and subsequent pressure release. Boiling would be expected to coincide with a release of H_2, which would, in turn, lead to higher fO_2. However, no significant differences in calculated *Fe#* were noted between the chaotic cores and oscillatory zoned rims, suggesting that boiling may not have played an overarching role in the formation of tourmaline.

Previous research has shown that tourmaline from porphyry systems typically has an average Mg content of ~2 *apfu* (Baksheev et al*.,* 2012), which is consistent with the results of this study. The predominance of Fe^{2+} in tourmaline could, in part, reflect (or be attributable to) an increase in the relative abundance of H_2S. High concentrations of Fe^{2+} is particularly relevant for sulphide formation if metals in mineralized porphyry systems are indeed transported in sulphide (or bisulphide) complexes (Heinrich et al*.,* 2004). The virtual absence of both F^- and Cl^- in tourmaline (which are common metal-complexing agents) may also support this supposition.

Calculated *Fe#* clearly demonstrate a predominance of Fe^{2+} in tourmaline, supporting crystallization under reducing conditions (i.e. low fO_2). Restricted increases in Fe^{3+} content is noted, perhaps reflecting local conditions of high fO_2 developed during alteration. The negative correlation between *Fe#* and FeO_{tot} (Fig. 4) observed in the samples from this study may be explained by both an increased concentration of H_2S (potentially transporting metals) during formation and by the crystallization of sulphides, notably pyrite, which is enriched in Fe^{2+} (rather than chalcopyrite, which is dominated by Fe^{3+}).

The trend of tourmaline compositions towards povondraite is noteworthy as povondraite shows not only a predominance of Fe^{3+} but also has its W-site dominated by O^{2-}, rather than by $(OH)^-$ or F^-. Therefore, chemical trends towards this component in the tourmaline may be suggestive of relatively lower H_2O content, but potentially higher fO_2, in the fluid or melt from which it crystallized. The observation that tourmaline from mineralized porphyry systems exhibits enrichment in the povondraite end-member composition has been previously reported by Baksheev et al. (2012) and is confirmed by the findings of this study.

CONCLUSIONS

1. Two generations of tourmaline have been recognized in the samples from Shaft Creek, Highland Valley and Casino: (a) an early, pre-sulphide tourmaline that dominates the cores of larger crystals and is characterized by a chaotic texture and (b) a later, pre- to syn-sulphide tourmaline that develops as rims and exhibits distinct oscillatory zonation. The core tourmaline is considered to have developed during pressure build-up and release and the rim is considered to have developed during a period of relative quiescence.
2. Chemical zonation (most notable under backscattered electron imaging) is primarily attributed to variations in Mg and Fe. Both the core and rim tourmaline show similar compositions (*Fe#*, *Mg#*, vacancy populations) and are chemically indistinguishable from one another.
3. Chemical analyses show major concentrations of Mg and Fe, with lesser amounts of Al. Calculations demonstrate that Fe^{2+} dominates but some tourmaline shows lesser, but potentially significant, concentrations of Fe^{3+}. Flourine and Cl were not observed above detection limits.
4. The tourmaline examined clearly plot along the dravite-schorl join, with most of the data plotting closer to the dravite end-member. A significant portion of the data shows limited enrichment towards the povondraite end-member.
5. Results suggest that (a) a direct genetic linkage between tourmaline and sulphide formation is tenuous. In most cases, sulphide crystallization appears to be post tourmaline; (b) the absence of significant halogens appears to be consistent with the hypothesis that metal transport in mineralized porphyry systems is primarily through sulphide complexes; (c) a predominance of Fe^{2+}, suggesting the tourmaline formed under relatively reducing conditions. This is also consistent with the presence of H_2S in the system, furthering the concept that metals are being transported in sulphide complexes in mineralized porphyry systems. (d) only slight Fe^{3+} enrichment was observed and may coincide with periods of alteration (as at Highland Valley) or possibly with the crystallization of sulphide minerals. Within the chaotic tourmaline cores; no variation in *Fe#* was observed, suggesting that boiling may not be responsible for their observed disaggregation.
6. The zonation patterns, the lack of significant vacancies in the X-site and the dominant compositional trend of tourmaline along the dravite-schorl join (with a weaker trend towards povondraite) collectively may serve as useful characteristics in recognizing tourmaline from mineralized porphyry systems.

REFERENCES

Baksheev, I.A., Yu Prokof'ev, V., Zaraisky, G.P., Chitalin, A.F., Yapaskurt, V.O., Nikolaev, Y.N.; Tikhomirov, P.L., Nagornaya, E.V., Rogacheva, L.I., Gorelikova, N.V., and Kononov, O.V., 2012. Tourmaline as a prospecting guide for the poryphyry-style deposits; *European Journal of Mineralogy*, v. 24, p. 957–979.

Heinrich, C.A., Driesner, T., Stefansson, A., and Seward, T.M., 2004, Magmatic vapor contraction and the transport of gold from the porphyry environment to epithermal ore deposits; *Geology*, v. 32, p. 761–764.

Lithosphere thickness determinations and kimberlite diamond potential

M.H. Seller

The De Beers Group of Companies, De Beers – Exploration Canada,
515 Consumers Road, Suite 300, Toronto, Ontario, Canada M2J 4Z2
(e-mail: michael.seller@debeersgroup.com)

Diamond exploration typically takes place in remote and inaccessible areas where it may take decades for an *economically viable* diamond deposit to be found, assessed, and ultimately mined. Various scientific skills and technical disciplines are required at all stages of the exploration process—from targeting, early or reconnaissance stages through discovery and advanced stages. Within the early stages of exploration, sampling of soil or stream sediments for the recovery of kimberlite indicator minerals (KIMs) is dependent on the environmental setting. With favourable results, more detailed sampling is conducted, then geophysical surveys are flown, and prospective targets are identified and drilled.

Not every kimberlite discovery is economically viable, in fact, the vast majority are not, however, assessment of the 'diamond potential' of a kimberlite can begin immediately upon discovery from the KIMs recovered from the samples collected. At this stage, the major element chemistry of the recovered KIMs are evaluated and compared to those from mantle studies and known inclusions in diamonds to highlight kimberlites with the 'highest' diamond potential (e.g. Gurney et al*.,* 1993; Nowkicki et al*.*, 2007; Stachel and Harris, 2008). This is critical as we only want to focus our continuing efforts on those kimberlites with the highest potential.

In addition to this traditional method of determining diamond potential, determining mantle pressure (P) and temperature (T) through thermobarometry of mantle xenoliths and garnet and clinopyroxene KIMs is key as the *P-T* data are a direct measure of the geothermal state (i.e. geotherm) of the continental lithospheric mantle at the time of emplacement.

PALEOGEOTHERM AND LITHOSPHERE THICKNESS

The estimation of paleogeotherms has traditionally been accomplished by calculating *P-T* data from recovered mantle xenoliths with reference to a family of geotherms (Pollack and Chapman, 1977). However, in the early stages of diamond exploration, the recovery of mantle xenoliths for tradition thermobarometry is very limited. Xenocrystic garnet and clinopyroxene from kimberlite concentrates are exceedingly more abundant than xenoliths, and it is common practice to analyse these for *P-T* data. As early as 1996, it became possible to use garnet xenocrysts to generate *P-T* data that could be used to produce a 'garnet geotherm'.

Temperature information for garnet xenocrysts can be determined by either of two methods. The first is an empirically derived Ni thermometer for peridotitic xenocrystic garnets from Griffin at al. (1989) and expanded upon in Ryan et al*.* (1996). This technique allows the temperatures for a single garnet to be calculated, assuming the grain has equilibrated with olivine. The second method is an experimentally derived Ni-in-garnet geothermometer developed by Canil (1994) and revised in Canil (1999). A garnet barometer (P_{Cr}) was initially developed by Ryan et al*.* (1996) and subsequent to this, Grütter et al*.* (2006) published the P_{38} Cr/Ca-in-pyrope barometer. Both barometers are limited in that they yield only minimum pressures in most circumstances. For the purposes of this paper, all temperatures and pressures presented for garnet xenocrysts will use the T_{Ni} formulation of Canil (1999) and the P_{38} barometer of Grütter et al*.* (2006). For a more comprehensive overview of these techniques, refer to Cookenboo and Grütter (2010).

An example of how kimberlite-derived garnet xenocryst *P-T* data has traditionally been used within the diamond exploration community is illustrated in Figure 1. It is evident that estimating a paleogeotherm in relation to the Pollack and Chapman (1977) reference geotherms is problematic, as the process is both manual and subjective, in addition, there does not appear to be a specific reference geotherm that adequately explains the data. To add further uncertainty in the process, P_{38} data are only minimum pressures so one must rely on using the maximum temperature for any given pressure (or depth) to define the geotherm. These issues will be further illustrated in subsequent figures.

Since *Exploration '07*, there have been advancements in reliable single-grain thermobarometry, specifically in the use of a single clinopyroxene for the derivation of *P-T* conditions of equilibration. In conjunction with this has been the development of a quantitative method for fitting a geotherm to *P-T* data. Nimis and Taylor (2000) presented a calibration of the Cr-in-

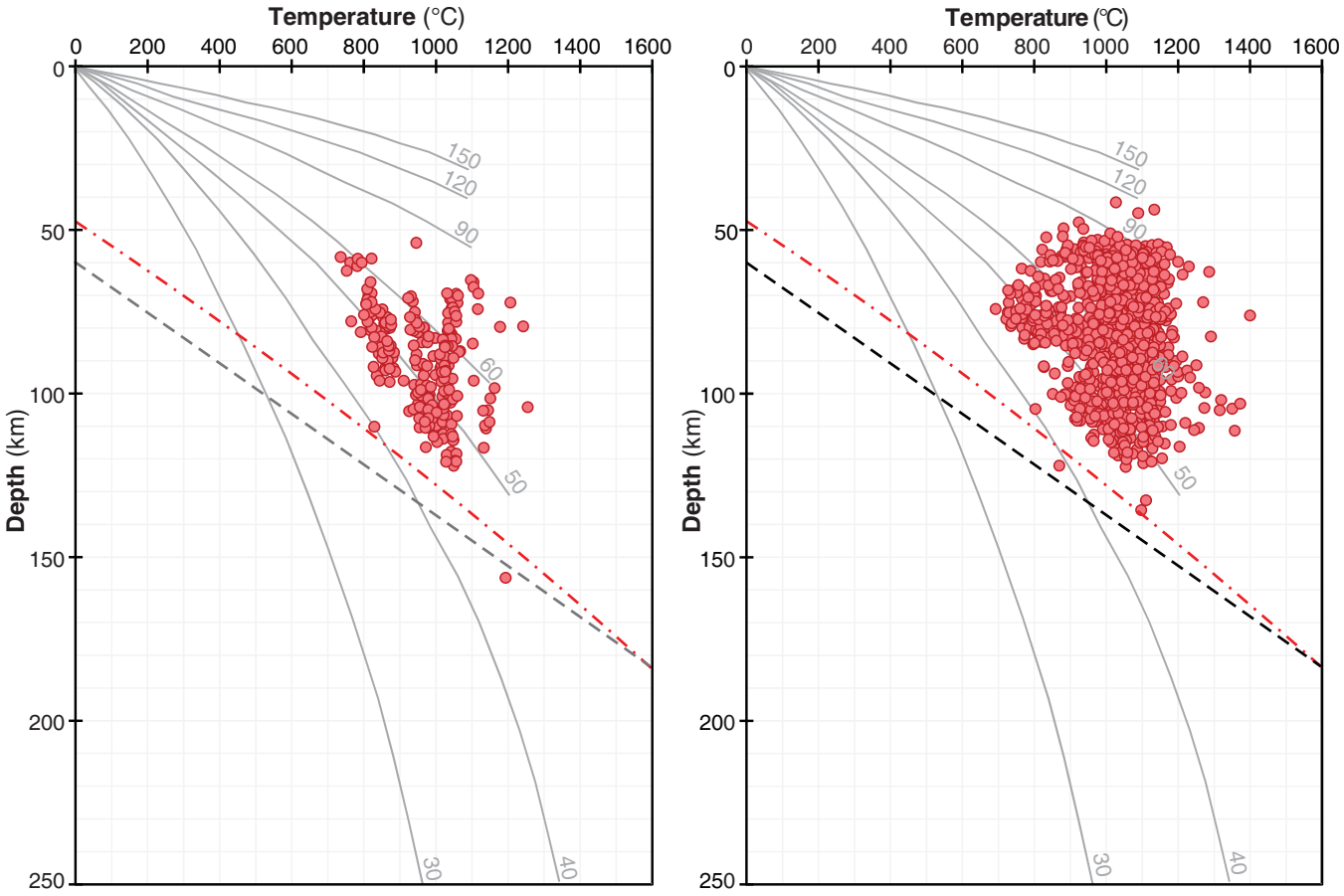

Figure 1. Garnet xenocryst pressure-temperature (*P-T*) data (at left) for the Charlie, Delta, Tango, and Whiskey kimberlites (241 garnets from Griffin et al., 2004; note, pressures have been converted to depth). At right is a selection of 997 garnet xenocrysts from the Victor kimberlite (De Beers data). The diamond-graphite transitions of Kennedy and Kennedy (1976) and Day (2012) are shown as the black dashed line and red dash-dot line, respectively. The seven represented geotherms (mW/m^2) were digitized from Figure 3 of Pollack and Chapman (1977).

clinopyroxene barometer and the enstatite-in-clinopyroxene thermometer for clinopyroxene grains derived from garnet peridotite. Grütter (2009) and Nimis and Grütter (2009) demonstrated the applicability of single-grain clinopyroxene-derived geotherms. In addition to this, a routine was presented for stringent filtering of the clinopyroxene data before any *P-T* calculations can be undertaken—further additions to the filters were made by Ziberna et al. (2016).

Despite this method for attaining reliable single-grain clinopyroxene thermobarometric data, P77 reference geotherms were still being used until Mather (2011) introduced *FITPLOT*, a program for numerical paleogeotherm fitting to *P-T* data. The origins of this quantitative approach are from McKenzie and Bickle (1988) and McKenzie et al. (2005). At the same time as Mather presented *FITPLOT*, Hasterok and Chapman (2011) introduced an updated set of preferred geotherm families, however, their approach is not numerical but replies on a manual method of comparing the *P-T* data to the reference geotherms.

To illustrate the value of *FITPLOT*, a few publicly available datasets are used to derive paleogeotherms at the time of kimberlite emplacement. Input parameters for *FITPLOT* require *P-T* data, upper and lower crustal thickness estimates (km), heat production values (mW/m^3) for the crust and mantle, and a potential temperature for the mantle. When clinopyroxene xenocrysts were used as inputs for this talk, pressures and temperatures were calculated using Nimis and Taylor (2000) and the filters outlined in Nimis and Grütter (2009) were employed. When *P-T*s from mantle xenoliths were inputs, they are entered "as is" from their respective sources. Crustal thickness data per location are from Tesauro et al. (2014)—the total crustal thickness was divided equally between the upper and lower crust. Heat production and mantle potential temperature are from McKenzie et al. (2005), 1.12 $\mu W/m^3$ for the upper crust, 0.4 $\mu W/m^3$ for the lower crust, and 0 $\mu W/m^3$ for the mantle, with a mantle potential temperature (isentrope) of 1315°C. Therefore, the only variable parameters are crustal thickness and the *P-T* data. Lastly, and most critical for diamond exploration, *FITPLOT* provides an estimate of lithosphere thickness

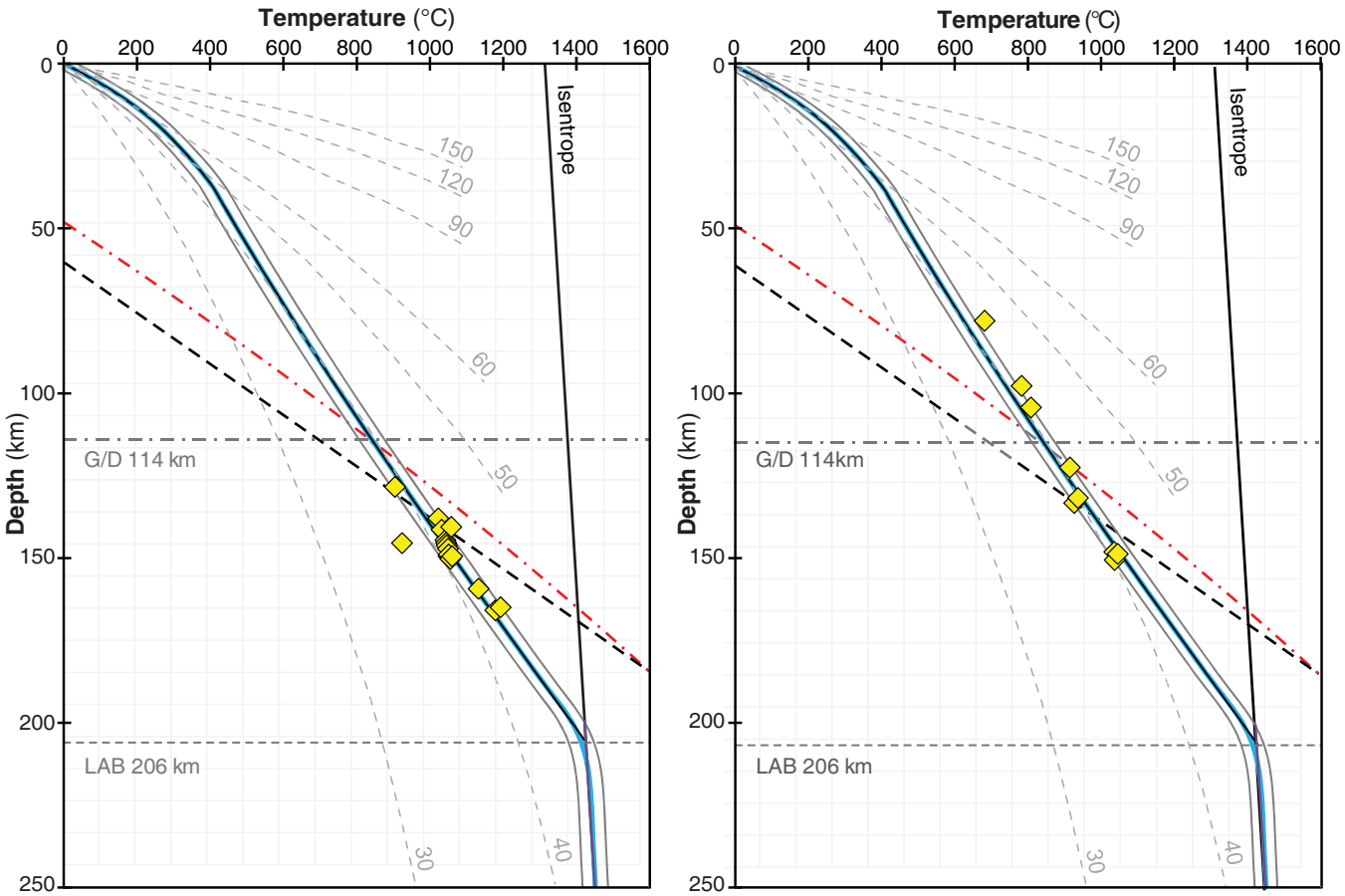

Figure 2. At the left is the *FITPLOT* paleogeotherm output for the pressure-temperature (*P-T*) data from clinopyroxene xenocrysts from the Victor mine (clinopyroxene data are from Sage, 2000). The output indicates that the paleogeotherm intersects the Day graphite-diamond transition (G/D) at ~114 km and meets the isentrope at ~206 km (i.e. the lithosphere/asthenosphere boundary; LAB) defining a diamond window of ~92 km. At the right is the *FITPLOT* output for *P-T* data for mantle xenoliths from Golf, Alpha, and Victor kimberlites (Scully, 2000). The outputs are identical to the clinopyroxene xenocryst data. The paleogeotherms are defined by the blue lines with their associated bounding error envelopes (grey lines). The seven Pollack and Chapman (1977) reference geotherms are indicated by the lines and labelled. All other reference lines are as those described in Figure 1. The *FITPLOT* crustal thickness terms were set at 18.85 km each for the upper and lower crust.

and the extent of the diamond window can be determined based on the intersection of the paleogeotherm with the graphite-diamond transition (Kennedy and Kennedy (1976) or Day (2012))—the position of the graphite-diamond transition within the continental lithospheric mantle is a fundamental control for diamond potential.

Paleogeotherms obtained through *FITPLOT* for the Attawapiskat kimberlite field (170–180 Ma; Januszczak et al., 2013) are shown in Figure 2. Pressure and temperature data for clinopyroxene xenocrysts from the Victor mine (Sage, 2000) and mantle xenoliths from the Golf and Alpha kimberlites and the Victor mine (Scully, 2000) were used as inputs. The fitted paleogeotherms are almost identical for both datasets with a lithospheric thickness of ~206 km and an extensive diamond window of ~92 km, beginning at a depth of ~134 km (using the graphite-diamond transition of Day (2012)). With respect to the reference geotherms of Pollack and Chapman (1977), the 40 mW/m^2 geotherm appears to fit the available data, however, it is impossible to determine lithosphere thickness as the geotherm does not meet the isentrope at a geologically reasonable depth.

Paleogeotherms for the Kyle Lake kimberlite in Ontario (1076.2 ±3.8 Ma: Heaman et al., 2004) and the Nikos kimberlite on Somerset Island (97 ±17 Ma: Schmidberger et al., 2001) are presented in Figure 3. Kyle Lake clinopyroxene xenocrysts (Sage, 2000) and low- and high-temperature peridotite xenoliths from Nikos (Schmidberger et al., 2001) were used for the *P-T* inputs. The fitted paleogeotherms indicate thinner lithospheres: the diamond window for Kyle Lake begins at ~134 km and ends at ~181 km (~47 km diamond window) and for Nikos, the diamond window begins at ~126 km and terminates at ~188 km (~62 km diamond window). None of the reference geotherms adequately fits the available *P-T* data, making it impossible to estimate the lithosphere thickness and the dia-

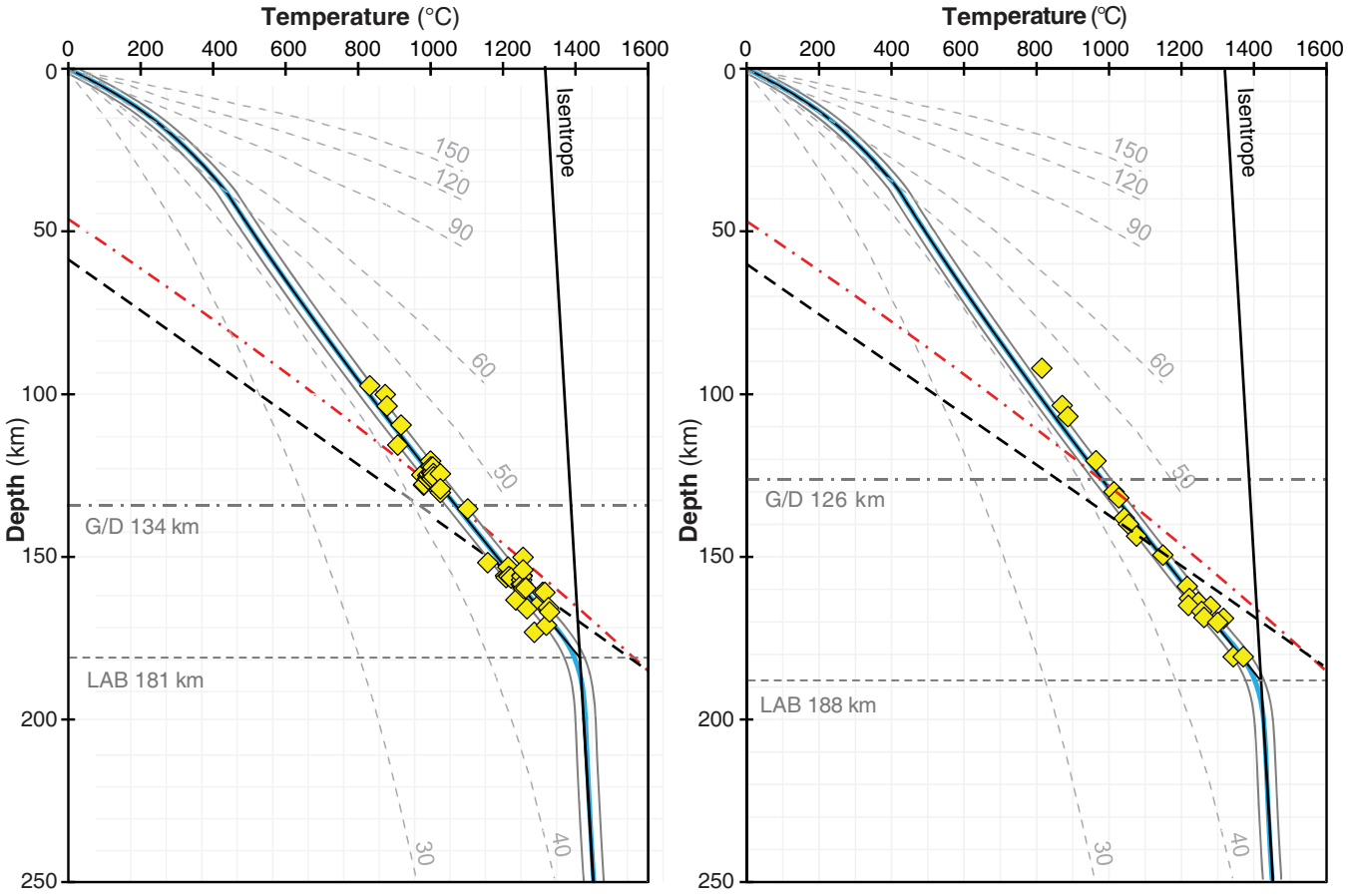

Figure 3. At the left is the *FITPLOT* paleogeotherm output for the clinopyroxene xenocrysts from Kyle Lake kimberlite (Sage, 2000). The output indicates that the paleogeotherm intersects the graphite-diamond transition (G/D) from Day (2012) at ~134 km and meets the isentrope at ~181 km (i.e. the lithosphere/asthenosphere boundary; LAB) defining a diamond window of ~47 km. At the right is the *FITPLOT* output for low- and high-temperature peridotite mantle xenoliths for the Nikos kimberlite, Somerset Island (Schmidberger et al., 2001). The output indicates that the paleogeotherm intersects the graphite-diamond transition (G/D) from Day (2012) at ~126 km and meets the isentrope at ~188 km, defining a diamond window of ~62 km. The paleogeotherms are defined by the blue lines with their associated bounding error envelopes (grey lines). The seven Pollack and Chapman (1977) reference geotherms are indicated by the lines and labelled. All other reference lines are as those described in Figure 1. The *FITPLOT* crustal thickness terms were set to 18.85 km for Kyle Lake and 18.5 km for Nikos.

mond window. Further examples will be presented during the workshop.

DIAMOND POTENTIAL

With a reliable and consistently reproducible method for obtaining paleogeotherms from *P-T* data and knowing where the paleogeotherm intersects the diamond stability field, the diamond potential of a kimberlite can now be further assessed using the available garnet xenocryst data. The process begins with each garnet xenocryst being projected onto the paleogeotherm to determine the location where the grain resided in the mantle before entrainment within the kimberlite magma. Using data for garnet xenocrysts from the Victor mine to illustrate the process (Fig. 4), the bulk of the garnet-bearing peridotitic mantle within Victor mine (~90%) was derived from the diamond stability field. Peak sampling occurred at ~150 km, with ~70% of the garnets recovered between 140 and 165 km. This information indicates a high diamond potential as there is little dilution of material from the graphite stability field.

CONCLUSIONS

The examples used in this talk are presented to illustrate the concept of assessing a kimberlite's diamond potential through determining the origins of garnet-bearing peridotitic mantle material within a kimberlite. This can be successfully and consistently accomplished through the determination of the paleogeotherm at the time of kimberlite emplacement using single-grain thermobarometry techniques and, at present, *FITPLOT*, a quantitative paleogeotherm fitting program. This technique is reliable and far more consistent and reproducible than using reference geotherms, such as those from Pollack and Chapman (1977), that do not appear to be geologically reasonable models of the lithospheric mantle.

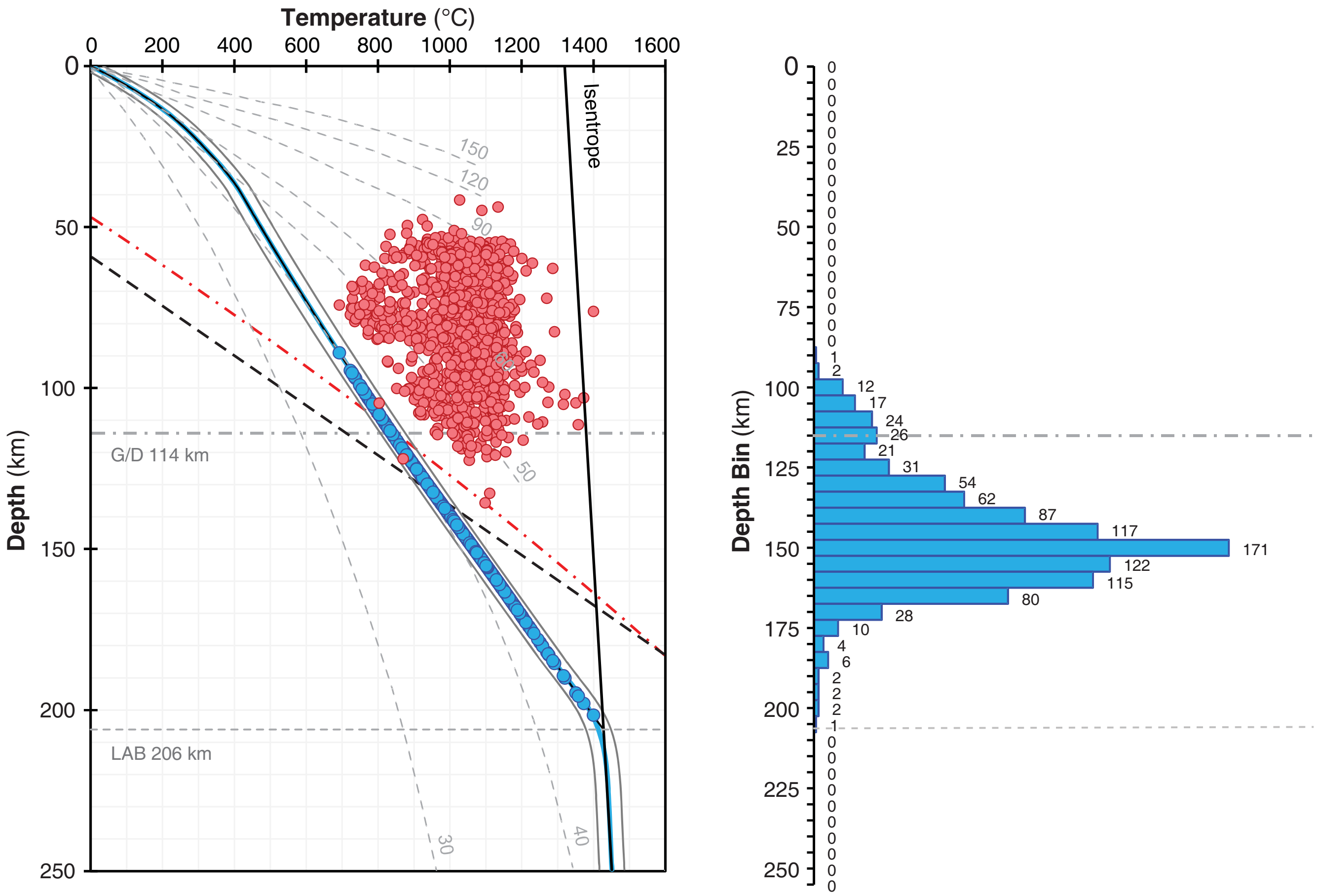

Figure 4. At left are the 997 Victor garnet xenocrysts (red circles) projected onto the clinopyroxene xenocryst derived paleogeotherm (blue circles). At right is a histogram grouping the garnet xenocryst data within 5 km bins—garnet counts per bin are listed. The histogram quickly portrays the amount of garnet-bearing mantle entrained by Victor, with ~90% originating within the diamond window and peak sampling occurring at ~150 km.

No single tool or technique supplies all the required answers. Although many of the tools have flaws and the data we use is invariably incomplete and uncertain, we should not let these limitations stop us from using the tools and data we have at hand to make decisions.

REFERENCES

Canil, D., 1994. An experimental calibration of the "Nickel in Garnet" geothermometer with applications; *Contributions to Mineralogy and Petrology*, v. 117, p. 410–420.

Canil, D., 1999. The Ni-in-garnet geothermometer: calibration at natural abundances; *Contributions to Mineralogy and Petrology*, v. 136, p. 240–246.

Cookenboo, H.O. and Grutter, H.S., 2010. Mantle-derived indicator mineral compositions as applied to diamond exploration; *Geochemistry: Exploration, Environment, Analysis*, v. 10, p. 81–95.

Day, H.W., 2012. A revised diamond-graphite transition curve; *American Mineralogist*, v. 97, p. 52–62.

Griffin, W.L., Cousens, D.R., Ryan, C.G., Sie, S.H., and Suter, G.F., 1989. Ni in chrome pyrope garnets: a new geothermometer; *Contributions to Mineralogy and Petrology*, v. 103, p. 199–202.

Griffin, W.L., O'Reilly, S.Y., Doyle, B.J., Pearson, N.J., Coopersmith, H., Kivi, K., Malkovets, V., and Pokhilenko, N., 2004. Lithosphere mapping beneath the North American plate; *Lithos*, v. 77, p. 873–922.

Grütter, H.S., 2009. Pyroxene xenocryst geotherms: Techniques and application; *Lithos*, v. 112, p. 1167–1178.

Grütter, H., Latti, D., and Menzies, A., 2006. Cr-saturation arrays in concentrate garnet compositions from kimberlite and their use in mantle barometry; *Journal of Petrology*, v. 47, p. 801–820.

Gurney, J.J., Helmstaedt, H., and Moore, R.O., 1993. A review of the use and application of mantle mineral geochemistry in diamond exploration; *Pure and Applied Chemistry*, v. 65, p. 2423–2442.

Hasterok, D. and Chapman, D.S., 2011. Heat production and geotherms for the continental lithosphere; *Earth and Planetary Science Letters*, v. 307, p. 59–70.

Heaman, L.M., Kjarsgaard, B.A., and Creaser, R.A., 2004. The temporal evolution of North American kimberlites; *Lithos*, v. 76, p. 377–397.

Januszczak, N., Seller, M.H., Kurszlaukis, S., Murphy, C., Delgaty, J., Tappe, S., Ali, K., Zhu, J., and Ellemers, P., 2013. A multidisciplinary approach to the Attawapiskat kimberlite field, Canada: accelerating the discovery-to-production pipeline, *In:* Pearson, D.G., Grütter, H.S., Harris, J.W., Kjarsgaard, B.A., O'Brien, H., Rao, N.V.C., and Sparks, S. (eds) *Proceedings of 10th International Kimberlite Conference: Volume 2*; New Delhi: Springer India, p. 157–171.

Kennedy, C.S. and Kennedy, G.C., 1976. The equilibrium boundary between graphite and diamond; *Journal of Geophysical Research*, v. 81, p. 2467–2470.

Mather, K.A., Pearson, D.G., McKenzie, D., Kjarsgaard, B.A., and Priestley, K., 2011. Constraints on the depth and thermal his-

tory of cratonic lithosphere from peridotite xenoliths, xenocrysts and seismology; *Lithos*, v. 125, p. 729–742.

McKenzie, D. and Bickle, M.J., 1988. The volume and composition of melt generated by extension of the lithosphere; *Journal of Petrology*, v. 29, p. 625–679.

Mckenzie, D., Jackson, J., and Priestley, K., 2005. Thermal structure of oceanic and continental lithosphere; *Earth and Planetary Science Letters*, v. 233, p. 337–349.

Nimis, P. and Grütter, H., 2009. Internally consistent geothermometers for garnet peridotites and pyroxenites; *Contributions to Mineralogy and Petrology*, v. 159, p. 411–427.

Nimis, P. and Taylor, W.R., 2000. Single clinopyroxene thermobarometry for garnet peridotites. Part I. Calibration and testing of a Cr-in-Cpx barometer and an enstatite-in-Cpx thermometer; *Contributions to Mineralogy and Petrology*, v. 139, p. 541–554.

Nowicki, T.E., Moore, R.O., Gurney, J.J., and Baumgartner, M.C., 2007. Diamonds and associated heavy minerals in kimberlite: A review of key concepts and applications, Chapter 46 *In:* Mange, M.A. and Wright, D.T. (eds.) *Heavy Minerals in Use; Developments in Sedimentology*, v. 58, p. 1235–1267.

Pollack, H.N. and Chapman, D.S., 1977. On the regional variation of heat flow, geotherms, and lithospheric thickness; *Tectonophysics*, v. 38, p. 279–296.

Ryan, C.G., Griffin, W.L., and Pearson, N.J., 1996. Garnet geotherms: Pressure-temperature data from Cr-pyrope garnet xenocrysts in volcanic rocks; *Journal of Geophysical Research: Solid Earth*, v. 101, p. 5611–5625.

Sage, R.P., 2000. *Kimberlites of the Attawapiskat area, James Bay Lowlands, northern Ontario*; Ontario Geological Survey, Open File Report 6019, 341 p.

Schmidberger, S.S., Simonetti, A., and Francis, D., 2001. Sr-Nd-Pb isotope systematics of mantle xenoliths from Somerset Island kimberlites: Evidence for lithosphere stratification beneath Arctic Canada; *Geochimica et Cosmochimica Acta*, v. 65, p. 4243–4255.

Scully, K.R., 2000. *Mantle xenoliths from the Attawapiskat kimberlite field*; M.Sc. thesis, University of Toronto.

Stachel, T. and Harris, J.W., 2008. The origin of cratonic diamonds — Constraints from mineral inclusions; *Ore Geology Reviews*, v. 34, p. 5–32.

Tesauro, M., Kaban, M.K., Mooney, W.D., and Cloetingh, S., 2014. $NACr_{14}$: A 3-D model for the crustal structure of the North American Continent; *Tectonophysics*, v. 631, p. 65–86.

Ziberna, L., Nimis, P., Kuzmin, D., and Malkovets, V.G., 2016. Error sources in single-clinopyroxene thermobarometry and a mantle geotherm for the Novinka kimberlite, Yakutia; *American Mineralogist*, v. 101, p. 2222–2232.

Trace element signatures of magmatic sulphides: petrogenetic implications and exploration applications

C.J. Duran[1*], S-J. Barnes[1], P. Pagé[1,2], H. Dubé-Loubert[3,4], M. Roy[4], and D. Savard[1]

[1]Université du Québec à Chicoutimi, 555 boulevard de l'Université, Chicoutimi, Quebéc, Canada G7H 2B1

[2]IOS services géoscientifiques, 1319 boulevard Saint-Paul, Chicoutimi, Quebéc, Canada G7J 3Y2

[3]Bureau de la Connaissance Géoscientifique du Québec, Ministère de l'Énergie et des Ressources Naturelles, 400 boulevard Lamaque, Val-d'Or, Québec, Canada J9P 3L4

[4]Université du Québec à Montréal, 201 avenue du Président-Kennedy, Montréal, Québec, Canada H2X 3Y7

*(*Corresponding author's e-mail: charley.duran@hotmail.fr)*

Sulphide minerals form in a wide variety of environments, e.g., crystallizing from magmatic sulphide liquid segregated from mafic/ultramafic magmas at 1200°C, to crystallizing from the reaction of detrital Fe-minerals with H_2S as a result of bacterial sulphate reduction during the shallow burial of sediments. The different conditions of sulphide formation lead to distinctive signatures in trace elements, which can now be easily determined through laser ablation inductively coupled plasma mass spectrometry (LA-ICP-MS). Although studies of sulphide trace element signatures in magmatic and hydrothermal environments have provided deeper insights into ore genesis (e.g. Barnes et al., 2008; Large et al., 2009; Duran et al., 2016; George et al., 2017), the chemistry of sulphide indicator minerals has not received attention, despite their abundance in ore deposits, rarity in barren rocks, and variable compositions. Sulphide minerals were neglected because of the popular belief that they cannot be preserved in surface media due to oxidation processes when exposed to the atmosphere or oxygenated surface water (e.g. Rosso and Vaughan, 2006). However, burial rates are fast in glaciated terrains and, in general, glacial sediments are relatively impermeable, which results in very limited chemical weathering. Thus, characterizing the mineral chemistry of these sulphide minerals, which are commonly preserved and can be abundant in till samples (e.g. Sarala and Peuraniemi, 2007; McClenaghan et al., 2011; Peuraniemi and Eskola, 2013), allows discrimination of different deposit styles at the geological province scale. This contribution presents a review of the trace element signatures of magmatic sulphides, with an emphasis on global petrogenetic implications and methods of discriminating magmatic and hydrothermal sulphides based on their trace element chemistry. Finally, an example from the Churchill Province in northern Quebec is presented that highlights the strong potential for magmatic and hydrothermal mineralization in this under-explored area as well as the usefulness of indicator mineral chemistry for exploration in glaciated terrains.

TRACE ELEMENT SIGNATURES OF MAGMATIC SULPHIDES AS PETROGENETIC INDICATORS

The trace element compositions of magmatic sulphides may be affected by several parameters: the degree of fractionation of the parental silicate magma, the silicate-to-sulphide ratio (R factor), contamination, deformation, and alteration (Duran et al., 2015, 2016 and references therein). The degree of fractionation of the parental silicate magma is reflected in the profile of primitive-mantle-normalized multi-element patterns. Pyrrhotite and pentlandite grains derived from primitive magmas, such as those from the komatiite at the Rosie Nickel Prospect, Western Australia, have relatively unfractionated platinum group element (PGE) patterns (Fig. 1a) whereas pyrrhotite and pentlandite grains derived from evolved magmas, such as those from Lac des Iles, Ontario, have very fractionated PGE patterns (Fig. 1a). The concentration of trace elements in magmatic sulphides is mainly controlled by their partition coefficients and the R factor. Elements with the highest partition coefficients for sulphides (i.e. PGE) are more enriched when the R factor increases, but the shape of the primitive mantle normalized multi-element patterns remains the same. This can be seen when comparing sulphides from the same system (Fig. 1a) that have different R factors (i.e. disseminated sulphides vs. massive sulphides). When the magma is contaminated, S and TABS (Te, As, Bi, Sb, and Sn) are added to the magma. Because these elements have low partition coefficients for sulphides, they are only weakly affected by the R factor. Thus, sulphides derived from strongly contaminated magmas have higher concentrations relative to sulphides derived from weakly contaminated magmas (Fig. 1a). When

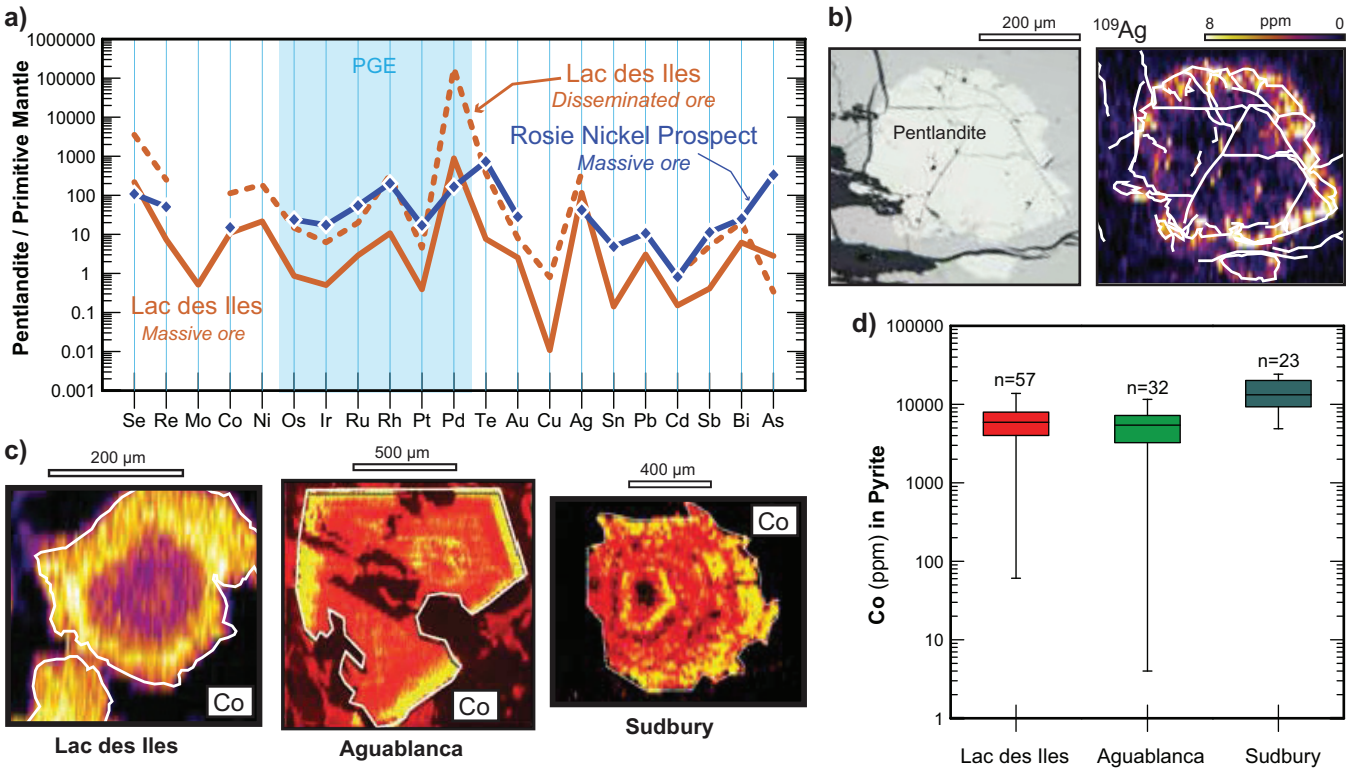

Figure 1. Examples of the use of trace element signatures of magmatic sulphides as petrogenetic indicator (modified from Duran et al., 2015, 2016). **a)** Primitive mantle normalized multi-element patterns of pentlandite from Lac des Iles massive and disseminated ores and Rosie Nickel prospect massive ore (see text for details). **b)** LA-ICP-MS elemental map of pentlandite from Lac des Iles showing enrichment of Ag along grain boundaries. **c)** LA-ICP-MS elemental maps of pyrite grains from Lac des Iles, Aguablanca, and Sudbury showing Co zonation. **d)** A box-and-whisker plot of Co concentrations in pyrite grains from Lac des Iles, Aguablanca, and Sudbury showing similar compositions.

the sulphides are deformed, elements with large ionic radii, such as Pb, Ag, and Bi, are concentrated along grain boundaries (Fig. 1b). Mineral replacement reactions during alteration of magmatic sulphides (replacement of pyrrhotite by pyrite) leads to the redistribution of the elements in the pyrite. Studies of magmatic ore deposits have shown that pyrite is similarly enriched in Co-Se and As-Rh-Ir-Os-Ru relative to pyrrhotite and pentlandite, and that these elements form antithetical concentric zonation (Fig. 1c,d). These features have been interpreted to be the result of a similar re-equilibration process occurring in magmatic ore deposits during alteration.

DISCRIMINATION OF SULPHIDES

Pentlandite essentially occurs in magmatic sulphide deposits, which may be broadly divided in two groups: PGE-dominated deposits and Ni-Cu sulphide deposits. Compilation of trace element data reveals that pentlandite from the PGE-dominated deposits (Oberthür et al., 1997; Barnes et al., 2006, 2008; Godel et al., 2007; Holwell and McDonald, 2007; Godel and Barnes, 2008; Djon and Barnes, 2012; Smith et al., 2014; Duran et al., 2016) can be distinguished from pentlandite from Ni-Cu sulphide deposits (Dare et al., 2010; Godel et al., 2012; Piña et al., 2012; Chen et al., 2014). Most pentlandite from PGE-dominated deposits has Pd concentrations of >10 ppm, whereas pentlandite from Ni-Cu sulphide deposits has Pd concentrations of <10 ppm. Moreover, pentlandite from PGE-dominated deposits has Rh concentrations of >1 ppm, whereas pentlandite from Ni-Cu sulphide deposits has Rh concentrations of <1 ppm. An exception to this is the pentlandite from Lac des Iles, which has Rh concentrations of between 0.01 and 1 ppm. However, pentlandite from Lac des Iles is still distinguishable from pentlandite from Ni-Cu sulphide deposits based on its higher Pd concentrations. These observations have a strong potential for use in discriminating between PGE-dominated and Ni-Cu sulphide deposits. A plot of Pd in pentlandite versus Rh in pentlandite (Fig. 2a) may be used to discriminate provenance (Duran et al., 2016).

In Ni-Cu-PGE deposits, pyrite typically occurs as an alteration product of a primary magmatic mineralization (Duran et al., 2015). A compilation of trace element data reveals that pyrite from Ni-Cu-PGE deposits can be distinguished from pyrite from hydrothermal deposits (volcanogenic massive sulphides (VMS), orogenic gold deposits, and Cu-porphyries). Pyrite from Ni-Cu-PGE deposits generally contains thousands of ppm of Co and hundreds of ppm of Se whereas hydrothermal pyrite generally contain a few to hun-

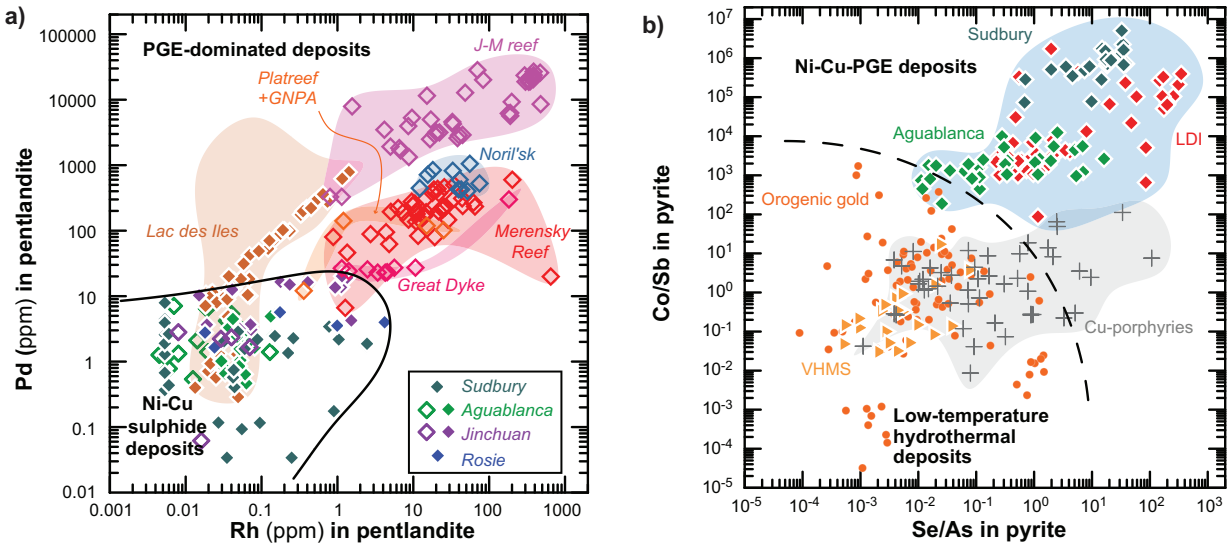

Figure 2. a) Binary plot of Pd versus Rh in pentlandite allowing discrimination between pentlandite from PGE-dominated deposits and pentlandite from Ni-Cu sulphide deposits (Duran et al., 2016). **b)** Binary plot of Co/Sb versus Se/As in pyrite allowing discrimination between pyrite from magmatic deposits and pyrite from hydrothermal deposits (Duran et al., 2015).

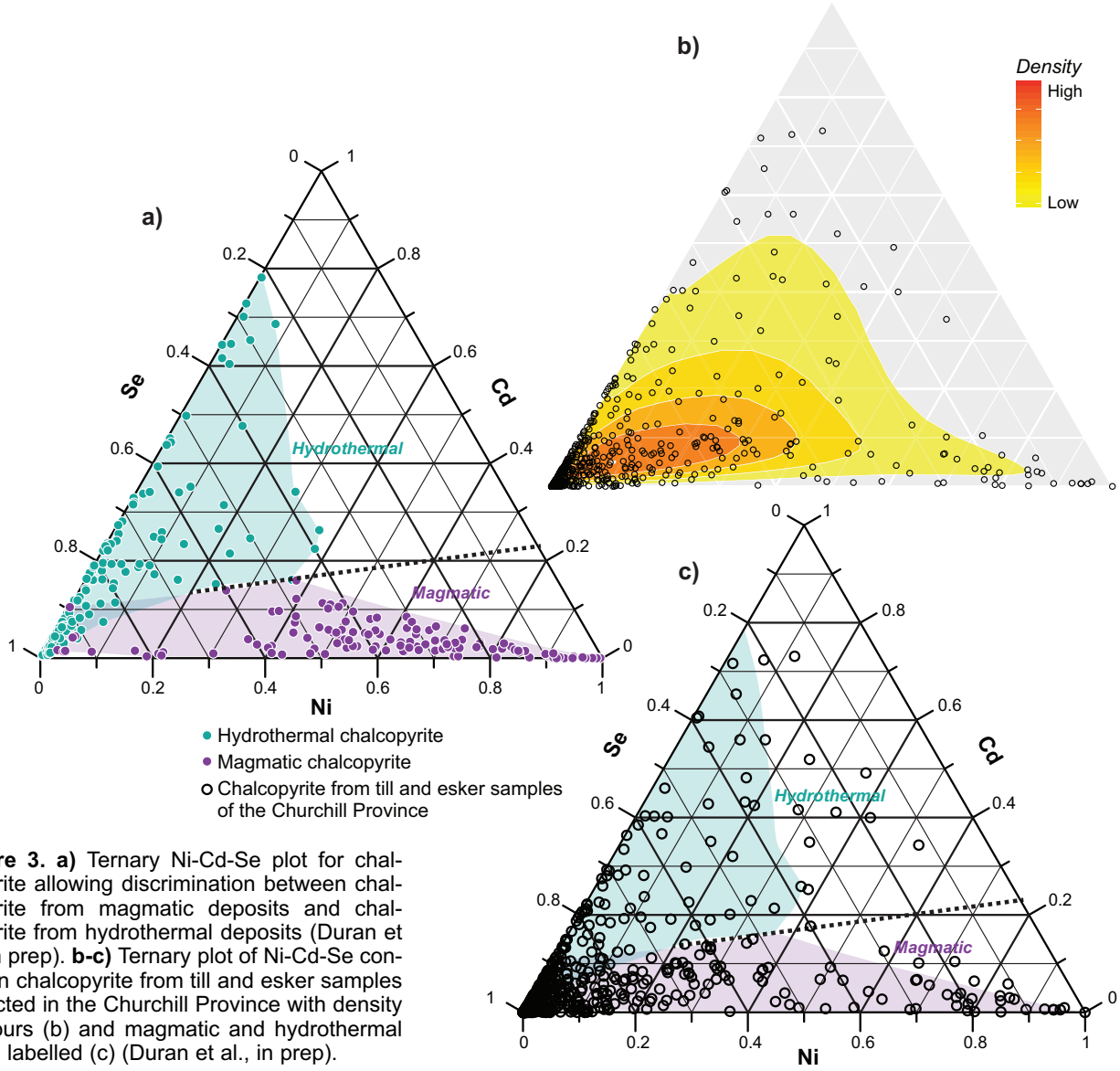

Figure 3. a) Ternary Ni-Cd-Se plot for chalcopyrite allowing discrimination between chalcopyrite from magmatic deposits and chalcopyrite from hydrothermal deposits (Duran et al., in prep). **b-c)** Ternary plot of Ni-Cd-Se content in chalcopyrite from till and esker samples collected in the Churchill Province with density contours (b) and magmatic and hydrothermal fields labelled (c) (Duran et al., in prep).

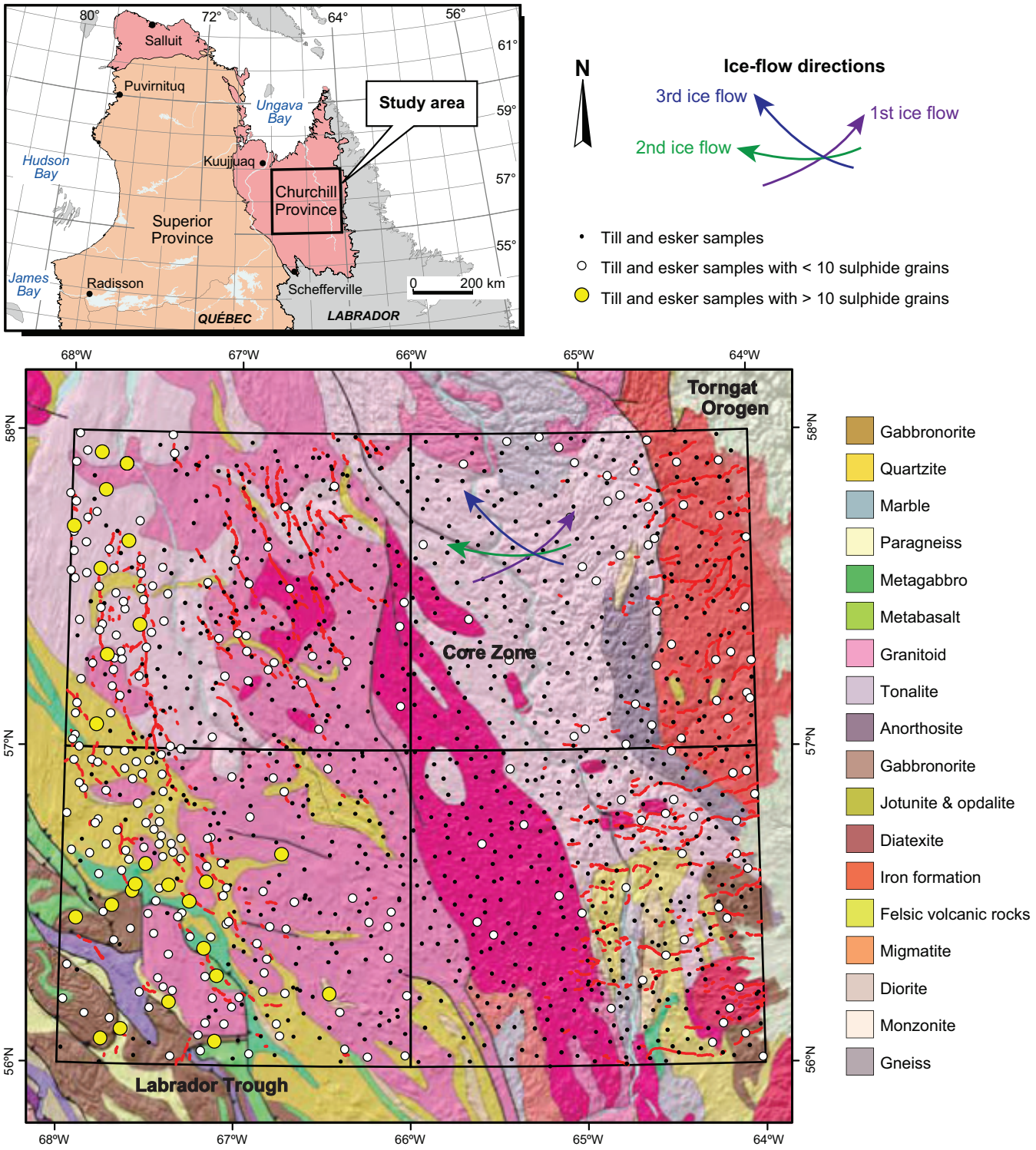

Figure 4. Bedrock geology map of the study area in the Churchill Province, northern Quebec, showing lithologies, till and esker samples with sulphide content, and ice-flow directions (three arrows) (Duran et al., in prep).

dreds of ppm of Co and a few ppm of Se. In contrast, hydrothermal pyrite generally contains thousands of ppm of As and hundreds of ppm of Sb, whereas pyrite from Ni-Cu-PGE deposits generally contains a few to hundreds of ppm of As and a few ppm of Sb. Therefore, a plot of Co/Sb versus Se/As (Duran et al., 2015) may be used to discriminate the provenance of the pyrite (Fig. 2b). Pyrite from Ni-Cu-PGE deposits (Dare et al., 2011; Piña et al., 2013; Duran et al., 2015) has high (~1000–10000000) Co/Sb and high (~0.01–1000) Se/As values whereas pyrite from low-temperature hydrothermal (i.e. orogenic gold deposits, VMS) and sedimentary deposits (Large et al., 2009; Maslennikov et al., 2009; Thomas et al., 2011; Revan et al., 2014)

has low (~1000–0.00001) Co/Sb and (~1–0.0001) Se/As values. Although pyrite from Cu-porphyries may have high (up to 100) Se/As values (Reich et al., 2013) as has pyrite from Ni-Cu-PGE deposits, it still may be discriminated based on its low Co content.

Chalcopyrite occurs in magmatic Ni-Cu-PGE deposits and in a variety of hydrothermal deposits (epithermal, skarn, VMS, sedimentary exhalative (SEDEX)). Unlike pentlandite and pyrite, chalcopyrite is only minimally enriched in trace elements because its composition is largely influenced by co-crystallizing sulphides. However, some elements do allow for the discrimination of magmatic and hydrothermal chalcopyrite. Magmatic chalcopyrite is usually richer in Ni (thousands of ppm) and Se (hundreds of ppm) and poorer in Cd (<10 ppm) (Barnes et al., 2008; Dare et al., 2010, 2011, 2014; Piña et al., 2012; Chen et al., 2014; Duran et al., 2016) relative to hydrothermal chalcopyrite (George et al., 2017). Hydrothermal chalcopyrite has also very variable Cd (1–100 ppm) and Se (1–1000 ppm) content (George et al., 2017). Thus, a ternary plot of Ni-Cd-Se (Fig. 3a) makes it possible to discriminate between magmatic and hydrothermal chalcopyrite: two trends are defined (1) a magmatic trend from the Se apex towards the Ni apex and (2) a hydrothermal trend from the Se apex towards the Cd apex (Duran et al., in prep).

APPLICATION FOR EXPLORATION: AN EXAMPLE FROM THE CHURCHILL PROVINCE, NORTHERN QUEBEC

The Churchill Province in northern Quebec consists of Archean to Proterozoic basement rocks, which have undergone a complex orogenic and metamorphic history (Clark and Wares, 2004; Lafrance et al., 2013). The vast majority of these rocks are covered by Quaternary glacial deposits that display a complex geomorphology that reflects important variations in the glacial dynamics (Clark et al., 2000; Dubé-Loubert et al., 2014a,b, 2016). Occasional mineralized outcrops have been identified in the area during mapping surveys. The area south from Ungava Bay in the Churchill Province has been under-explored owing to the sedimentary cover, which has limited the effectiveness of conventional exploration methods. However, as a result this area is ideal to test the use of sulphide indicator mineral chemistry for mineral assessment and vectoring.

Till and esker samples were collected in the area and heavy mineral concentrates were prepared. The concentrates of the samples collected along the boundary between the Labrador Trough and the Core Zone (Fig. 4) were found to contain thousands of sulphide grains, namely pyrite and chalcopyrite with lesser amounts of arsenopyrite/löllingite, which is indicative of the

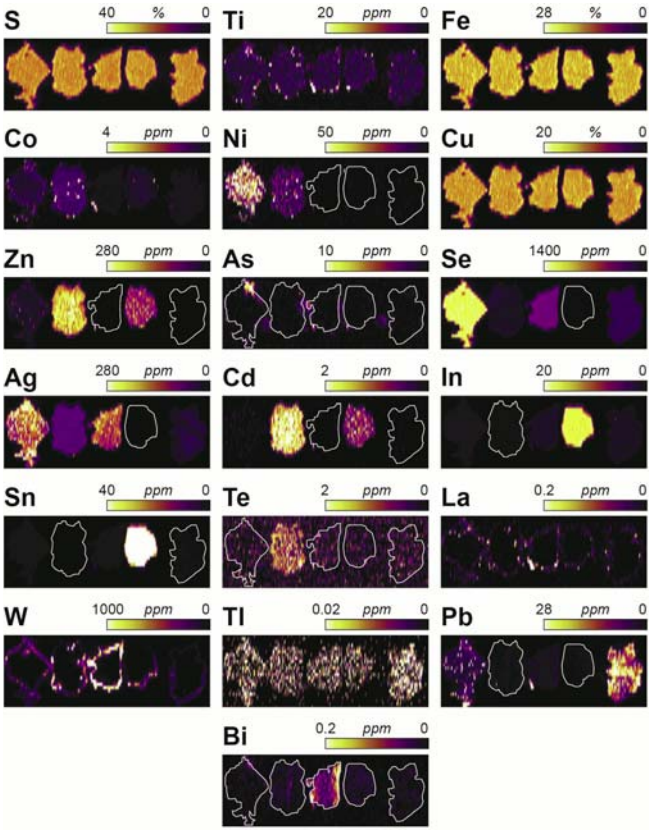

Figure 5. Multi-grain LA-ICP-MS elemental map of chalcopyrite grains from this study showing various trace element compositions. From Duran et al., (in prep).

underlying mineralized rocks. The sulphide grains ranged from unaltered to moderately altered with a thin oxidation corona that is enriched in W and La (Fig. 5), which is a reflection of the mobility of theses elements in the sediment matrix. No other elements were found to display this relationship with the oxidation corona (Fig. 5), indicating that the concentrations of the other elements in the sulphides reflect the original composition. Most pyrite grains display trace element zoning patterns similar to those observed in pyrite from magmatic and hydrothermal deposits. However, on a binary plot of Co/Sb versus Se/As (not shown), most of the pyrite grains plotted in the magmatic field. Only a small population of pyrite falls in the hydrothermal field and these grains appear to be enriched in Au. Chalcopyrite grains do not display zoning patterns (Fig. 5). However, multi-grain LA-ICP-MS elemental maps exhibit strong compositional variations (Fig. 5). On a ternary Ni-Cd-Se plot (Fig. 3b,c), chalcopyrite grains were found to follow the magmatic and hydrothermal trends.

The results of this study reveal multiple sources for the sulphide minerals present in the glacial deposits and suggest there is strong potential for magmatic and hydrothermal mineralization. Future work aims at reconciling the chemistry of the sulphide indicator miner-

als with the geology of the glacial deposits to delineate vectors toward potential economic targets.

CONCLUSIONS

Sulphide grains collected from heavy mineral concentrates of till and esker samples display trace element compositions that are a reflection of the environment of their formation. Important information can be learned about ore-forming processes from the trace element signatures of magmatic sulphides, such as the degree of fractionation of the parental silicate magma, R factor, contamination, deformation, and alteration. Pentlandite from PGE-dominated deposits can be discriminated from pentlandite from Ni-Cu sulphide deposits based on Pd and Rh concentrations. Pyrite from magmatic deposits can be differentiated from pyrite from hydrothermal deposits based on Co/Sb and Se/As values. Chalcopyrite from magmatic deposits can be discriminated from chalcopyrite from hydrothermal deposits based on Ni, Cd, and Se concentrations.

With discovery of outcropping and subcropping ore deposits on the wane, developing new exploration methods for targeting deeply buried ore deposits has become critical. There are vast areas that have been affected by glaciation and are covered with thick glacial deposits, limiting the usefulness of conventional mineral-targeting methods. To overcome this, till geochemical and indicator mineral methods are evolving to provide vectors to underlying mineral resources (e.g. McClenaghan, 2005; McClenaghan et al., 2014). These methods have proved to be effective in exploration for a wide range of ore deposit types (Averill, 2001, 2011). In addition, the chemistry of indicator minerals can be used to amplify the ore signature, which can be diluted by the till background signature. As shown in this example utilizing glacial deposits of the Churchill Province, the trace element signatures of sulphide minerals can be used to discriminate different deposit styles. These promising results indicates that further work is warranted to identify more discriminants and to test other cases.

ACKNOWLEDGEMENTS

The work presented here has been financially supported by North American Palladium and the Ministère de l'Énergie et des Ressources Naturelles of Québec via the Canada Research Chair in Magmatic Ore deposits.

REFERENCES

Averill, S., 2001. The application of heavy indicator mineralogy in mineral exploration, with emphasis on base metal indicators in glaciated metamorphic and plutonic terrain, *In:* McClenaghan, M.B., Bobrowsky, P.T., Hall, G.E.M., and Cook, S.J. (eds), *Drift Exploration in Glaciated Terrain*; Geological Society, London, Special Publications 185, p. 69–81.

Averill, S.A., 2011. Viable indicator minerals in surficial sediments for two major base metal deposit types: Ni-Cu-PGE and porphyry Cu; *Geochemistry: Exploration, Environment, Analysis*, v. 11, p. 279–291.

Barnes, S-J., Cox, R.A., and Zientek, M.L., 2006. Platinum-group element, gold, silver and base metal distribution in compositionally zoned sulfide droplets from the Medvezky Creek Mine, Noril'sk, Russia; *Contributions to Mineralogy and Petrology*, v. 152, p. 187–200.

Barnes, S-J., Prichard, H.M., Cox, R.A., Fisher, P.C., and Godel, B., 2008. The location of the chalcophile and siderophile elements in platinum group element ore deposits (a textural, microbeam and whole rock geochemical study): implications for the formation of the deposits; *Chemical Geology*, v. 248, p. 295–317.

Chen, L-M., Song, X-Y., Danyushevsky L.V., Wang, Y-S., Tian, Y-L., and Xiao, J-F., 2014. A laser ablation ICP-MS study of platinum-group and chalcophile elements in base metal sulfide minerals of the Jinchuan Ni–Cu sulfide deposit, NW China; *Ore Geology Reviews*, v. 65, p. 955–967.

Clark, T. and Wares, R., 2004. Synthèse lithotectonique et métallogénique de l'Orogène du Nouveau-Québec (Fosse du Labrador); Ministère des Ressources naturelles, de la Faune et des Parcs, Québec, MM 2004-01.

Clark, C.D., Knight, J.K., and Gray, J.T., 2000. Geomorphological reconstruction of the Labrador sector of the Laurentide Ice Sheet; *Quaternary Science Reviews*, v. 19, p. 1343–1366.

Dare, S.A.S., Barnes, S-J., and Prichard, H.M., 2010. The distribution of platinum group elements and other chalcophile elements among sulfides from the Creighton Ni–Cu–PGE sulfide deposit, Sudbury, Canada, and the origin of Pd in pentlandite; *Mineralium Deposita*, v. 45, p. 765–793.

Dare, S.A.S., Barnes, S-J., Prichard, H.M., and Fisher, P.C., 2011. Chalcophile and platinum-group element (PGE) concentrations in the sulfide minerals from the McCreedy East deposit, Sudbury, Canada, and the origin of PGE in pyrite; *Mineralium Deposita*, v. 46, p. 381–407.

Dare, S.A.S., Barnes, S-J., Prichard, H.M., and Fisher, P.C., 2014. Mineralogy and geochemistry of Cu-rich ores from the McCreedy East Ni-Cu-PGE deposit (Sudbury, Canada): Implications for the behavior of platinum group and chalcophile elements at the end of crystallization of a sulfide liquid; *Economic Geology*, v. 109, p. 343–366.

Djon, M.L.N. and Barnes, S-J., 2012. Changes in sulphides and platinum-group minerals with the degree of alteration in the Roby, Twilight, and High-Grade Zones of the Lac des Iles Complex, Ontario, Canada; *Mineralium Deposita*, v. 47, p. 875–896.

Dubé-Loubert, H., Daubois, V., and Roy, M., 2014a. *Géologie des dépôts de surface de la région du lac Saffray (24G)*; Ministère de l'Énergie et des Ressources naturelles, Québec, RP-2014-06.

Dubé-Loubert, H., Daubois, V., and Roy, M., 2014b. *Géologie des dépôts de surface de la région du lac Brisson (24A)*; Ministère de l'Énergie et des Ressources naturelles, Québec, RP-2016-03.

Dubé-Loubert, H., Daubois, V., and Roy, M., 2016. *Géologie des dépôts de surface de la région du lac Henrietta (24H)*; Ministère de l'Énergie et des Ressources naturelles, Québec, RP-2016-01.

Duran, C.J., Barnes, S-J., and Corkery, J.T., 2015. Chalcophile and platinum-group element distribution in pyrites from the sulfide-rich pods of the Lac des Iles Pd deposits, Western Ontario, Canada: Implications for post-cumulus re-equilibration of the ore and the use of pyrite compositions in exploration; *Journal of Geochemical Exploration*, v. 158, p. 223–242.

Duran, C.J., Barnes, S-J., and Corkery, J.T., 2016. Trace element distribution in primary sulfides and Fe–Ti oxides from the sulfide-rich pods of the Lac des Iles Pd deposits, Western Ontario,

Canada: Constraints on processes controlling the composition of the ore and the use of pentlandite compositions in exploration; *Journal of Geochemical Exploration*, v. 166, p. 45–63.

George, L.L., Cook, N.J., Crowe, B.B.P., and Ciobanu, C.L., 2017. Trace elements in hydrothermal chalcopyrite; *Mineralogical Magazine*, doi.org/10.1180/minmag.2017.081.021

Godel, B. and Barnes, S-J., 2008. Platinum-group elements in sulfide minerals and the whole rocks of the J-M Reef (Stillwater Complex): Implication for the formation of the reef; *Chemical Geology*, v. 248, p. 272–294.

Godel, B., Barnes, S-J., and Maier, W.D., 2007. Platinum-group elements in sulfide minerals, platinum-group minerals, and whole-rocks of the Merensky Reef (Bushveld Complex, South Africa): Implications for the formation of the reef; *Journal of Petrology*, v. 48, p. 1569–1604.

Godel, B., González-Álvarez, I., Barnes, S.J., Barnes, S-J., Parker, P., and Day J., 2012. Sulfides and sulfarsenides from the Rosie Nickel Prospect, Duketon greenstone belt, Western Australia; *Economic Geology*, v. 107, p. 275–294.

Holwell, D.A. and McDonald, I., 2007. Distributions of platinum-group elements in the Platreef at Overysel, northern Busveld Complex: A combined PGM and LA-ICP-MS study; *Contribution to Mineralogy and Petrology*, v. 154, p. 171–190.

Lafrance, I., Simard, M., and Bandyayera, D., 2013. *Géologie de la région du lac Saffray (SNRC 24G, 24F)*; Ministère des Ressources Naturelles, Rapport Géologique 2014-02.

Large, R.R., Danyushevsky, L., Hollit, C., Maslennikov, V., Meffre, S., Gilbert, S., Bull, S., Scott, R., Emsbo, P., Thomas, H., Singh, B., and Foster, J., 2009. Gold and trace element zonation in pyrite using a laser imaging technique: implications for the timing of gold in orogenic and carlin-style sediment-hosted deposits; *Economic Geology*, v. 104, p. 635–668.

Maslennikov, V.V., Maslennikova, S.P., Large, R.R., and Danyushevsky, L.V., 2009. Study of trace element zonation in vent chimneys from the Silurian Yaman-Kasy volcanic-hosted massive sulfide deposit (Southern Urals, Russia) using laser ablation-inductively coupled plasma mass spectrometry (LA-ICPMS); *Economic Geology*, v. 104, p. 1111–1141.

McClenaghan, M.B., 2005. Indicator mineral methods in mineral exploration; *Geochemistry: Exploration, Environment, Analysis*, v. 5, p. 233–245.

McClenaghan, M.B., Averill, S.A., Kjarsgaard, I.M., Layton-Matthews, D., and Matile, G., 2011. Indicator mineral signatures of magmatic Ni-Cu deposits, Thompson Nickel Belt, central Canada, *In:* McClenaghan, B., Peuraniemi, V., and Lehtonen, M. (eds), *Indicator Mineral Methods in Mineral Exploration*; Workshop in the 25th International Applied Geochemistry Symposium 2011, 22-26 August 2011 Rovaniemi, Finland. Vuorimiesyhdistys, p. B92-4.

McClenaghan, M.B., Plouffe, A., and Layton-Matthews, D. (eds), 2014. *Application of indicator mineral methods to mineral exploration*; Geological Survey of Canada, Open File 7553.

Oberthür, T., Cabri, L.J., Weiser, T.W., McMahon, G., and Müller P., 1997. Pt, Pd and other trace elements in sulphides of the Main sulfide zone, Great Dyke, Zimbabwe: A reconnaissance study; *The Canadian Mineralogist*, v. 35, p. 597–609.

Peuraniemi, V. and Eskola, T., 2013. Glacial dispersal and mode of occurrence of metals in till and esker gravel at Kumpuselkä, northern Finland; *Geochemistry: Exploration, Environment, Analysis*, v. 13, p. 195–203.

Piña, R., Gervilla, F., Barnes, S-J., Ortega, L., and Lunar, R., 2012. Distribution of platinum- group and chalcophile elements in the Aguablanca Ni–Cu sulfide deposit (SW Spain): Evidence from a LA-ICP-MS study; *Chemical Geology*, v. 302–303, p. 61–75.

Piña, R., Gervilla, F., Barnes, S-J., Ortega, L., and Lunar, R., 2013. Platinum-group elements-bearing pyrite from the Aguablanca Ni-Cu sulphide deposit (SW Spain): a LA-ICP-MS study; *European Journal of Mineralogy*, v. 25, p. 241–252.

Reich, M., Deditius, A., Chryssoulis, S., Li, J-W., Ma, C-Q., Parada, M.A., Barra, F., and Mittermayr, F., 2013. Pyrite as a record of hydrothermal fluid evolution in a porphyry copper system: A SIMS/EMPA trace element study; *Geochimica and Cosmochimica Acta*, v. 104, p. 42–62.

Revan, M.K., Genç, Y., Maslennikov, V.V., Maslennikova, S.P., Large, R.R., and Danyushevsky, L.V., 2014. Mineralogy and trace-element geochemistry of sulfide minerals in hydrothermal chimneys from the Upper Cretaceous VMS deposits of the eastern Pontide orogenic belt (NE Turkey); *Ore Geology Reviews*, v. 63, p. 129–149.

Rosso, K.M. and Vaughan, D.J., 2006. Reactivity of sulfide mineral surfaces; *Reviews in Mineralogy and Geochemistry,* v. 61, p. 557–607.

Sarala, P. and Peuraniemi, V., 2007. Exploration using till geochemistry and heavy minerals in the ribbed moraine area of southern Finnish Lapland; *Geochemistry: Exploration, Environment, Analysis*, v. 7, p. 195–205.

Smith, J.W., Holwell, D.A., and McDonald, I., 2014. Precious and base metal geochemistry and mineralogy of the Grasvally Norite-Pyroxenite-Anorthosite (GNPA) member, northern Bushveld Complex, South Africa: implications for a multistage emplacement; *Mineralium Deposita*, v. 49, p. 667–692.

Thomas, H.V., Large, R.R., Bull, S.W., Maslennikov, V., Berry, R.F., Fraser, R., Froud, S., and Moye, R., 2011. Pyrite and pyrrhotite textures and composition in sediments, laminated quartz veins, and reefs at Bendigo gold mine, Australia: insights for ore genesis; *Economic Geology*, v. 106, p. 1–31.

Scheelite as a possible ore-deposit discriminator based on luminescence, trace-element chemistry, $\delta^{18}O$ signature, fluid inclusions, and U-Pb geochronology

D.J. Kontak[1*], A.M. McDonald[1], R. Poulin[1], J. Petrus[1], and M.B. McClenaghan[2]

[1]Harquail School of Earth Sciences, Laurentian University, Sudbury, Ontario, Canada P3E 2C6
[2]Geological Survey of Canada, 601 Booth Street, Ottawa, Ontario, Canada K1A 0E8
*(*Corresponding author's e-mail: dkontak@laurentian.ca)*

Scheelite and wolframite are the main host minerals for tungsten and their production is dominated by intrusion-related ore deposit settings, specifically skarns (i.e. calc-silicate assemblages), and quartz-vein types, respectively (Kwak, 1987). The high density and robustness of tungsten combined with its high melting point and ability to alloy with other metals facilitates its numerous technical applications (e.g. X-ray tubes, welding, superalloys, radiation shields, projectiles). The primary global supplier of tungsten is China due to a few very large skarn-type deposits. The most recent production figures (2016, https://minerals.usgs.gov/minerals/pubs/commodity) indicate that of the approximately 90,000 T of global production, China accounted for 73,000 T, with Vietnam a distant second at 5,600 T and Canada fifth at 1,680 T, the latter from the intermittently open Cantung deposit in the Northwest Territories. The price of ferrotungsten has varied over the past 10 to 15 years between US$25 and US$55 per kg; the price has currently (2017) retreated to the low end of this range. The large fluctuation in price reflects, in part, the dominance of a single supplier and related stockpiles reflects the opening and closing of several producers globally, including producers of both scheelite and wolframite. The forecast however is for tungsten to gain strength due to an increase in demand; this bodes well for such deposits as the world-class Sisson W-Mo deposit in New Brunswick, Canada. Given the importance of tungsten for specific high-tech applications, ensuring a steady supply has become an issue of concern for many countries, several of which have targeted it as a critical metal requiring attention.

The presence of tungsten in the form of both scheelite and wolframite is not uncommon in other deposit types, which includes both orogenic and intrusion-related gold, some epithermal settings, and some rare-metal pegmatites, to name but a few examples (see Kwak (1987) for a review of tungsten deposits). In fact, there has even been historical production of W, as scheelite, from some of these deposits, with the sediment-hosted orogenic Au-W deposits in the Otago Schists, New Zealand, and the Meguma Group, Nova Scotia, being classic examples.

The fact that tungsten occurs as an accessory phase in a variety of deposit types provides the focus of this paper. This latter feature, combined with the high density and hardness of its two main host minerals, and hence its robustness during transport and weathering, provided the basis of exploring the potential of scheelite and wolframite as pathfinder or indicator minerals, also called resistate indicator minerals (RIMs), in a similar manner as garnet is used in exploration for diamondiferous kimberlites. McClenaghan et al. (2013) provide a review of the use of tungsten indicator minerals and in subsequent work the successful application of this concept with a case study of the Sisson W-Mo deposit, where they demonstrated that both minerals were dispersed during glacial erosion and transport and could, therefore, prove useful in exploration locally and elsewhere in similar geological settings and terrains (McClenaghan et al., 2017). An unanswered part of their study, however, was whether these minerals also had the ability to discriminate ore-deposit types, which is a critical aspect in exploration. The latter is particularly relevant for scheelite, as it is also associated with, for example, orogenic- and intrusion-related gold (IRG) deposits. Thus, as part of the Geological Survey of Canada's Targeted Geoscience Initiative program (TGI-4), a project was initiated to address this deficiency and to provide the first geochemical database specifically for scheelite using laser ablation inductively coupled mass spectrometry (LA ICP-MS). The latter method, with the capacity to rapidly and cost-effectively analyse small grains at low levels of detection (ppm), provided the means to explore the chemistry of scheelite.

This paper summarizes the results of our study on scheelite chemistry, which formed the basis of a M.Sc. project at Laurentian University (Poulin, 2016). This work addressed two aspects, the nature of luminescence in scheelite and its minor- and trace-element geochemistry. In addition, a preliminary investigation into the use of its $\delta^{18}O$ signature was also undertaken. The results of the former have recently been published (Poulin et al., 2016a), whereas the latter work on chemistry and isotopes has been presented at a variety of venues (e.g. Poulin et al., 2016b) and is currently under

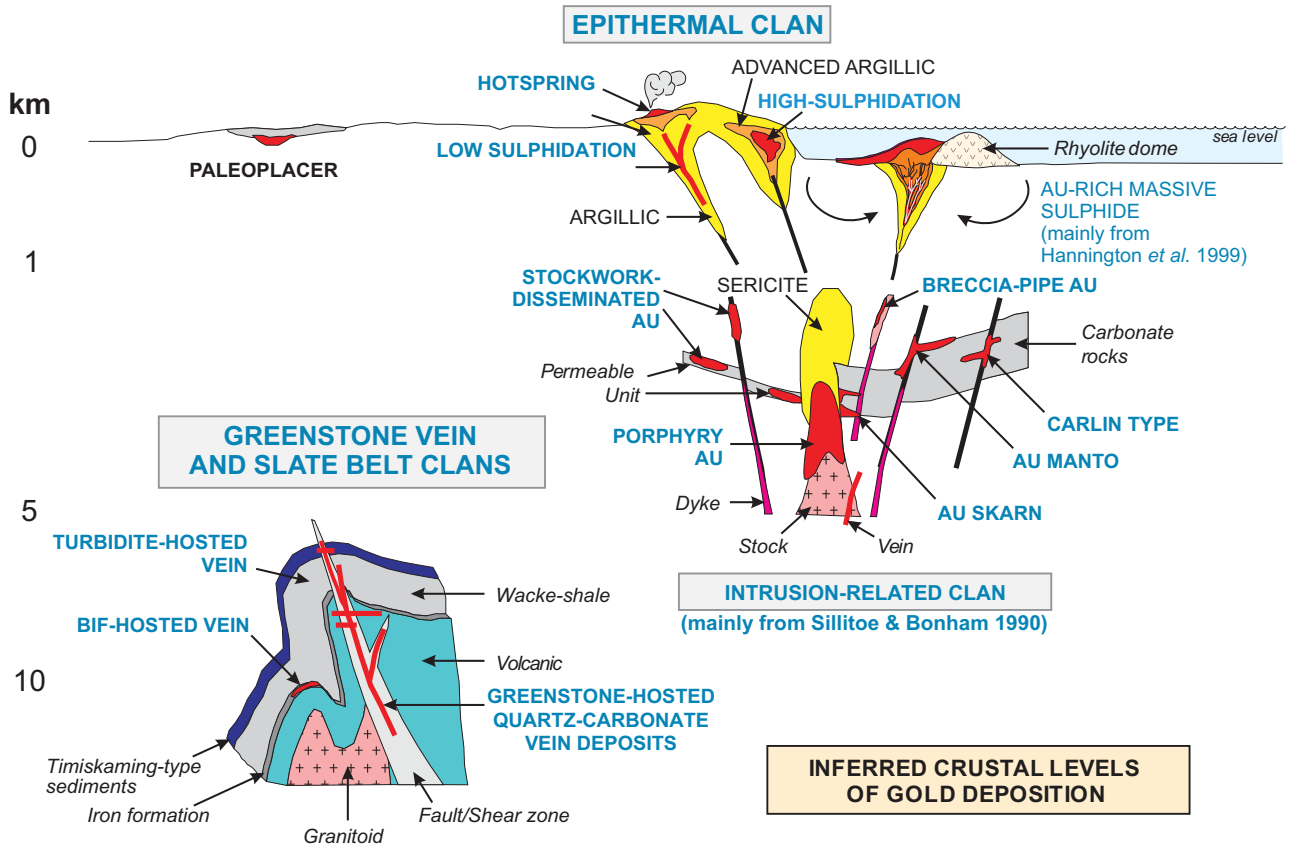

Figure 1. Schematic summary of different gold deposit settings from Dubé et al. (2015) that in many cases include an Au-W association, such as the orogenic metasediment-hosted gold deposits and various intrusion-related gold settings, including vein, skarn, and greisen.

review (Poulin et al.,, submitted). Importantly, this latter work provides and discusses the basis of the first discriminant diagram for scheelite, this being a plot of Eu_A versus Sr/Mo. Since this study we have explored additional aspects, following on the recent work of others (e.g. Wintzer et al., 2016; Poitrenaud et al., 2017; Raith et al., 2017). Aspects under investigation include the use of fluid inclusions and the potential use of scheelite as a chronometer, the latter of which is particularly significant as it would mean that scheelite could be used to both discriminate an ore-deposit and directly date it, even though its presence may not be known.

TUNGSTEN: ORE DEPOSIT SETTINGS AND SOURCE OF W

In the present study, two main ore deposit types hosting W mineralization are prominent, these being metamorphic- and intrusion-related, as summarized in Figure 1. In a very general sense therefore, these deposits conform to the orogenic gold deposit group, which are generally Au-dominant with or without lesser Ag, Te, Cu, Zn, Pb, and Te (Bierlein and Crowe, 2000; Hagemann and Cassidy, 2000; Goldfarb et al., 2005), and the intrusion- or magmatic-related deposits where W, with associated Cu, Mo, Au, Sn, Pb, and Zn mineralization, is present as veins, greisens and skarns (e.g. Hart et al., 2002; Ĉerný et al., 2005). Whereas W is rarely produced from the former (see exceptions noted above), it is an important commodity extracted from the latter deposits. In the context of this study, a few pertinent comments are provided as they relate to the interpretation of the results presented below.

Orogenic gold systems are found in terranes dominated by either mafic volcanic rocks or metasedimentary rocks, the latter often including mudstones, with variable amounts of graphite. In a very general sense, these two sequences are relatively reduced with Fe±As sulphides and various carbonates, which is relevant when considering the chemistry of fluids generated during metamorphism (i.e. H_2O-CO_2±CH_4). When W is present in these deposits, it is invariably as scheelite, which reflects enrichment of the system in Ca. Although the origin of these deposits remains debated (see Goldfarb and Groves (2015) for recent synthesis), most agree they are not of magmatic derivation. Particularly relevant to the current study, however, is both the source and the relative paragenesis of Au versus W. Whereas Au is likely released from Fe-sulphides during metamorphism based on its apparent enrichment in such phases (e.g. Pitcairn et al., 2006; Large et al., 2011), recent work suggests W is liberated from the breakdown of Fe-Ti phases, such as ilmenite and rutile

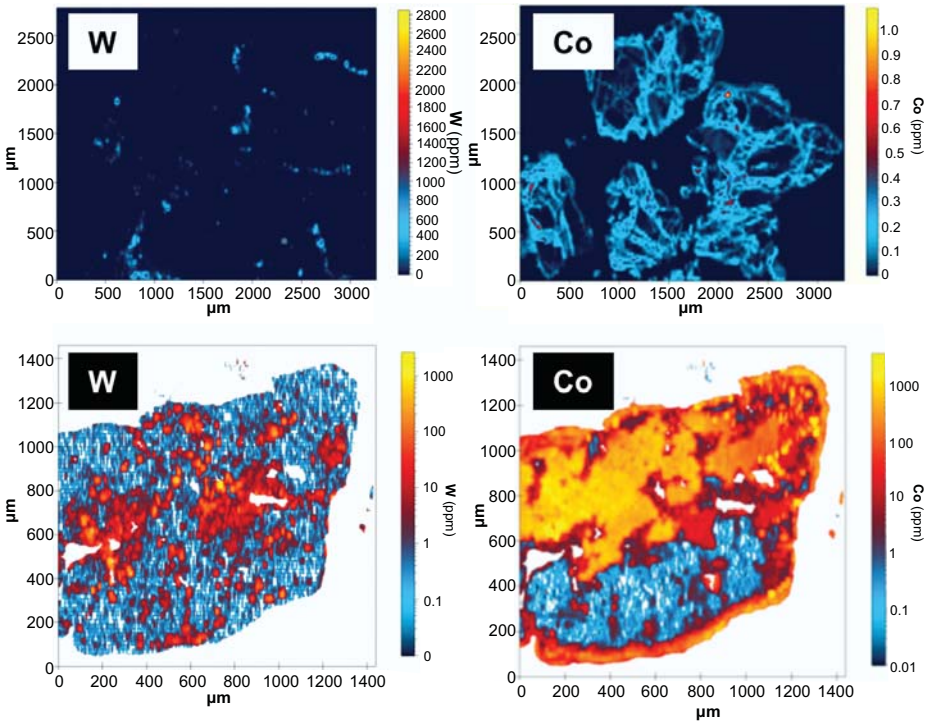

Figure 2. LA ICP-MS elemental maps of pyrite showing the distribution of W (left) and Co (right) with concentrations shown on the cold-to-hot colour bars. The samples from the Archean Bisset gold deposit (top), Manitoba (Neyedley et al., 2017) and the Archean/ Proterozoic Vickers gold deposit (bottom), Pistol Bay, Nunavut (from S. Tokayrk, M.Sc. in prep.). Note that in the former, W post-dates pyrite growth, as indicated by the Co map, whereas in the latter W may occur within the pyrite but it still post-dates pyrite as it traverses the Co pattern that mimics the growth of pyrite.

(Cave et al., 2015). This becomes relevant when using scheelite as a RIM phase, as it may be decoupled from the Au and therefore represent a different process and even mineralizing event, or related to the same event but reflect a different reservoir depending on scaling. To illustrate this point, we present representative LA ICP-MS-generated element maps of pyrite from two of many orogenic gold systems we have studied (Fig. 2). These maps show that W has a varied paragenesis in these systems and generally post-dates the pyrite that in these and most other cases is enriched in Au, which means that W must post date at least some of the gold.

The magmatic-related W ore systems can be subdivided into two general groups: skarn settings where scheelite dominates, and vein and greisens where wolframite dominates (Kwak, 1987; Ĉerný et al., 2005). In general, these reflect the nature of the enclosing host rock, with calcareous sequences in the former (e.g., Cantung deposit, NWT; Rasmussen et al., 2011) and metasiltstones in the latter (e.g. Panasqueira, Portugal; Lecumberri-Sanchez et al., 2017). In both cases, the mineralizing fluids are inferred to be sourced from highly fractionated felsic magmas, hence depleted in, for example Sr, and in the case of skarn settings the progenitor granite is generally oxidizing (i.e. magnetite stable).

Although not considered in detail here due to the nature of the sampling, another deposit setting is relevant in a general sense to the application of scheelite as a RIM phase, this being reduced intrusion-related gold (RIRG) deposits (e.g. Hart et al., 2002), such as Fort Knox, Alaska.These deposits form a sub-type in the gold deposit classification and, in general, relate to mineralization associated with reduced, ilmenite-bearing intrusions. They are best studied in the contiguous Yukon-Alaska gold belt where many deposits have been discovered. In these settings, there is a strong Au-W-(Te, Bi, As) association, which is therefore similar to that of the orogenic group. We refer to this deposit type in the context of suggestions of future work below.

Thus, in comparing the two main deposit settings above, two aspects are apparent that relate to analysis of the data presented below: (1) there is a difference in the overall chemical environment of these systems that will affect element valence, hence substitution (see below), $\delta^{18}O$ scheelite, and the nature of fluid inclusions; and (2) the coupling or decoupling of W with Au and other elements.

SCHEELITE: PHYSICAL PROPERTIES AND CRYSTAL CHEMISTRY

Scheelite ($CaWO_4$) is part of the tetragonal system and in its euhedral form appears as dipyramidal pseudo-octahedra, although a massive form is most common. It is vitreous and the colour is highly variable from golden yellow, brown to brownish green, pinkish to red-grey, orange and colourless. The samples in this study were mostly shades of orange to orange-brown, cloudy white, and colourless. Of particular relevance for scheelite as a RIM is its high specific gravity (5.9–6.1), hardness (MOH 4.5–5), and brittle nature. These properties combine to ensure breakage of scheelite with subsequent survival of grains during physical transport and ease of separation during heavy mineral processing of till samples. An additional feature of scheelite is its ability to fluoresce under short-wave

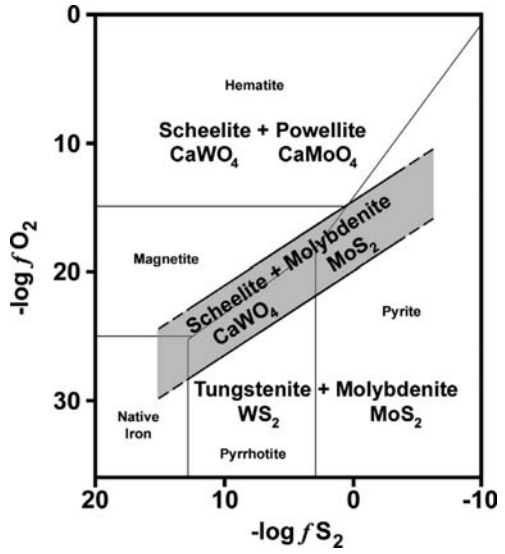

Figure 3. A plot of -logfO_2 versus –logfS_2 showing the stability field of scheelite and powellite at 577°C and 1000 bars fluid pressure (modified after Hsu, 1977).

ultraviolet (UV) light, which also aids with its identification and separation.

The crystal-chemistry of scheelite ($CaWO_4$) is important in the present context of using it as an indicator and discriminator mineral as there are two sites available for elemental substitution: an octahedral [8] coordinated Ca site and a tetrahedral [4] coordinated W site. The latter site is of particular interest as it can accommodate highly charged, smaller cations (e.g. Mo^{6+}, As^{5+}, Nb^{5+}). As the octahedral Ca(2+) and tetrahedral W(4+) sites have different coordination numbers, valences, and preferred radii, this is what dictates what elements can substitute into these sites. The latter are governed by the principles of substitution, which dictate that both charge and radius are important, with the latter taking priority. Furthermore, as some of the relevant elements considered below have multiple valence states, such as Mo (4+, 6+) and As (3+, 5+), redox conditions will in part determine whether substitutions are permitted. A good example of this is the occurrence of powellite, the Mo-rich form of scheelite, which is favoured under oxidization conditions such that Mo^{6+} is stabilized. Thus, the presence of this component, which can be verified using short wavelength UV light (i.e. change from whitish-blue to yellow as Mo increases), indicates the scheelite is from an oxidized environment (Fig. 3).

SAMPLE SUITE AND ANALYTICAL METHODS

The details of the sample suite used are provided elsewhere (Poulin, 2016; Poulin et al., 2016a) and hence are only briefly summarized here. Samples from 37 deposit sites, which represent a wide range of mineralization styles, were collected from archived suites. Based on a review of the relevant literature on each of these deposit sites, samples were categorized into subgroups, which included sediment- and greenstone-rock hosted orogenic gold deposits, magmatic or intrusion-related greisen, porphyry- and skarn-type deposits, and other hydrothermal settings (massive sulphide, epithermal, and general if the details provided of deposits were not specific enough). In the plots below, the samples are therefore organized into these subgroups.

The full analytical methods are provided in Poulin (2016) with a brief summary below. Samples were either mounted as grains (<10 mm) in epoxy pucks or prepared as thick (65 μm) polished sections. The material was examined for chemical zoning at Laurentian University using backscatter imaging and X-ray mapping methods complemented with cathodoluminescence (CL) using a JEOL 6400 SEM-EDS with a GatanChromaCL attachment. Subsequently LA ICP-MS analysis were done (also at Laurentian University), using a Thermo X SERIES II quadrupole ICP-MS in a two-volume Laurin Technic sample cell using a pulsed ArF excimer laser (RESOlution M-50) emitting at 193 nm and a repetition rate of 10 Hz. A 47 μm beam was used for all the analyses, which included Li, B, Na, K, Ti, V, Cr, Mn, Fe, Co, Ni, Cu, Zn, As, Rb, Sr, Y, Mo, Ag, Sn, Ba, and the rare earth elements (REE). The most informative of these elements was found to be Sr, Mo, As, and the REEs and, as such, are only elements discussed in further detail below. In addition, in situ U-Pb dating was done on select samples in polished thin section and for this a 140 μm beam was utilized. Oxygen isotopes were done on high-purity scheelite separates at the Queen's Facility for Isotope Research (QFIR) following the standard BrF_5 dissolution method using a Finnigan MAT 252 mass spectrometer. The results are reported in standard per mil (‰) nomenclature referenced to SMOW with reproducibility (2σ) of $\delta^{18}O$ values at ±0.2‰.

RESULTS

Provided below is a brief summary of several factors considered to potentially be relevant in using scheelite as an ore-deposit discriminator. The details of each is beyond the scope of this paper, hence the interested reader is forwarded to the relevant publications for further details.

Cathodoluminescence

Cathodoluminescence (CL) results from the emission of photons in the UV, visible, and infrared range of the electromagnetic spectrum when material is bombarded with high-energy electrons. There are multiple elemental substitutions that influence the CL response of a mineral, such as activators (promote a CL response; e.g. Mn^{2+}, REEs) and quenchers (inhibit or eliminate a CL response; e.g. Fe^{2+}), and thus there is a balance

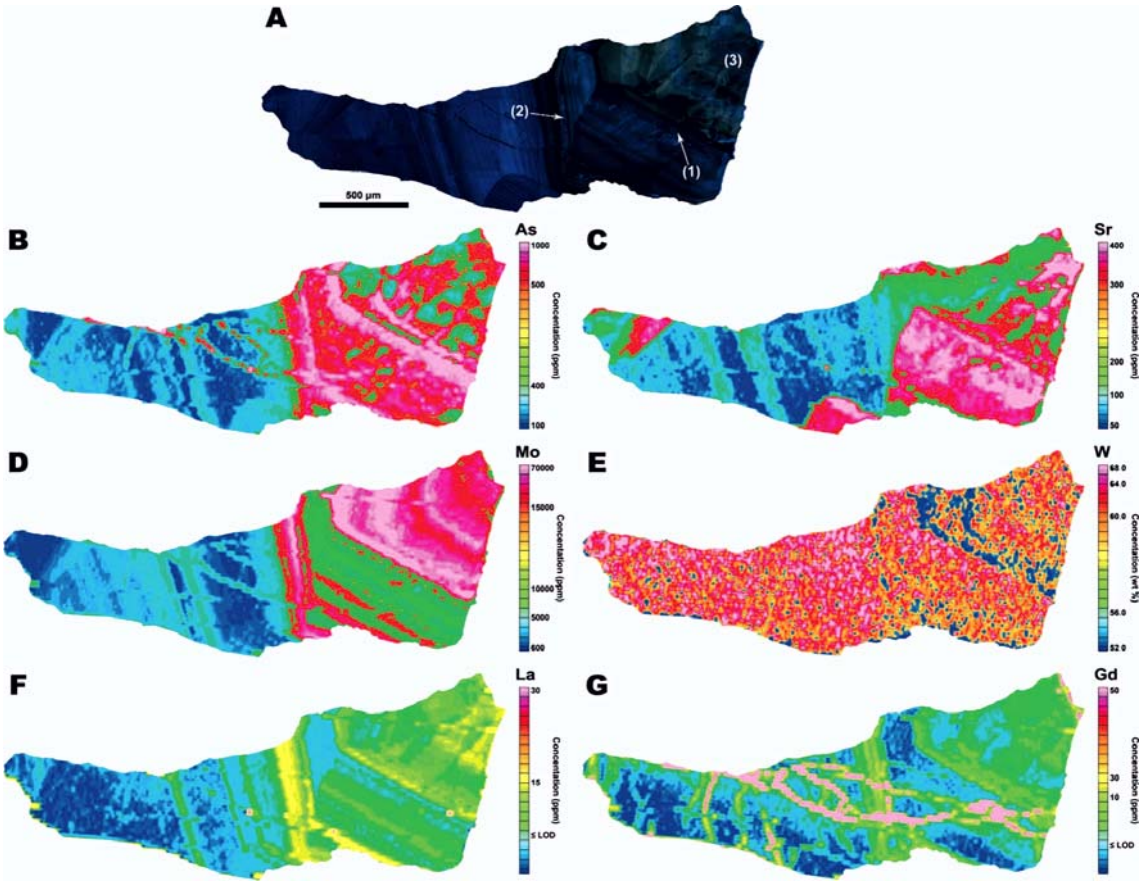

Figure 4. A cathodoluminescence image **(a)** and equivalent false-coloured LA ICP-MS elemental maps **(b–g)** for major and trace elements in a scheelite grain for a sample (CMN80145B) from Zinnwald–Cinovec, Germany–Czech Republic. See Poulin et al. (2016a) for details of the image.

between the absolute and relative concentrations of activators and quenchers, both of which impact on the overall intensity and colour of a CL response. Poulin et al. (2016a) provide a review of the relevant theory of CL response and the results of an investigation of the relationship between CL and scheelite chemistry. As the details of this study are not pertinent to the intent of this paper, they are not repeated here. What is relevant, however, is that scheelite does generate exceptional CL images and this appears to be both ore deposit and chemistry dependent, as summarized below:

1. Cathodoluminescence zonation patterns appear to discriminate between differing mineralized environments, with scheelite from orogenic Au deposits exhibiting a homogenous CL response, whereas those from intrusion-related systems (e.g. porphyries, skarns, and greisens) show strong oscillatory zoning (<1 µm to >300 µm).
2. Maps generated from CL imaging and LA-ICP-MS mapping reveal a strong negative correlation between CL intensity and Mo content, whereas enrichment in Sr, As, and RREE + Y does not appear to be correlated with CL response.
3. Qualitative Mo and W X-ray maps, produced using the less time and cost-intensive method of SEM-EDS analysis, correlate with the corresponding LA-ICP-MS maps of scheelite and successively delineate the zonation patterns observed under CL.

Table 1. Relevant data for elemental substitution for Ca and W in scheelite; NA = not applicable.

Element	IV Coordination	VIII Coordination
Ca^{2+}	NA	1.00
W^{6+}	0.42	0.62
Sr^{2+}	NA	1.18
Mo^{6+}	0.41	0.59
Mo^{4+}	NA	0.65
As^{3+}	NA	0.58
As^{5+}	0.34	0.46

To illustrate the above points, an example of the correlation of CL response and element maps is provided in Figure 4. What is important to note in this figure is that although there is complex oscillatory zoning, there are also cross-cutting relationships, which indicates this sample has a protracted history of elemental paragenesis; i.e., multiple fluid events that may not be related. In addition, the complex chemical maps provide visible evidence of the potential pitfalls of doing a point analyses without context.

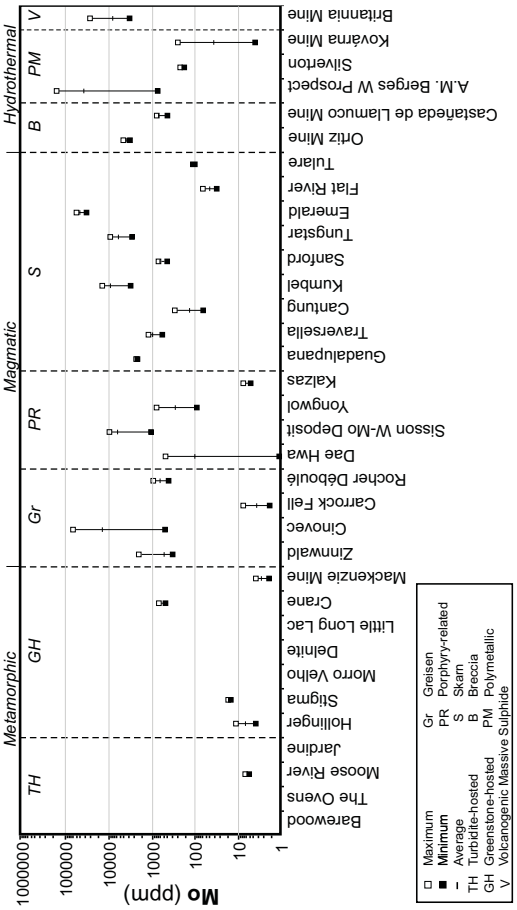

Figure 6. Summary of Mo contents (log scale) in scheelite from various ore-deposit settings (from Poulin, 2016).

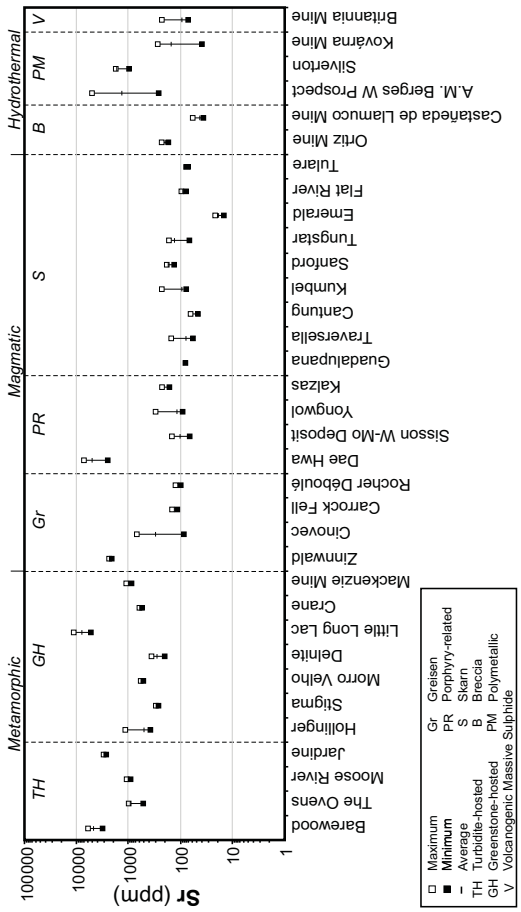

Figure 5. Summary of Sr contents (log scale) in scheelite from various ore-deposit settings (from Poulin, 2016).

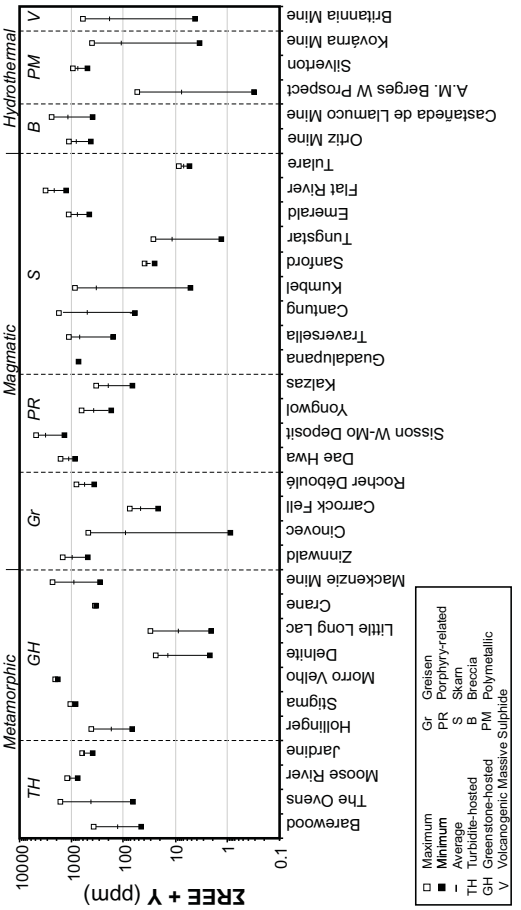

Figure 8. Summary of Mo contents (log scale) in scheelite from various ore-deposit settings (from Poulin, 2016).

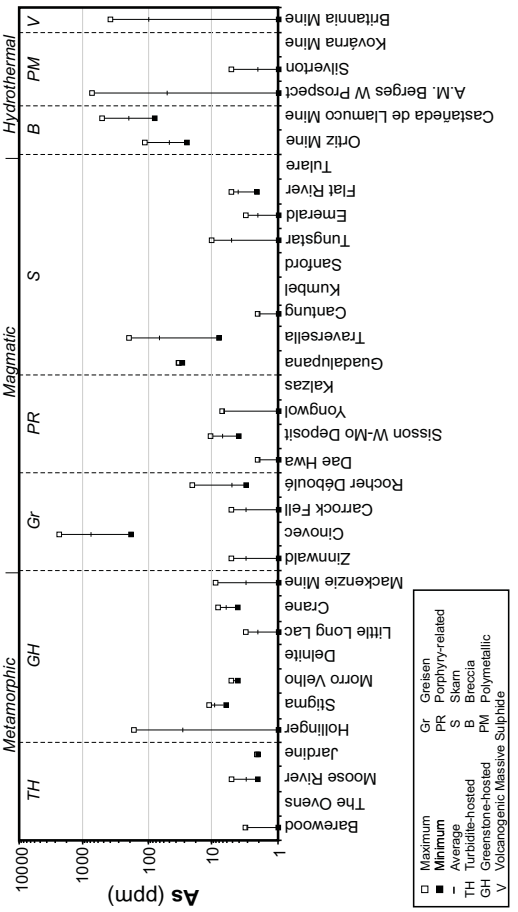

Figure 7. Summary of Sr contents (log scale) in scheelite from various ore-deposit settings (from Poulin, 2016).

Geochemistry

Approximately 700 in situ LA ICP-MS analyses for trace element chemistry were made for 36 scheelite grains from 34 deposit settings; the complete data set is provided in Poulin (2016). The most informative elements of those analysed were Sr, Mo, As, and the REEs. We highlight below the important aspects of the scheelite chemistry and note that a more thorough discussion of the data is presented in Poulin et al. (submitted).

Strontium

There is a clear enrichment of Sr in scheelite from metamorphic settings compared to magmatic-hydrothermal settings (Fig. 5) with the former containing up to 10 000 ppm whereas the latter rarely contains a few 100 ppm. This difference is strongly suggestive of a host-rock influence, as mafic volcanic and metasedimentary rocks are generally enriched in Sr, whereas fluids exsolved from fractionated felsic magmas, the progenitor to the W mineralization, would not be expected to be enriched in Sr. As Sr is not a redox-sensitive element, its enrichment or depletion is not a reflection of this parameter.

Molybdenum

There is a clear enrichment of Mo in scheelite from magmatic-hydrothermal settings compared to metamorphic settings (Fig. 6) with the former having up to several 1000 ppm Mo whereas the latter rarely exceeds 10 ppm (note the single exception). This difference is marked and is interpreted to reflect the redox-sensitive nature of Mo such that Mo^{6+} is preferentially accommodated by scheelite in its tetrahedral site (Table 1).

Arsenic

In general, As is not abundant in scheelite with contents ≤10s ppm, except rarely where it is 100s to a few 1000 ppm (Fig. 7), which is almost always in magmatic-related settings where prevailing oxidation may have favoured As^{5+} over As^{3}. We note one case in particular to illustrate the latter point, this being the setting at The Ovens deposit, southern Nova Scotia, Canada, where arsenopyrite is abundant in the metasedimentary host rocks (i.e. 10–30 modal% locally), but evidently not in the cogenetic scheelite. This example highlights the redox-sensitivity of As, such that the oxidized form as As^{5+} is favoured over its reduced counterpart As^{3+} in substituting for W in the tetrahedral site. The latter is what is inferred to have occurred at The Ovens deposit.

Rare earth elements

The rare earth element (REE) content of scheelite varies considerably with ΣREE+Y, which ranges from 1 to 1000s ppm with no apparent pattern among the samples studied (Fig. 8). In addition, the chondrite-normalized (CN) profiles are also somewhat similar across the deposit types, for which we only provide a few comments as a more detailed discussion is provided in Poulin et al. (submitted). The CN patterns mimic, in general, the results from other studies, which have mostly focused on scheelite from single deposits rather than a number of deposits; the work of Dostal et al. (2009) being one of the few exceptions. Regardless, the CN patterns generally show both concave and convex shapes, with similar patterns recorded in individual deposits. There is also a change in the maximum enrichment such that the "hump" can migrate across the middle REEs (MREEs), consistent with these REEs being the most compatible for substitution based on their radii. The similarity of patterns within single samples but with large ranges of ΣREE+Y is consistent with fluid distillation and progressive depletion of REEs with time (e.g. Brugger et al., 2000). Of relevance to characterizing scheelite in ore systems is the degree of the Eu anomaly, which is generally higher in metamorphic samples, suggesting a redox effect with Eu^{2+} favoured over Eu^{3+}.

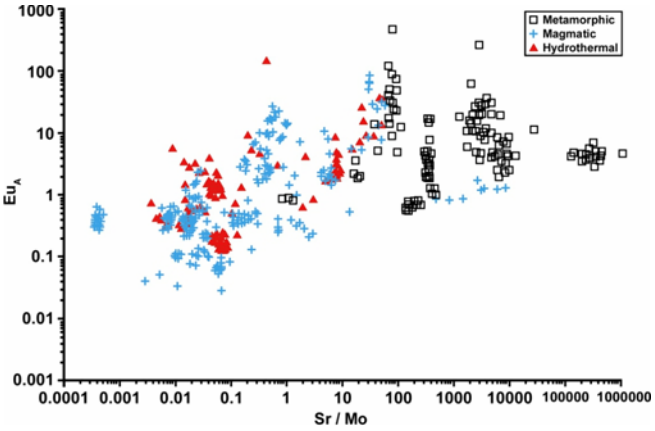

Figure 9. A proposed discriminant plot for scheelite, which separates samples from reduced orogenic-type gold settings (from Poulin, 2016).

Based on the results and examination of the geochemical data, a discriminatory plot was derived of Eu_A versus Sr/Mo (Fig. 9). The basis of this diagram is that the redox-sensitive elements Eu and Mo provide the means to separate scheelite from reduced versus oxidized settings; Sr reflects relative enrichment and depletion, respectively, in contrast, these same settings due to the control of host rock and magmatic fractions (see discussion above).

Oxygen isotopes

The oxygen isotopic composition of hydrothermal fluids has long been used as a monitor of source reservoirs given the different signatures recorded for fluids generated from contrasting sources, such as primitive magmas, during metamorphism, burial of sedimentary

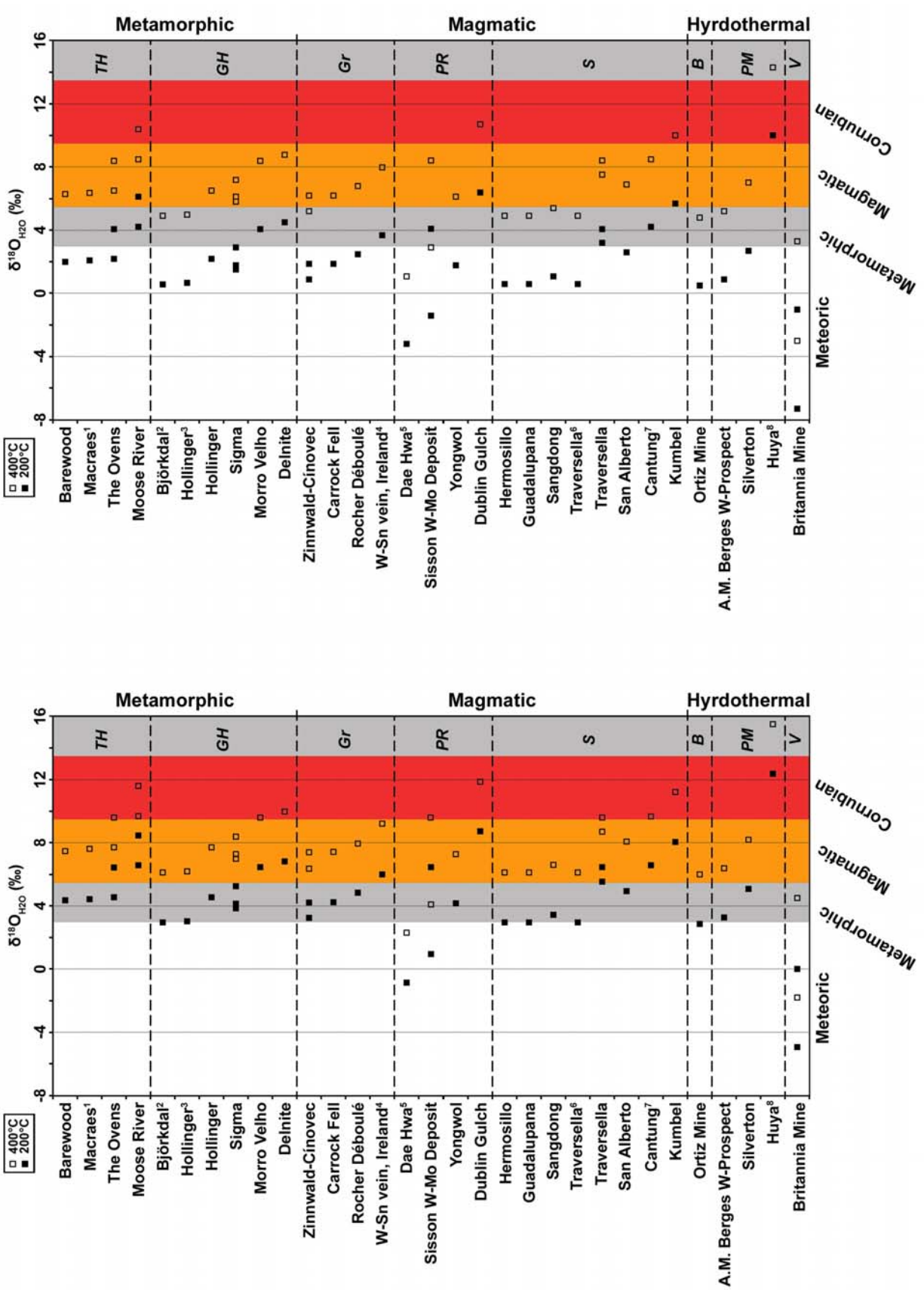

Figure 10. Summary of the calculated $\delta^{18}O_{H_2O}$ values (shown as numbers in the white boxes) in equilibrium with scheelite at 200 and 400°C using fractionation equations of Wesolowski and Ohmoto (1986; left) and Zheng (1992; right); diagram from Poulin (2016). The data are grouped by deposit type on the vertical axis and fluid type is indicated on the horizontal axis. Coloured boxes show $\delta^{18}O_{H_2O}$ for metamorphic fluids (grey box, +3 to +20‰), magmatic fluids (orange box, +5.5 to +9.5‰), and Cornubian fluids (red box, +9.5 to +13.2‰), as indicated by Sheppard (1986).

basins, or near surface environments (e.g. Taylor, 1979; Sheppard, 1986). Given the limited amount of data on scheelite (see Poulin et al. (submitted) for a summary), this aspect was explored to see if it could also be used to discriminate its source and deposit setting based on the large difference in $\delta^{18}O_{H_2O}$ for the aforementioned reservoirs.

The results from calculating the $\delta^{18}O_{H_2O}$ in equilibrium with scheelite at appropriate formation temperatures (i.e. 200–400°C) are shown in Figure 10 and are summarized as follows: (1) metamorphic settings 14 to 6‰; (2) magmatic settings 11 to -3‰; and (3) other settings 14 to -6‰. The spread of these data is large and in all cases indicates that several processes and oxygen reservoirs have influenced the $\delta^{18}O_{H_2O}$ of the systems.

To account for the large variation in $\delta^{18}O$ values, different plausible models were evaluated (Poulin et al., under review), which includes contamination from impurities (e.g. quartz), cooling-induced fractionation, closed- versus open-system fractionation, wall-rock interaction, and fluid mixing. The results suggest that some combination of closed system fractionation (i.e. distillation) and fluid mixing are the most plausible cause for the observed range in $\delta^{18}O_{scheelite}$ and calculated $\delta^{18}O_{H_2O}$ values. Thus, based on our data set and a compilation of previous work, it appears that $\delta^{18}O_{scheelite}$ does not offer a simple discriminant for evaluating ore deposit settings.

Fluid inclusions

Fluid inclusions (FI) are used extensively to trace the fluid evolution of hydrothermal ore systems; excellent reviews are provided by Wilkinson (2001), Kesler (2007), and Bodnar et al. (2014). That the pressure-temperature-composition (PTX) conditions of the relevant chemical systems, namely H_2O-CO_2 (Diamond, 2003) and H_2O-NaCl (Dreisner and Heinrich, 2007), are well defined means it is possible to characterize the PTX characteristics of minerals using their contained FI; the caveat of the latter is of course that the FI were trapped close to the time of mineral formation (see Bodnar (2003) for discussion). Thus, scheelite in general porphyry-type settings, including skarns, have two important features about their FI: (1) a low-density near critical parental fluid with high homogenization temperatures (Th); and (2) an unmixed fluid pair, derived from the latter, and characterized as an assemblage of coexisting vapor(V)-rich and hypersaline (L_{H_2O}-V-Halite) FI. In contrast, quartz-hosted FI in orogenic systems are generally characterized as a low-salinity (i.e. 5–10 wt% equiv. NaCl), H_2O-CO_2±CH_4 type; this fluid may also unmix to produce CO_2-rich and H_2O-rich type FI. With some experience, it is possible to recognize petrographically these different FI and by inference assign a general setting to the sample.

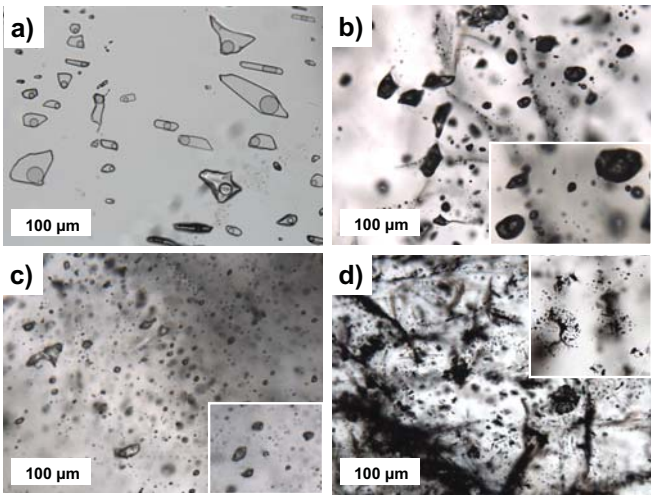

Figure 11. Photomicrographs of scheelite-hosted fluid inclusions; note that all images are at the same scale to better illustrate the highly variable nature of the inclusions. **a)** Kumbel (Kara-Urkurt), Kyrgystan, oxidized skarn with the most impressive inclusions seen in any of the scheelite samples studied. **b)** Castañeda de Llamuco, Chile, breccia pipe/porphyry setting showing the opacity of inclusions in scheelite; close-up shows these are low-density, near critical types expected in such an environment. **c)** Hollinger-McIntryre, Ontario orogenic deposit showing scheelite inundated with CO_2-rich inclusions (see inset for enlarged examples). **d)** The Ovens, Nova Scotia, orogenic deposit showing an exceptional example of decrepitated inclusions. The inset image is to highlight what such inclusions look like in detail.

In our study of FI, we routinely fragmented vein quartz and with the mm-size material bathed in immersion oil (refractive index (RI) ~1.54) looked for FI. This provided a fast, inexpensive, and effective means of examining the FI present. The hindrance of using this approach with scheelite is its high RI (i.e. mineral is uniaxial (+), nw = 1.918–1.921, nε 1.935–1.938), hence most if not all FI appear opaque when such chips are viewed using plane transmitted light; a similar problem occurs with FI in sphalerite. However, using doubly polished thick sections (~50–80 µm) one can overcome to some extent this problem and observe FI. Representative examples are shown in Figure 11, which were photographed at the same scale to better illustrate the large range of sizes and shapes to be expected. In this regard, a few comments are provided to illustrate that useful information can be extracted: (1) if high-density (i.e. low- to moderate-temperature FI) dominate, this likely indicates aqueous fluids of ≤200 to 250°C. Such fluids might be found in high-level, epizonal settings or represent CO_2-poor metamorphic fluids (Fig. 11a); (2) if abundant 3-phase (L_{H_2O}-L_{CO_2}-V_{CO_2}) FI with or without monophase FI (i.e. CO_2-rich) are present, these are typical of orogenic systems (Fig. 11c); and (3) if near critical type (i.e. high Th values) or coexisting V-rich and L_{H_2O}-V-H, then

these likely represent a magmatic-hydrothermal fluid such as those found in a porphyry setting (Fig. 11d). Another aspect to note is the textures of the inclusions, which can be modified post-entrapment due to pressure cycling (Bodnar, 2003; Diamond and Tarantola, 2015). Of relevance here is that in orogenic gold systems, FI commonly have such textures (Fig. 11b), thus their presence alludes to such an environment.

U-Pb geochronology

Recent success of dating scheelite using the in situ U-Pb LA ICP-MS method, which is commonly applied to zircon, titanite, and monazite, provides yet another tool to trace the origin of scheelite and potentially differentiate the source of this mineral. Examples of successful dating of scheelite mineralization include (1) the world-class Felbertal scheelite-skarn in Austria, dated at 335 ±4 Ma (Raith et al., 2017); (2) the Salau W-Au skarn, France, where U-Pb dating of coexisting apatite and scheelite gave similar ages of ca. 287 Ma (Poitrenaud et al., 2017); and (3) scheelite from the Yellow Pine Au-Sb-W mining area, Idaho, USA, where two distinct scheelite events could be recognized at ca. 44 and 35 Ma (± 0.5–1 Ma) by dating texturally different scheelite (Wintzer et al., 2016). Importantly, the U content of scheelite in these various studies varied from <1 to 1120 ppm, which means most scheelite should have sufficient U that U-Pb dating is possible.

Unfortunately U was not part of the element list in our initial study (Poulin, 2016) and we were not aware of the potential for in situ U-Pb dating! Thus, to evaluate the application of this U-Pb dating method, we selected a range of samples from the original study suite of polished thin sections in which scheelite was present as coarse grains. Using conventional analytical methods, the following results were obtained, based on about 20 analysis per sample, and plotted in Tera-Wasserburg diagrams due to the large amount of common Pb that was present, as has been noted by others (e.g. Wintzer et al., 2016): (1) 300 ±10 Ma for the Kumbel deposit, Kyrgyzstan, which agrees with its age constraint based on previous work; (2) 390 ±10 Ma for The Ovens, Nova Scotia, Canada, which overlaps known absolute age constraints; and (3) 1500 ±35 Ma for the famed McIntyre-Hollinger Au deposit, Timmins, Ontario, Canada. This age is much younger than the inferred ca. 2670 Ma for mineralization. A fourth sample from the Rocher Déboulé porphyry-type setting in British Columbia, Canada, had a very uniform U content in all the analyses and, hence, limited spread in the associated plots, which precluded an age calculation. Thus our preliminary examination confirms the work of others, which indicates the potential of using scheelite as a powerful chronometer in ore systems.

FUTURE WORK

The results of this study have demonstrated the potential application of scheelite as an ore deposit discriminator. In addition, that it can also be dated in situ adds a dimension to using scheelite as a RIM to assess the timing of ore-forming events. Continued advances in the LA ICP-MS as a micro-analytical tool also means that data can be acquired more rapidly, thus lower cost, and at lower detection limits. In addition, although not explored as part of this study, in situ measurement of Sr isotopes could also be integrated as part of the analytical protocol to assess source reservoirs. It is also recommended, based on the initial results of this study, that $\delta^{18}O_{scheelite}$ be done using secondary ion mass spectrometry (SIMS) versus conventional bulk methods, as SIMS is a relatively fast, efficient, and cost-effective means of acquiring such data at a high spatial resolution. Thus, an important outcome of this work is that all of the aforementioned data could then be obtained in situ on the same grains which provide the means to completely trace individual scheelite grains.

As noted above, this study did not include samples from the reduced intrusion related gold (RIRG) settings, which is a gold deposit setting gaining more attention in recent years, the success of exploration in the Yukon area of Canada being an excellent example. As noted before, distinguishing between RIRG versus orogenic gold systems, particularly those hosted in metasedimentary rocks, has been an issue (Goldfarb et al., 2005; Goldfarb and Groves, 2015). The application of the protocol reviewed here may therefore provide a means to assess the similarities and differences in these systems and is seen as an area requiring immediate and high-priority research.

ACKNOWLEDGEMENTS

This project would not have been possible without the financial support of the TGI program through the Geological Survey of Canada. In addition, we thank the Natural History Museum of Canada and the Miller Museum, Queen's University, for providing some of the scheelite specimens used in this study, and lastly the Queen's Facility for Isotope Research for the oxygen isotopic analysis.

REFERENCES

Bierlein, F.P. and Crowe, D.E., 2000. Phanerozoic orogenic lode gold deposits, *In:* Hagemann, D.G. and Brown, P.E. (eds), *Gold in 2000*; Society of Economic Geologists, Reviews in Economic Geology, v. 13, 103–139.

Bodnar, R.J., 2003. Re-equilibration of fluid inclusions, *In:* Samson, I., Anderson, A., and Marshall, D. (eds) *Fluid Inclusions: Analysis and Interpretation*; Mineralogical Association of Canada, Short Course 32, p. 213–230.

Bodnar, R.J., Lecumberri-Sanchez, P., Moncada, D., and Steele-MacInnis, M., 2014. Fluid inclusions in hydrothermal ore

deposits, *In:* Holland, H.D. and Turekian, K.K. (eds), *Treatise on Geochemistry 2nd edition;* Elsevier, p. 120–137.

Brugger, J., Lahaye, Y., Costa, S., Lambert, D., and Bateman, R., 2000. Inhomogeneous distribution of REE in scheelite and dynamics of Archaean hydrothermal systems (Mt. Charlotte and Drysdale gold deposits, Western Australia); *Contributions to Mineralogy and Petrology*, v. 139, p. 251–264.

Cave, B.J., Stepanov, A.S., Craw, D., Large, R.R., Haplin, J.A., and Thompson, J., 2015. Release of trace elements through the sub-greenschist facies breakdown of detrital rutile to metamorphic titanite in the Otago Schist, New Zealand; *The Canadian Mineralogist*, v. 53, p. 379–400.

Ĉerný, P., Blevin, P.L., Cuney, M., and London, D., 2005. Granite-related deposits, *In:* Hedenquist, J.W., Thompson, J.F.H., Goldfarb, R.J., and Richards, J.P. (eds), *100th Anniversary Volume*; Society of Economic Geologists, p. 337–370.

Diamond, L.W., 2003. Introduction to gas-bearing aqueous fluid inclusions, *In:* Samson, I., Anderson, A. and Marshall, D. (eds) *Fluid Inclusions: Analysis and Interpretation*; Mineralogical Association of Canada, Short Course 32, p. 101–157.

Diamond, L.W. and Tarantola, A., 2015. Interpretation of fluid inclusions in quartz deformed by weak ductile shearing: Reconstruction of differential stress magnitude and pre-deformation fluid properties; *Earth and Planetary Science Letters*, v. 417, p. 107–119.

Dostal, J., Kontak, D.J., and Chatterjee, A.K., 2009. Trace element geochemistry of scheelite and rutile from metaturbidite-hosted quartz vein gold deposits, Meguma Terrane, Nova Scotia, Canada: genetic implications; *Mineralogy and Petrology*, v. 97, p. 95–109.

Dreisner, T. and Heinrich, C.A., 2007. The system H_2O-NaCl. Part I: Correlation formulae for phase relations in temperature-pressure-composition space from 0 to 1000°C, 0 to 5000 bar, and 0 to 1 X_{NaCl}; *Geochimica Cosmochimica Acta*, v. 71, p. 4880–4901.

Dubé, B., Mercier-Langevin, P., Castonguay, S., McNicoll, V.J., Bleeker, W., Lawley, C.J.M., De Souza, S., Jackson, S.E., Dupuis, C., Gao, J.-F., Bécu, V., Pilote, P., Goutier, J., Beakhouse, G.P., Yergeau, D., Oswald, W., Janvier, V., Fontaine, A., Pelletier, M., Beauchamp, A.-M., Katz, L.R., Kontak, D.J., Tóth, Z., Lafrance, B., Gourcerol, B., Thurston, P.C., Creaser, R.A., Enkin, R.J., El Goumi, N., Grunsky, E.C., Schneider, D.A., Kelly, C.J., and Lauzière, K., 2015. Precambrian lode gold deposits — a summary of TGI-4 contributions to the understanding of lode gold deposits, with an emphasis on implications for exploration, *In:* Dubé B. and Mercier-Langevin, P. (eds), *Targeted Geoscience Initiative 4: Contributions to the Understanding of Precambrian Lode Gold Deposits and Implications for Exploration*; Geological Survey of Canada, Open File 7852, p. 1–24.

Goldfarb, R.J. and Groves, D.I., 2015. Orogenic gold: Common or evolving fluid and metal sources through time; *Lithos*, v. 233, p. 2–26.

Goldfarb, R.J., Baker, T., Dubé, B., Groves, D.I., Hart, C.J.R., Robert, F., and Gosselin, P., 2005. World distribution, productivity, character, and genesis of gold deposits in metamorphic terranes, *In:* Hedenquist, J.W., Thompson, J.F.H., Goldfarb, R.J., and Richards, J.P. (eds), *100th Anniversary Volume*; Society of Economic Geologists, p. 407–450.

Hagemann, S.G. and Cassidy, K.F., 2000. Archean orogenic lode gold deposits. *In:* Hagemann, D.G. and Brown, P.E. (eds), *Gold in 2000*; Society of Economic Geologists, Reviews in Economic Geology, v. 13, p. 9–68.

Hannington, M.D. Poulsen, K.H., Thompson, J.F.H., and Sillitoe, R., 1999.Volcanogenic gold in the massive sulfide environment, *In:* Barrie, C,T. and Hannington, M.D. (eds), *Volcanic-associated Sulfide Deposits: Processes and Examples in Modern and Ancient Setting*; Society of Economic Geologist, Reviews in Economic Geology 8, p. 325–356.

Hart, C.J.R., McCoy, D., Goldfarb, R.J., Smith, M., Roberts, P., Hulstein, R., Bakke, A.A., and Bundtzen, T.K., 2002. Geology, exploration and discovery in the Tintina gold province, Alaska and Yukon. *In:* Goldfarb, R.J. and Nielsen, R.L. (eds) *Integrated Methods for Discovery: Global Exploration in the 21st Century*; Society of Economic Geologists, Special Publication 9, p. 241–274.

Hsu, L.C., 1977. Phase relations of some tungstate minerals under hydrothermal conditions. *American Mineralogist*, v. 66, p. 298–308.

Kesler, S.E., 2007. Ore-forming fluids; *Elements*, v. 12, p. 13–18.

Kwak, T.A.P. (ed), 1987. *W-Sn Skarn Deposits and Related Metamorphic Skarns and Granitoids*; Developments in Economic Geology, v. 24, Elsevier.

Large, R.R., Bull, S.W., and Maslennikov, V.V., 2011. A carbonaceous sedimentary source-rock model for Carlin-type and orogenic gold deposits; *Economic Geology*, v. 106, p. 331–358.

Lecumberri-Sanchez, P., Vieira, R., Heinrich, C.A., Pinto, F., and Wälle, M., 2017. Fluid rock interaction is decisive for the formation of tungsten deposits; *Geology*, v. 45, p. 579–582.

McClenaghan, M.B., Parkhill, M.A., Seaman, A.A., Pronk, A.G., McCurdy, M., and Kontak, D.J., 2013. Overview of tungsten indicator minerals scheelite and wolframite with examples from the Sisson W-Mo deposit, Canada, *In: Application of Indicator Mineral Methods to Mineral Exploration, Short Course 07*; 26th International Applied Geochemistry Symposium, Association of Applied Geochemists, p. 58–67.

McClenaghan, M.B., Parkhill, M.A., Pronk, A.G., Seaman, A.A., McCurdy, M., and Leybourne, M.I., 2017. Indicator mineral and till geochemical signatures associated with the Sisson W-Mo deposit, New Brunswick, Canada; *Geochemistry: Exploration, Environment, Analysis*. doi:10.1144/geochem2015-396

Neyedley, K., Hanley, K., Fayek, M., and Kontak, D.J., 2017. Textural, fluid inclusion, and stable O isotope constraints on vein formation and gold precipitation, 007 deposit, Bissett, Manitoba, Canada; *Economic Geology*, v. 112, p. 629–660.

Pitcairn, I.K., Teagle, D.A.H., Craw, D., Olivo, G.R., Kerrich, R., and Brewer, T.S., 2006. Sources of metals and fluids in orogenic gold deposits: insights from the Otago and Alpine Schists, New Zealand; *Economic Geology*, v. 101, p. 1525–1546.

Poitrenaud, T., Poujol, M., Augier, R., and Marcoux, E., 2017. U/Pb and REE LA-ICPMS analyses on apatite and scheelite as tracers of fluid circulations for the polyphased W-Au Salau ore deposit (France); Goldschmidt Conference Abstract, *Mineralogical Magazine*.

Poulin, R.S., 2016. A *Study of the crystal chemistry, cathodoluminescence, geochemistry and oxygen isotopes in Scheelite: application towards discriminating among different ore-deposit systems*; M.Sc. thesis, Laurentian University, Sudbury, Ontario.

Poulin, R.S., McDonald, A.M., Kontak, D.J., and McClenaghan, M.B., 2016a. On the relationship between cathodoluminescence and the chemical composition of scheelite from geologically diverse ore-deposit environments; *The Canadian Mineralogist*, v. 54, p. 1147–1173.

Poulin, R.S., McDonald, A.M., Kontak, D.J., and McClenaghan, B., 2016b. Scheelite revealed by CL imaging and LA ICP-MS elemental mapping and analysis: Not so simple after all, *In: Program with Abstracts;* Geological Association of Canada, Mineralogical Association of Canada, Whitehorse, Yukon, Canada, p. 39.

Poulin, R., Kontak, D.J., McDonald, A.M., Petrus, J., and McClenaghan, M.B. (submitted): Assessing scheeite as an ore

deposit discriminator using its trace element chemistry, $\delta^{18}O$ signature and potential as a U-Pb geochronometer.

Raith, J.G., Gerdes, A., and Cornell, D.H., 2017. In situ U-Pb dating of scheelite: Constraints on the age and genesis of the Felbertal tungsten deposit; Goldschmidt Conference Abstract, *Mineralogical Magazine*.

Rasmussen, K.L., Lentz, D.R., Falck, H., and Pattison, D., 2011 Felsic magmatic phases and the role of late-stage aplitic dykes in the formation of the world-class Cantung Tungsten skarn deposit, Northwest Territories, Canada; *Ore Geology Reviews*, v. 41, p. 75–111.

Robert, F., Poulsen, H., and Dubé, B., 1997. Gold deposits and their geological classification, *In:* Gubins, A.G. (ed), *Proceedings of Exploration 97*; Fourth Decennial International Conference on Mineral Exploration 1997, p. 209–220

Sheppard, S.M.F., 1986. Igneous Rocks: III. Isotopic case studies of magmatism in Africa, Eurasia, and Oceanic Islands. *In:* Valley, J.V., Taylor, H.P. Jr., and O'Neil, J.R. (eds), *Stable Isotopes in High Temperature Geological Processes*; Mineralogical Society of America, Reviews in Mineralogy and Geochemistry v. 16, p. 319–372.

Sillitoe, R.H. and Bonham, H.F., 1990.Sediment-hosted gold deposits: distral products of magmatic-hydrothermal systems; *Geology*, v. 18, p. 157–161.

Taylor, H.P. Jr., 1979. Oxygen and hydrogen isotope relationships in hydrothermal mineral deposits, *In:* Barnes, H.L. (ed.), *Geochemistry of Hydrothermal Ore Deposits, 2nd edition*; Wiley, New York, p. 236–318.

Wesolowski, D. and Ohmoto, H., 1986. Calculated oxygen isotope fractionation factors between water and the minerals scheelite and powellite; *Economic Geology,* v. 81, p. 471–477.

Wilkinson, J.J., 2001. Fluid inclusions in hydrothermal ore deposits; *Lithos* .v. 55, p. 229–272.

Wintzer, N.E., Gillerman, V.S., and Schmitz, M., 2016. U-Pb scheelite LA-ICP-MS dates of stibnite-scheelite mineralization in the Yellow Pine Au-Sb-W mining area, Central Idaho, USA, *In: Program with Abstracts;* The Geological Society America (GSA) Annual Meeting, Denver, Colorado, 25-28 September, 2016.

Zheng, Y.F., 1992. Oxygen isotope fractionation in wolframite;. *European Journal of Mineralogy*, v. 4, p. 1331–1335.

The past is the key to the future: understanding and successfully applying the lessons learned from 40 years of indicator mineral exploration

S.A. Averill

Overburden Drilling Management Limited, 107-15 Capella Court, Nepean, Ontario, Canada K2E 7X1
(Author's e-mail: stuaverill@storm.ca)

Transported gold grains from sediments have been used as an indicator of mineralization for millennia by prospectors searching for the "mother lode", and kimberlite indicator minerals (KIMs) have been used successfully in diamond exploration for more than 100 years. However, the development of the systematic indicator mineral techniques that are used today in the search for many types of mineral deposits (e.g. McClenaghan, 2005; McClenaghan and Cabri, 2011; McClenaghan and Paulen, in press) only began in 1966 during pre-production stripping of Texas Gulf Sulphur's giant Kidd Creek volcanogenic massive sulphide (VMS) deposit in the renowned Abitibi Greenstone Belt near Timmins in Canada (Averill, 2003).

The Kidd Creek orebody was covered by tens of metres of glacial sediments, which are typical of the Abitibi region and consisted of a layer of till overlain by thick, varved glaciolacustrine clay and silt. When the pit reached bedrock, Texas Gulf's geological team, which was headed by George Mannard Sr. and included other visionaries such as Bob Ginn and Dave Rogers, were attracted by the presence of numerous, unoxidized ore boulders in the lower part of the till horizon. Since the sulphide minerals in these boulders were not oxidized, the team reasoned that for every ore boulder in the clast fraction of the till, millions of sulphide mineral grains must be present in the silt-sand matrix. In short, they recognized that the till overlying and glacially down-ice from the Kidd Creek ore deposit contained a train of fresh, physically dispersed mineral grains that are indicative of the deposit — an indicator mineral dispersal train — and that this dispersal train should be a much longer, more systematic, and more readily detectable exploration target than the corresponding boulder train.

The Texas Gulf team then worked with Bradley Brothers Limited of Timmins to develop an efficient, mobile, self-contained, off-road drill that could rapidly obtain representative samples of the till at any depth. The result was a reverse circulation (RC) rotary drill rig mounted on a wide-tracked vehicle and fully enclosed to allow the drillers, geologist, and samplers to work together in any weather. The Geological Survey of Canada tested the prototype in the winter of 1971–72 by drilling a transect across the Abitibi Greenstone Belt from west to east (Skinner et al., 1972). Drills of this type, with significant improvements including the use of an adjustable air-water mixture rather than water alone as the drilling fluid to obtain full sample recovery in sediments of any consistency and degree of saturation, remain the industry standard today (Fig. 1).

Figure 1. Example of a reverse circulation (RC) drill purpose-built for till and bedrock sampling in areas of deep overburden.

Since the most useful indicator minerals for VMS exploration were sulphides, heavy mineral separation could be used to concentrate them. This greatly improved the detection limit, facilitating recognition of even the low-grade margins and distal tail of a dispersal train and thereby effectively increasing the size of the exploration target, reducing the number of drill holes required to find it and lowering exploration costs. Increasing the sample size to recover more indicator mineral grains further lowered the detection limit and extended the effective length of the dispersal train, i.e., the distance from which a VMS deposit could be detected. For till, 10 kg of the -2 mm matrix fraction proved to be ideal, providing a km-scale detection range. A matching hole diameter of ~7.5 cm was chosen to deliver this weight of sample from a 1 m interval while minimizing the weight of the drill rig.

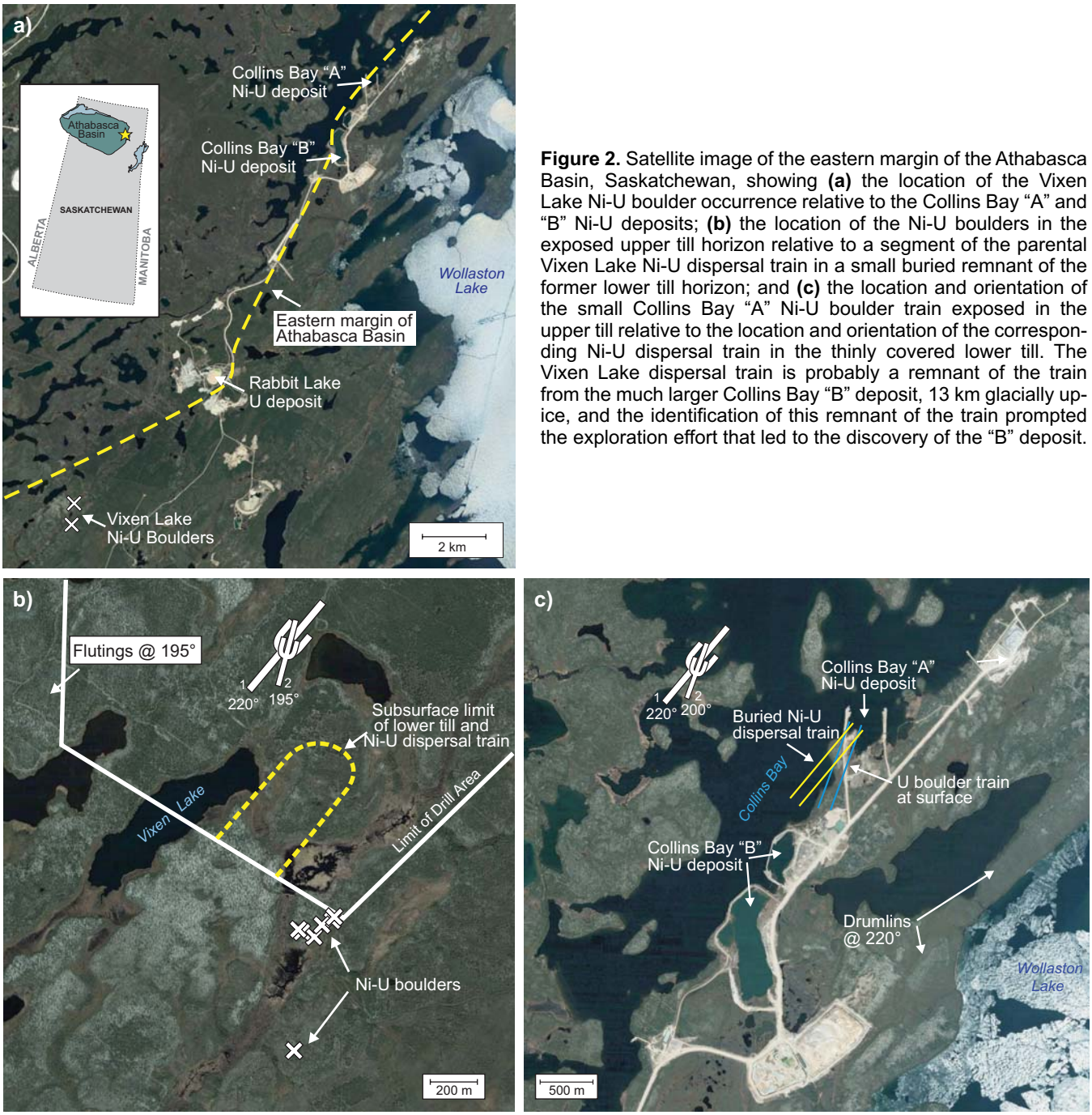

Figure 2. Satellite image of the eastern margin of the Athabasca Basin, Saskatchewan, showing **(a)** the location of the Vixen Lake Ni-U boulder occurrence relative to the Collins Bay "A" and "B" Ni-U deposits; **(b)** the location of the Ni-U boulders in the exposed upper till horizon relative to a segment of the parental Vixen Lake Ni-U dispersal train in a small buried remnant of the former lower till horizon; and **(c)** the location and orientation of the small Collins Bay "A" Ni-U boulder train exposed in the upper till relative to the location and orientation of the corresponding Ni-U dispersal train in the thinly covered lower till. The Vixen Lake dispersal train is probably a remnant of the train from the much larger Collins Bay "B" deposit, 13 km glacially up-ice, and the identification of this remnant of the train prompted the exploration effort that led to the discovery of the "B" deposit.

THE COLLINS BAY U DISCOVERY: A PROMISING START

Though the initial concept was to use glacially dispersed grains of sulphide minerals, principally chalcopyrite and sphalerite, to find VMS deposits from afar, in practice little direct use was made of these minerals because it was much simpler to analyze the heavy mineral concentrates (HMCs) for Cu and Zn than to examine them for chalcopyrite and sphalerite grains. The benefit of identifying the indicator minerals present in a HMC, in addition to analyzing the HMC for the elements in these minerals, was first demonstrated in 1976 by Gulf Minerals while using RC drilling to explore for unconformity-hosted uranium deposits along the eastern edge of the Athabasca Basin in Saskatchewan (Fig. 2; Geddes, 1982). Seven Ni-U boulders with no logical source had been found by scintillometer prospecting near Vixen Lake, 5 km southwest of the Rabbit Lake uranium mine (Fig. 2a), and the objective of the RC drilling was to determine and locate their probable source.

The initial RC drilling showed that the matrix of the till beneath the mineralized boulders was only patchily anomalous in Ni and U, i.e., the boulders appeared to

Figure 3. Photograph of a typical till sample pit in non-permafrost terrain. The sample is normally collected at a depth of 0.5 to 1 m from the C-horizon of the soil profile, which is less oxidized than the overlying B-horizon but still depleted of sulphide minerals as illustrated by the extracted heavy mineral concentrate. At this site, duplicate 10 kg samples of sieved till matrix were taken for quality control. Source: Overburden Drilling Management archives.

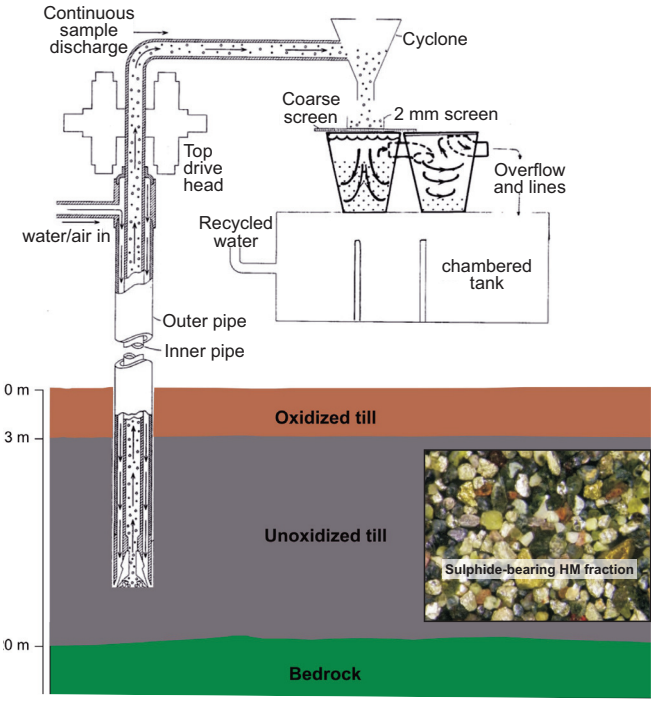

Figure 4. Schematic cross section of a reverse circulation drill rig sampling till. Note that the till below 3 m is unoxidized; therefore, any sulphide mineral grains that were entrained during glaciation are preserved.

be erratics. However, step-out drilling 300 m to the northwest intersected a Ni-U dispersal train in a buried remnant of an older, underlying till horizon in a hidden bedrock valley. A stereo air-photo study determined that the direction of ice flow for the upper till was 195° and that the mineralized boulders on its surface had been plucked from the Ni-U dispersal train in the lower till and transported 300 to 800 m down-ice to their present locations.

The buried remnant of the dispersal train was only 500 m long but appeared to be oriented at 220°, subparallel to the edge of the Athabasca Basin, and the coarse fraction of the till contained very few sandstone clasts derived from the basin. In addition, the dispersal train was found to be confined to the upper part of the till remnant, indicating that the source was very distal and must be large to have produced such a long train.

A zoned U and Ni-U deposit had previously been found at Collins Bay on Wollaston Lake, 16 km to the northeast, by tracing a 1.5 km long train of U-bearing (no Ni) boulders identified in 1970 by a team that included the author. This boulder train (Fig. 2b) occurred in the upper till, which at Collins Bay forms only a thin veneer over the lower till horizon which, instead of being only patchily preserved, has undergone so little erosion that drumlinoid ridges oriented in the 220° direction of till transport are still visible. The orientation of this boulder trend was 200°, similar to the 195° direction of boulder displacement from the Vixen Lake dispersal train. Its source, the Collins Bay deposit that lay 400 m offshore beneath the bay, appeared to be too small to have produced a 16 km long dispersal train.

In conjunction with the RC drilling at Vixen Lake, Gulf performed orientation drilling on the Collins Bay boulder train. This drilling showed that the U boulder train in the upper till was underlain by lower till containing a zoned U and Ni-U dispersal train of the same 1.5 km length as the boulder train. The strike of this train was 215°, essentially the same as the 220° strike of the Vixen Lake train, and the two trains were directly in line. However, the Ni to U ratio was much lower in the Collins Bay train than in the Vixen Lake train.

To prove that the Vixen Lake train was indeed a new dispersal train from an undiscovered source of exploration interest, the Ni-U mineralogy of anomalous HMCs from both trains was investigated. Although the instrumentation was primitive by today's standards — U was determined by fluorimetry and the minerals were determined by x-ray diffraction analysis of single grains — the test was very definitive. The principal Ni and U minerals in the Vixen Lake train were determined to be niccolite and pitchblende and those in the Collins Bay train were rammelsbergite and coffinite.

From the above evidence, it was deduced that the Vixen Lake train originated from an undiscovered large Ni-U deposit and that this deposit lay somewhere along a 220° line between Collins Bay and Vixen Lake. With the aid of an electromagnetic survey, the Collins Bay "B" deposit was found beneath the bay, 13 km up-ice from Vixen Lake and 2.5 km down-ice from the origi-

nal "A" deposit. The "B" deposit was subsequently mined, producing more than $1 billion of uranium.

SHIFT TO GOLD EXPLORATION: SUCCESS AT CASA BERARDI

A few years later, due to a major increase in the price of gold, RC drilling began to be applied to exploration for this metal, particularly in the clay-covered Abitibi region. It was soon determined that significant anomalies indicative of a gold dispersal train could be identified much more reliably by studying the gold grains recovered in the HMCs than by analyzing the HMCs for Au, although analyzing the HMCs for elements such as As was useful for rapidly identifying the presence in the till of gold pathfinder minerals such as arsenopyrite. In 1984, the discovery of the Casa Berardi East gold mine on the northern frontier of the Abitibi Greenstone Belt from a strong gold grain anomaly identified by RC drilling, at a cost of just $248,000 (Sauerbrei et al., 1987), started an exploration rush so large that it created a job for every geologist remaining unemployed from the 1980–1984 recession.

TRANSITION FROM DEEP TILL SAMPLING TO SURFACE SAMPLING

The use of gold grains in exploration was soon extended to areas where the till was thinner and not covered by clay. Reverse circulation drilling was not required in these areas; suitable till samples could be obtained simply by digging pits ~1 m deep, either by hand or mechanically, to reach the C-horizon of the soil profile where the till is still compact and undisturbed. However, the till at this depth is significantly oxidized (Fig. 3) unlike the fresh till obtained from drill holes (Fig. 4) and thus it now contains few if any of the sulphide mineral grains that were dispersed during glaciation. Therefore, the only remaining gold pathfinder minerals are oxide or silicate minerals, mainly those produced by hydrothermal alteration and/or metamorphism, such as the abundant spessartine garnet that occurs in the gold dispersal train of the Blackwater deposit in British Columbia (Averill, 2017).

An important consideration when working with chemically resistant silicate and oxide indicator minerals such as spessartine or KIMs is that their presence in a HMC generally cannot be detected by chemical analysis because the i*ndicator elements* in these minerals (i.e. Mn in spessartine and Mg and/or Cr in KIMs) are plentiful in other, non-indicator minerals in the HMC. Moreover, the required detection limit for most of these minerals is one grain per 10 kg sample — too low for the minerals to be identified and/or quantified by automated scanning electron microscope (SEM) analysis (Averill and Huneault, 2017). Therefore, visual analysis of the HMC is required.

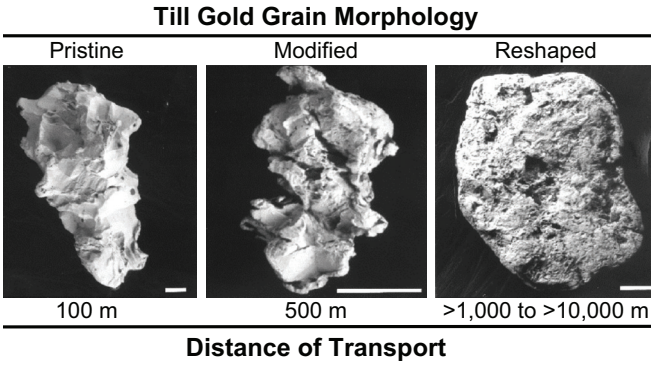

Figure 5. Backscatter electron images of gold grains from till illustrating the relationship between grain wear and distance of transport. The wear processes are compressional (infolding and compaction) and do not reduce the mass of the gold grain. Scale bars = 50 µm. From Averill (2001).

LEARNING FROM THE DIAMOND EXPLORERS

The demand in Canada for KIM identification in thousands of till samples that were collected from surface pits and frost boils following the discovery, in 1991, of the Ekati diamond mine in the Northwest Territories led to the recognition of a heavy mineral suites that could potentially be used as indicators for other types of mineral deposits (Averill, 2001). The most suitable deposit types for indicator mineral exploration have proved to be those that, like kimberlite, have (a) a large variety of distinctive heavy minerals, particularly alteration minerals given the instability of most ore minerals in the surficial environment; and (b) a high concentration of at least one of these minerals.

In Canada, the most useful indicator mineral suites identified to date have been those associated with Ni-Cu-PGE (e.g. Averill, 2011; McClenaghan et al., 2011), porphyry Cu (e.g. Plouffe and Ferbey, 2016), and skarn (e.g. Palmer et al., 2015) deposits. Indicator minerals have also proved to be very useful in unglaciated regions, particularly for porphyry Cu and epithermal Au exploration (e.g. Averill, 2011). For a given deposit type, the number of available indicator minerals may vary with the type of climate (e.g. Averill, 2013). In the hyper-arid parts of Chile and Arizona, for example, chalcopyrite and arsenopyrite have been converted to chemically stable turquoise and scorodite, respectively, allowing the sample size for porphyry Cu exploration to be reduced from 10 kg to 1 kg (Averill, 2011).

BENEFITING FROM THE PAST

In the 40 years since it was demonstrated at Collins Bay that the power of indicator mineralogy for locating mineral deposits from afar was not limited to gold and diamond deposits, some indicator mineral patterns

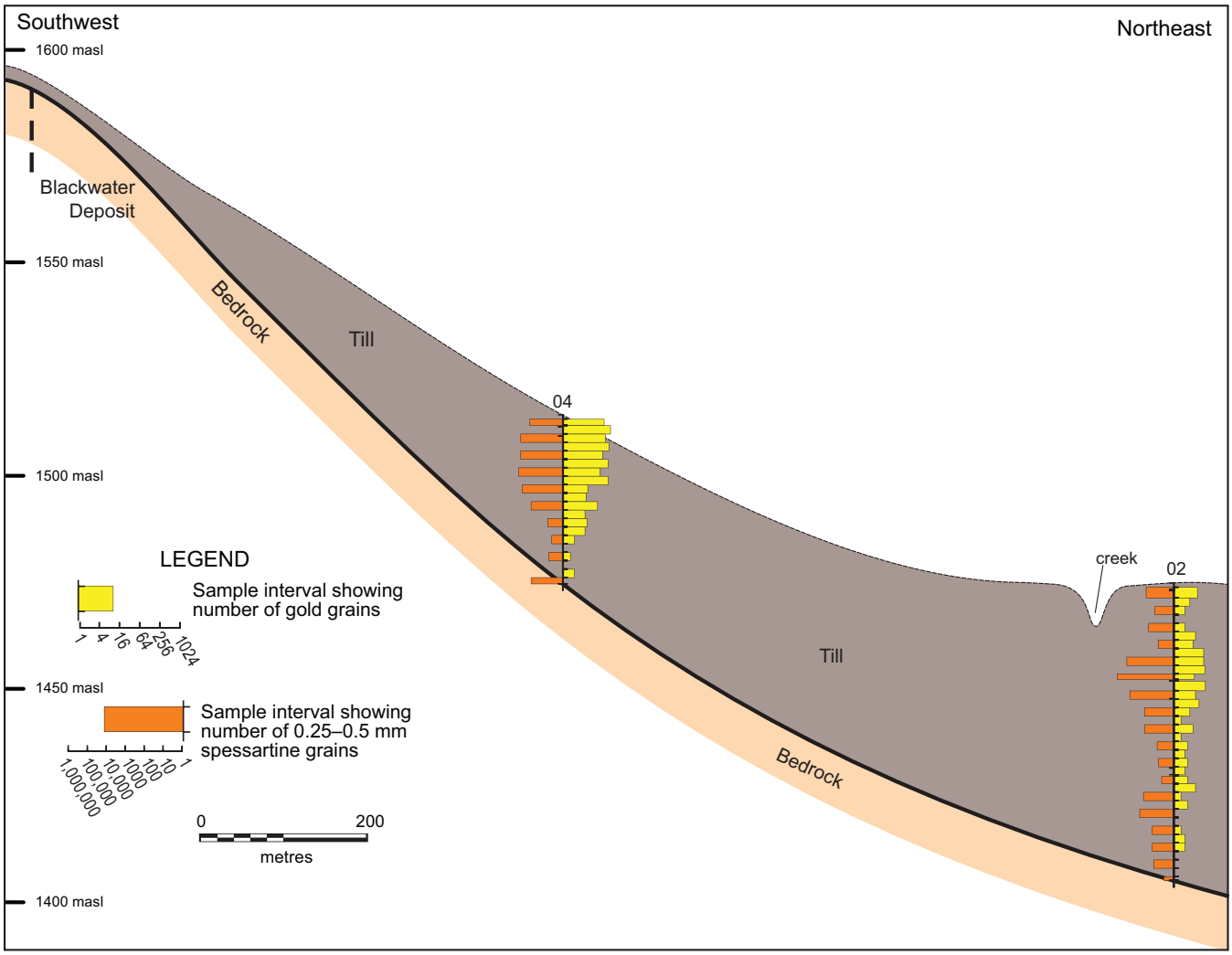

Figure 6. Longitudinal section of the Blackwater dispersal train showing the concentrations of gold and 0.25–0.5 mm spessartine grains in the heavy mineral fraction of the till samples. Note that the dispersal train is thick and rises within the till in the down-ice direction, leaving a barren zone at the base. From Averill (2017).

have become so well established that they can now be considered basic rules for indicator mineral exploration. These fundamental rules include but are not limited to the following:

1. Till exposed at surface in Canada has been oxidized following glaciation to a depth of only 2 to 3 m (Fig. 4); below this depth it is as fresh as at the time of deposition ~10,000 to 15,000 years ago.
2. Till in frost boils in northern permafrost regions is oxidized to the same degree as till in the C-horizon further south but may contain unoxidized felsenmeer blocks if it is less than 2 m thick.
3. Gold naturally tends to crystallize in bedrock as silt-size (<63 µm) grains and because gold is malleable, the grains do not break down into smaller grains during glacial transport. Therefore >90% of gold grains in mineralized zones are silt size, even in gold deposits where most of the gold value resides in coarse, nuggety grains.
4. Low-density quartz and feldspar grains settle in water almost as slowly as silt-size gold grains (Stokes Law) and because >90% of gold grains are of this size, high-energy, gravel-depositing streams, whether pre-glacial, glacial or modern, actually expel most of the gold grains; only the largest grains lag behind and eventually accumulate in placers. Therefore, a gravel sample normally contains less than one-tenth as many gold grains as a neighbouring till sample.
5. During glacial transport, the pristine primary form of a gold grain becomes progressively modified until the grain is reshaped to a simpler, physically stable form (Fig. 5). This process is normally complete after ~1 km of glacial transport, which can be readily observed in gold dispersal trains hosted at depth by fresh till. Many dispersal trains exposed at surface, however, also

contain gold grains that were chemically liberated in situ from inclusion-bearing sulphide mineral grains by post-glacial oxidation. These gold grains chemically liberated from gold inclusions tend to be smaller than 25 μm and are pristine regardless of the distance of glacial transport.

6. Sulphide minerals have varying chemical stability in oxidized acidic (carbonate-poor) till, and a similar range of stabilities in fluvial sediments in unglaciated regions with moderate climates and significant relief (e.g. the hilly to mountainous parts of Peru, Turkey and Tanzania), and their general order of stability has been established (e.g. Averill, 2011, 2013). Only cinnabar and molybdenite are completely stable, though molybdenite is susceptible to physical degradation. Sperrylite, a Pt-arsenide mineral. is also stable. Chalcopyrite is marginally more stable than pyrite. By comparing the number of surviving chalcopyrite grains in a sediment sample to the number of surviving pyrite grains, an estimate can be made of the original number of chalcopyrite grains that were present before the sediment was oxidized, and thus the true strength of a chalcopyrite anomaly. In carbonate-rich sediments, most sulphide minerals are stable.
7. Dispersal trains in till, which originate at the till-bedrock interface, rise progressively above bedrock with increasing distance of glacial transport. Both the thickness of the train and its separation from bedrock may increase markedly if the bedrock source is located at a higher elevation than the train, as can be observed at the Blackwater deposit (Fig. 6; Averill, 2017). In drill holes, therefore, the till must be sampled from top to bottom to ensure identification of the train. The term "basal till sampling" is a misnomer; it has no place in mineral exploration.

INTO THE FUTURE

Over the last 40 years, the indicator mineral story has been progressively evolving from an innovative concept for deep sampling of till in Canada to shallow sampling of a variety of surficial sediments in increasingly diverse regions and landscapes for a growing variety of mineral deposit types. Recent years have seen a shift from indicator mineralogy to indicator mineral chemistry (e.g. Spry and Teal, 2009; Layton-Matthews et al., 2014; Agnew, 2015), and this trend can be expected to continue over the next decade. However, many regions of the world, including significant parts of Canada (e.g. the Interior Plateau of British Columbia; Ferbey et al., 2014), are ripe for indicator mineral exploration using existing technology in combination with the extensive knowledge gained over the last four decades. For these regions, the past is the key to the future.

REFERENCES

Agnew, P.G., 2015. Micro-analytical innovation for indicator mineral exploration, *In: Application of Indicator Mineral Methods to Exploration*; 26th International Applied Geochemistry Symposium (IAGS), Short Course SC02, Tucson, p. 18.

Averill, S.A., 2001. The application of heavy indicator mineralogy in mineral exploration with emphasis on base metal indicators in glaciated metamorphic and plutonic terrains, *In:* McClenaghan, M.B., Bobrowsky, P.T., Hall, G.E.M., and Cook, S.J. (eds), *Drift Exploration in Glaciated Terrains*; Geological Society, London, Special Publication 185, p. 69–81.

Averill, S.A., 2003. Indicator mineralogy: A tool for reviving mineral discoveries in the Abitibi; New Technologies and New Frontiers, Exploration 2003, Quebec, Quebec, p. 88.

Averill, S.A., 2011. Viable indicator minerals in surficial sediments for two major base metal deposit types: Ni-Cu-PGE and porphyry Cu; *Geochemistry: Exploration, Environment, Analysis*, v. 11, p. 279–292.

Averill, S.A., 2013. Indicator mineral fingerprints in surficial sediments near Cu-Au deposits of the porphyry-epithermal-volcanogenic suite, *In:* McClenaghan, M.B., Plouffe, A., and Layton-Matthews, D. (eds.) *Application of Indicator Mineral Methods to Mineral Exploration*; Geological Survey of Canada, Open File 7553, p. 35–44.

Averill, S.A., 2017. The Blackwater gold-spessartine-pyrolusite dispersal train, British Columbia, Canada: Influence of sampling depth on indicator mineralogy and geochemistry; *Geochemistry: Exploration, Environment, Analysis*, v. 17, p. 43–60.

Averill, S.A. and Huneault, R.G., 2016. Basic indicator mineral math: Why visual analysis of the entire heavy mineral fraction of large sediment samples is required on indicator mineral exploration programs in glaciated terrains; *The Association of Applied Geochemists, Explore Newsletter*, v. 172, p. 1–14.

Ferbey, T., Plouffe A., and Anderson, R.G., 2014. An integrated approach to search for buried porphyry-style mineralization in central British Columbia using geochemistry and mineralogy: A TGI-4 project; Geological Survey of Canada, Current Research 2014-2. doi:10.4095/ 293130

Geddes, R.S., 1982. The Vixen Lake indicator train, northern Saskatchewan, *In:* Davenport, P.H. (ed), *Prospecting in Glaciated Terrain*; Canadian Institute of Mining and Metallurgy, p. 264–283.

Layton-Matthews, D., Hamilton, C., and McClenaghan, M.B., 2014. Mineral chemistry: modern techniques and applications to exploration, *In:* McClenaghan, M.B., Plouffe, A., and Layton-Matthews, D. (eds), *Application of Indicator Mineral Methods to Mineral Exploration*; Geological Survey of Canada, Open File 7553, p. 10–18.

McClenaghan, M.B., 2005. Indicator mineral methods in mineral exploration; *Geochemistry: Exploration, Environment, Analysis*, v. 5, p. 233–245.

McClenaghan, M.B. and Cabri, L.J., 2011. Gold and platinum group element indicator minerals in surficial sediments; *Geochemistry: Exploration, Environment, Analysis*, v. 11, p. 251–263.

McClenaghan, M.B., and Paulen, R.C., in press. Mineral exploration in glaciated terrain, *In:* Menzies, J. and van der Meer, J.J-M. (eds), *Past Glacial Environments (Sediments, Forms and Techniques) A new and revised edition*; Elsevier.

McClenaghan, M.B., Layton-Matthews, D., and Matile, G., 2011. Till geochemical signatures of magmatic Ni-Cu deposits,

Thompson Nickel Belt, Manitoba, Canada; *Geochemistry: Exploration, Environment, Analysis*, v. 11, p. 145–159.

Palmer, E.M., McFarlane, C.R.M., Lentz, D.R., and Falck, H., 2015. Gold mineralization in the Cantung W-skarn deposit, Northwest Territories: an examination of distribution, mineralogy, and petrogenesis, *In:* Rogers, N. (ed.), *TGI 4 - Intrusion Related Mineralization Project: New Vectors to Buried Porphyry-Style Mineralization*; Geological Survey of Canada, Open File 7843, p. 415–428.

Plouffe, A. and Ferbey, T., 2016. *Till geochemistry, mineralogy and textural data near four Cu porphyry deposits in British Columbia;* Geological Survey of Canada, Open File 8038.

Sauerbrei, J.A., Pattison, E.F., and Averill, S.A., 1987. Till sampling in the Casa–Berardi area, Quebec: A case history in orientation and discovery; *Journal of Geochemical Exploration*, v. 28, p. 297–314.

Skinner, R.G., 1972. Drift prospecting in the Abitibi clay belt, overburden drilling program, methods and costs; Geological Survey of Canada, Open File 116.

Spry, P.G. and Teal, G.S., 2009. Gahnite composition as a guide tin the search for metamorphosed massive sulphide deposits, *In:* McClenaghan, M.B. and Thorleifson, L.H. (convenors), *Workshop B: Indicator Mineral Methods in Mineral Exploration*; 24th International Applied Geochemistry Symposium, Fredericton, New Brunswick, May 2009, p. 27–34.

Porphyry indicator minerals and their mineral chemistry as vectoring and fertility tools

J.J. Wilkinson[1,2,3*], D.R. Cooke[4], M.J. Baker[3,4], Z. Chang[5], C.C. Wilkinson[1], H. Chen[6], N. Fox[3], P. Hollings[7], N.C. White[3,8], J.B. Gemmell[3,4], M.A. Loader[1,2], A. Pacey[1,2], R.H. Sievwright[1,2], L.A. Hart[1,2], and E.R. Brugge[1,2]

[1]London Centre for Ore Deposits and Exploration (LODE), Department of Earth Sciences, Natural History Museum, Cromwell Road, London SW7 5BD, UK

[2]Department of Earth Science and Engineering, Imperial College London, Exhibition Road, London SW7 2AZ, United Kingdom

[3]CODES, the Australian Research Council's Centre for Excellence in Ore Deposits, University of Tasmania, Private Bag 79. Hobart, Tasmania, 7001, Australia

[4]Transforming the Mining Value Chain, an ARC Industrial Transformation Research Hub, University of Tasmania, Private Bag 79, Hobart, Tasmania, 7001, Australia

[5]EGRU (Economic Geology Research Centre) and Academic Group of Geosciences, College of Science and Engineering, James Cook University, Townsville, Queensland 4811, Australia

[6]Guangzhou Institute of Geochemistry, Chinese Academy of Sciences, 511 Kehua Street, Tianhe, PO Box 1131, Guangzhou, China, 510640

[7]Geology Department, Lakehead University, 955 Oliver Road, Thunder Bay, Ontario, Canada P7B 5E1

[8]Ore Deposit and Exploration Centre (ODEC), School of Resources and Environmental Engineering, Hefei University of Technology, Hefei, Anhui, China, 230009

*(*Corresponding author's e-mail: j.wilkinson@nhm.ac.uk)*

Intrusion-centred mineral districts host a diversity of ore deposits of variable metal associations, alteration assemblages and genesis. Porphyry systems represent particularly important exploration targets but the prioritization of conventional geochemical or geophysical anomalies that might represent a deposit, particularly when systems are buried, is extremely difficult. Three key questions arise: (1) Is the alteration (particularly when only propylitic alteration is observed) related to a porphyry system? (2) How can the fertility of a system be assessed at an early stage of exploration in order to reduce exploration risk? (3) How can the centre of the system (in 3 dimensions) be predicted ahead of extensive, potentially deep, drilling? These fertility and vectoring challenges have been the subject of recent work, primarily based on mineral chemistry, in a series of AMIRA projects based out of the University of Tasmania, now also being continued at the Natural History Museum in London.

The approach to assessing the possible presence of a porphyry system has been to establish mineral chemical criteria that discriminate between porphyry and non-porphyry environments based on (1) the composition of igneous minerals (e.g. plagioclase, zircon, apatite, magnetite); and (2) the composition of hydrothermal alteration phases, particularly those developed in the propylitic domain (epidote, chlorite, magnetite, calcite, quartz). Many of these phases may be reworked via erosion into paleo or modern sediment transport systems and are thus available for assessment from catchment areas. Some of the characteristics of these minerals may allow the distinction between extensively mineralized and ostensibly barren environments (the system "fertility") by tracing key igneous processes (Wilkinson, 2013); clearly these features are of significant exploration utility (Fig. 1).

The vectoring challenge has been addressed by the completion of numerous orientation studies on known porphyry systems to establish any systematic spatial variations in mineral chemistry that may exist, primarily within the propylitic environment. These studies have shown that characteristic and, to variable degrees, reproducible patterns of major and trace element variation exist that enable vectoring towards the centre of a hydrothermal system, as well as discrimination between porphyry-related and non-porphyry mineral assemblages (Cooke et al., 2014a, 2015, 2017; Baker et al., 2015, 2017; Wilkinson et al., 2015a, 2017). In particular, chlorite has proven to be particularly effective for prediction of absolute distances to the system centre, even allowing estimation of the depth of a buried system. Both epidote and chlorite appear to contain signals that reflect the potential metal endowment of a system. The ability to define these characteristics of a system from a limited number of samples of distal "green rocks" marks a major step-change in the way

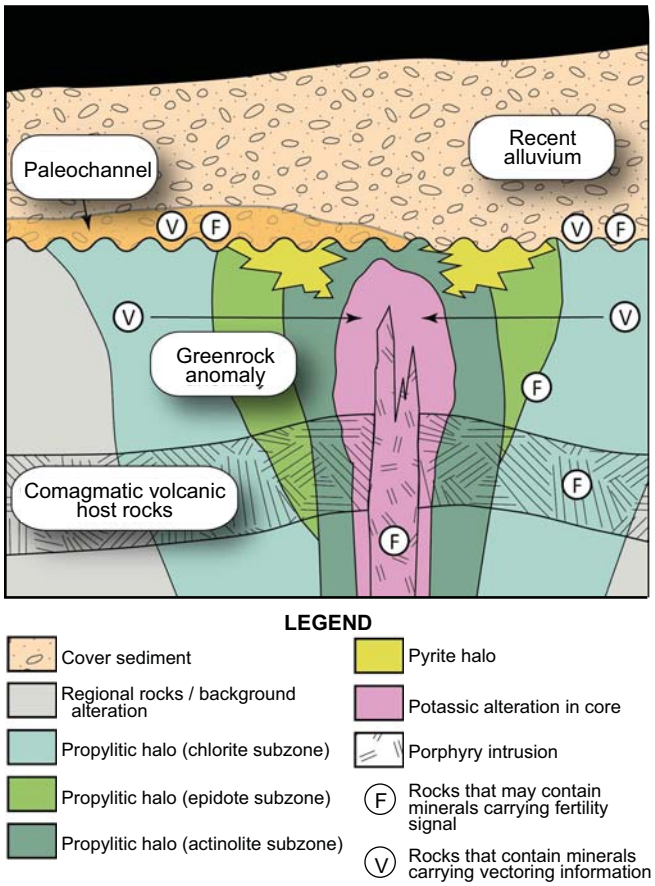

Figure 1. Schematic diagram of an eroded and reburied porphyry system illustrating potential sources of fertility and vectoring information.

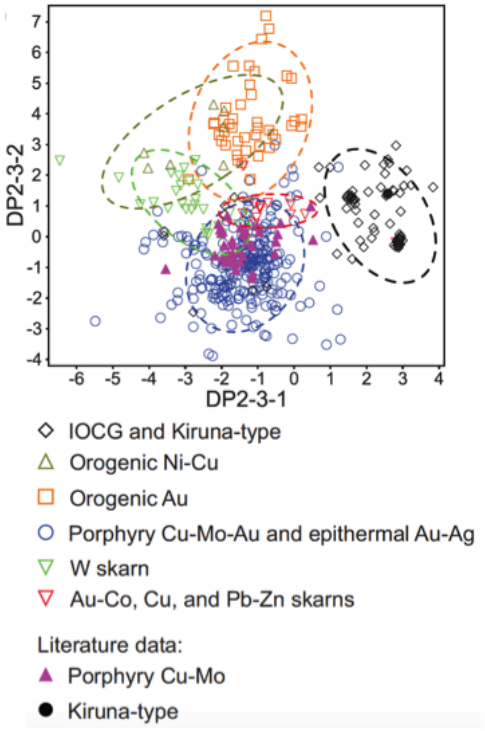

Figure 2. Discriminant projection plot separating apatite from porphyry-epithermal systems from other deposit types. There is significant overlap between porphyry and skarn-related apatite on this diagram. Elements used are Mg, Mn, Y, Ce, Eu, Dy, Yb, Pb, Th, and U. From Mao et al. (2016).

that exploration for porphyry systems can be done (Fig. 1).

PORPHYRY INDICATOR MINERALS

The ability to discriminate minerals from a porphyry magmatic-hydrothermal system as opposed to other kinds of hydrothermal, geothermal, or metamorphic environments would be a valuable addition to the porphyry exploration toolbox. Clearly, the field recognition of characteristic mineral assemblages is an obvious first step, as well as delineating these assemblages and their textural variations. Extending this to transported grains is possible, where the occurrence of relatively characteristic minerals (e.g. molybdenite) and, more usefully, composite grains (containing typical mineral associations) may be indicative of an eroded bedrock porphyry source. However, many minerals that occur in porphyry-type deposits are not diagnostic, even when occurring in mineral assemblages. This is particularly true in the distal, propylitic alteration environment, where there is little chance of finding anything that could be indicative of a nearby porphyry centre.

As a result, recent work has increasingly focused on mineral chemistry, particularly trace element chemistry, in the hope that distinctive "porphyry" signatures may exist. Much of this work has been made possible by the development and decreasing cost of laser ablation inductively-coupled-plasma mass spectrometry (LA-ICP-MS). This technique, with its high spatial resolution (generally 25–50 μm) and low limits of detection (in the 10s of ppb range for many elements), now allows the simultaneous determination of approximately 40 elements in a wide range of silicate, oxide, and sulphide minerals—subject to careful checks on analytical artefacts such as mass spectrometer interferences.

Apatite

Limited work has been done on assessing the utility of apatite for porphyry discrimination. Mao et al. (2016) analysed 20 samples from a variety of porphyry system types and found that these types could be distinguished quite effectively from one another using multivariate discriminant projection. Porphyry-type deposits in general could also be distinguished to some degree from other hydrothermal ore types (Fig. 2), but the authors made no attempt to compare porphyry-related apatite with that from unmineralized rocks. Rukhlov et al. (2016) also analysed apatite from a variety of porphyry systems and showed that alkalic porphyry systems could be discriminated from calc-alkalic systems, probably due to the more oxidized state and less

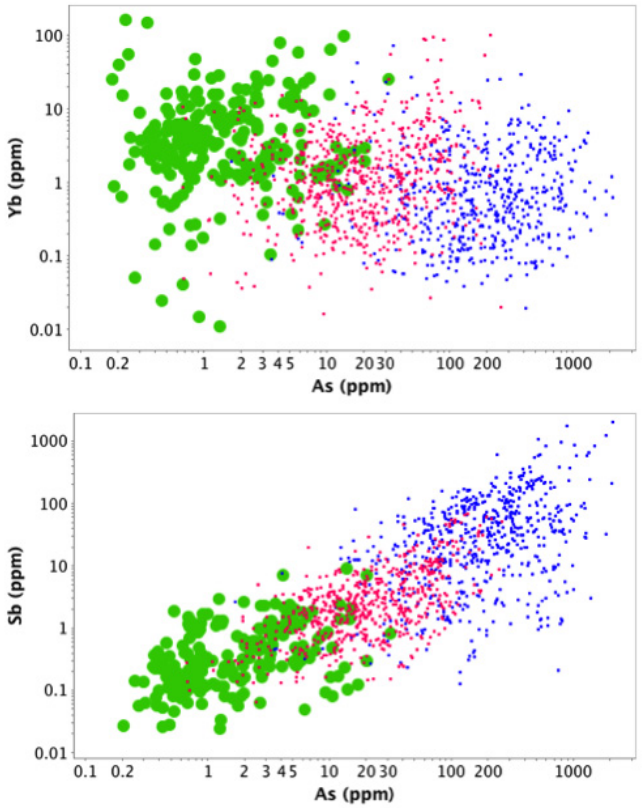

Figure 3. Epidote compositions from Cu-Au (pink dots) and Cu-Mo (blue dots) porphyry systems (Baguio district, El Teniente, Resolution) compared with metamorphic epidote (large green dots) from the Dalradian and Moine Supergroups in Scotland (n = 288), and the Proterozoic Georgetown Inlier (n = 29) and Harts Range (n = 46) in Australia. Note that a large proportion of metamorphic analyses (not shown) were below the limit of detection for As and Sb (typically ~1 ppm for As and 0.1 ppm for Sb). Data from AMIRA P1060 project.

evolved magmas associated with the former. Bouzari et al. (2016) carried out a similar study and showed that apatite associated with different porphyry alteration styles could be discriminated by cathodoluminescence colour and certain chemical characteristics such as Mn/Fe ratio. Again, however, there was no explicit discrimination of porphyry-related apatite from other sources of the mineral.

Epidote

The potential utility of epidote as an indicator mineral for porphyry systems stems from its frequent occurrence within porphyry alteration assemblages. It can occur within the potassic zone (e.g. El Teniente, Chile: Vry et al., 2010) and within two surrounding domains (actinolite and epidote subzones; Cooke et al., 2014b; *see also* Fig. 1). However, epidote frequently also occurs in regional metamorphic rocks (e.g. Wilson and Leake, 1972) and geothermal systems (Bird and Spieler, 2004), as well as in other hydrothermal settings such as skarn deposits and granite-associated veins (e.g. Lindgren, 1933). In addition, it is generally only abundant in intermediate to mafic volcanic country rocks and is much less common in felsic igneous rocks, such as those that host many deposits in southwest USA.

Although a full evaluation of epidote discrimination between such settings using major and trace element chemistry remains to be done, some initial findings provide hope that this may be possible. For example, skarn-associated epidote may be relatively depleted in heavy rare earth elements (HREE) (if coeval with garnet) or enriched in HREE (if it has replaced garnet), and is typically enriched in As, Sb, Sn, Ga, Ge, Pb, U, and Th relative to other types of epidote (Wilkinson et al., 2015a,b). Porphyry-related epidote tends to be enriched in elements that are fluxed by porphyry-hydrothermal fluids and that are compatible in the epidote structure, such as As, Sb, Zn, and Pb (Fig. 3), and also in Au, Ag, and Bi, which could be hosted by nano-inclusions (e.g. Cooke et al., 2014a; Pacey, 2017). By contrast, metamorphic epidote is conspicuously depleted in these elements, plus Ta, U, and Th, and tends to be relatively enriched in Hf, Y, and the HREE (e.g. Fig. 3). In addition, there is a difference between epidote from Cu-Mo and Cu-Au systems, with the former being enriched in As and Sb and depleted in Yb.

The application of multivariate statistical methods is increasingly being used in attempts to discriminate indicator minerals formed in different environments (e.g. Mao et al., 2016). In a study of the Oyu Tolgoi porphyry Cu-Au system, Hart et al. (2015) used this approach to distinguish epidote that was associated with the ore-forming system from a later generation unrelated to ore (Fig. 4). The second event overprints post-ore Carboniferous volcanic rocks and granitoids, as well as the host rock sequence; clearly, recognizing two distinct events within the same sequence is critical for a realistic interpretation of vectoring or fertility information.

Chlorite

Chlorite is widely developed in porphyry systems, occurring in late chlorite-sericite assemblages in more proximal positions, and throughout the epidote and chlorite subzones of the propylitic domain. From work done in the AMIRA projects (Cooke et al., 2015, 2017; Wilkinson et al., 2017), we know that it falls into the compositional range of clinochlore but with significant minor and trace element variation. As with epidote, chlorite is very common in many other geological environments, meaning that the discrimination of porphyry-related propylitic chlorite is critical for identifying the distal parts of potentially mineralized hydrothermal systems.

Again, it is fairly early in the development of tools for the discrimination of porphyry-related chlorite.

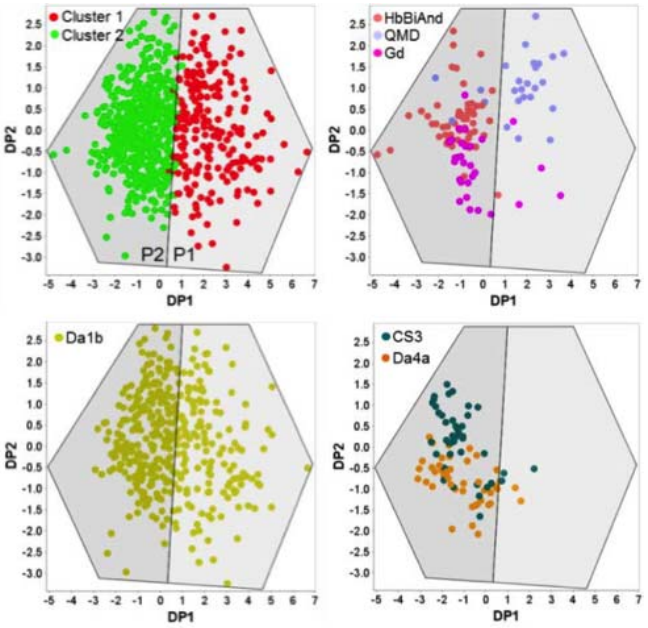

Figure 4. Discriminant projection plots of epidote data from the Oyu Tolgoi district, Mongolia (from Hart et al., 2015). All epidote data were classified into two groups (P1, P2) based on cluster analysis. Epidote data from intrusive units (top right) shows that the Devonian causative intrusions (QMD) classify in P1 whereas Carboniferous granodiorite- and hornblende-biotite andesite-hosted epidote mostly classify in P2. Data from the Devonian augite basalt host rocks (lower left) classify in both groups, which is consistent with primary propylitic and secondary overprinting (Carboniferous) epidote. Epidote data from the post-mineralization, allochthonous Heruga Sequence basaltic volcanic breccia (Da4a) and post-mineralization Carboniferous basaltic-andesitic volcanics (CS3) classify in P2.

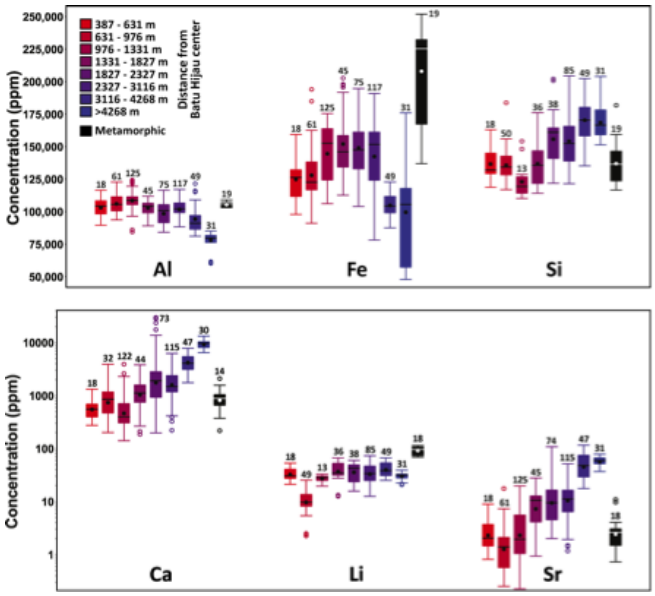

Figure 5. Comparison of metamorphic chlorite compositions (black symbols) with chlorite from Batu Hijau binned by the distance of the samples from the porphyry centre (warm colours are more proximal). Box-and-whisker symbols show: mean value (black/white dot), median (horizontal line), second and third quartiles (extent of box), whiskers (maximum and minimum values that are not outliers), circles (outliers that are greater than 1.5 times the interquartile range from the box). Numbers of analyses included in each bin are shown. From Wilkinson et al. (2015a).

However, comparison of spatial mineral chemistry data from the propylitic halo of the Batu Hijau Cu-Au system, Indonesia (Wilkinson et al., 2015a), showed Fe and Li contents in metamorphic chlorite were fairly distinct from those of porphyry-related chlorite (Fig. 5). Although metamorphic compositions overlap with proximal chlorite compositions for Al, Si, Ca, and Sr, there is a clear distinction between those from distal propylitic chlorite (Wilkinson et al., 2015a). This is the key capability; it is only for the porphyry-distal chlorites in very nondescript propylitic rocks without whole rock geochemical anomalies that discrimination is of paramount importance for exploration.

Other elements that are useful for discrimination purposes are Ag, Sb, and As. Probably for similar reasons as epidote, these elements appear to be taken up at low concentrations in chlorite in the propylitic halos of porphyry systems but are not present at significant levels in metamorphic fluids, and/or are not partitioned into crystallizing metamorphic chlorite.

Magnetite

Magnetite offers significant promise as a tool for discrimination of different kinds of magmatic and hydrothermal environments because of its wide range of potential element substitutions. Furthermore, its magnetism and relatively robust character mean that it survives within, and is easily sampled from, sediments and soils.

The Ca + Al + Mn vs. Ti + V plot developed by Dupuis and Beaudoin (2011) was one of the first attempts to distinguish magnetite derived from porphyry, iron-oxide Cu-Au, skarn, Kiruna-type, Fe-Ti and V deposits, and banded iron formations. Calcium contributes only negligible amounts to the overall cation sum (typically 1–2 orders of magnitude less than the concentrations of Al and Mn) and can effectively be dropped from the y-axis (cf. Nadoll et al., 2014). Ga and Sn have also been identified as useful in the discrimination of magnetite from various hydrothermal systems, with porphyry- and skarn-related hydrothermal magnetite having elevated Ga (>10 ppm) relative to other types (Nadoll et al., 2014), potentially due to a higher temperature of formation.

The Ti vs. Ni/Cr plot proposed by Dare et al. (2014) for the discrimination of hydrothermal and igneous magnetite from felsic magmatic-hydrothermal systems has been shown to be ineffective (Sievwright, 2017). In fact, the simplest and most robust way to separate the two types is based on Ti alone, with a cut-off at 1 wt% correctly separating them in 97.5% of cases in the database of Sievwright (2017). The correct identification of

hydrothermal and igneous populations of magnetite in either rock, heavy mineral concentrates, or soils is a key first-step in the interpretation of its mineral chemistry. Although hydrothermal magnetite is relatively easy to identify we do not yet have a robust tool for identifying porphyry-related populations from those developed in other types of system. However, it is possible to discriminate porphyries of different metal tenor (Sievwright, 2017).

PORPHYRY FERTILITY INDICATORS

"Fertility" — the mineralization potential — of a porphyry system can be assessed at several stages and on several scales of exploration. The fertility of arc segments can be evaluated using a variety of igneous minerals (e.g. zircon, magnetite, apatite) and can indicate whether magmas were suitably hydrous, oxidized, and sulphur-rich to be capable of developing extensive hydrothermal systems with mineralization potential. These tools can also be used on a district scale to identify magmatic complexes, or individual intrusions within such complexes, that may be most likely to host mineralization. Such tools are thus particularly useful as a way of prioritizing geophysical targets. Once a hydrothermal system has been identified, but potentially just its distal propylitic domain, other minerals can be used to evaluate whether it may be extensively mineralized or not (e.g. epidote, chlorite, hydrothermal magnetite).

Zircon

Zircon is extremely useful in the study of igneous and metaorhic petrogenesis because of its robustness through weathering, its utility as a geochronometer, the sensitivity of certain trace element substitutions to intensive parameters, and its resistance to high-temperature diffusive re-equilibration.

One aspect of zircon chemistry that has received significant recent interest is the effect of magmatic redox conditions on partitioning rare earth elements Ce and Eu. Experimental studies have shown that the magnitude of Ce and Eu anomalies varies as a function of melt fO_2 (e.g. Burnham and Berry, 2012), such that zircons from more oxidized systems have larger positive Ce anomalies, and smaller negative Eu anomalies. This redox sensitivity is of particular relevance in the exploration for porphyry deposits because they appear to form from especially oxidized arc magmas (Sillitoe, 2010; Richards, 2014). Zircons from magmatic rocks closely associated with mineralization have been shown to have high values of Ce^{4+}/Ce^{3+} and Eu/Eu*, with moderately elevated Ce/Ce* (Fig. 6; *see* Loader et al., 2017), ascribed by most authors to oxidizing conditions at the time of crystallization (e.g. Dilles et al., 2015; Shen et al., 2015; Lu et al., 2016). It was suggested by these authors that this characteristic may be used to distinguish magmatic systems with high and low ore-forming potential.

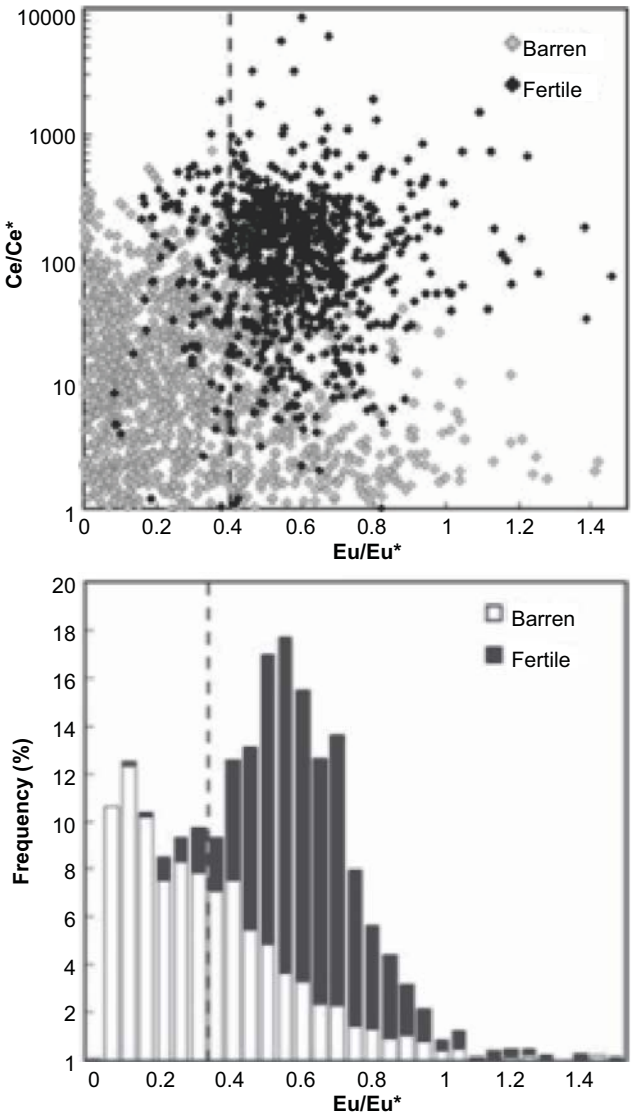

Figure 6. Comparison of Eu/Eu* and Ce/Ce* zircon data from barren and fertile igneous suites. From Loader et al. (2017).

However, as shown by Buret et al. (2016), the co-crystallization or prior crystallization of apatite and/or titanite can significantly impact zircon trace element chemistry. Furthermore, Loader et al. (2017) demonstrated that titanite crystallization can have a major effect on Eu anomalies. It was recommended that only high-Ta zircons (>0.2 ppm Ta) should be used to test for magmatic redox because these are not likely to have had their chemistry modified by titanite crystallization. Ce/Ce* may be unaffected but is difficult to determine accurately; Loader et al. (2017) proposed the use of the formulation $Ce^* = Nd_N^2/Sm_N$ to estimate Ce* in the absence of precise analytical data for La and/or Pr. A lot of overlap exists between barren and fertile magmas in terms of Ce/Ce* but values above ~100 are only rarely seen in barren suites and, when combined with

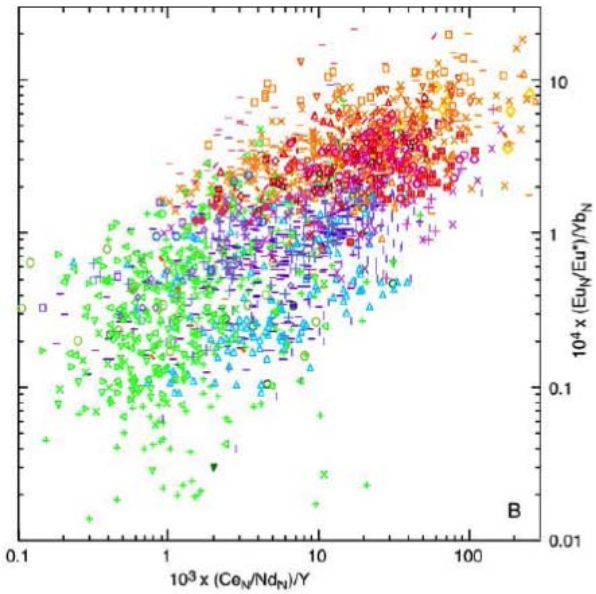

Figure 7. Comparison of (Eu_N/Eu^*)/Yb_N versus (Ce_N/Nd_N)/Y for zircon from barren (blue/green) and fertile (orange/red) igneous suites. From Loucks et al. (2016).

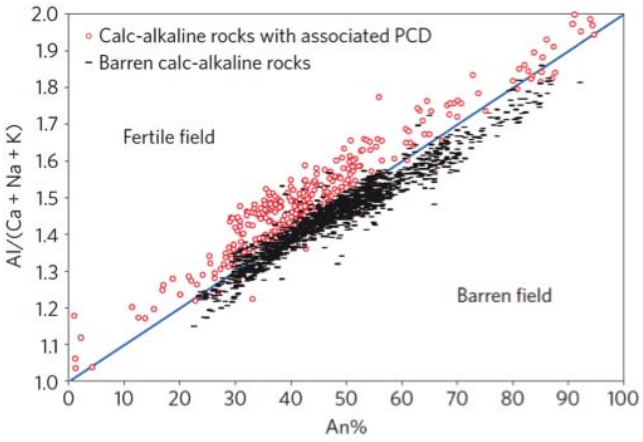

Figure 8. Plot of excess Al in plagioclase (atomic proportion of Al/Ca+Na+K) as a function of anorthite content. Plagioclase from barren systems falls on or below the stoichiometric line shown, whereas grains from mineralized systems fall above the line. From Williamson et al. (2016).

robust Eu/Eu* values above 0.4 (Fig. 6), provides a powerful discriminator of fertile rocks.

Loucks et al. (2016) developed some additional parameters in zircon ($Eu_N/Eu^*/Yb_N$ and $Ce_N/Nd_N/Y$) that can help to discriminate barren and fertile igneous suites. Zircons are thought to inherit the negligible negative Eu anomaly that characterizes fertile magmas as recognized in whole rock data and also to acquire a large positive Ce anomaly in fertile, oxidized melts. Normalizing either of these "fertile-high" parameters to HREE that are typically low in fertile magmas (assuming that zircon inherits this feature too), such as Yb or Y (as a proxy for Ho), enhances the fertility signal (Fig. 7). Because of the difficulty in precisely measuring Ce/Ce*, the Ce anomaly proxy Ce_N/Nd_N was proposed.

Plagioclase

Recent interest in the potential application of plagioclase as a fertility indicator has come from the recognition that it appears to be unusually enriched in Al – above normal stoichiometric levels – in fertile porphyry systems (Williamson et al., 2016; *see* Fig. 8). Although these results are promising, there remains more work to be done to confirm that this behaviour is systematically observed in mineralized systems and, indeed, what it represents. Experimental studies by Kyono and Kimata (2001) suggested that this may be due to substitution of water into vacancy sites [ ]Si_4O_8 as a result of high H_2O_{melt}.

Apatite

Limited work has investigated apatite chemistry as a potential tool for assessment of fertility, although it undoubtedly offers significant potential because it can track key melt parameters, such as halogen content (or Cl/H_2O ratio), sulphur content, redox sensitive elements like Mn (Miles et al., 2013), and tracers of melt evolution like the REE.

Belousova et al. (2002) showed that low Mn, low Y/ΣREE, high La/Sm and high Ce/Th characterized apatite from more oxidized igneous rocks, but these authors did not study porphyry systems specifically. Rukhlov et al. (2017) evaluated apatite composition as a proxy for the oxidation states of porphyry Cu-Mo-Au deposits and concluded that S, V, and Eu correlated with the oxidation state of the magmas. However, there was no explicit assessment of differences between mineralized and unmineralized systems. Recently, Brugge et al. (2017) illustrated the complexity of apatite chemistry that can be observed in a single porphyry system (Chuquicamata, Chile; *see* Fig. 9), emphasizing that our understanding of its chemistry in porphyry deposits is in its infancy.

Epidote

The chemistry of propylitic epidote in part reflects metasomatic mass transfer by magmatic-hydrothermal fluids, as well as crystallization conditions, precursor phase chemistry (if formed by replacement), and competition with co-crystallizing minerals. Cooke et al. (2014a) suggested that chalcophile metalloids As and Sb, which may be incorporated into epidote, are preferentially sequestered by pyrite within the pyrite halo of porphyry systems, leading to low concentrations in other phases. However, in the more distal propylitic zones where H_2S has been consumed, their concentrations in epidote increase. Assuming As and Sb are primarily derived from magmatic-hydrothermal fluids, the levels attained in epidote may be a qualitative proxy for the total metal flux in the system.

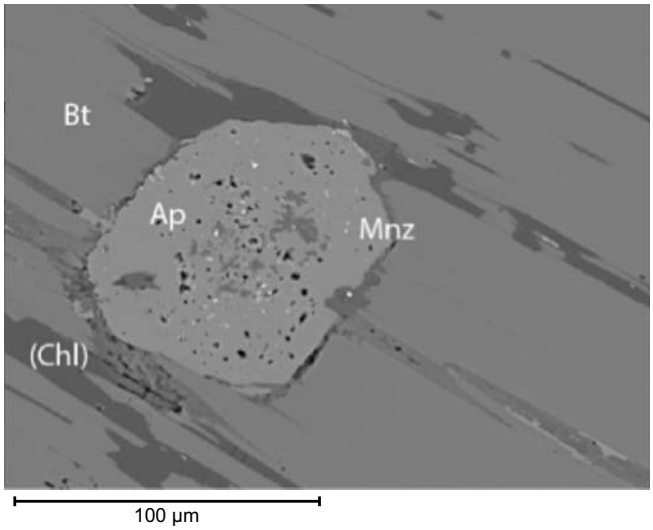

Figure 9. Primary igneous apatite in biotite from Chuquicamata, Chile, overprinted by secondary alteration resulting in crystallization of monazite and pitting (from Brugge et al., 2017). Note: Ap = apatite; Bt = biotite; Chl = chlorite; and Mnz = monazite.

Enrichments of other fluid-mobile metals that can be incorporated into epidote, such as Zn, may also prove to be useful for assessing metal endowment in porphyry systems but remain to be evaluated.

Chlorite

Chlorite chemistry offers a lot of potential as a fertility tool, but there is no information in the public domain to date. However, results from the AMIRA projects show that the Mn and Zn contents in chlorite are potential indicators of endowment in porphyry systems (Fig. 10). It is also evident that these elements reach a peak concentration in chlorite at distances of ~1-3 km from porphyry centres, coincident with the whole rock geochemical maxima that are commonly observed for these metals (e.g. Pacey, 2017).

PORPHYRY VECTORING TOOLS

Epidote

Propylitic epidote shows some fairly systematic spatial variations in relation to the ore zone of porphyry systems. In the Baguio district, Philippines, Cu, Mo, Au, and Sn were found to be high proximal to the known porphyry centres but it is not yet clear if this is related to substitution of these elements into the epidote structure or if it reflects an increased abundance of nano-inclusions (Cooke et al., 2014a). Similar to chlorite, Mn and Zn are enriched in epidote just outside the pyrite halo, as are La, Y, Zr, and Sr. Elements that are enriched most distally are As, Sb, and Pb. Broadly similar patterns are reported for the El Teniente system, Chile (Fig. 11), indicating that epidote shows comparable behaviour in both Cu-Au and Co-Mo porphyry environments (Wilkinson et al., 2017).

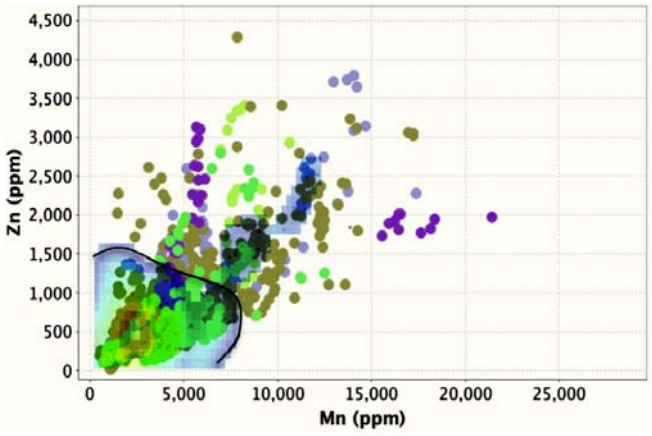

Figure 10. Zn versus Mn plot (n = 5015) for chlorite from porphyry systems. Contoured data are from metamorphic background, prospects, and small deposits (West Scotland, Georgetown Inlier, Harts Range, Shebandowan Greenstone Belt, Central Chile, Baguio district); 97.7% of the data from these systems fall below the black line indicated. A large proportion of the giant porphyry system data (coloured symbols: Batu Hijau, El Teniente, Collahuasi District) also fall below the line, but the majority of data that fall above it (95.0%) are from these fertile settings. Thus, chlorite with elevated Mn and Zn content are fairly characteristic of the propylitic halo of economic porphyry deposits. Data from AMIRA P1060 project.

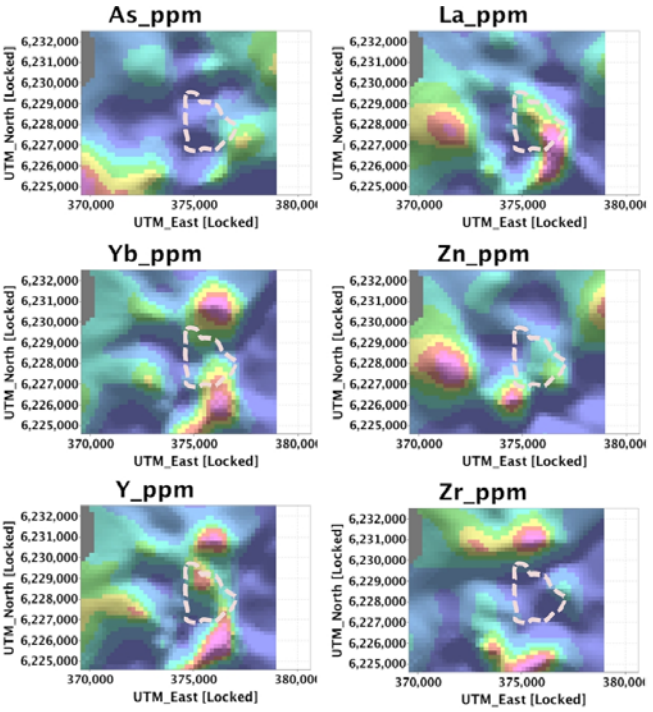

Figure 11. Gridded epidote compositional data (log of sample average, cell size 200 m, minimum smoothing distance 4 cells) for trace elements in epidote from El Teniente, Chile, showing proximal lows and highs just outboard of the ore zone. Outline of the 0.5 wt% Cu shell is shown for reference. Note the apparent westward offset between some of the epidote anomalies and the location of the orebody at depth, possibly due to post-ore westward tilt. From Wilkinson et al. (2017).

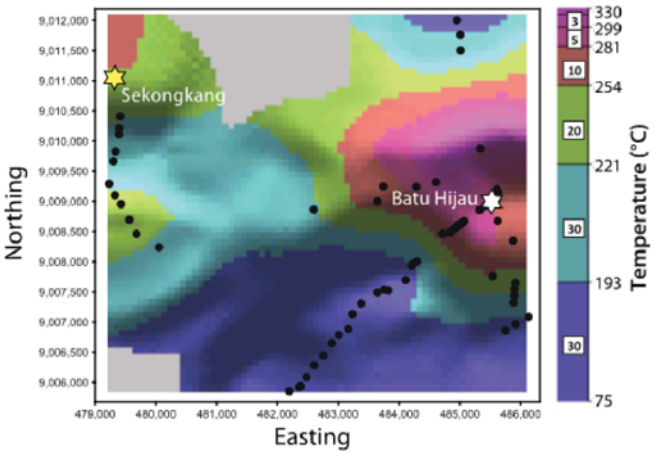

Figure 12. Gridded chlorite geothermometry results (sample mean data, 100 m pixels) for the Batu Hijau porphyry Cu-Au system, Indonesia. Chlorite clearly maps out the thermal anomaly associated with the ore deposit as well as a west-northwest-trending ridge that follows the underlying intrusive complex and a zone of elevated (inner propylitic) grade at surface. Sample locations are shown. From Wilkinson et al. (2015a).

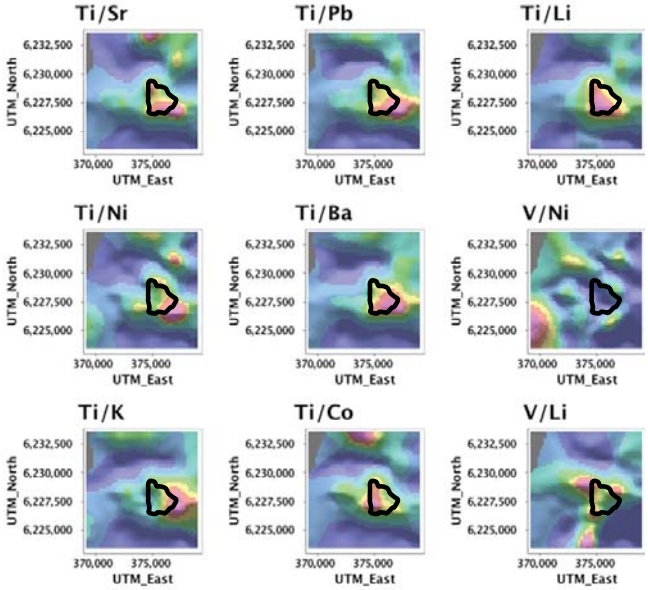

Figure 13. Gridded chlorite trace element ratios (log of sample average, cell size 200 m, minimum smoothing distance 5 cells) for samples from El Teniente, Chile. Outline of the 0.5 wt% Cu shell is shown for reference. From Wilkinson et al. (2017).

These systematic zonation patterns can be used as a broad vectoring tool within the propylitic halos of porphyry systems. Decreases in As, Sb, and Pb content in epidote would be expected as the centre is approached, with a range of other elements increasing to a maximum on the fringes of the pyrite halo. Proximal high elements should be supportive of other geological evidence (potassic alteration, whole rock anomalism of normal porphyry pathfinder elements) indicating that a hydrothermal centre is nearby. They may even be indicative of mineralization as opposed to just a barren hydrothermal system, but this has yet to be tested.

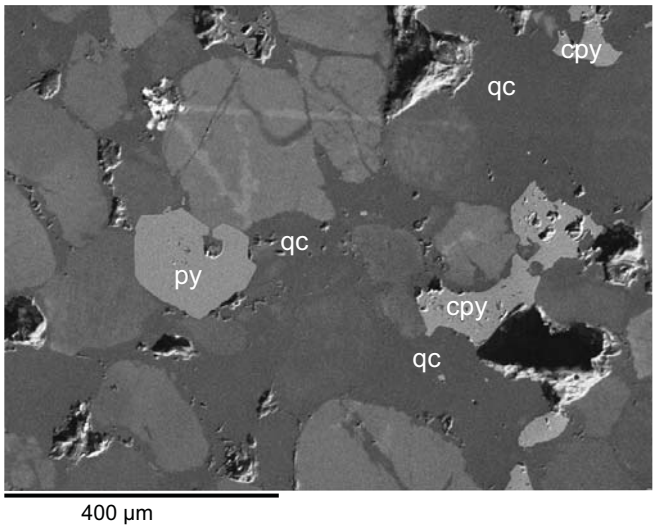

Figure 14. Scanning electron microscope-cathodoluminescence image of quartzite from the Bingham Canyon porphyry system, Utah. The sample, which was collected 1310 m from the deposit centre, shows dull grey luminescent quartz cement (qc) that has overgrown and cuts detrital grains, and is associated with pyrite (py) and chalcopyrite (cpy). Image courtesy of Jo Taylor, AMIRA P1060 project.

Chlorite

Propylitic chlorite has been convincingly demonstrated to delineate the thermal anomaly associated with porphyry systems (Fig. 12) as well as display systematic major and trace element variations as a function of distance from the hydrothermal centre (Baker et al., 2015; Wilkinson et al., 2015a, 2017). Furthermore, trace element ratios can be used to predict the absolute distance to the system centre. A range of ratios have been proposed (e.g. Ti/Sr, Ti/Ni, Ti/Li, Ti/Pb, Ti/Ba, Mg/Sr, Mg/Ca, V/Ni) that vary up to four orders of magnitude and therefore provide clearly recognizable, roughly exponential gradients (e.g. Fig. 13). Thus, chlorite is extremely useful for exploring within fairly unremarkable greenrock terrains and for buried deposits.

Quartz

Quartz veins are ubiquitous in all but some alkalic porphyry systems but form over a wide range of temperature and from diverse fluids. Consequently, a significant degree of heterogeneity might be expected in quartz trace-element chemistry, as indicated by microprobe studies (Rusk et al., 2008). However, in some sediment-hosted porphyry systems, such as Bingham Canyon, quartzite host rocks are pervasively cemented by hydrothermal quartz (Fig. 14) that can show more systematic trace element behaviour.

At Bingham, quartz cements show consistent decreases of over ~3 orders of magnitude in trace element ratios, including Ti/As, Cu/Sr, Cu/Li and Ti/Li,

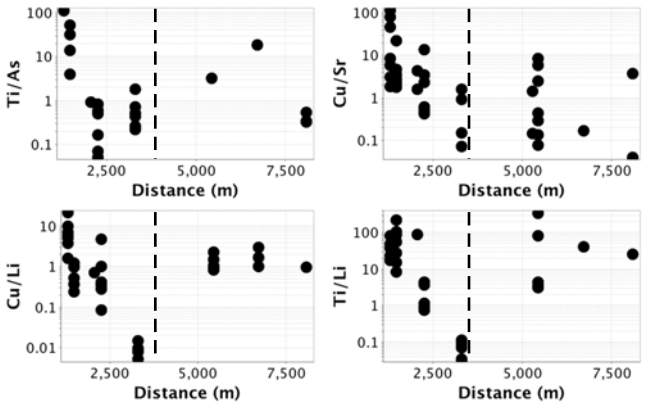

Figure 15. Chemistry of quartz cement in quartzites from the halo of the Bingham Canyon porphyry system. Systematic, approximately exponential, decreases in trace element ratios are observed out to ~3.5 km. Data from AMIRA P1060 project.

out to ~3.5 km (Fig. 15), beyond which there is either a lot of scatter or ratios stabilize to a constant value (e.g. Cu/Li). Ti substitution in quartz is known to be thermally controlled (Wark and Watson, 2006) so the high proximal concentrations observed at Bingham are not unexpected. Copper also appears to substitute into quartz in greater concentrations near the orebody, although the existence of nano-inclusions of sulphides cannot be ruled out. Trace elements that are low in proximal quartz are the same as those that are depleted in proximal chlorite, suggesting that chemical controls on partitioning are not important; we assume that fluid properties and complexation behaviour of these elements prevent their incorporation into silicates at the elevated temperature and lower pH/higher fO_2 conditions likely to exist in more proximal regions.

Hydrothermal magnetite

Hydrothermal magnetite is common in the potassic zone of porphyry systems and is particularly abundant in porphyry Cu-Au deposits. However, it also extends beyond the typical potassic zone in biotite-magnetite domains (e.g. Northparkes, New South Wales; Pacey, 2017) and further into the propylitic domain. Sievwright (2017) showed that hydrothermal overprinting of precursor igneous magnetite is common in propylitic rocks, with euhedral overgrowth of magnetite on igneous titanomagnetite and/or partial recrystallization/re-equilibration of igneous magnetite (e.g. Fig. 16).

In exploration, just the proportion of hydrothermal magnetite in a stream sediment concentrate may be a useful indicator of the likely location of a hydrothermal centre relative to stream catchments. Sievwright (2017) developed this further and showed that the alteration association of hydrothermal magnetite (i.e. whether magnetite was derived from potassic, propylitic, phyllic, or intermediate argillic domains) could be discrim-

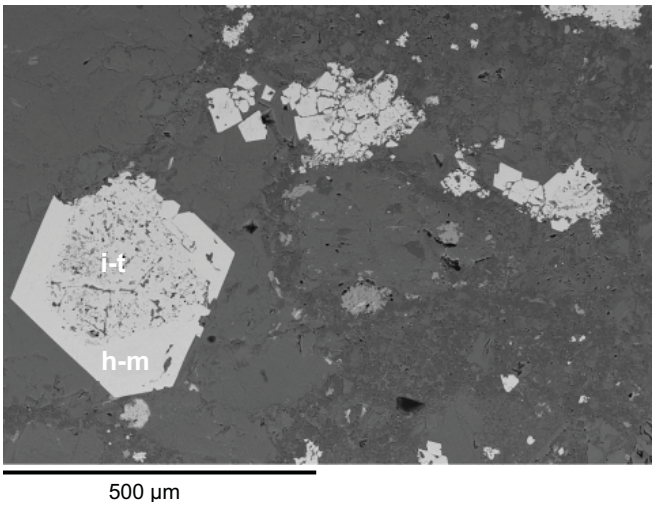

Figure 16. Backscattered scanning electron microscope image showing euhedral hydrothermal magnetite overgrowth (h-m) on an igneous titanomagnetite (i-t) core. Volcanic lithic breccia sample collected 1.1 km from the deposit centre, Batu Hijau, Indonesia. Image from AMIRA P1060 project.

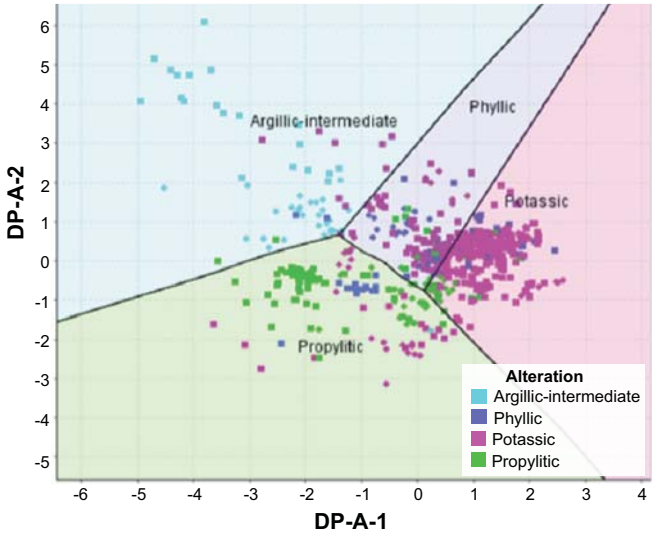

Figure 17. Discriminant projection plot showing that hydrothermal magnetite from different alteration domains can be quite effectively discriminated using multivariate trace element geochemistry (from Sievwright, 2017).

inated (Fig. 17). Similar vectoring potential is offered by apatite (Bouzari et al., 2016). Given the instability of magnetite in phyllic and intermediate argillic alteration, it is assumed that magnetite present in these domains is a partially overprinted relic from precursor potassic or propylitic assemblages. The magnetite discrimination plot allows hydrothermal magnetite from different domains to be identified, which would be particularly useful when using stream sediments to map catchment areas.

SUMMARY

The major and trace element chemistry of a range of igneous and alteration phases associated with porphyry

systems provide a valuable record of processes that resulted in the genesis of these major ore deposits. Recognizing and deciphering these fingerprints remain, for the most part, in their infancy but there is now clear evidence that valuable information is locked up in these indicator minerals that can be utilized as valuable discrimination, fertility, and vectoring tools. In concert with conventional approaches, these methods have a good chance of improving discovery success for porphyry ore deposits, particularly under cover.

Acknowledgements

The authors are grateful to Sarah Gilbert, Leonid Danyushevsky at CODES and Martina Bertini and William Brownscombe at LODE for support of LA-ICP-MS analyses. We thank Karsten Goemann, Central Science Laboratories, University of Tasmania, and John Spratt and Anton Kearsley, Imaging and Analysis Centre, Natural History Museum, for assistance with microprobe and SEM analyses. Alan Goode and Adele Seymon provided project management for the AMIRA-sponsored research. We are grateful to all the sponsors of AMIRA P765A and P1060, and to Rio Tinto, who are specifically acknowledged for their support of the Ph.D. studies of Matt Loader, Rob Sievwright, and Emily Brugge.

REFERENCES

Baker, M.J., Wilkinson, J.J., Wilkinson, C.C., Cooke, D.R., and Inglis, S., 2015. Chlorite trace element chemistry as an exploration tool: a case study from the Collahuasi mining district, northern Chile, *In: World-Class Ore Deposits: Discovery to Recovery*; Society of Economic Geology 2015 Conference, Hobart, Tasmania, September 27-30, 2015.

Baker, M.J., Cooke, D.R., Hollings, P.N., and Piquer, J., 2017. Identification of hydrothermal alteration related to mineralisation using epidote mineral chemistry, *In: Proceedings;* 15th Biennial Society for Geology Applied to Mineral Deposits (SGA) Conference*,* Quebec City, August 20-23, 2017, 1069–1071.

Belousova E.A., Griffin W.L., O'Reilly S.Y., and Fisher N.I., 2002. Apatite as an indicator mineral for mineral exploration: Trace-element compositions and their relationship to host rock type; *Journal of Geochemical Exploration*, v. 76, p. 45–69.

Bird, D.K. and Spieler, AR., 2004. Epidote in geothermal systems. Mineralogical Society of America; *Reviews in Mineralogy and Geochemistry*, v. 56, p. 35–300.

Bouzari, F., Hart, C.J.R., Bissig, T., and Barker, S., 2016. Hydrothermal alteration revealed by apatite luminescence and chemistry: a potential indicator mineral for exploring covered porphyry copper deposits; *Economic Geology*, v. 111, p. 1397–1410.

Brugge, E., Wilkinson, J.J., and Miles, A., 2017. Habit and chemistry of apatite at Chuquicamata, Chile, *In: Proceedings;* 15th Biennial Society for Geology Applied to Mineral Deposits (SGA) Conference, Quebec City, August 2017, 287–290.

Buret, Y., von Quadt, A., Heinrich, C., Selby, D., Wällea, M., and Peytcheva, I., 2016. From a long-lived upper-crustal magma chamber to rapid porphyry copper emplacement: Reading the geochemistry of zircon crystals at Bajo de la Alumbrera (NW Argentina); *Earth and Planetary Science Letters*, v. 450, p. 120–131.

Burnham, A.D. and Berry, A.J., 2012. An experimental study of trace element partitioning between zircon and melt as a function of oxygen fugacity; *Geochimica Cosmochimica Acta*, v. 95, p. 196–212.

Cooke, D.R., Baker, M., Hollings, P., Sweet, G., Chang, Z., Danyushevsky, L., Gilbert, S., Zhou, T., White, N., Gemmell, J.B., and Inglis, S., 2014a. New advances in detecting the distal geochemical footprints of porphyry systems - Epidote mineral chemistry as a tool for vectoring and fertility assessments, *In:* Kelley K.D. and Golden H.C. (eds.), *Building Exploration Capability for the 21st Century*; Society of Economic Geologists, Special Publication 18, p. 127–152.

Cooke, D.R., Hollings, P., Wilkinson, J.J., and Tosdal, R.M., 2014b. Geochemistry of porphyry deposits, *In:* Holland, H.D. and Turekian, K.K. (eds), *Treatise on Geochemistry 13, Second edition*; Elsevier, Oxford, p. 357–381.

Cooke, D.R., Wilkinson, Jamie J., Baker, M., Agnew, P., Wilkinson, C.C., Martin, H., Chang, Z., Chen, H., Gemmell, J.B., Inglis, S., Danyushevsky, L., Gilbert, S., and Hollings, P., 2015. Using mineral chemistry to detect the location of concealed porphyry deposits – an example from Resolution, Arizona, *In: Proceedings*; International Applied Geochemistry Symposium, Tucson, Arizona.

Cooke, D.R., Agnew, P., Hollings, P., Baker, M., Chang, Z., Wilkinson, J.J., White, N.C., Zhang, L., Thompson, J., Gemmell, J.B., Fox, N., Chen, H., and Wilkinson, C.C., 2017. Porphyry indicator minerals (PIMS) and porphyry vectoring and fertility tools (PVFTS) – indicators of mineralization styles and recorders of hypogene geochemical dispersion halos, *In: Proceedings*; Exploration 17, Toronto, October 22-25, 2017.

Dare, S.A.S., Barnes, S.J., Beaudoin, G., Méric, J., Boutroy, E., and Potvin-Doucet, C., 2014. Trace elements in magnetite as petrogenetic indicators; *Mineralium Deposita*, v. 49, p. 785–796.

Dilles, J.H., Kent, A.J.R., Wooden, J.L., Tosdal, R.M., Koleszar, A., Lee, R.G., and Farmer, L.P., 2015. Zircon compositional evidence for sulfur-degassing from ore-forming arc magmas; *Economic Geology*, v. 110, p. 241–251.

Dupuis, C. and Beaudoin, G., 2011. Discriminant diagrams for iron oxide trace element fingerprinting of mineral deposit types; *Mineralium Deposita*, v. 46, p. 319–335.

Hart, L.A., Wilkinson, J.J., Armstrong, R.N., and Araujo, D., 2017. Classifying propylitic alteration in complex porphyry systems; a case study of the Oyu Tolgoi Cu-Au porphyry deposits, Southern Mongolia, *In: Proceedings;* 14th Biennial Society of Geology Applied to Mineral Deposits (SGA) conference, Quebec City, August 20–23, 2017.

Kyono, A. and Kimata, M., 2001. Refinement of the crystal structure of a synthetic non-stoichiometric Rb-feldspar; *Mineral Magazine*, v. 65, p. 523–531.

Lindgren W., 1933. *Mineral Deposits*; McGraw-Hill Book Co., New York.

Loader, M.A., Wilkinson, J.J., and Armstrong, R.N., 2017. The effect of titanite crystallisation on Eu and Ce anomalies in zircon and its implications for the assessment of porphyry Cu deposit fertility; *Earth and Planetary Science Letters*, v. 472, p. 107–119.

Loucks, R.R., Fiorentini, M.J., and Lu, Y-J., 2016. Detrital zircon chemistry. Centre for Exploration Targeting, University of Western Australia. http://www.cet.edu.au/news-and-media/news/news-details/2016/ 09/02/detrital-zircon-chemistry.

Lu, Y.-J., Loucks, R.R., Fiorentini, M., McCuaig, T.C., Evans, N.J., Yang, Z.-M., Hou, Z.-Q., Kirkland, C.L., Parra-Avila, L.A., and Kobussen, A., 2016. Zircon compositions as a pathfinder for porphyry Cu ±Mo ±Au deposits, *In:* Richards, J.P. (ed.)

Tectonics and Metallogeny of the Tethyan Orogenic Belt; Society of Economic Geologists, Special Publication 19, p. 329–347.

Mao, M., Rukhlov, A.S., Rowins, S.M., Spence, J., and Coogan, L.A., 2016. Apatite trace element compositions: A robust new tool for mineral exploration; *Economic Geology*, v. 111, p. 1187–1222.

Miles, A.J. Graham, C.M., Hawkesworth, C.J., Gillespie, M.R., Hinton, R.W., Bromiley, G.D., and EMMAC, 2014. Apatite: A new redox proxy for silicic magmas? *Geochimica et Cosmochimica Acta*, v. 132, p. 101–119.

Nadoll, P., Angerer, T., Mauk, J.L., and Walshe, J., 2014. The chemistry of hydrothermal magnetite: A review; *Ore Geology Reviews*, v. 61, p. 1–32.

Pacey, A., 2017. *The characteristics, geochemistry and origin of propylitic alteration in the Northparkes porphyry Cu-Au system*; Ph.D .thesis, Imperial College London, 631 p.

Richards, J.P., 2014. The oxidation state, and sulfur and Cu contents of arc magmas: implications for metallogeny; *Lithos*, p. 233, p. 27–45.

Rukhlov, A.S., Plouffe, A., Ferbey, T., Mao, M., and Spence, J., 2016. Application of trace-element compositions of detrital apatite to explore for porphyry deposits in central British Columbia, *In: Geological Fieldwork 2015*; British Columbia Ministry of Energy and Mines, British Columbia Geological Survey Paper 2016-1, p. 145–179.

Rukhlov, A.S., Rowins, S.M., Mao, M., Coogan, L.A., and Spence, J., 2017. *Apatite compositions as a proxy for the oxidation states of porphyry Cu-Mo-Au deposits*; British Columbia Ministry of Energy and Mines, British Columbia Geological Survey GeoFile 2017-2.

Rusk, B.G., Lowers, H.A., and Reed, M.H., 2008. Trace elements in hydrothermal quartz: Relationships to cathodoluminescent textures and insights into vein formation; *Geology*, v. 36, p. 547–550.

Shen, P., Hattori, K., Pan, H., Jackson, S., and Seitmoratova, E., 2015. Oxidation condition and metal fertility of granitic magmas: zircon trace-element data from porphyry Cu deposits in the Central Asian Orogenic Belt; *Economic Geology*, v. 110, p. 1861–1878.

Sievwright, R., 2017. *Developing magnetite chemistry as an exploration tool for porphyry copper deposits*; Ph.D. thesis, Imperial College London, 340 p.

Sillitoe, R.H., 2010. Porphyry copper systems; *Economic Geology,* v. 105, p. 3–41.

Vry, V.H., Wilkinson, J.J., Seguel, J., and Millan, J., 2010. Multistage intrusion, brecciation, and veining at El Teniente, Chile: Evolution of a nested porphyry system; *Economic Geology*, v. 105, p. 119–153.

Wark, D.A. and Watson, E.B., 2006. The TitaniQ: a Titanium-in-quartz geothermometer; *Contributions to Mineralogy and Petrology*, v. 152, p. 743–754.

Williamson, B., Herrington, R.J., and Morris, A., 2016. Porphyry copper enrichment linked to excess aluminium in plagioclase; *Nature Geoscience*, v. 9, p. 237–241.

Wilkinson, J.J., 2013. Triggers for the formation of porphyry ore deposits in magmatic arcs; *Nature Geoscience*, v. 6, p. 917–925.

Wilkinson, J.J., Chang, Z., Cooke, D.R., Baker, M.J., Wilkinson, C.C., Inglis, S., Chen, H., and Gemmell, J.B., 2015a. The chlorite proximitor: A new tool for detecting porphyry ore deposits; *Journal of Geochemical Exploration*, v. 152, p. 10–26.

Wilkinson, C.C., Harman, E.M., and Wilkinson, J.J., 2015b. Epidote chemistry in contrasting hydrothermal and metamorphic environments, *In: World-Class Ore Deposits: Discovery to Recovery*; Society of Economic Geology 2015 Conference, Hobart, Tasmania, September 27-30, 2015

Wilkinson, J.J., Baker, M.J., Cooke, D.R., Wilkinson, C.C., and Inglis, S., 2017. Exploration targeting in porphyry Cu systems using propylitic mineral chemistry: a case study of the El Teniente deposit, Chile, *In: Proceedings;* 14th Biennial Society of Geology Applied to Mineral Deposits (SGA) conference, Quebec City, August 20–23, 2017.

Wilson, J.R. and Leake, B.E., 1972. The petrochemistry of the epidiorites of the Tayvallich Peninsula, North Knapdale, Argyllshire; *Scottish Journal of Geology*, v. 8, p. 215–252.

Rare earth element indicator minerals: an example from the Strange Lake deposit, Quebec and Labrador, eastern Canada

M.B. McClenaghan[1*], R.C. Paulen[1], I.M. Kjarsgaard[2], and R. Fortin[1]

[1]Geological Survey of Canada, 601 Booth Street, Ottawa, Ontario, Canada K1A 0E8
[2]Mineralogical Consultant, 15 Scotia Place, Ottawa, Ontario, Canada K1S 0W2
*(*Corresponding author's e-mail: beth.mcclenaghan@canada.ca)*

Currently no rare earth element (REE) metals are mined or processed in Canada, however, significant REE resource potential exists. Because Canada has a glaciated landscape, indicator mineral methods have the potential to be useful exploration tools. The focused recovery of REE indicator minerals from glacial sediments such as till, however, is relatively new. Simandl et al. (2015) summarized potential REE indicator minerals that could be of use in glaciated terrain, which include pyrochlore (e.g. DiLabio, 1988, 1995; Lehtonen et al., 2011), columbite-tantalite (Mackay and Simandl, 2015), phosphates (e.g. monazite, rhabdophane) (Lehtonen et al., 2011), carbonates (e.g. bastnaesite, kainosite, parasite, synchysite), barite, Na-pyroxenes (e.g. aegirine), Na- and K-amphiboles (e.g. arfvedsonite, richterite) (e.g. Hawthorne et al., 2001), baddeleyite, Nb-rutile, Ti-Zr garnet, magnetite, apatite (e.g. Belusova et al., 2002a), fluorite (e.g. Makin et al., 2014), and zirconosilicates such as gittinsite, zircon, and elpidite (e.g. Birkett et al., 1992; Salvi and Williams-Jones, 1995; Belusova et al., 2002b; Lehtonen et al., 2011).

The undeveloped Strange Lake peralkaline complex in eastern Canada (Fig. 1) is one of the world's largest deposits of Zr, Y, and heavy rare earth elements (HREE) (Zajac, 2015). The Geological Survey of Canada, under the auspices of the Geo-Mapping for Energy and Minerals Program (GEM2), collected bedrock and till samples at the deposit to evaluate and test modern indicator mineral methods for detecting REE deposits using glacial sediments. This chapter provides an overview of the indicator mineral methods tested and the results.

GEOLOGY

Bedrock geology

The bedrock geology of the area is summarized below from Miller (1986, 1988, 1990, 1996), Sinclair et al. (1992), Kerr (2013), and Gowans et al. (2014). The Strange Lake pluton is a Mesoproterozic peralkaline granite dated at 1240 +/- 2 Ma (Miller et al., 1997) that intruded along the contact between older quartzo feldspathic and amphibolitic gneisses to the north and quartz monzonite to the south (Fig. 1). The complex consists of at least three varieties of peralkaline granite, which have been divided into four granitic subunits by Miller (1986, 1990, 1997) based on their mineralogy and the presence of inclusions (Fig. 2). The highest grade of mineralization is in pegmatite-aplite dykes that are associated with the exotic-rich granite in the central part of the intrusion (Main Zone) and the northwest edge (B Zone) (Fig. 1). Table 1 provides a list of potential indicator minerals contained in the deposit and the elements they host; this list is summarized from Jambor et al. (1996,1998), Birkett et al. (1992, 1996), Miller et al. (1997), and Zajac (2015).

The Strange Lake intrusion was discovered by the Iron Ore Company of Canada in 1979 in the follow-up of a lake sediment anomaly reported by the GSC (Hornbrook et al., 1979; McConnell and Batterson, 1987; Zajac, 2015). From 1980 to 2006, several companies explored the property and two mineralized zones were identified, the Main Zone (formerly the A Zone) and the B Zone (Fig. 2). The B Zone is the largest resource with indicated mineral resources of 278 Mt at 0.93% total rare earth element oxide (TREO) and inferred mineral resources of 214 Mt at 0.85% TREO (Gowans et al., 2014). The resource for the smaller Main Zone has been estimated at 55.8 Mt with a grade of 2.99% ZrO_2, 0.38% Y_2O_3, 0.29% Nb_2O_5, 0.08% BeO (Kerr and Rafuse, 2012; Kerr, 2013). The Strange Lake intrusion has a strong gamma-ray signature (Geological Survey of Canada, 1980), as can be seen in Figure 3, and it also has a glacial dispersal train of radioactive boulders and minerals in till at least 50 km down-ice to the east-northeast.

Surficial geology

During the Wisconsin glacial event, the Strange Lake deposit was strongly scoured by the Laurentide Ice Sheet flowing outward from an ice dome over central Quebec (Dyke and Prest, 1987). Most of the landscape is covered by till of variable thickness, from <2 m to over several metres. The morphology is characterized by streamlined landforms that were carved out by fast glacial flow from an ice stream that flowed toward the east-northeast (Paulen et al., 2017). Boulders, cobbles, and glacial sediment have been dispersed in a ribbon-shaped train that can be traced for more than 50 km down-ice to the northeast and can be detected by boul-

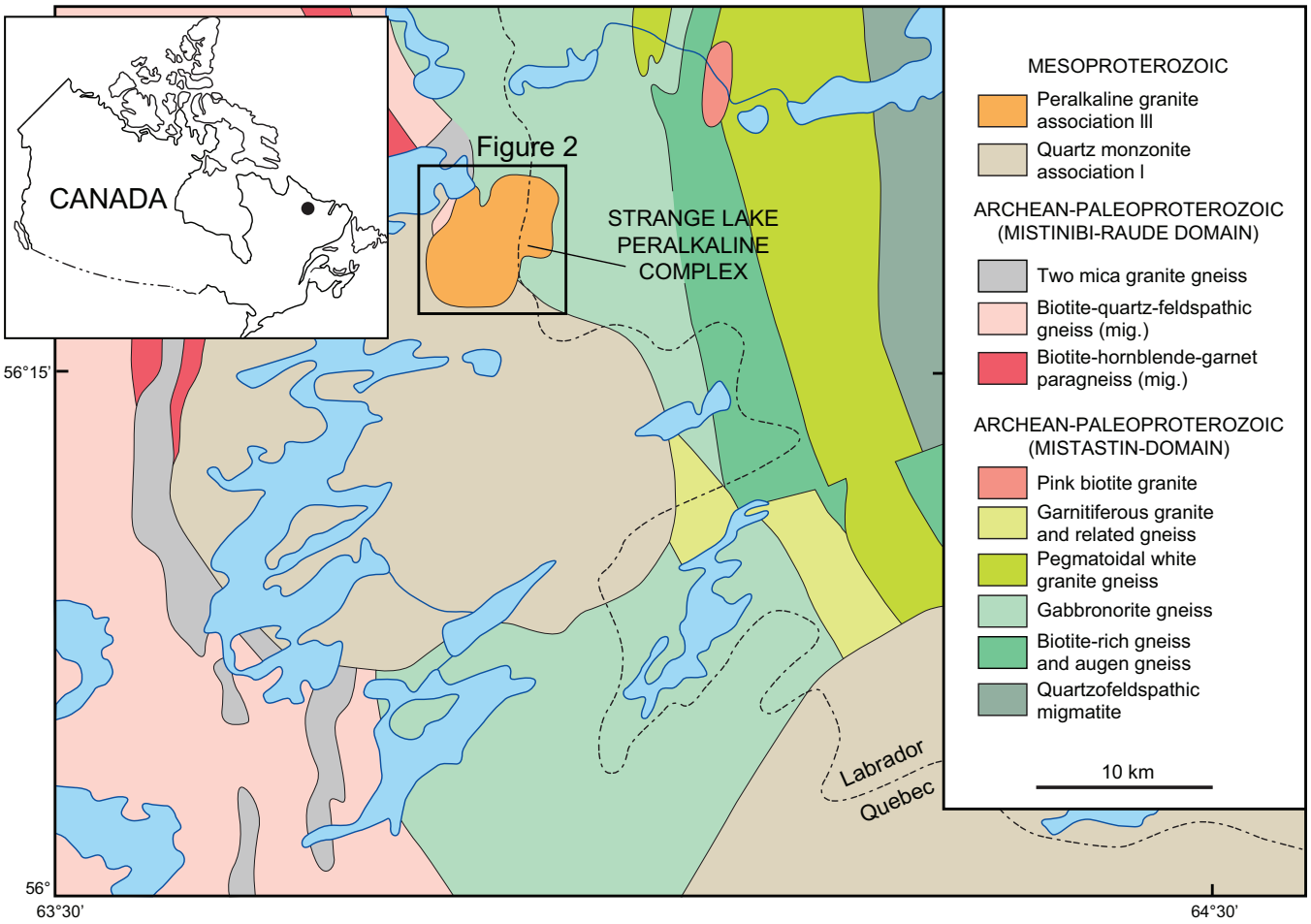

Figure 1. Location of the study area in eastern Canada (inset) and regional bedrock geology map of the Strange Lake area (modified from Miller et al., 1997).

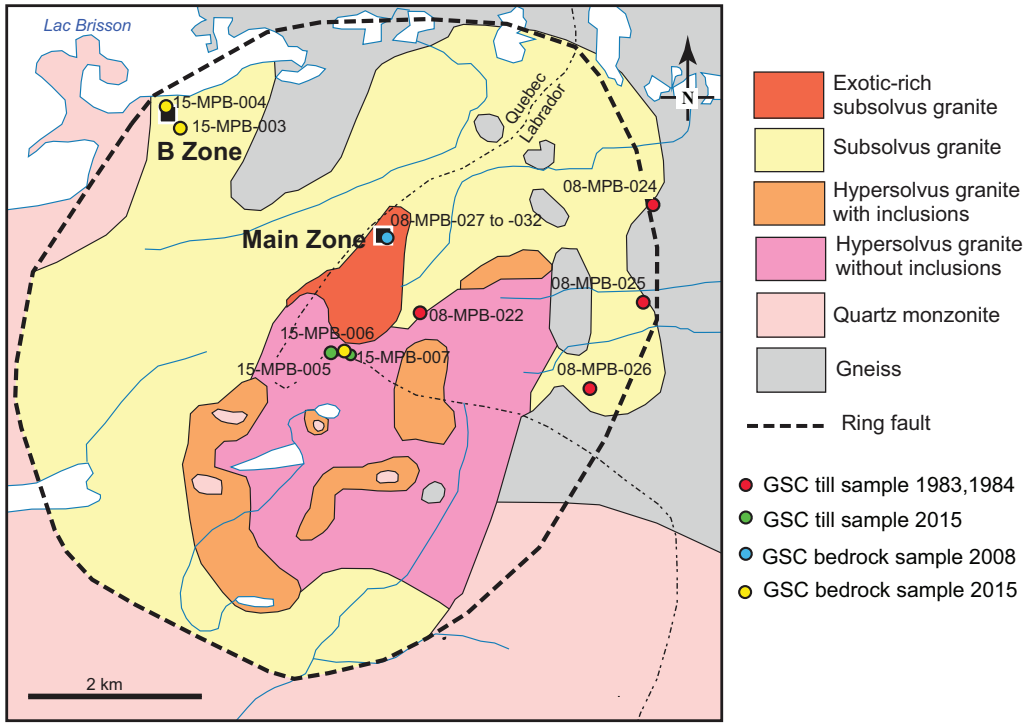

Figure 2. Simplified bedrock geology map of the Strange Lake intrusion, modified from Kerr (2013), after Miller (1986) and Miller et al. (1997).

Table 1. List of potential indicator minerals in the Strange Lake deposit compiled from Birkett et al. (1992, 1996), Sinclair (1992), Miller (1996), Jambor et al. (1996, 1998), Roelofson and Veblen (1999), and Gowans et al. (2014). Indicator minerals recovered from bedrock and till samples in the study by McClenaghan et al. (2017) are indicated.

Mineral	Formula	Hardness*	Density*	Reported by others	Seen in bedrock PTS in this study	Seen in bedrock HMC in this study	Seen in till HMC in this study	Element source in glacial dispersal train
U, Th minerals								
cerianite	$(Ce,Th)O_2$	*not determined*	7.2	no	no	yes	no	Ce, Th
thorite	$Th(SiO_4)$	5.0	4–6.7	Miller (1996)	no	yes	yes	Th
thorianite	ThO_2	6.0	10.0	no	yes	yes	yes	Th
uraninite	UO_2	5–6	6.5–10.95	no	yes	yes	no	U
Zr minerals								
elpidite	$Na_2ZrSi_6O_{15}•3(H_2O)$	7	2.54	Birkett et al. (1992)	yes	no	yes	Zr
hilairite	$Na_2ZrSiO_3O_9•3H_2O$	4.5	2.72	Roelofson & Veblen (1999)	no	no	no	Zr
dalyite	$K_2ZrSi_6O_{15}$	7.5	2.84	Birkett et al. (1992)	no	no	no	Zr
vlasovite	$Na_2ZrSi_4O_{11}$	6	2.97	Birkett et al. (1992)	no	no	no	Zr
zircon	$ZrSiO_4$	7.5	4.6–4.7	Birkett et al. (1992)	yes	yes	yes	Zr
armstrongite	$CaZrSi_6O_{15}•3(H_2O)$	4.5	2.7	Birkett et al. (1992)	no	no	no	Zr
catapleiite	$NaZrS_33O_9•2(H_2O)$	4.5–5	2.8	Birkett et al. (1992)	yes	yes	no	Zr
Ca-catapleiite	$CaZrSi_3O_9•2(H_2O)$	4.5–5	2.8	Birkett et al. (1992)	yes	yes	no	Zr
calciohilairite	$CaZrSi_3O_9•3(H_2O)$	4	2.68	Birkett et al. (1992)	no	no	no	Zr
gittinsite	$CaZrSi_2O_7$	3.5-4	3.6	Birkett et al. (1992)	yes	yes	yes	Zr
Ti minerals								
aeschynite	$(Y,Ca,Fe)(Ti,Nb)_2(O,OH)_6$	5–6	4.9–9.1	no	yes	no	no	Y
ilmenite	$FeTiO_3$	5–5.5	4.7	Birkett et al. (1996)	no	yes	no	
narsarsukite	$Na_2(Ti,Fe)Si_4(O,F)_{11}$	7	2.7	Miller (1996)	no	no	no	
bafertisite	$Ba(Fe,Mn)_2TiSi_2O_7(O,OH)_2$	5	3.96–4.25	Birkett et al. (1996)	no	no	no	
neptunite	$KNa_2Li(Fe,Mn)_2Ti_2Si_8O_{24}$	5–6	3.23	Birkett et al. (1996)	no	no	no	
aenigmatite	$(Na,Ca)_4(Fe,Ti,Mg)_{12}Si_{12}O_{40}$	5–6	3.7–3.9	Birkett et al. (1996)	no	yes	yes	
astrophyllite	$K_2Na(Fe,Mn)_7Ti_2Si_8O_{26}(OH)_4$	3-3.5	3.3–3.4	Birkett et al. (1996)	yes	no	no	
titanite	$CaTiSiO_5$	5–5.5	3.4–3.56	Miller (1996)	yes	yes	yes	
komarovite	$(Ca,Mn)_2(Nb,Ti)_2Si_2O_7(O,F)_2•3.5(H_2O)$	4	3.61–3.76	no	no	no	yes	Nb
chevkinite	$(Ce,La,Ca,Th)_4(Fe,Mg)_2(Ti,Fe)_3Si_4O_{22}$	5–5.5	4.5	no	no	no	yes	Ce, La, Th
Phosphate minerals								
xenotime	YPO_4	4–5	4.4–5.1	no	no	no	yes	Y
monazite	$(La,Ce,Y,Th)PO_4$	5–5.5	4.8–5.5	Miller (1996)	yes	yes	yes	Ce, La, Y, Th
fluorapatite	$Ca_5(PO_4)_3F$	5.0	3.1–3.2	no	no	yes	no	
apatite	$Ca_5(PO_4)_3(OH,F,Cl)$	5.0	3.2	Gowans et al. (2014)	yes	yes	yes	
britholite	$(Ce,Ca,Th,La,Nd)_5(SiO_4,PO_4)_3(OH,F)$		4.2–4.7	no	yes	no	no	Ce, La, Th
rhabdophane	$(Ce,La)PO_4•(H_2O)$	3.5	4.0	no	no	yes	yes	Ce, La
Other minerals								
gadolinite group	$Be_2(Ca,REE,Fe)_3Si_2O_{10}$	6.5–7	4.2	Miller (1996)	no	no	no	Be, Ce, La, Y
arfvedsonite	$Na_3Fe_4Fe(Si_8O_{22})(OH)_2$	5.5–6	3.44–3.45	Miller (1996)	yes	yes	yes	
aegerine	$NaFe(Si_2O_6)$	6.0	3.5–3.6	Miller (1996)	yes	yes	yes	
pyrochlore	$(Na,Ca)_2Nb_2O_6(OH,F)$	5–5.5	4.2–6.4	Miller (1996)	yes	yes	yes	Nb
bastnaesite	$Ce(CO_3)F$	4-5	4.95–5	Miller (1996)	no	no	yes	Ce
parisite	$Ca(Ce,La)_2(CO_3)_3F_2$	4.5	4.4	no	no	yes	yes	Ce, La
kainosite	$Ca_2(Y,Ce)_2Si_4O_{12}(CO_3)•H_2$Oleif	5–6	3.4–3.6	Miller (1996)	no	no	yes	Ce, Y
anthophyllite	$Mg_7(Si_8O_{22})(OH)_2$	5–6	2.9–3.6	no	no	no	yes	
allanite	$(Ce,Ca,Y)_2(Al,Fe)_3(SiO_4)_3(OH)$	5.5	3.3–4.2	Birkett et al. (1992)	yes	no	yes	Ce, Y
milarite	$K_2Ca_4Al_2Be_4Si_{24}O_{60}•(H_2O)$	6	2.52	Gowans et al. (2014)	no	no	no	Be
gerenite	$(Ca,Na)_2(Y,REE)_3Si_6O_{18}•2(H_2O)$	5	3.3–3.52	Jambor et al. (1998)	no	no	no	Ce, La, Nd, Y
leifite	$Na_2(Si,Al,Be)_7(O,OH,F)_{14}$	6	2.57	Sinclair et al. (1992)	no	no	no	Be
danburite	$CaB_2Si_2O_8$	7.0	3.0	no	no	yes	no	
zajacite-(Ce)	$Na(REE_xCa_{1-x})(REE_yCa_{1-y})F6$ where $(x \neq y)$	3.5	4.4–4.6	Jambor et al. (1996)	no	no	no	Ce, La, Nd
gagarinite-(Y)	$NaCaY(F,Cl)_6$	4.5	4.2	Jambor et al. (1996)	yes	no	no	Y
sphalerlite	(Zn,Fe)S	3.5–4	3.9–4.2	Miller (1996)	no	no	no	
molybdenite	MoS_2	1.0	5.5	no	no	yes	no	
galena	PbS	2.5	7.2–7.6	Miller (1996)	no	no	no	
fluorite	CaF_2	4.0	3.0–3.3	Miller (1996)	yes	yes	yes	

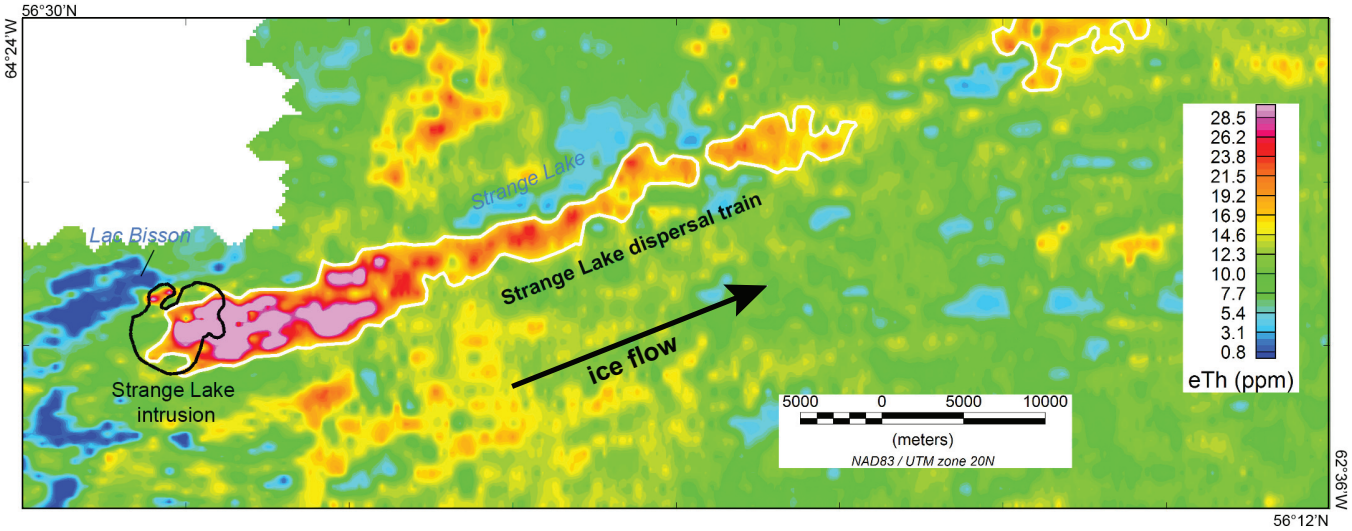

Figure 3. Equivalent Th (ppm) from airborne gamma-ray spectrometry data for the Strange Lake intrusion (black outline) and the northeast-trending glacial dispersal train (white outline). Data from Geological Survey of Canada (1980).

der mapping (Batterson et al., 1985; Batterson, 1989), matrix till geochemistry—most notably Be (Fig. 4), Ce, Zr, La, Nb, Pb, Rb, Th, U, and Y (McConnell and Batterson, 1987; Batterson, 1989; Batterson and Taylor, 2009)—and airborne gamma-ray spectrometry (Fig. 3).

METHODS

Several bedrock samples were collected from the Strange Lake Main and B zones. Colour photographs of sample sites and polished bedrock sample slabs, hand sample descriptions, and petrographic descriptions are reported in McClenaghan et al. (2017). Several till samples were collected around (up-ice, overlying, down-ice) the Strange Lake deposit in 1981 and 1983, and again in 2015 (Fig. 4).

Till and bedrock samples were processed to produce heavy mineral concentrates (HMC) for indicator min-

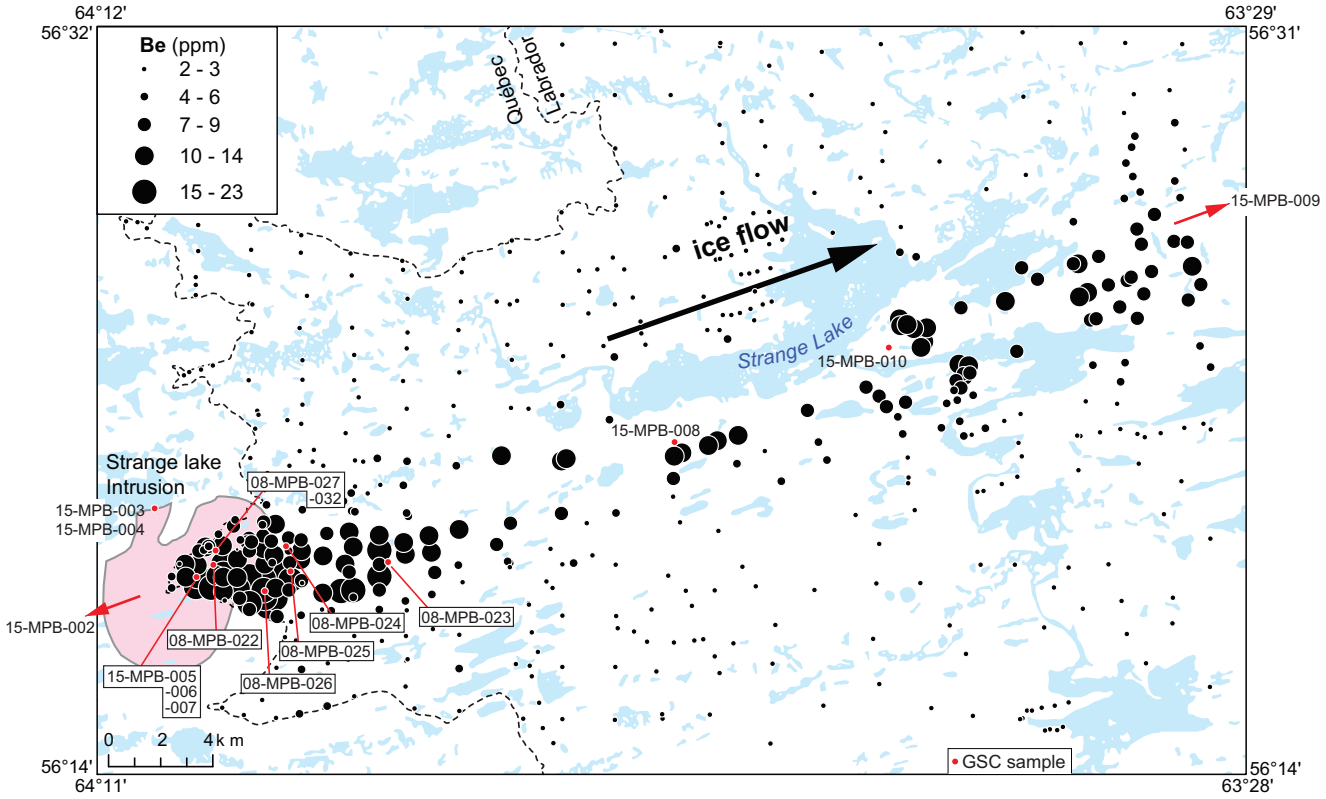

Figure 4. Distribution of Be (ppm) in the <0.063 mm fraction of till samples (total digestion/ICP-ES) collected overlying and down-ice of the Strange Lake intrusion (modified from Batterson and Taylor, 2009). Locations of Geological Survey of Canada bedrock and till samples are shown as red dots.

eral examination using procedures described in Spirito et al. (2011) and McClenaghan et al. (2013, 2017). Bedrock samples were disaggregated using an electric pulse disaggregator prior to processing. The <2.0 mm material from each bedrock and till sample was processed following tabling and heavy liquid methods described by McClenaghan (2011) and McClenaghan et al. (2017) to produce a non-ferromagnetic HMC (>3.2 specific gravity (SG)) and a mid-density (3.0–3.2 SG) mineral concentrate for examination of indicator minerals. The non-ferromagnetic HMC (SG >3.2) of bedrock and till samples was sieved and the 0.25–0.5, 0.5–1.0, and 1.0–2.0 mm size fractions examined. The 0.25–0.5 mm portion of the mid-density (SG 3.0–3.2) fraction of bedrock and till samples was also examined. Mineral grains were identified using a binocular microscope and potential indicator minerals of the REE mineralization at Strange Lake were counted. Some mineral grains were removed from the samples and set aside for further analyses. The visual identification of some mineral species was verified with a scanning electron microscope (SEM) and electron microprobe analysis (EMPA).

RESULTS

Indicator minerals that were observed in bedrock samples are listed in Table 1. Most indicator minerals in bedrock HMC were difficult to identify visually because of their small size, tendency to be intergrown with other indicator minerals and quartz, and discolouration from hematite staining. Minerals observed in bedrock samples in the recent Strange Lake study (McClenaghan et al., 2017) but not reported in earlier studies of the deposit include cerianite, uraninite, komarovite, chevkinite, fluorapatite, rhabdophane, parasite, thorianite, danburite, and molybdenite.

Indicator minerals observed in till samples in the recent study (McClenaghan et al., 2017) are listed in Tables 1 and 2 and include minerals not reported in earlier studies of the Strange Lake deposit (e.g. komarovite, chevkinite, parasite, anthophyllite, thorite, thorianite, and rhabdophane). Colour photographs of some of the minerals recovered from bedrock and till samples are shown in Figure 5. The most abundant minerals recovered from till are discussed below.

Zircon was difficult to distinguish from Ca-rich gittinsite if the zircon was intergrown with calcite or a REE carbonate mineral, such as parasite. Thus, some zircon grains may have been reported as gittinsite, which is a common post-magmatic mineral phase in the Strange Lake intrusion and is a valuable ore mineral for Zr. It is present in both bedrock and till samples. It may be a useful indicator mineral proximal (<2 km) to highly altered REE deposits such as Strange Lake. Zircon grains recovered from bedrock and till in

Table 2. Number of grains of select indicator mineral species in the 0.25 to 0.5 mm non-ferromagnetic heavy mineral fraction (SG >3.2) and mid-density fraction (SG 3.0–3.2) of bedrock, float, and till samples examined in the study by McClenaghan et al. (2017). Counts for bedrock and float are normalized to a 1 kg sample mass of <2 mm (table feed) material. Counts for till samples are normalized to a 10 kg mass of the <2 mm (table feed) fraction.

Sample	Material	Mass <2 mm (kg)	Titanite	Pyrochlore	Rhabdophane /monazite	Gittinsite	Parisite	Bastnaesite	Kainosite	Chevkinite	Zircon	Allanite	Thorite/ thorianite	Aegerine	Arfvedsonite	Fluorite 3.0-3.2 SG
08-MPB-027	Main Zone	bedrock	0.43	0	84	1397	4657	0	0	0	0	3492	0	5	0	34924	582
08-MPB-028	Main Zone	bedrock	0.25	8	0	0	0	0	0	0	0	237	0	0	0	12	0
08-MPB-029	Main Zone	bedrock	0.14	29155	15	1093	21866	0	0	0	0	0	0	0	87464	7289	1822
08-MPB-030	Main Zone	bedrock	0.12	0	40	96	48	2005	0	0	0	0	16	0	16	120289	642
08-MPB-031	Main Zone	bedrock	0.36	0	0	0	0	0	0	0	0	8	0	0	0	0	0
15MPB-006	Main Zone	bedrock	0.79	0	1	12593	151	0	0	0	0	0	0	2519	37779	10074	16
15MPB-004B	B Zone	bedrock	0.17	0	293	0	0	6	0	0	0	58514	59	0	29	0	1463
15MPB-004A02	B Zone	bedrock	0.18	0	450	0	0	0	0	0	0	28106	84	0	56211	56	5621
15MPB-003	B Zone	bedrock	0.38	395	132	8	5	0	0	0	0	0	10535	2107	79010	118515	132
15MPB-010A	35 km down-ice	cobble	0.20	0	15	978	0	0	0	0	0	391	29	293	12219	122190	0
15-MPB-002	2 km up-ice	till	6.3	476	0	6	0	0	0	0	0	0	0	0	0	0	0
08-MPB-022	overlying	till	3.6	2222	6	56	111	3	8	6	0	556	25	11	56	83333	17
15-MPB-005	overlying	till	6.2	24	0	6	8	0	0	0	10	194	2	0	32	97	0
15-MPB-007	overlying	till	7.2	21	0	18	4	0	1	0	31	139	1	1	28	278	0
08-MPB-026	1.8 km down-ice	till	4.0	1250	63	250	625	0	18	0	5	3750	5	0	100	125000	0
08-MPB-025	2.5 km down-ice	till	4.8	1250	25	25	73	0	6	0	48	104	6	0	83	5208	0
08-MPB-024	3 km down-ice	till	2.2	3636	100	123	455	0	9	1136	14	6818	95	14	3636	45455	0
08-MPB-023	5 km down-ice	till	2.7	926	7	7	444	4	7	0	0	9259	4	0	74	74074	7
15-MPB-008	16 km down-ice	till	7.7	2597	0	5	0	0	0	0	1	909	649	0	26	7792	0
15-MPB-010	35 km down-ice	till	10.1	1	5	3	8	0	1	0	6	792	1485	0	50	9901	0
15-MPB-009	50 km down-ice	till	6.9	4348	0	6	0	9	0	0	0	217	43	1	145	5797	0

bedrock normalized to 1 kg <2 mm; till normalized to 10 kg <2 mm

Figure 5. Colour photographs of select indicator minerals from till and bedrock samples overlying and down-ice of the Strange Lake deposit: **a)** pyrochlore, sample 15-MPB-010; **b)** bastnaesite, till sample 15-MPB-007; **c)** arfvedsonite, till sample 15-MPB-010; **d)** aegerine, till sample 15-MPB-008; **e)** chevkinite, till sample 15-MPB-010; **f)** zircon, till sample 15-MPB-008. Photographs provided by Michael J. Bainbridge Photography.

the recent study (McClenaghan et al., 2017) are not individual grains but fragile aggregates with other minerals and are often red, indicating the presence of hematite (Fig. 5f).

Titanite at Strange Lake is occasionally Sn-bearing (McClenaghan et al., 2017) and this feature may help to link some of the titanite grains recovered from till to titanite in the deposit. It is otherwise unremarkable in its occurrence.

Monazite and rhabdophane are both RE-phosphate minerals with very similar compositions, which makes it difficult to reliably distinguish between the two based on EMPA or SEM-EDS data alone. Their high RE-content makes them useful indicators of the presence of RE-rich rocks.

Pyrochlore occurs as a common primary euhedral phase in the Strange Lake granite and is also a valuable ore mineral for Nb. The Strange Lake pyrochlore is moderate brown to orange in colour (Fig. 5a). It is considered to be a useful indicator mineral because of its compact habit (usually octahedra), high density, resistate nature, and ease of recognition in HMC.

Bastnaesite (Fig. 5b) is a source of Ce in the deposit and kainosite is an important ore mineral of Y in the deposit. Both minerals are rare in till samples but their presence is a strong indication of the presence of REE mineralization up-ice. Chevkinite is a REE-silicate that is visually distinct (Fig. 5e) and sufficiently abundant in the till at Strange Lake to be considered a useful indicator mineral of REE mineralization. Allanite is a REE-silicate that is visually distinct and sufficiently abundant in the till at Strange Lake to be considered a useful indicator mineral of REE mineralization. Parisite has a distinctive reddish brown colour and compact habit and could, when grain size is sufficiently large, be a useful indicator mineral for RE-rich rocks. A few grains were observed in proximal till samples in this recent study (McClenaghan et al., 2017).

Arfvedsonite (Fig. 5c) and aegirine (Fig. 5d) are common major minerals in sodic alkaline rocks and hence good indicators of their presence. However, these minerals reveal little about the rare metal content of their host rocks. Thorite and thorianite are heavy dark brown minerals found in pegmatite. They were difficult to distinguish between in bedrock and till HMC and thus were counted and reported as one group (McClenaghan et al., 2017).

Distance of transport

A glacial dispersal train trends east-northeast from the Strange Lake deposit for at least 50 km and has been defined using airborne gamma-ray spectrometry, radioactive boulders, lake sediment geochemistry, and till geochemistry. Indicator minerals are most abundant in till samples collected directly overlying the Strange Lake intrusion and between 2 and 5 km down-ice (Table 2). However, a few grains of pyrochlore, gittinsite, bastnaesite, and chevkinite were still detectable in till up to 35 km down-ice, and a few grains of rhabdophane, parasite, and allanite were recovered from till 50 km down-ice.

Advantages of indicator mineral methods

The advantages of REE indicator mineral methods over geochemical analysis of the till matrix are that the indicator mineral grains (1) are visible and can be examined with a binocular or scanning electron microscope; (2) may be chemically analyzed to provide information about the nature of the mineralizing system; (3) provide physical evidence of the presence or absence of mineralization or alteration; (4) may be present in very low abundances (a few grains in a 10 kg till sample) that can be readily detected by indicator mineral methods but not by till geochemical methods (Averill, 2001; McClenaghan, 2011). Also, spacing of regional indicator mineral samples is typically broader (>5 km) than till geochemical samples (>2 km) and thus fewer samples need to be collected in a regional survey.

There are several benefits from visually examining the >0.25 mm fraction of till samples to identify indicator minerals: (1) the method described here is well established and has been used by industry and governments for more than 30 years and thus it is possible to compare results from surveys conducted during different years or by different organizations; (2) the method is fast and moderately priced; (3) identification of REE-minerals can be conducted as part of any indicator mineral survey undertaken for other purposes, i.e., precious and base metal exploration; and (4) the grains in this fraction are sufficiently large enough to be manipulated and their 3-dimensional shape and surface textures examined.

CONCLUSIONS

The Strange Lake study is the first detailed investigation of the indicator mineral signature of a major REE deposit in glaciated terrain. The deposit contains a large number of oxide and silicate, phosphate, and carbonate indicator minerals, some of which were observed in till overlying and up to 50 km down-ice. Several minerals were observed in bedrock and/or till samples in this recent study (McClenaghan et al., 2017) that had not been previously reported for the Strange Lake deposit.

The most useful indicator minerals of the REE mineralization include Zr-silicates (secondary gittinsite and many other hydrated Zr±Y±Ca-silicates), pyrochlore, thorite/thorianite, monazite/rhabdophane, chevkinite, parasite, bastnaesite, kainosite, and allanite.

The Strange Lake test site is exceptional for two reasons. First, a large volume of debris was glacially eroded from the deposit and second, the debris was glacially transported a long distance by a paleo ice stream of the Laurentide Ice Sheet. The net result is a remarkably long ribbon-shaped dispersal train formed by unidirectional ice-flow. This remarkable dispersal train was ideal for the collection of metal-rich till at varying distances down-ice to test and develop REE indicator mineral methods. The indicator mineral abun-

dances for till that are reported here offer a guide to contents in till that might be expected proximal and distal to other REE mineralization in the region, and elsewhere.

This case study demonstrates that REE indicator minerals can now be added to a large suite of indicator minerals that are used to explore glaciated terrain for a broad range of deposit types and commodities. This broad suite of indicator minerals can be recovered from the same till or stream sediment samples collected during exploration for diamonds, precious metals, base metals, strategic metals, and/or rare metals.

ACKNOWLEDGEMENTS

The recent Strange Lake study (McClenaghan et al., 2017) was initiated as part of the Geological Survey of Canada's (GSC) Targeted Geoscience Initiative (TGI-3) Program and completed as part of the GSC's Geomapping for Energy and Minerals (GEM) Program (2014–2018) in the Hudson-Ungava region. The authors thank D. Lentz (University of New Brunswick) for providing bedrock samples that he collected from the deposit in 2008. The authors acknowledge Quest Rare Minerals Limited, in particular E. Walker and J. Renaud, for providing access to the Strange Lake property in 2015. H. Dubé-Loubert, Ministère de l'Énergie et des Ressources naturelles du Québec, and J. Rice, Ph.D. student at the University of Waterloo, are thanked for providing assistance with the collection of till and bedrock samples in 2015. Discussions with R.N.W. DiLabio and S. Zajac were helpful to this research. Photographs shown in Figure 5 were provided by Michael J. Bainbridge Photography.

REFERENCES

Averill, S.A., 2001. The application of heavy indicator minerals in mineral exploration with emphasis on base metal indicators in glaciated metamorphic and plutonic terrain, *In:* McClenaghan, M.B., Bobrowsky, P.T., Hall, G.E.M. and Cook, S. (eds.), *Drift Exploration in Glaciated Terrain*; Geological Society of London, Special Volume 185, p. 69–82.

Batterson, M.J., 1989. Glacial dispersal from the Strange Lake alkalic complex, northern Labrador, *In:* DiLabio, R.N.W. and Coker, W.B. (eds.), *Drift Prospecting*; Geological Survey of Canada, Paper 89-20, p. 31–40.

Batterson, M.J. and Taylor, D.M., 2009. *Geochemical re-analysis of till samples from the Strange Lake area, Labrador (NTS Map Sheets 14D/5 and 24A/8)*; Government of Newfoundland and Labrador, Department of Natural Resources, Geological Survey, Open File LAB/1479.

Batterson, M.J., Taylor, D.M., and Vatcher, S.V., 1985. Quaternary mapping and drift exploration in the Strange Lake areas, Labrador, *In: Current Research*. Newfoundland Department of Mines and Energy, Mineral Development Division, Report 85-1, 4–10.

Belusova, E.A., Griffin, W.L., O'Reilley, S.Y., and Fisher, N.I., 2002a. Apatite as an indicator mineral for mineral exploration: trace-element compositions and their relationship to host rock type; *Journal of Geochemical Exploration*, v. 76, p. 45–69.

Belusova, E.A., Griffin, W.L., O'Reilley, S.Y., and Fisher, N.I., 2002b. Igneous zircon: trace element composition as an indicator of source rock type' *Contributions to Mineralogy and Petrology*, v. 143, p. 602–622.

Birkett, T.C., Miller, R.R., Roberts, A.C., and Mariano, A.N., 1992. Zirconium-bearing minerals of the Strange Lake intrusive complex, Quebec-Labrador; *The Canadian Mineralogist*, v. 30, p. 191–205.

Birkett, T.C., Trzcienski, Jr., and Stirling, J.A.R., 1996. Occurrence and compositions of some Ti-bearing minerals in the Strange Lake intrusive complex, Quebec-Labrador boundary; *The Canadian Mineralogist*, v. 34, p. 779–801.

DiLabio, R.N.W., 1988. Residence sites of gold, PGE and rare lithophile elements in till, *In: Prospecting in Areas of Glaciated Terrain – 1988*; Canadian Institute of Mining and Metallurgy, p. 121–140.

DiLabio, R.N.W., 1995. Residence sites of trace elements in oxidized till, *In:* Bobrowsky, P.T. Sibbick, S.J., Newell, J.M., and Matysek, P.F. (eds), *Drift Exploration in the Canadian Cordiller;* British Columbia Ministry of Energy, Mines and Petroleum Resources, Paper 1995-2, p. 139–148.

Dyke, A.S. and Prest, V.K., 1987. Late Wisconsin and Holocene history of the Laurentide Ice Sheet; *Géographie physique et Quaternaire*, v. 41, p. 237–263.

Geological Survey of Canada, 1980. *Airborne gamma ray spectrometric map, Dihourse Lake Quebec-Newfoundland*; Geological Survey of Canada, Geophysical Series, Map 35124(08)G.

Gowans, R.M., Lewis, W.J., Shoemaker, S., Spooner, J., and Zalnieriunas, R.V., 2014. *Quest Rare Minerals Ltd. NI-43-101 Technical report on the preliminary economic assessment (PEA) for the Strange Lake Property, Quebec, Canada*; Micon International Limited, www.SEDAR.com.

Hawthorne, F.C., Oberti, R., Cannillo, E., Ottolini, L., Roelofsen, J., and Martin, R.F., 2001. Li-bearing arfvedsonitic amphiboles from the Strange Lake peralkaline granite Quebec; *The Canadian Mineralogist*, v. 39, p. 1161–1170.

Hornbrook, E.H.W., Maurice, Y.T., and Lynch, J.J., 1979. *Regional lake sediment and water geochemical reconnaissance data, Labrador*; Geological Survey of Canada, Open File 559.

Jambor, J.L., Roberts, A.C., Owens, D.R., and Grice, J.D., 1996. Zajacite-(Ce), a new rare-earth fluoride from the Strange Lake deposit, Quebec-Labrador; *The Canadian Mineralogist*, v. 34, p. 1299–1304.

Jambor, J.L., Roberts, A.C., Grice, J.D., Birkett, T.C., Groat, L., and Zajac, S., 1998. Gerenite-(Y), $(CaNa)_2(Y,REE)_3Si_6O_{18}•2H_2O$, a new mineral species and an associated Y-bearing gadolinite-group mineral, from the Strange Lake peralkaline complex, Quebec-Labrador; *The Canadian Mineralogist*, v 36, p. 793–800.

Kerr, A., 2013. Rare-Earth-Element (REE) behavior in the Strange Lake intrusion, Labrador: resource estimation using predictive methods, *In: Current Research*; Newfoundland and Labrador Department of Natural Resources, Geological Survey Report 13-1, p. 117-136.

Kerr, A. and Rafuse, H., 2012. Rare-earth element (REE) behavior in the Strange Lake intrusion: resource estimation using predictive methods, *In: Current Research*; Newfoundland and Labrador Department of Natural Resources, Geological Survey Report 12-1, p. 39–60.

Lehtonen, M., Laukkanen, J., and Sarala, P., 2011. Exploring RE and REE mineralization using indicator minerals, *In: Indicator Mineral Methods in Mineral Exploration, Workshop 3*; 25th International Applied Geochemistry Symposium, Rovaniemi, Finland. Association of Applied Geochemists, p. 13–18.

Mackay, D.A.R. and Simandl, G.J., 2015. Pyrochlore and columbite-tantalite as indicator minerals for specialty metal

deposits; *Geochemistry: Exploration, Environment, Analysis*, v. 15, p. 167–178.

Mackay, D.A.R., Simandl, G.J., Grcic, B., Li, C., Luck, P., Redfearn, M., and Gravel, J., 2015. Evaluation of Mozley C800 laboratory mineral separator for heavy mineral concentration of stream sediments in exploration for carbonatite-related specialty metal deposits: case study at the Aley carbonatite, British Columbia (NTS 094B), Canada, *In: Geoscience BC Summary of Activities 2014*; Geoscience BC, Report 2015-1, p. 111–122.

Makin, S.A., Simandl, G.J., and Marshall, D., 2014. Fluorite and its potential as an indicator mineral for carbonatite-related rare earth element deposits, *In: Geological Fieldwork 2013*; British Columbia Ministry of Energy and Mines, British Columbia Geological Survey, Paper 2014-1, p. 207–212.

McClenaghan, M.B., 2011. Overview of common processing methods for recovery of indicator minerals from sediment and bedrock in mineral exploration; *Geochemistry: Exploration, Environment, Analysis*, v. 11, p. 265–278.

McClenaghan, M.B., Plouffe, A., McMartin, I., Campbell, J.E., Spirito, W.A., Paulen, R.C., Garrett, R.G., and Hall, G.E.M., 2013. Till sampling and geochemical analytical protocols used by the Geological Survey of Canada; *Geochemistry: Exploration, Environment, Analysis*, v. 13, p. 285–301.

McClenaghan, M.B., Paulen, R.C., Kjarsgaard, I.M., and Fortin, R., 2017. *Indicator mineral signatures of the Strange Lake REE deposit, Labrador*; Geological Survey of Canada, Open File 8420.

McConnell, J.W. and Batterson, M.J., 1987. The Strange Lake Zr-Y-Nb-Be-REE deposit, Labrador: a geochemical profile in till, lake and stream sediment, and water; *Journal of Geochemical Exploration*, v. 29, p. 105–127.

Miller, R.R., 1986. Geology of the Strange Lake alkali complex and the associated Zr-Y-Nb-Be-REE mineralization, *In: Current Research 1986*; Newfoundland Department of Mines and Energy, Report 86-1, p. 11–19.

Miller, R.R., 1988. Yttrium (Y) and other rare metals (Be, Nb, REE, Ta, Zr) in Labrador, *In: Current Research 1988*; Newfoundland Department of Mines and Energy, Report 88-1, p. 229–245.

Miller, R., 1990. The Strange Lake pegmatite-aplite-hosted rare-metal deposit, Labrado, *In: Current Research 1990*; Newfoundland Department of Mines and Energy, Report 90-1, p. 171–182.

Miller, R.R., 1996. Structural and textural evolution of the Strange Lake peralkaline rare-element (NYF) granite pegmatite, Quebec-Labrador; *The Canadian Mineralogist*, v. 34, p. 349–371.

Miller, R.R., Heaman, L.M., and Birkett, T.C., 1997. U-Pb zircon age of the Strange Lake peralkaline complex: implications for Mesoproterozoic peralkaline magmatism in north central Labrador; *Precambrian Research*, v. 81, p. 67–82.

Paulen, R.C., Stokes, C.R., Fortin, R., Rice, J.M., Dubé-Loubert, H., and McClenaghan, M.B., 2017. Dispersal trains produced by ice streams: an Example from Strange Lake, Labrador, Canada, *In: Proceedings of the Sixth Decennial International Conference on Mineral Exploration*, Toronto, Canada.

Roelofson, J.N. and Veblen, D.R., 1999. Relationships among zirconosilicates: examination by cathodoluminescence and transmission electron microscopy; *Mineralogy and Petrology*, v. 67, p. 71–84.

Salvi, S. and Williams-Jones, A.E., 1995. Zirconosilicate phase relations in the Strange Lake (Lac Brisson) pluton, Quebec-Labrador, Canada; *American Mineralogist*, v. 80, p. 1031–1040.

Sinclair, W.D., Jambor, J.L., and Birkett, T.C., 1992. Rare earths and the potential for rare-earth deposits in Canada; *Exploration and Mining Geology*, v. 1, p. 265–281.

Spirito, W.A.,McClenaghan, M.B., Plouffe, A., McMartin, I. Campbell, J.E., Paulen, R.C., Garrett, R.G., and Hall, G.E.M., 2011. *Till sampling and analytical protocols for GEM Projects from field to archive*; Geological Survey of Canada, Open File 6850.

Zajac, S.I., 2015. John Jambor's contributions to the mineralogy of the Strange Lake peralkaline complex, Quebec-Labrador; Canada. *The Canadian Mineralogist*, v. 53, p. 885–894.